LRRK2 GENETICS AND EXPRESSION IN THE PARKINSONIAN BRAIN

Thesis submitted in fulfilment of the degree of Doctor of Philosophy

2010

Queen Square Brain Bank, Department of Molecular Neuroscience, Institute of Neurology
& Institute of Human Genetics and Health,
University College London

Simone Sharma

Declaration

I hereby declare that the work described in this thesis is solely that of the author, unless stated otherwise in the text. None of the work has been submitted for any other qualification at this or any other university.

Simone Sharma

Abstract

Mutations in *LRRK2* have been established as a common genetic cause of Parkinson's disease (PD). Variation in gene expression of PARK loci has previously been demonstrated in PD pathogenesis, although it has not been described in detail for LRRK2 expression in the human brain. This study further elucidates the role of LRRK2 in development of PD by describing an investigation into the role of LRRK2 genetics and expression in the human brain.

The G2019S mutation is a common *LRRK2* mutation that exhibits a clinical and pathological phenotype indistinguishable from idiopathic PD. Thus, the study of G2019S mutation is a recurrent theme. The frequency of G2019S was estimated in unaffected subjects that lived or shared a cultural heritage to the predicted founding populations of the mutation, and was found not to be common in these populations.

Morphological analysis revealed a ubiquitous expression for LRRK2 mRNA and protein in the human brain. *In-situ* hybridisation data suggests that LRRK2 mRNA is present as a low copy number mRNA in the human brain. A semi-quantitative analysis of LRRK2 immunohistochemistry revealed extensive regional variation in the LRRK2 protein levels, although the weakest immunoreactivity was consistently identified in the nigrostriatal dopamine region. No difference was observed in the morphological localisation of LRRK2 mRNA and protein in unaffected, IPD or G2019S positive PD subjects.

Dysregulation of LRRK2 mRNA expression and the effects of *cis*- acting genetic variation on these levels were demonstrated. A widespread decrease of LRRK2 mRNA was observed in IPD and G2019S positive PD subjects in comparison to unaffected controls. Furthermore, non-coding genetic variation was also demonstrated to have an effect on the LRRK2 transcriptional activity in PD subjects. Collectively, these findings suggest that LRRK2 has an important physiological role, and a dysregulation in its levels could affect auxiliary mechanisms that contribute to PD pathogenesis. This data also supports the possibility of a shared mechanism contributing to the identical phenotype of IPD and G2019S linked PD.

Acknowledgements

Firstly, I would like to thank the Institute of Human Genetics and Health (IHGH) and my principal supervisor Prof. Nick Wood for giving me the opportunity and support to undertake this project. I am extremely grateful and owe a special thanks to my secondary supervisors, Dr. Janice Holton and Dr. Rina Bandopadhyay for their guidance, constant encouragement, an infinite amount of patience and the much needed strictness that really helped bring this project together.

Thanks are given to all the lab colleagues at the Department of Molecular Neuroscience, Queen Square Brain Bank and Reta Lila Weston Institute for their guidance and assistance. I would especially like to thank Drs. Ann Kingsbury and Tammaryn Lashley for teaching me the many joys of the histochemical work. Profs. Tamas Revesz and John Hardy, and Dr. Rohan de Silva have given me some very useful advice over the years and I thank them for that. I am also grateful to Dr. Costas Kallis for advising me on the statistics, and to Drs. Carles Vilarino Guell and Alan Pittman for all their help with the genetics in the early days. I would also like to thank Dr. Patrick Lewis for his critical reading and insightful comments on the final section of this thesis. I am grateful to all the patients and their families, without whom none of this research would have been possible.

I would like to thank the IHGH team, especially Prof. Steve Humphries and Dr. Neil Bradman for their support and guidance in the project. The interdisciplinary training gained through IHGH was very helpful in making me appreciate the point view of other disciplines. A special thanks goes to my friends and fellow IHGH PhD students: Alan Renton and Alex Calladine for all the giggles and the debates- be it about housekeeping genes, genetic reductionism or just general existential crisis! I am thankful to Jutta Palmen and Dr. Andrew Smith (Rayne Institute, UCL) for all their assistance, and also to my current colleagues for their patience during the writing procedure.

A huge thank you to my mum and dad, and the rest of the family and friends for their understanding, support and for dealing with my whingeing all these years!

Lastly, this thesis is dedicated with love to all my grandparents who continue to be a source of great love and inspiration.

Table of contents

List of figures

List of tables

Abbreviations

AD	autosomal dominant
AR	autosomal recessive
AR-JP	autosomal recessive forms of juvenile parkinsonism
bp	base pair
BCA	bicinchoninic acid
BSA	bovine serum albumin
CBD	corticobasal degeneration
CD-CV	common disease –common variant
cDNA	complementary DNA
CEPH	Centre Humain d'Etude du Polymorphisme
CI	confidence interval
CNS	central nervous system
CO_2	carbon dioxide
COR	c-terminal of ROC
CSF	cerebrospinal fluid
Ct	threshold cycle
DAB	diaminobenzidine
DAergic	dopaminergic
DAE	differential allelic expression
ddH_2O	double distilled water
DEPC	diethyl pyrocarbonate
DLB	dementia with Lewy body
DLBD	diffuse Lewy body disease
DMNV	dorsal motor nucleus of the vagus nerve
dNTPs	deoxynucleoside triphosphates

DTT	dithiothreitol
ECACC	European collection of cell cultures
EDTA	ethylenediaminetetraacetic acid
EMSA	electrophoretic mobility shift assay
EtBr	ethidium bromide
eQTL	quantitative trait loci for expression
F-DOPA	fluorodopa
FPD	familial Parkinson's disease
FTDP-17	frontotemporal dementia with parkinsonism-*17*
FTDP-17/PPND	frontotemporal dementia of the pallido-ponto-nigral degeneration type linked to the chromosome 17
FTLD	frontotemporal lobar degeneration
FTLD-U/NII	frontotemporal lobar degeneration with ubiquitinated neuronal intranuclear inclusions
GCI	glial cytoplasmic inclusions
GPe	globus pallidus external
GPi	globus pallidus internal
GWA	genome wide association
HapMap	International HapMap project
Haemotoxylin & Eosin	H & E
H_2O_2	hydrogen peroxidase
HRP	horseradish peroxidase
HWE	Hardy- Weinberg Equilibrium
IHC	immunohistochemistry
INAD	infantile neuroaxonal dystrophy
IPD	idiopathic Parkinson's disease

ISH	*in-situ* hybridisation
kb	kilobase
kDA	kilodalton
KRS	Kufor-Rakeb syndrome
LB	Lewy body
LC	locus coeruleus
LD	linkage disequilibrium
Maneb	manganese ethylenebisdithiocarbamate
MAPKKK	mitogen- activated protein kinase kinase kinase
MENA	Middle Eastern- North African
miRNA	micro-RNA
MLK	mixed-lineage kinase
MMSE	mini mental state examination
MSA	multiple system atrophy
MPP+	1-methyl-4-phenylpyridinium
MPTP	1-methyl-4-phenyl-1,2,3,6-tetrahydropyridine
nbM	nucleus basalis of Meynert
NCBI	National Centre for Biotechnology Information
NBIA	neurodegeneration with brain iron accumulation
NFT	neuro fibrillary tangle
NPC	Neimann-Pick Type C
OR	odds ratio
6-OHDA	6-hydroxydopamine
PBS	phosphate buffered saline
PD	Parkinson’s disease
PDD	Parkinsonism with dementia
PET	positron emission tomography

PPS	Parkinsonian-pyramidal syndrome
PSP	progressive supranuclear palsy
RIPK	receptor interaction protein kinase
RT-PCR	reverse transcriptase PCR
RNAi	RNA interference
ROC	ras of complex
ROS	reactive oxygen species
qPCR	quantitative real-time PCR
SEM	standard error of the mean
SN	substantia nigra
SNpc	substantia nigra pars compacta
SNpr	substantia nigra pars reticulata
SNP	single nucleotide polymorphisms
TFBS	transcription factor binding site
TSA	tyramide signal amplification
TKL	tyrosine kinase like
tRNA	transfer RNA
tSNPs	tagging SNPs
UCSC	University of California Santa Cruz genome browser
UPS	ubiquitin protease system
VTA	ventral tegmental area

Gene abbreviations

ALD-C	Aldolase-C
APOE	apolipoprotein E
ATP13A2	ATPase Type 13A2
COMT	catechol-o-methyl transferase
GBA	glucocerebrosidase
GIGYF2	Grb10-Interacting GYF Protein-2
G6PD	Glucose 6 –phosphate-1-dehydrogenase
HPRT1	Hypoxanthine Phosphoribosyl-transferase 1
LRRK2	Leucine rich repeat kinase 2
MAPT	microtubule associated protein tau
Nurr1/NR4A2	Nuclear receptor related 1
PINK1	PTEN-induced kinase 1
PLA2G6	phospholipase A2
PRKN	Parkin
RPL13A	Ribosomal Protein L13a
SNCA	α-synuclein
SPR	sepiapterin reductase
TBP	TATA binding protein
UCH-L1	ubiquitin C-terminal hydrolase 1

Chapter 1

1 Introduction

1.1 Parkinson's Disease

Parkinson's Disease (PD) is an insidious and a progressive disease that affects approximately 1% of the population over the age of 65 years. It has a broad clinical spectrum which is usually defined by a combination of any of the following six motor features: rest tremor, bradykinesia, rigidity, loss of postural reflexes, flexed posture, and freezing of gait (Lees et al. 2009). At least two of these cardinal symptoms should be present before a clinical diagnosis of PD can be made. The symptoms usually present themselves asymmetrically, and levodopa (L-DOPA) replacement therapy offers relief to the initial clinical symptoms of resting tremor, bradykinesia and rigidity, but this does not halt the progression of the disease.

Age is the biggest risk factor for the disease, and majority of PD cases are idiopathic (IPD) with less than 10% reporting a family history (Lees et al. 2009). Despite the rarity of monogenic inheritance in PD, mendelian genes collectively known as the PARK loci have been shown to be associated with familial inheritance. Some PARK loci have also been implicated in the idiopathic forms of the disease, suggesting that shared mechanistic pathways might contribute to familial and idiopathic disease pathogenesis.

1.2 Clinical phenotype

The clinical diagnosis published by James Parkinson in 1817 entitled 'An essay on the shaking palsy', set the precedent for further investigation into this debilitating disease. He identified the progressive nature of the disease along with the cardinal symptoms of akinesia (impaired muscle movement), resting tremor, bradykinesia (slow movement) and postural instability, and referred to the disease as Shaking Palsy or Paralysis Agitans (Lees 2007).

The clinical signs were expanded upon by Charcot in 1881 who observed that "*You easily recognise how difficult it is for them to do things even though rigidity or*

tremor is not the limiting factor. Instead even a cursory exam demonstrates that their problem relates more to slowness in execution of movement rather than to real weakness." (translation of Charcot, 1881 (Goetz 2002)). Based on his extensive and detailed observations of the tremor associated with the disease, he added rigidity to the characteristic features of the Paralysis Agitans. However, as Charcot did not consistently observe rest tremor, he argued that Paralysis Agitans was an inaccurate description, and suggested that the disease be referred to as 'Parkinson's Disease' (PD).

The cardinal features based on the motor symptoms as described by Parkinson and Charcot still remain essential for the clinical diagnosis of PD. However, it has long been acknowledged that there are various non-motor symptoms that include autonomic and neuropsychiatric symptoms. Some of the disturbance of autonomic functions precede the motor symptoms and can include sleep disturbances, constipation, sexual dysfunction, and hyposmia (impairment of smell) (Bohnen et al. 2007; Lim et al. 2009). The neuropsychiatric symptoms appear later in the course of disease and include depression and anxiety, followed by cognitive decline (Emre 2003; Lim et al. 2009). The complexity presented by the broad spectrum of PD symptoms has made it necessary to include the non-motor symptoms in clinical diagnosis of the disease. As a result, the unified Parkinson's diseases rating scale was revised by the UK movement disorder society to incorporate these symptoms as well as the cardinal motor symptoms (Litvan et al. 2003). This combination of motor and non-motor symptoms has resulted in PD being described as a highly complex disease, and poses a tough challenge to the scientists studying PD pathogenesis and the relevant therapeutics.

1.3 Pathological phenotype

1.3.1 Nigral cell loss

The pathology of PD is frequently characterised by the pallor of specific subnuclei of the substantia nigra pars compacta. The dopaminergic (DAergic) neurons of the substantia nigra (SN) contain cytoplasmic neuromelanin, a pigment which gives these nuclei a macroscopical black appearance (Forno 1996). A loss of this pigment correlates with severe degeneration (approximately ~50%) of the DAergic neurons in SN of PD subjects (see Figure 1.1).

The neuronal cell loss in SN is not uniform in PD. The ventrolateral tier of neurons in the pars compacta (A9) are the most vulnerable to PD, degenerating earlier and more severely than the dorsal medial regions (Fearnley & Lees 1991). Differing amounts of neuromelanin in DAergic neurons of the ventrolateral versus the dorsal medial regions have been suggested to be a cause of the selective vulnerability of the nigral neurons (Gibb & Lees 1991). This is interesting in terms of PD pathogenesis as the ventrolateral tier of the nigra projects to the dorsal putamen which is predominantly involved in motor co-ordination, and the relatively spared areas of the medial and ventral tegmental areas (VTA) project to the caudate which is involved in cognition (Fearnley & Lees 1991).

The DAergic neurons of the ventral tier contain a smaller amount of neuromelanin than those in the dorsal medial areas, but whether neuromelanin is protective or toxic remains undecided (Zecca et al. 2003). Furthermore, the DAergic neurons within the red nucleus, are relatively protected from degeneration despite having similar levels of neuromelanin to the neurons in the ventrolateral nigra (Gibb 1992). These observations along with weak expression of neurotrophic factors, such as brain derived neurotrophic factor (BDNF) in SN has led to the suggestions that weakened trophic support plays a central role in the regional vulnerability of dopamine neurons (Howells et al. 2000). Higher cell density of midbrain DAergic neurons have also been suggested to add to their

vulnerability (Gibb 1992). Cells with disproportionately large axons in comparison to the somata, or with long thin-caliber axons that are un- or poorly myelinated have also been suggested to be susceptible to PD degeneration (Braak et al. 2004). In contrast, local circuit neurons and projection cells with short axons (e.g., the small pyramidal cells of neocortical layers II and IV and the granule cells of dentate fascia) remain relatively resistant (Braak et al. 2004).

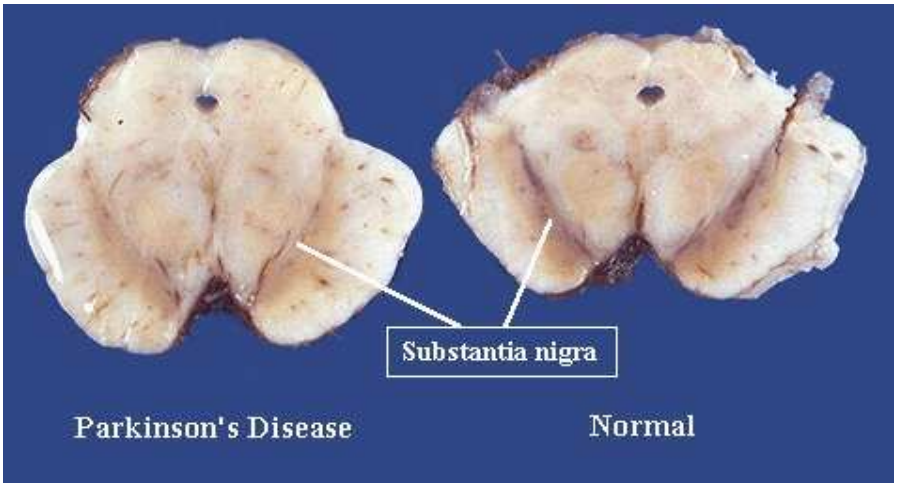

Figure 1.1: Degeneration of dopaminergic neurons in substantia nigra of PD patients. Loss of pigment is evident in PD when compared to the substantia nigra in the normal brain. This image was obtained from- http://www.gwc.maricopa.edu/class/bio201/parkn/parkn1.jpg.

1.3.2 Lewy body inclusions

In the early 1900's, Friederich H. Lewy examined PD brains and described spherical pathological inclusions in the dorsal motor nucleus of the vagus nerve (DMVN), nucleus basalis of Meynert, paraventricular nucleus and lateral thalamic nucleus. Further examination led him to conclude that this inclusion body pathology was predominantly observed, but not limited to the brainstem and basal ganglia structures. Lewy described these pathological inclusions as having a 'dense core' with a 'transparent and lighter-stained cytoplasmic sheath'. The lesions in the SN were first identified by Tŕetiakoff in patients with PD and in those with encephalitis lethargica, leading him to coin the term "corps de Lewy" or Lewy bodies (LB) (Lees 2007).

Later confirmed in all pigmented neurons of the brainstem including locus coeruleus (LC), the most consistent lesions were observed in SN, securing their position as the pathological hallmark of PD (Forno 1996). The principle component of these inclusions was identified as α-synuclein, (a protein expressed in presynaptic nerve terminals) in 1997 (Spillantini et al. 1997).

In PD, these pathological inclusions develop either as globular LBs in the neuronal perikarya, or as spindle- or thread like Lewy neurites (LNs) in cellular processes (Braak et al. 2003). Classical brainstem or intraneuritic LBs are usually presented as spherical and weakly acidophilic inclusion bodies with a smooth halo. LBs are typically located within the deposits of lipofuscin or neuromelanin granules of the cells vulnerable to degeneration. The selective pattern of nigral cell death is mirrored by the initial appearance of LBs in ventrolateral regions, followed by the presence in more medial and dorsal regions of the SN (Gibb & Lees 1991). LNs are thought to ante-date the appearance of LBs, and are only visible using immunohistochemical methods, whereas LBs can be observed using routine histological staining (e.g. haemotoxylin and eosin) (Braak et al. 2003).

Unlike brainstem LBs, cortical LBs lack the typical well defined halo. In PD pathology, cortical LBs and LNs are predominantly found in areas containing non-pigmented and less vulnerable neurons that typically display weak immunoreactivity for α-synuclein. These inclusions can be seen in hippocampus amygdala, neocortex, and olfactory bulb (Braak et al. 2003). Cortical LBs are distinct from another pale staining cytoplasmic inclusion which is found in the pigmented neurons of SN and LC, and is termed the ‘pale body’. It has been suggested that cortical LBs and pale bodies are early lesions that precede the classical LBs (Braak et al. 2003).

1.3.3 Extra-nigral pathology

As first noted by Lewy, PD pathology is not limited to the nigrostriatal system but instead involves various extranigral regions that include the mesocortical DAergic system, noradrenergic, serotonergic, cholinergic brainstem nuclei, and the limbic

system (Jellinger 1999). In cases with severe damage, lesions can also be observed in various regions of the neocortex (Braak et al. 2003).

1.3.3.1 Sub- cortical pathology

Apart from severe degeneration and lesions in SN, neuronal loss can also occur in other regions of the brainstem (although not as severe as in SN). These include noradrenergic nuclei of dorsal motor nucleus of the glossopharyngeal and vagal nerves (dorsal IX/X motor nucleus, respectively) of the medulla oblongata, and the locus coeruleus (LC) (Jellinger 1999). The melanised noradrenergic neurons of the LC project bilaterally to various locations including the cerebral cortex, limbic system and spinal cord. Like the loss of nigral neurons in SN, a complete degeneration of the LC complex can also be seen in PD subjects with long duration of illness. Lesions are frequently observed in these nuclei in addition to the anterior olfactory nucleus (Braak et al. 2004).

The other regions affected in midbrain, although not to the same extent as the nigral neurons (A9 cell group) are the DAergic neurons of VTA (A10 cell group, origin of DAergic cell bodies) which are involved in the mesocorticolimbic dopamine system and the red nucleus which is involved in motor coordination (German et al. 1989). The dorsal raphè which is the largest serotonergic nucleus in the brainstem also undergoes degeneration in PD, and a deficit of neurons in the mesocorticolimbic and noradrenergic systems has been suggested to contribute to the cognitive symptoms associated with PD (Jellinger 1999).

1.3.3.2 Limbic and Cortical pathology

PD-related LB inclusions can be frequently and consistently observed in the nucleus basalis of Meynert (nbM), and this group of cholinergic nerve cells in the substantia innominata have wide projections to the neocortex and limbic areas, such as hippocampus and amygdala, both of which are known to have PD pathology (Braak et al. 2003). The limbic areas of anterior cingulate gyrus and temporal cortex are more severely affected than the frontal and parietal cortices with the occipital areas being relatively spared (Braak & Braak 2000). Pathology within limbic structures

(amygdaloid nucleus, CA2/3 neurons of the hippocampal formation, limbic thalamic nuclei with prefrontal projections) has been correlated with dementia and other cognitive related symptoms in PD (Jellinger 2004; Junqué et al. 2005).

1.3.4 Neuropathological stages associated with PD progression

Despite the extensive degeneration of DAergic neurons of the SN in PD, it has been shown that the pathology in nigral and extranigral system does not evolve simultaneously, but instead follows a coherent sequence of disease related alterations (Braak et al. 2003). Braak and colleagues investigated the assumption that the lesions in PD appear prior to the somato-motor dysfunctions, and were able to produce a detailed topographical map of how the progression of PD lesions can be used to stage the pathological process. As such, they were able to demonstrate the extent to which extranigral impairment contributes to the somato-motor dysfunctions in PD pathogenesis (Braak & Braak 2000; Braak et al. 2003).

Braak and colleagues detail that in the course of PD, major components of somato-motor and emotional motor systems suffer a gradually evolving deterioration as a result of LB pathology which develops in 6 different stages (Braak et al. 2003; Braak et al. 2004). They were able to demonstrate that the LB pathology in PD begins in the lower brainstem nuclei and assumes an upward course, eventually extending into the cerebral cortex (see Figure 1.2). Stages 1 and 2, involve and remain virtually confined to the medulla oblongata, whereas in stage 3 the lower and upper brainstem is also involved. By stage 4, LB lesions can be observed in anteromedial temporal mesocortex. At stage 5, the olfactory areas are severely affected along with the limbic areas of the allocortex. By stage 6, the LB pathology is conspicuous in nearly all of the neocortex (Braak et al. 2003; Braak et al. 2004). Mesocortical and neocortical areas that undergo late myelination have been suggested to develop lesions earlier and at higher densities than those that begin to myelinate earlier, thereby recapitulating the process of cortical myelination in reverse order (Braak & Del Tredici 2004).

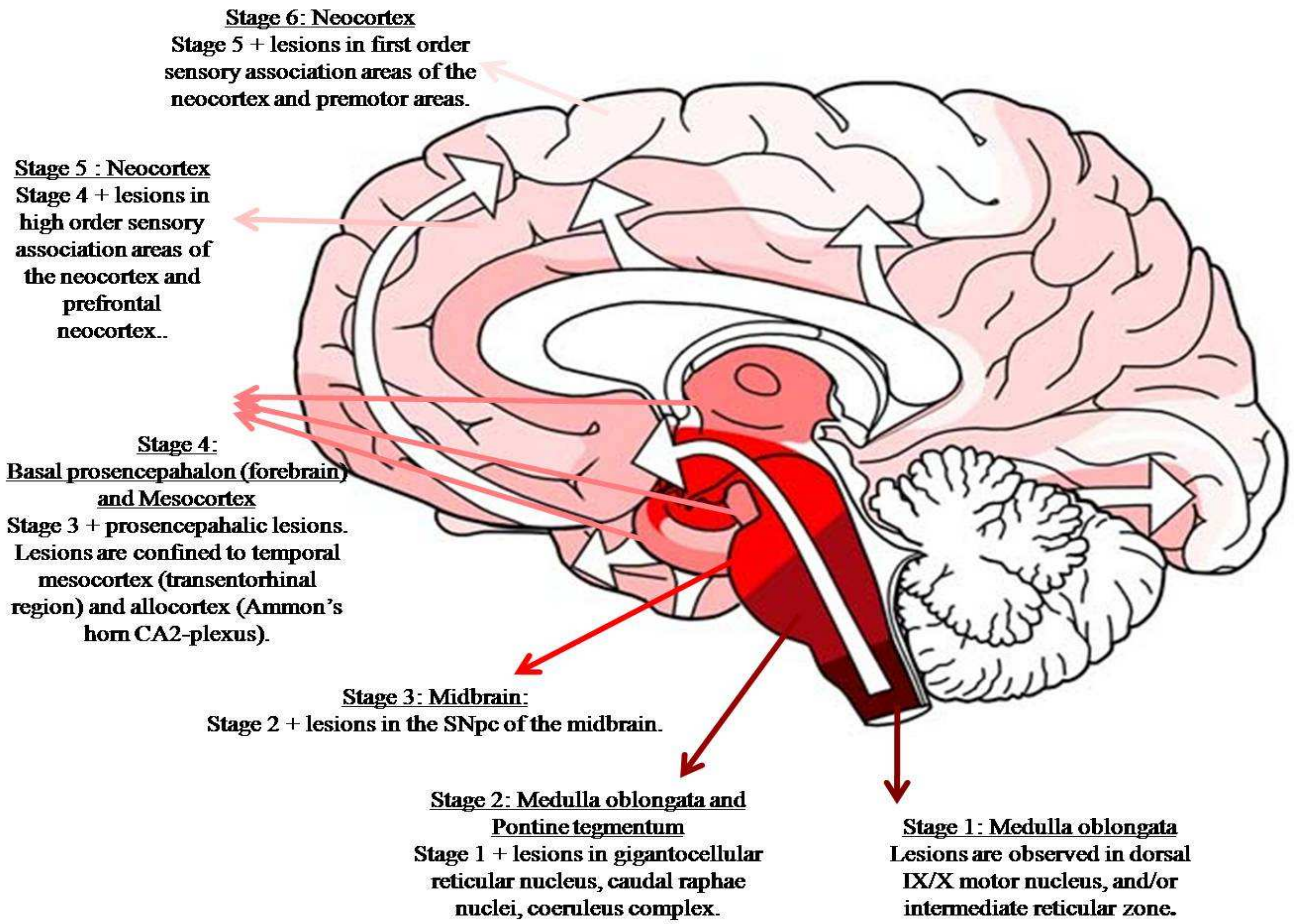

Figure 1.2: Braak staging related to PD pathology. The six stages of PD progression are illustrated. The thick white arrows identify the anatomical progression of LB pathology with medulla oblongata being the first to be affected followed by pontine tegmentum, midbrain and finally the neocortex. This image was adapted and modified from (Braak et al. 2003).

The Braak PD staging system has also been investigated in other disorders that are associated with LBs, and although the system fits most cases, there are exceptions. For example, the staging system does not have relevance to LBs that occur in Alzheimer's disease, where many of these inclusions are confined to the amygdala (Uchikado et al. 2006). LBs have also been demonstrated in brains of asymptomatic subjects, thought to represent the early disease stages and is known as incidental LB disease (Parkkinen et al. 2003). As a result, the dementia with Lewy bodies (DLB) Consortium proposed a new scheme for the pathologic assessment of LBs and LNs, taking into account both Lewy-related and Alzheimer-type pathology (McKeith et al. 2005). Under this scheme, the lesion density is graded semi-quantitatively, but the pattern of regional involvement is deemed more important than total LB count, and can be divided into predominantly brainstem (IX-X cranial nerve nucleus, LC and SN), transitional (nbM, amygdala, transentorhinal, cingulate gyrus) or diffuse neocortical pathology (temporal, frontal and parietal cortices). A probability of the clinical DLB syndrome can be assigned based on this assessment.

Figure 1.3: Staging of α-synuclein pathology according to the dementia with Lewy bodies (DLB) consortium. This image presents the grading criteria of LB pathology in cerebral cortex of DLB cases as defined by the DLB consortium. The LB pathology is scored as stages 1 to 4: Stage 1 = sparse LBs and LNs; Stage 2 = >1 LB per high power field and sparse LNs; Stage 3 = ≥4 LBs and scattered LNs in low power field; Stage 4 = numerous LBs and LNs. This image was obtained from (McKeith et al. 2005)**.**

1.3.5 PD pathology and autonomic symptoms

The involvement of non-motor autonomic symptoms has been suggested to predate the PD-associated motor symptoms by many years. Extensive LB pathology in PD subjects has been reported in the regions central to the autonomic functions, such as lower brainstem autonomic nuclei, hypothalamus, spinal cord and enteric plexus (Braak et al. 2006). The DMVN is involved in oesophageal motility, and the pathology of this nucleus has been suggested to lead to gastrointestinal dysfunctions, such as drooling, dysphagia (swallowing difficulties) and gastroesophageal reflux (Wolters & Braak 2006). Most PD patients also have an impaired sense of smell which has been attributed to severe degeneration of olfactory bulbs in PD patients (Del Tredici et al. 2002). Neuronal cell loss of serotonergic neurons of the dorsal raphè nuclei, and cholinergic neurons of the pedunculopontine tegmental nucleus are thought to be involved in the sleep disturbances associated with the PD phenotype (Jellinger 1999). Constipation and sexual dysfunction are the other autonomic symptoms that often precede the motor symptoms of PD, thereby supporting the notion that the PD pathology might begin in the peripheral nervous system, and not the central nervous system (Micieli et al. 2003).

1.3.6 Glial cell loss

Glial cells have been suggested to have varying degrees of involvement in PD pathology, and can be involved either by reacting to, or by directly being affected by the existing pathology (Croisier & Graeber 2006). Microglia and astrocytes are sensitive to changes in cellular environment, and can be activated upon reaction to toxins and pathological conditions, resulting in an immune response and inflammation. However, the role of inflammation (neuroprotective or toxic), and the little reactive astrocytosis observed in PD brains makes their role in the disease pathogenesis debatable (reviewed in (Teismann & Schulz 2004).

Although α-synuclein immunoreactivity in PD is mostly limited to the neuronal populations, instances of glia (oligodendroglia and astrocytes) immunoreactive for α-synuclein in midbrain, basal ganglia, cerebral cortex, cerebellum and spinal cord have

been described (Arai et al. 1999; Wakabayashi et al. 2000; Hishikawa et al. 2001). Fibrillary glial inclusions composed of α-synuclein, however, remain characteristic of multiple system atrophy (MSA). Therefore, the significance of glial pathology in PD is still unknown and requires further elucidation.

1.4 Basal ganglia circuitry

The progressive degeneration of the SN is associated with the DAergic denervation of the striatum. This positive correlation between dopamine deficiency in the striatum and nigral cell loss in PD patients led Hornykiewicz to describe PD as a 'striatal dopamine deficiency syndrome' (Hornykiewicz 2008). The loss of SN DAergic neurons that project towards the striatum results in a dopamine deficiency causing the earliest PD symptom in posterior putamen. As such, most symptomatic therapies are aimed at replacing dopamine.

There is no diagnostic laboratory test for PD, and the diagnosis relies on clinical features. Neuroimaging techniques such as positron emission tomography (PET) using fluorodopa ([^{18}F]-DOPA) are used to measure levodopa uptake into dopamine nerve terminals. In PD subjects a decline in striatal dopamine uptake of up to 5% per year can be observed (Fearnley & Lees 1991). Loss of dopamine causes a downstream dysfunction in the circuit anatomy of basal ganglia, resulting in the motor fluctuations observed in PD.

The basal ganglia encompasses the striatum (putamen and caudate), globus pallidus which contains external and internal segments (GPe and GPi, respectively), SN pars compacta and pars reticulata (SNpc and SNpr, respectively), and the subthalamic nucleus (STN) (see Figure 1.4a). Information from all parts of the cerebral cortex is received by the basal ganglia which projects back through frontal cortex via partially closed loops. The striatum and the STN are the two main entry points for receiving input for the basal ganglia.

The intrinsic circuitry of the basal ganglia is described as having two projection systems: a 'direct' pathway extending between striatum and GPi/SNpr, and an

‘indirect’ pathway with excitatory projections between striatum to GPe to STN. These pathways differ in their functionality as the corticostriatal afferents primarily act to facilitate or excite the ‘direct’ pathway, but inhibit the ‘indirect pathway’. In the direct pathway, cortical activity excites the inhibitory GABAergic neurons in striatum, leading to inhibition of GPi and SNpr, which in turn removes their tonic inhibition from the thalamus. In contrast, cortical activity that excites glutamatergic neurons in the striatum in the indirect pathway, performs an overall inhibition of the thalamus. It does this by using inhibitory GABAergic projections between striatum-GPe-STN, and excitatory (glutamatergic) between STN-GPi/SNpr (see Figure 1.4b).

Dopamine from the SN stimulates dopamine receptors, and modulates glutamatergic (excitatory) effects on corticostriatal inputs by exerting a dual effect on the striatal neurons: exciting D1 receptors in the direct pathway and inhibiting D2 receptors in the indirect pathway. Dopamine depletion in PD disrupts this fine corticostriatal balance leading to decreased activity in the direct circuit and an increased activity in the indirect circuit. The tonic inhibition on the thalamus needs to be removed for the purpose of voluntary movement. During PD, a lack of dopamine results in D1 receptors (in the direct pathway) not being able to exert their excitatory effect on striatum resulting in a removal of subsequent inhibition from GPi/STN. This means the tonic inhibition on the thalamus cannot be removed and the afferent signals are sent to the cortex for movement to continue. In the indirect pathway, a depletion of dopamine results in the D2 receptors not being able to exert an inhibition on the striatum which means the subsequent inhibition on the GPe and STN is removed, resulting in excitatory signals from STN increasing the inhibitory output from GPi/SNpr. Replacing dopamine in the form of its precursor levodopa (L-DOPA) addresses this imbalance and allows for basal ganglia to function normally. Although this is by no means a definitive cure, L-DOPA in combination with a dopa-decarboxylase inhibitor is an effective therapy that improves the quality and functional capacity of PD subjects (Lees et al. 2009).

(A) **(B)**

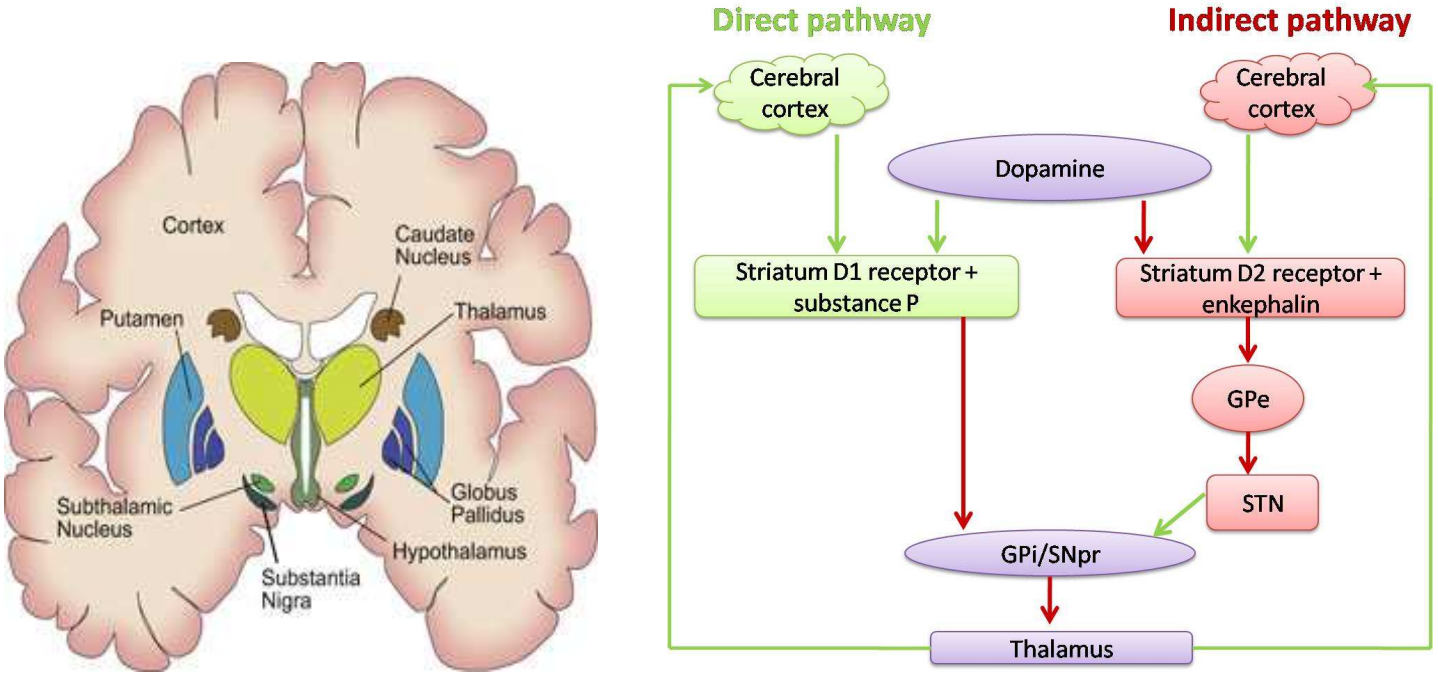

Figure 1.4: Basal ganglia components and circuitry. (A) Anatomical components that form the basal ganglia circuitry. The image was obtained from http://www.dana.org/uploadedImages/Images/Spotlight_Images/BW_JanFeb07_basal_ganglia_spot.jpg. (B) A simplified schematic of direct and indirect pathways of basal ganglia. Arrows in green show excitatory effect and in red show an inhibition. Dopamine serves to activate the direct pathway over the indirect pathway, and thus increase the signal to the thalamus by removing the inhibition from GPi/SNpr, whereas in the indirect pathway, the STN increases the tonic inhibition on thalamus via GPi/SNpr.

1.5 Disease Aetiology

1.5.1 Environmental factors

Up until the late 20th century, PD was thought to mainly result from environmental insults, and there is some clinical and epidemiological evidence that supports the notion of PD occurring as a result of a neuronal infection, for example, neuro-virulent strains of influenza A virus (Takahashi & Yamada 1999). The enteric system has been shown to be affected in the earlier stages of PD pathogenesis, leading the authors to speculate that a viral pathogen could infect the CNS via the postganglionic enteric neurons (Braak et al. 2003). A variety of other mechanisms, including inhibition of complex I of the mitochondrial respiratory chain, displacement of dopamine from vesicular stores, and formation of mitochondrial or cytosolic reactive oxygen species (ROS) have also been proposed as the means for harmful agents to exert their neurotoxic effects (Richardson et al. 2007). Cellular and animal models have been created to mimic parkinsonian symptoms following exposure to neurotoxins, thereby emphasising the role of environmental toxins in PD aetiology.

6-hydroxydopamine (6- OHDA) was one of the first neurotoxins to be isolated (Schober 2004). It was found to selectively degenerate catecholaminergic neurons, as a result of decreased mitochondrial complex I function and increased production of reactive oxygen species (ROS) (Betarbet et al. 2002). Another neurotoxin found to mimic parkinsonian symptoms in animal models is the 1-methyl-4-phenyl-1,2,3,6-tetrahydropyridine (MPTP). It was discovered in 1982, when a group of young heroin addicts were diagnosed with parkinsonian symptoms after injecting a synthetic drug, a major contaminate of which was the neurotoxin MPTP (Langston et al. 1983). MPTP has since been successfully used to develop cellular and animal models of PD. In the brain, MPTP crosses the blood brain barrier and is metabolised by monoamine oxidase B into 1-methyl-4-phenylpyridinium (MPP+), a potent mitochondrial complex I inhibitor. MPP+ displays a selective toxicity for DAergic neurons in SN, thereby replicating PD symptoms (Richardson et al. 2005). MPTP is now widely used to disrupt the nigrostriatal dopamine pathway in non-human primate models. Another

mitochondrial complex I inhibitor that successfully mimics PD symptoms and neuropathology in rodent animal models is the pesticide rotenone (Betarbet et al. 2002). Rotenone is administered systemically, and can inhibit mitochondrial complex I uniformly, as opposed to 6-OHDA and MPTP, both of which display a selectivity for catecholaminergic neurons. Despite the widespread mitochondrial complex I inhibition by rotenone, it results in degeneration of nigral-striatal DAergic neurons (Betarbet et al. 2002). The specific degeneration of these neurons by a wide range of neurotoxins that display complex I inhibition, and thus inhibit the respiratory chain suggests an important role for mitochondrial dysfunction in PD pathogenesis.

Exposure to agricultural products has also been suggested to increase sensitivity of DAergic neurons to toxins later in life (Richardson et al. 2006). Paraquat or 1,1'-dimethyl-4, 4'-bipyridinium is a herbicide that is structurally similar to MPP+ and crosses the blood brain barrier to cause degeneration of DAergic neurons, and cause locomotor dysfunction in mice (Brooks et al. 1999). Unlike MPTP or rotenone, paraquat does not require dopamine transporter nor does it inhibit mitochondrial complex I. Paraquat exerts its effects by oxidising the cytosolic form of thioredoxin and activating Jun N-terminal kinase (JNK), followed by caspase-3 activation, whereas MPTP and rotenone oxidize the mitochondrial form of thioredoxin and do not activate JNK-mitogen-activated protein kinase and caspase-3 (Ramachandiran et al. 2007). When administered together with manganese ethylenebisdithiocarbamate (maneb), a fungicide that enhances the neurotoxic effects of MPTP on locomotion in mice, a greater toxicity towards the nigral dopamine system was observed, than when either of them were administered individually to the rodent model (Thiruchelvam et al. 2000).

Apart from the ATP depletion, complex I inhibition can increase cellular levels of mitochondrial reactive oxygen species (ROS) (Adam-Vizi 2005). Increase in ROS production and subsequent respiratory inhibition, leading to oxidative stress has been suggested as a possible mechanism for nigral cell death (Kushnareva et al. 2002). The relevance of PD models (cellular and animal) that recapitulate PD symptoms resultant from mitochondrial dysfunction was further emphasised by the identification of point

mutations in mitochondrial transfer RNA (tRNA) genes in the SN of PD cases (neuropathologically confirmed) (Kösel et al. 1998; Grasbon-Frodl et al. 1999). The knowledge obtained from these PD models is instrumental in understanding the impact of oxidative stress and complex I inhibition on mitochondrial dysfunction, and is fast becoming a major contribution to the explanation of PD pathogenesis.

1.5.2 Genetics of PD

Identification of PD causing toxins and the low concordance rate in monozygotic and dizygotic twin studies perpetuated the idea that PD was not caused by genetic elements. However, PET studies utilising F-DOPA uptake have shown reduced levels of striatal dopamine in unaffected twins and relatives of PD patients when compared to controls, suggesting a familial component to PD aetiology (Brooks 1991). Moreover, in the last two decades several genes linked to familial PD have been reported. Linkage mapping using positional cloning in large kindreds or autozygosity mapping in small families have been used to identify dominant and recessive genes for PD, respectively. These mendelian genes have collectively come to be known as the PARK loci.

Many genes associated with PD have also been identified by candidate gene association studies and are continuously being updated at PD Gene (http://www.pdgene.org). Majority of these genes were investigated either due to their functional relevance in a mechanistic pathway, or for their role in other diseases that displayed parkinsonian symptoms. Investigations into recessive disorders such as Gaucher's disease, or diseases with LBs but complex phenotypes such as Neimann-Pick Type C (NPC), infantile neuroaxonal dystrophy (INAD) and neurodegeneration with brain iron accumulation (NBIA) have provided many new candidates for PD research (Hardy et al. 2009).

Locus	Chromosome	Gene	Mode of inheritance and phenotype
PARK1	4q21-q23	***SNCA***	AD, Mid-late with DLB features
PARK2	6q25.2-q27	***PRKN***	AR, EO, slow progression, no LBs
PARK3	2p13	**Unknown**	AD, Classic PD with LBs
PARK4	4q21	***SNCA*** **(triplication)**	AD, EO with DLB features
PARK5	4q14	***UCH-L1***	Unclear transmission, Classic PD
PARK6	1p35-p36	***PINK1***	AR, EO, slow progression with LBs
PARK7	1p36	***DJ1***	AR, EO, slow progression
PARK8	12p11.2-q13.1	***LRRK2***	AD, Classic PD with heterogenous pathology
PARK9	1p36	***ATP13A2***	AR, Atypical -Kufor-Rakeb syndrome
PARK10	1p32	**Unknown**	Unclear transmission, Classic PD
PARK11	2q36-q37	***GIGYF2***	AD, Classic PD
PARK12	Xq21-q25	**Unknown**	Classic PD
PARK13	2p12	***HTRA2/OMI***	Classic PD
PARK14	22q13.1	***PLAG26***	AR, parkinsonism-dystonia phenotype, NBIA-type2, with LBs
PARK15	22q12-q13	***FBXO7***	AR, parkinsonian pallidal syndrome
-	17q21.1	***MAPT***	Frontotemporal dementia with parkinsonism linked to chromosome- 17.
-	1q21	***GBA***	Parkinsonism with LBs
-	5q23.1-q23.3	***Synphilin-1***	Classic PD
-	2q22-q23	***NR4A2/Nurr1***	Classic PD

Table 1.1: Autosomal dominant and recessive genes linked to PD. This table describes the familial PARK loci (1-15), and genes shown to be associated to PD in non-familial forms. AD: autosomal dominant, AR: autosomal recessive, EO: early onset, LB: Lewy body. Classic PD refers to the late- onset clinical IPD phenotype unless otherwise stated.

1.5.2.1 PARK loci and familial PD

1.5.2.1.1 PARK 1/4 (*SNCA*)

A genome wide linkage analysis mapped an Italian family (Contrusi kindred) with autosomal dominant form of PD, to a locus on chromosome 4q21 (PARK1) in 1996 (Polymeropoulos et al. 1996). This locus contained *SNCA*, which became the first gene to be implicated in familial PD (FPD). The *SNCA* gene spans 117 kb and contains 6 exons that encode for a 140 amino acid protein known as α-synuclein. Three missense mutations, A53T, A30P and G46L were identified in the original Italian (Contrusi kindred), German and Spanish families, respectively (Polymeropoulos et al. 1997; Krüger et al. 1998; Zarranz et al. 2004). The protein encoded by this locus (α-synuclein) was also demonstrated as a principal component of the LBs (Spillantini et al. 1997; Spillantini et al. 1998).

Various studies have reported multiplications of the wild-type *SNCA* locus in families with parkinsonism. Initially, designated the PARK4 locus, duplications of the *SNCA* gene have been reported in two French (Chartier-Harlin et al. 2004; Ibáñez et al. 2004a), an Italian, a Swedish (Fuchs et al. 2007), and two Japanese (Nishioka et al. 2006) families. *SNCA* triplications have also been identified in American (Singleton et al. 2003) and Swedish-American kindreds (Farrer et al. 2004). However, screening of large cohorts of patients has suggested that missense mutations and multiplications of the wild-type *SNCA* are a rare cause of parkinsonism (Hope et al. 2004; Johnson et al. 2004; Lockhart et al. 2004).

The clinical phenotype resulting from a duplication of the wild-type gene has a mid-late onset with a slow progression that is clinically similar to IPD (Chartier-Harlin et al. 2004; Ibáñez et al. 2004a; Nishioka et al. 2006). In contrast, *SNCA* triplications result in an earlier age of onset with a faster progression, and a more severe presentation of the phenotype that includes dementia, autonomic dysfunction, and a reduced lifespan (although this varies in different cases) (Singleton et al. 2003; Farrer et al. 2004; Fuchs et al. 2007). This pathologic gain of function demonstrates the importance of a critical dosage of the *SNCA* locus, and how alterations in the gene

copy number can impact on the severity of the clinical phenotype. The role of SNCA mRNA upregulation was further supported by the identification of NACP-Rep1 polymorphism in the promoter region of the *SNCA* gene. Consistently, identified as a risk factor in various populations, an *in-vitro* increase in transcription is associated with the risk allele of NACP-Rep1 (Chiba-Falek & Nussbaum 2001; Maraganore et al. 2006). Therefore, the importance of gene dosage effects of *SNCA* can be observed in both the familial and idiopathic forms of PD.

The physiological role of α-synuclein remains unclear but it has been implicated in synaptic plasticity, vesicle recycling, chaperone mechanisms, storage and regulation of neurotransmitters (Schiesling et al. 2008). As mentioned previously, wild-type α-synuclein has been identified as the principal component of LBs and LNs, and as such plays a crucial role in PD. Phosphorylation of wild-type α-synuclein results in increased oligomerisation and eventual accumulation as the major insoluble fibrillar component of the LBs (Goldberg & Lansbury 2000). An overexpression model using *Drosophila melanogaster* showed an adult-loss of DAergic neurons, α-synuclein positive intraneuronal inclusions and a loss of locomotor activity (Feany & Bender 2000). Whether aggregation of wild-type α-synuclein or toxic oligomeric intermediates cause cell death is debatable, but the processes leading to the fibrillisation of the protein seems to form a strong link to the pathology.

1.5.2.1.2 PARK2 (*PRKN)*

A locus mapping to chromosome 6q25.2-27, designated PARK2 was linked to autosomal recessive forms of juvenile parkinsonism (AR-JP), with a typical age of onset of 40 years of age (Matsumine et al. 1997). The causative gene was later identified as parkin (*PRKN*), and shown to contain 12 exons that span 1.53 Mb and encode a 465 amino acid (52 kDa) protein (Kitada et al. 1998).

Homozygous deletions of exons 1 and 5 were identified in Japanese families with AR-JP (Kitada et al. 1998), and deletion of exons 5, 6 and 7 were also confirmed in a two individuals from a Greek pedigree with early onset parkinsonism (Leroy et al. 1998a). Since then a multitude of mutations in *PRKN* including deletions, exon

multiplications, point and frameshift mutations have been identified as a cause for early onset parkinsonism (<50 years of age) (reviewed in (Schiesling et al. 2008)). *PRKN* mutation carriers display typical signs of IPD with a slower progression of the disease, a more symmetric onset, and dystonia as a possible initial sign (Lohmann et al. 2003). To date over 100 mutations in early onset PD cases (< 45 years of age) have been identified in *PRKN*, accounting for about 50% of familial and 20% of PD cases with no family history (Abbas et al. 1999; Lücking et al. 2000). Heterozygous mutations in *PRKN* have been shown to be present at a similar frequency in PD patients and controls (Lincoln et al. 2003; Kay et al. 2007). However, functional brain imaging studies have shown alterations of nigrostriatal DAergic projections in asymptomatic heterozygous *PRKN* mutation carriers, leading to suggestions that heterozygosity might constitute a risk factor by causing haploinsufficiency of the *PRKN* gene in PD (Hilker et al. 2001).

Parkin is an ubiquitin E3 ligase that is responsible for the addition of ubiquitin to specific substrates which are then targeted for degradation by the proteasome in the ubiquitin protease system (UPS). *PRKN* mutations lead to a loss of ligase function which affects the ubiquitination and degradation of the protein, thereby strengthening the hypothesis that protein degradation and aggregation might play a central role in PD pathogenesis (Shimura et al. 2000). Post-mortem analysis of *PRKN* brains report a typical neuron loss in SN, but LBs are rarely observed in the brains of *PRKN* mutation carriers (Farrer et al. 2001), however, parkin has been shown to be a component of LBs in PD and DLB brains (Schlossmacher et al. 2002).

1.5.2.1.3 PARK3

The third PARK locus was mapped to chromosome 2p13 in 1998, and indicates association with autosomal dominant PD with a late onset and a pathological phenotype that includes LBs (Gasser et al. 1998). Many genes in this region have been excluded as potential candidates, although polymorphisms in the sepiapterin reductase gene in the PARK3 region have been suggested to modulate the onset or risk of PD (Sharma et al. 2006).

1.5.2.1.4 PARK5 (*UCH-L1*)

The locus for PARK5 was mapped onto chromosome 4p14, and the gene linked to FPD was identified as the multifunctional ubiquitin C-terminal hydrolase 1 (*UCH-L1*), and a single missense mutation (I93M) was reported in affected siblings from a German kindred, presenting typical PD symptoms (Leroy et al. 1998b). *UCH-L1* produces a neuron-specific enzyme that is part of the UPS pathway. Biochemical studies reveal a dual role for UCH-L1 protein; as a ubiquitin hydrolase and also as an E3 ligase. *In-vitro* studies have demonstrated how UCH-L1 uses these two opposing enzymatic activities to exert its influence on α-synuclein degradation (Liu et al. 2002).

UCH-L1 has also been shown to be present in LBs of IPD brains (Lowe et al. 1990). Only a single neuropathology report has been presented on I93M mutation carriers, describing LBs in the affected regions, and also demonstrating co-localisation of UCH-L1 with α-synuclein in cortical LBs (reviewed in (Schiesling et al. 2008). This mutation has not been found in other PD families, thereby leading some to challenge the credibility of *UCH-L1* gene as a PARK locus.

1.5.2.1.5 PARK6 (*PINK1*)

The PARK6 locus was mapped to chromosome 1p35-p36 in a large Sicilian family known as the 'Marsala kindred' with autosomal recessive PD, clinically characterised by an early age of onset (32-48 years), and exhibiting a typical parkinsonism phenotype (Valente et al. 2001). Identified as the PTEN-induced putative kinase 1 (*PINK1*), the gene spans 18 kb, and the 8 exons encode a 581 amino acid protein (63 kDa) (Valente et al. 2004). Mutations in *PINK1* account for 1-7% of early onset PD cases (depending on the ethnicity), and are therefore regarded as the second most common cause of early-onset PD (Tan et al. 2006).

PINK1 variants result in a loss-of function, and include point mutations as well as insertions and deletions that lead to frameshift and subsequent truncation of the protein. Typically associated with a recessive transmission, a homozygous mutation (W437X) in the *PINK1* gene has also been shown to be associated with autosomal

dominant parkinsonism (Criscuolo et al. 2006). Heterozygous *PINK1* mutations have been shown to be more frequent in IPD patients compared with controls, and have been suggested to act as a risk for developing PD via haploinsufficiency or even a dominant-negative effect (Abou-Sleiman et al. 2006). Brain imaging studies performed on asymptomatic heterozygous carrier of *PINK1* mutations identified reduced striatal F-DOPA uptake in PET studies, lending support to haploinsufficiency contributing to pathogenic influences in PD (Khan et al. 2002).

PINK1 is a protein kinase that has been shown to have a neuroprotective effect by phosphorylating specific mitochondrial proteins (modulating their function), and loss of PINK1 function can be rescued by parkin (Clark IE et al. 2006; Park et al. 2006; Yang et al. 2006; Exner et al. 2007). Post-mortem analysis of *PINK1* carriers present typical features of IPD with neuronal loss and LB inclusions in affected areas, and the protein has been shown to be immunoreactive in a proportion of LBs in PD and DLB (Gandhi et al. 2006; Murakami et al. 2007). The heterozygous nature of the mutations, however, makes it difficult to determine whether mutant or wild-type PINK1, or both forms accumulate in the neuronal inclusions.

1.5.2.1.6 PARK7 (*DJ-1*)

The PARK7 locus was mapped to chromosome 1p36 in a Dutch family who presented with an autosomal recessive form of PD (van Duijn et al. 2001). The candidate for this locus was identified as the oncogene, *DJ-1*, which spans 24 kb and contains 8 exons that produce a 189 amino acid (20 kDa) protein (Bonifati et al. 2003a). Patients with mutations in *DJ-1* show typical PD symptoms, plus dystonic features and/or psychiatric signs (van Duijn et al. 2001).

The first mutations identified were a large homozygous chromosomal deletion of 14 kb in the Dutch kindred, and a homozygous point mutation in an Italian family (Bonifati et al. 2003b). Although additional mutations in *DJ-1* have been identified, they remain a rare cause of early-onset PD (<1%) (reviewed in (Schiesling et al. 2008)). A decreased F-DOPA uptake in patients with homozygous *DJ-1* deletions was reported, but asymptomatic individuals with heterozygous mutations showed no

alterations in F-DOPA PET imaging (Dekker et al. 2004). Even though *DJ-1* mutation carriers show an early-onset phenotype comparable to *PINK1* and *PRKN* mediated PD, an unremarkable F-DOPA metabolism in asymptomatic heterozygous *DJ-1* carriers is in stark contrast to the other two recessive genes.

DJ-1 controls gene transcription and stability of mRNA regulation (Bonifati et al. 2003), and is thought to have neuroprotective effects by acting as an oxidative stress sensor within cells (Taira et al. 2004). Histopathological studies relating to the brains of *DJ-1* mutation carriers have not been reported, but it has been shown to have a mainly astrocytic expression in the brain with higher levels in subcortical areas that are affected in PD (Bonifati et al. 2003; Bandopadhyay et al. 2004). DJ-1 is not a component of LBs and LNs, but it has been identified in glial-positive inclusions and tangles associated with tauopathies such as Pick's disease, progressive supranuclear palsy (PSP), corticobasal degeneration (CBD) and Alzheimer's disease (Rizzu et al. 2004).

1.5.2.1.7 PARK8 (*LRRK2*)

The PARK8 locus was originally identified in 2002 in a large Japanese family known as the Sagamihara kindred, after the area in which the family resides (Funayama et al. 2002). The affected members in the family presented with autosomal dominant parkinsonism that responded to levodopa. A genome-wide linkage analysis revealed a novel locus for FPD on chromosome 12p11.2-q13.1. Further analysis identified a disease associated haplotype shared by the affected and unaffected members of the family, suggesting a low disease penetrance. Linkage to the PARK8 locus was also identified in European families (German Canadian and Nebraskan) (Zimprich et al. 2004a), thereby further highlighting its importance as a monogenic cause of PD across different populations. PARK8 linked parkinsonism displays a wide spectrum of clinical and pathological phenotypes. The Sagamihara kindred showed no dementia and pure nigral degeneration with no LB pathology whereas the European families reported by Zimprich and colleagues were clinically heterogenous and presented with signs of dementia, PSP, or motor-neuron degeneration (Funayama et

al. 2002; Zimprich et al. 2004a; Wszolek et al. 2004). These European subjects were found to have tau and α-synuclein pathology (Wszolek et al. 2004)

The gene responsible for PARK8 linked PD was identified as Leucine rich repeat kinase 2 (*LRRK2*) by two independent groups in 2004 (Paisán-Ruíz et al. 2004; Zimprich et al. 2004b). *LRRK2* spans 144 kb and contains 51 exons that encode a >250 kDa protein. Paisan-Ruiz and colleagues (2004) identified missense mutations, Y1654C and R1396G in *LRRK2* gene in British and Spanish families, respectively. Since a number of families identified by them were of a Basque origin, they named the gene product dardarin from the Basque word *dardara* meaning tremor. Zimprich and colleagues also identified a total of four mis-sense (Y1699C; R1441C; I1122V and I2020T) and one putative splice site (L1114L) mutation in the families that they initially identified the PARK8 linkage in. Over 50 variants have since been identified in *LRRK2*, many of which are regarded as pathogenic (see (Schiesling et al. 2008; Lesage & Brice 2009) for review). However, the G2019S mutation identified in exon 41 of *LRRK2*, has come to be regarded as the most common genetic cause of PD in Europeans, North African Berbers and Ashkenazi Jewish populations (Ozelius et al. 2006; Lesage et al. 2006; Healy et al. 2008).

An interesting feature of the *LRRK2* mutations is the pleiomorphic pathology they display. The *LRRK2* linked pathology can include not only classic nigral degeneration with or without LB pathology, but also pathologies associated with Alzheimer's disease, multiple system atrophy (MSA), or PSP (Wszolek et al. 2004; Miklossy et al. 2006; Ross et al. 2006). Both G2019S and I2020T mutations occur in adjacent codons in the conserved activation loop of the kinase catalytic domain, and cause a dominant gain-of function effect which increases the protein's kinase activity *in vitro* (West et al. 2005; Gloeckner et al. 2006; Greggio et al. 2006). However, they display different pathological phenotypes. The I2020T mutation in the original Sagamihara kindred presents pure nigral degeneration without α-synuclein positive inclusions (Funayama et al. 2005), whereas G2019S mutation exhibits classical IPD pathology which includes selective degeneration of SN and LC neurons accompanied with α-synuclein positive LBs in the brainstem and limbic cortex (Ross et al. 2006). Ross

and colleagues (2006) also reported that G2019S mutation carriers can occasionally contain NFTs in addition to extensive LB pathology in the amygdala. However, an isolated case with G2019S linked PD has been reported to have nigral degeneration with no pathological inclusions (Gaig et al. 2007). The mutations R1441C and Y1699C also display neuronal loss and gliosis in SN, and R1441C carriers present classic α -synuclein pathology with LBs localised either just to the brainstem or a more widespread LB and LN pathology pattern (Zimprich et al. 2004b). Tau immunoreactive neuronal and glial lesions reminiscent of PSP pathology was observed in Y1699C mutation carriers who displayed signs of dementia. The I1371V mutation, on the other hand, shows ubiquitin as well as α-synuclein positive LB pathology (Giordana et al. 2007). A case of the basque R1441G *LRRK2* mutation has been shown to have mild neuronal loss without α-synuclein, tau, LRRK2, or ubiquitin cytoplasmic inclusions (Martí-Massó et al. 2009). LRRK2 is a large and a complex multidomain protein that functions as a kinase, acts as a mediator in synaptic endocytosis, plays a role in the maintenance of neuronal viability and possibly functions as a scaffolding protein for cell signalling pathways, thereby suggesting that LRRK2 might be an important physiological protein with a central role to play in a variety of neurodegenerative diseases (Greggio & Cookson 2009).

1.5.2.1.8 PARK9 (*ATP13A2*)

Initially described in a Jordanian family, Kufor-Rakeb syndrome (KRS) is a rare form of recessively inherited, juvenile onset parkinsonism with additional symptoms including pyramidal degeneration, upward gaze palsy, spasticity and dementia (al-Din et al. 1994). The PARK9 locus linked to KRS was mapped to chromosome 1p36 (Hampshire et al. 2001). Identification of compound heterozygous deletion and splice site mutation in affected members of a large Chilean family resulted in the candidate gene being identified as ATPase Type 13A2 (*ATP13A2*) which spans 29 kb and encodes 29 exons (Ramirez et al. 2006). The same research group also identified a 22 bp homozygous duplication in the original Jordanian family to whom the locus was originally linked to. It has been suggested that the aggregation of the mutant protein in the endoplasmic reticulum causes proteasomal or lysosomal dysfunction (Ramirez

et al. 2006). Other variants in the gene, both heterozygous and homozygous have been reported to be associated with early-onset parkinsonism in Brazil and Italy (Di Fonzo et al. 2007). A knockdown of the *ATP13A2* ortholog in *Caenorhabditis elegans* enhances α-synuclein misfolding, and the yeast ortholog of *ATP13A2* has also been shown to protect cells from manganese toxicity, thereby revealing an interaction between PD genetics and environmental risk factors (Gitler et al. 2009). So far nothing has been reported on the histopathology associated with mutations in this gene.

1.5.2.1.9 PARK10

A genomic screen investigating the influence of age of onset on PD found significant linkage to chromosome 1 (Li et al. 2002). Designated PARK10, this locus was mapped to chromosome 1p32 in an Icelandic IPD population with late-onset using genome wide linkage analysis (Hicks et al. 2002). Various genes have been suggested as possible candidates with the strongest association being observed in the *CDCP2* gene (Maraganore et al. 2005). However, this association remains to be confirmed.

1.5.2.1.10 PARK11

The autosomal dominant model of disease transmission associated with the PARK11 locus was confirmed in a large number of families mapping to chromosome 2q36-q37 (Pankratz et al. 2003; Maraganore et al. 2005). Heterozygous mutations have suggested that Grb10-Interacting GYF Protein-2 (*GIGYF2*) gene might be a possible candidate for the PARK11 locus (Lautier et al. 2008). However, the presence of *GIGYF2* mutation (N457T) in neurologically normal controls, and a lack of genotypic and haplotypic association (Sutherland et al. 2009a) suggests that this gene is not strongly related to the development of PD.

1.5.2.1.11 PARK12

This FPD locus was mapped to chromosome Xq21-q25 (Pankratz et al. 2002; Hicks et al. 2002), but a candidate gene(s) has not yet been identified.

1.5.2.1.12 PARK13 (*HTRA2/OMI*)

The candidate gene for the PARK13 locus is located within the PARK3 linkage locus, and was mapped to 2p12-2p13 (Gray et al. 2000; Faccio et al. 2000). Mutational screening of *HTRA2/OMI* in German patients with PD identified novel heterozygous mutations in this 3.8 kb gene (Strauss et al. 2005). The novel variants identified in the German case-control cohort by Strauss and colleagues (2005) interfere with the serine protease activity of the protein, and were shown to induce mitochondrial dysfunction *in-vitro*. The protein has been detected in LBs (Strauss et al. 2005), and has been shown to be phosphorylated by PINK1 (Plun-Favreau et al. 2007). This led the authors to hypothesise that mitochondrial dysfunction plays an important role in neurodegeneration observed in a fraction of PD patients.

1.5.2.1.13 PARK14 (*PLA2G6)*

Mutations in phospholipase A2 (*PLA2G6*) on chromosome 22q13.1 are associated with INAD and NBIA-type 2 in unrelated consanguineous families (Morgan et al. 2006; Khateeb et al. 2006; Gregory et al. 2008). Linkage analysis in adult-onset levodopa-responsive dystonia-parkinsonism with pyramidal signs and cognitive/ psychiatric features (but no iron in basal ganglia) identified *PLA2G6* as the candidate (Paisan-Ruiz et al. 2009). The mutation R632W in *PLA2G6* was shown to segregate with disease in a consanguineous Iranian dystonia-parkinsonism pedigree (Sina et al. 2009). This gene is now referred to as PARK14 (Hardy et al. 2009).

1.5.2.1.14 PARK15 (*FBXO7*)

A genome wide linkage analysis on a large Iranian pedigree affected with autosomal recessive, early-onset parkinsonian-pyramidal syndrome (PPS) showed linkage to chromosome 22 which was designated the PARK15 locus. Subsequent candidate gene screening revealed a disease-associated homozygous variation (R378G) in F-Box only protein 7 (*FBXO7*), thought to have a role in the UPS degradation pathway (Shojaee et al. 2008). Mutations in *FBXO7* have also been found in Italian and Dutch families, all of which display a complex PPS phenotype similar to *ATP13A2* and *PLA2G6* families (Hardy et al. 2009).

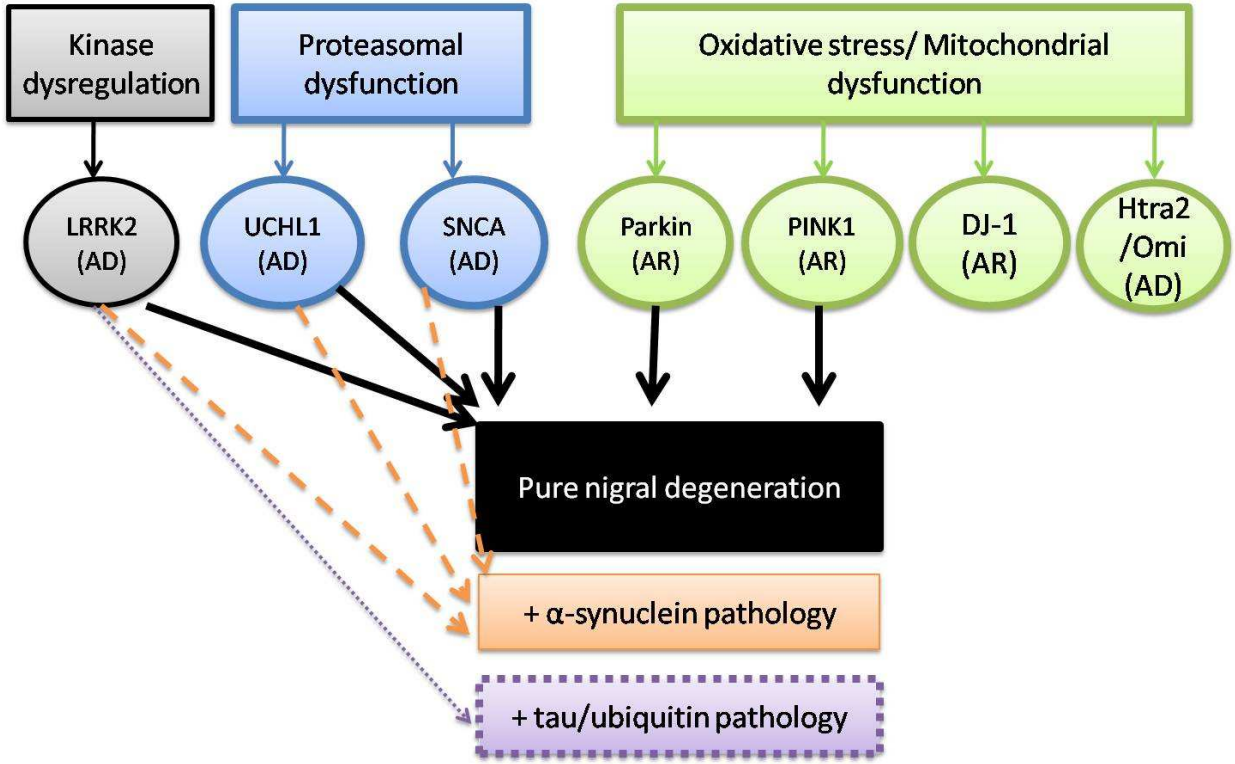

Figure 1.5: A schematic view of the pathology associated with the familial PARK loci. The major molecular mechanisms involved in PD, have been determined from *in-vitro* and *in-vivo* studies of the proteins encoded by mutant genes implicated in PD. Histopathological findings associated with mutations in PARK genes are indicated. *LRRK2* mutations exhibit the most heterogenous pathology. Neuropathological findings have not yet been reported for *DJ-1* and *Htra2/Omi* mutations and *PRKN* mutation carriers are usually negative for LB pathology. α-synuclein pathology has been reported for rare cases with *PINK1* mutations. AD= autosomal dominant, AR= autosomal recessive.

1.5.2.2 Common genetic variation in PD

Genetic variation acting as a susceptibility factor forms the basis of the common disease –common variant (CD-CV) hypothesis. Since the identification of the first mendelian PD gene, many studies have focused on the basic tenets of the CD-CV hypothesis in order to identify common genetic variants within the population (>1%) that may lead to an increased risk rather than directly cause PD. The completion of the 'International Haplotype Map (HapMap) project', and current technological advances have allowed researchers to test genomic variation at a much larger scale than was previously afforded by traditional candidate gene association studies. The high-throughput ability of genome wide association (GWA) studies is now frequently used to assess the contributions of common variants in the mechanistic foundations of the disease. Data from GWA studies can be used not only to identify novel risk loci that might be potential interactors of the established PARK loci, but also to discover novel pathways in the disease pathogenesis.

The first GWA PD study was used to screen ~200,000 SNPs in a cohort of discordant sib-pairs (Maraganore et al. 2005). To assess the influence of 3,035 SNPs identified in these sib-pairs, the group replicated the study in an unrelated patient-control series along with hypothesis-based SNPs previously selected for PD loci. Combined results from both the cohorts, nominated a small number of SNPs in various genes as being significantly associated with PD. The second PD GWA study produced around 220 million genotypes in a case-control cohort of over 500 individuals (Fung et al. 2006a). This information was publicly released with the premise that future researchers could mine these data to identify genetic variability that poses a mild or moderate risk of PD. The initial GWA studies reported many susceptible loci for PD, but the marker densities, sample sizes, and population substructures could have contributed to the data not being replicable. The ever increasing precision of the microarray technology with higher SNP density and superior data mining techniques have resulted in better consistency across GWA studies. Replication for a SNP identified by Maraganore and colleagues in the *Phactr2* gene was recently reported in a GWA study comprising IPD samples in populations from US, Canada and Ireland

but not in Norway (Wider et al. 2009). This emphasizes how important it is to have an accurate and a standardised interpretation of GWA studies, as an inaccurate analysis could not only produce false positives but also result in true positives being missed in the vast amount of data generated by these platforms.

Prior to the arrival of GWA studies, case-control associations focused on specific candidate genes. Conflicting results and a lack of replication are frequently reported as an observation of these studies. Nevertheless, this approach has been highly influential in establishing the basis of identifying common genetic variation that could alter the risk of PD in PARK and other loci. Variants in the promoter of *SNCA* have consistently been shown to be associated with increased expression and risk of PD, especially the dinucleotide repeat polymorphism, NACP-Rep1 allele (Maraganore et al. 2006). Associations have been reported in the 3'block around exons 5 and 6 of the *SNCA* gene (Mueller et al. 2005). Multiple SNPs in *SNCA* were identified as risk factors in a case-control cohort from Japan (Mizuta et al. 2006). The high level of linkage disequilibrium (LD) in the *SNCA* gene has been suggested to be one of the causes for multiple risk factors identified in this locus. Regardless of this, the consistent association of *SNCA* variants with PD risk suggests that there are functional variant(s) that act as risk modifiers. For example, a meta-analysis confirmed that the allele size of NACP-Rep1 is a susceptibility factor that acts by altering *SNCA* mRNA expression levels (Maraganore et al. 2006), and a 3' SNP (rs356219) is reportedly associated with *SNCA* mRNA levels in SN and cerebellum (Fuchs et al. 2008). Recent GWA studies have consistently shown that common variants in *SNCA* are associated with both the familial and idiopathic forms of PD (Pankratz et al. 2009; Sutherland et al. 2009b).

Case-control association studies for the mis-sense polymorphism Ser18Tyr (Lincoln et al. 1999) in the *UCH-L1* gene showed a reduced risk for IPD with this variant (Maraganore et al. 1999). The 50% frequency of this variant in Japanese and Chinese (Satoh & Kuroda 2001; Toda et al. 2003), and a meta-analysis of published studies further suggested a positive association for a protective risk in IPD. This association has been refuted by other studies, although a recent GWA study reported an

association with a different SNP (rs10517002) in *UCH-L1* and IPD subjects (Sutherland et al. 2009b).

Certain genetic variants in *LRRK2* gene have provided the strongest evidence that common genetic variation within the general population leads to an increased risk of PD. Both G2019S and G2385R mutations have been observed in a number of PD patients, although the association remains ethnicity dependent. On the basis of data from 24 different populations, the International *LRRK2* Consortium concluded that G2019S related PD was a common cause of PD (familial and idiopathic) in European and certain Middle-Eastern populations (up to 40%) (Healy et al. 2008). In contrast, the G2385R variant is more prevalent in the far Eastern populations, and has been associated with an increased risk for developing PD in several independent Chinese (Singapore/Taiwan), Japanese and Korean populations (Tan et al. 2007a). The variant G2385R is not found in Europeans (Berg et al. 2005; Di Fonzo et al. 2006), and is also not common in Indians or Malays (Tan et al. 2007b). This highlights the importance of sample group choice in association studies. The variant R1682P has also been identified as a risk factor in certain Chinese populations (Tan et al. 2008; Ross et al. 2008), and an intronic SNP has also been shown to be reportedly associated in a Singaporean IPD cohort (Skipper et al. 2005). Apart from a strong association for G2019S mutation, *LRRK2* association studies have not always yielded positive results for European IPD cases (Biskup et al. 2005; Paisán-Ruíz et al. 2005), but an association has been reported for the SNP rs2723264 and PD in a Greek population (Paisán-Ruíz et al. 2006). A tSNP correlated to rs2723264 was recently shown to have a modest association with PD samples in an Australian cohort. The same group also identified modest associations to two other SNPs (rs10784486 and rs10878405) and IPD (Sutherland et al. 2009b). However, no associations for *LRRK2* were observed in a GWA study for familial PD samples (Pankratz et al. 2009).

It has been suggested that young onset-PD cases might have a stronger genetic component (Tanner et al. 1999). Despite this, there is only limited information on association between common variants in recessive PARK loci and PD, although pathogenic mutations have been identified. A polymorphism in the promoter of

PRKN gene (-28 T/G) has been shown to be a risk factor for IPD affecting the age of onset (West et al. 2002; Sutherland et al. 2007), but similar findings were not observed for other SNPs in the *PRKN* promoter (Mata et al. 2002; Ross et al. 2007). In familial PD samples, Maraganore and colleagues demonstrated common variation in *DJ-1* as being associated with PD risk in related females, but not as a risk factor for overall PD (Maraganore et al. 2004). However, GWA studies have not identified any strong associations for common genetic variation in the recessive genes (*PRKN*, *PINK1* and *DJ-1)* and PD.

The susceptibility risk for PD is not limited to the familial PARK loci and includes various other genes, some of which are associated with a parkinsonism plus phenotype. Like the NACP-Rep1 allele for *SNCA*, a consistent association is reported for the common microtubule associated protein tau (*MAPT*) H1 haplotype for an increased risk for familial and idiopathic PD (Skipper et al. 2004; Healy et al. 2004; Zhang et al. 2005; Tobin et al. 2008). Mutations in *MAPT* were originally identified in rare families with autosomal dominant frontotemporal dementia linked to chromosome 17 with parkinsonism (FTDP-17), and linkage of PD to *MAPT* was initially reported in 2001 (Hutton et al. 1998; Scott et al. 2001). Aggregation of tau is a pathological hallmark for several neurodegenerative disorders collectively known as tauopathies, and Alzheimer's disease is the most common example. Tau pathology also underlies several diseases with parkinsonian features, such as PSP, CBD and FTDP-17. The *MAPT* locus is comprised of two extended LD blocks, designated H1 and H2, and associations for the common H1 haplotype have been reported for the parkinsonian disorder PSP (Baker et al. 1999; Pittman et al. 2005). The region around *MAPT* has a complex linkage disequilibrium (LD) structure, and this has led to the suggestions that multiple susceptible genes (or alleles) could be present in this large LD block. For example, allele Q of saitohin gene which is contained in intron 9 of the *MAPT* gene is in complete LD with H1 clade (Levecque et al. 2004). There is evidence that the complex genomic region around *MAPT* H1 clade acts as a susceptibility factor in PD risk, and a fine mapping of a large number of cases would identify the functional variant(s) modulating this risk (Zabetian et al. 2007).

Homozygous mutations in glucocerebrosidase (*GBA*) gene cause Gaucher's disease, a recessive lysosomal storage disease that is clinically recognised by liver damage, but can also present neurological problems, and at autopsy can reveal LBs (Hardy et al. 2009). The discovery of *GBA* as risk factor for PD was a serendipitous clinical observation, where it was noted that the parents and second degree relatives of Gaucher's patients frequently had PD (Goker-Alpan et al. 2004). This was the first study to show that heterozygous mutations in *GBA* gene were a risk factor for parkinsonism (in a familial cohort), and it was later confirmed in PD populations comprising Ashkenazi Jewish subjects (Aharon-Peretz et al. 2004; Gan-Or et al. 2008). A lack of association between *GBA* variants and PD in Europeans (Toft et al. 2006; Mata et al. 2008; Sutherland, et al. 2009b) has been reported. However, recent studies have shown that *GBA* mutations confer an increased risk of familial and idiopathic PD in Europeans (Bras et al. 2009; Neumann et al. 2009; Nichols et al. 2009).

Search for common genetic variation and its modulation of PD risk has also been extended to PARK interacting partners, transcription factors and micro-RNAs (miRNA), although these remain to be verified. Synphilin-1, an interacting partner for α-synuclein has been shown to produce LB- like cytosolic inclusions *in-vitro* (Engelender et al. 1999). Variants in this gene have been reported in isolated PD cases, and the variant R621C has also been assigned a functional relevance (Marx et al. 2003). A recent association study did not find any of the previously reported synphilin-1 variants to be associated with risk for PD, although the authors did report a marginal association of microsatellite markers in the synphilin regions (5q21) and IPD (Myhre et al. 2008).

Nuclear receptor related 1 (*Nurr1/ NR4A2*) functions as a transcription factor which has been shown to be critical for nigral DAergic cell development and differentiation (Martinat et al. 2006). Therefore, many studies have attempted to ascertain whether defects in this gene could contribute to PD. A polymorphism in intron 6 of the gene, (7048insG) was identified in familial and idiopathic PD patients (Xu et al. 2002;

Zheng et al. 2003; Hering et al. 2004), along with other heterozygous mutations (-291delT and -245T-G) (Le et al. 2003). Subsequent studies were not able to replicate these findings (Zimprich et al. 2003; Ibáñez et al. 2004b; Healy et al. 2006). A recent investigation into PD risk-conferring polymorphism in fibroblast growth factor 20 (*FGF20*), revealed a strong association with a SNP in the 3' untranslated region of the gene (G. Wang et al. 2008). Functional analysis showed that the risk allele disrupts a binding site for microRNA-433 (miRNA), leading to an increased translation of *FGF20* both *in vitro* and *in vivo*. A correlation with an increased expression of α-synuclein in a cell-based system and in PD brains led the authors to suggest that common variation can alter regulation of miRNAs and could be a novel mechanism that modulates PD risk.

1.6 *LRRK2* – a link between familial and idiopathic PD

Majority of PD develops as a result of complex interactions between genetic and environmental agents. Establishing the contribution of genetic components to the development of idiopathic PD (IPD) is paramount to understanding the multifactorial characteristics of the disease, and the study of familial PARK loci is the first step to understanding these genetic contributions.

LRRK2 was only identified as the causative gene for PARK8 linked autosomal dominant PD in 2004, however, it has come to be regarded as a key player in both the familial and idiopathic forms of the disease. Many pathogenic variants have since been identified in *LRRK2* (see Figure 1.6, reviewed in (Lesage & Brice 2009)). The pathogenic G2019S mutation in *LRRK2* is the most common cause of hereditary *LRRK2* associated PD, accounting for 3 per 100,000 PD cases in white population (based on an estimate of 200 per 100,000 with a hereditary PD rate of 15% by the International *LRRK2* Consortium (Healy et al. 2008)). The widespread frequency of G2019S mutation amongst IPD cases has resulted in it being termed as a common risk factor for non-familial PD (see Table 1.2). The variant R1441G is frequently reported in Spanish PD subjects of the Basque origin (Mata et al. 2005), and the variants G2385R and R1628P have also been identified as risk factors in Chinese

populations (Tan et al. 2007a). The identification of genetic variation in *LRRK2* as susceptibility factors in IPD subjects, qualifies this mendelian gene as a major candidate in bridging the gap between familial and idiopathic PD.

1.6.1 *LRRK2* gene structure and function

As previously mentioned, the *LRRK2* gene contains 51 exons that span 144 kb. A 9kb mRNA transcript has been identified in various tissues including the brain, and is predicted to encode a ~250 kDa (2,482-amino acids) multi-domain protein that is expressed in various tissues including the brain (Zimprich et al. 2004b; Paisán-Ruíz et al. 2004). The LRRK2 protein belongs to the ROCO superfamily that contain functional domains of ROC (Ras of complex proteins), COR (C-terminal of ROC), followed by a kinase domain belonging to the mitogen- activated protein kinase kinase kinase (MAPKKK) subfamily (see Figure 1.6), but the LRRK2 kinase domain has also been suggested to have structural similarities with the receptor-interacting protein kinases (RIPK) (Greggio & Cookson 2009). These functional domains are flanked by armadillo, ankyrin and 13 leucine rich repeats at the N-terminus and 7 WD40 repeats at the C-terminus which serve as modules for protein-protein interactions (Guo et al. 2006). The *LRRK2* paralog *LRRK1* has an identical domain structure, but a smaller N-terminus than *LRRK2*, and is also widely expressed in brain and other tissues (reviewed in (Mata et al. 2006a)). Both genes are reportedly conserved in vertebrates, and may have diverged from a common ancestral *LRRK* ortholog.

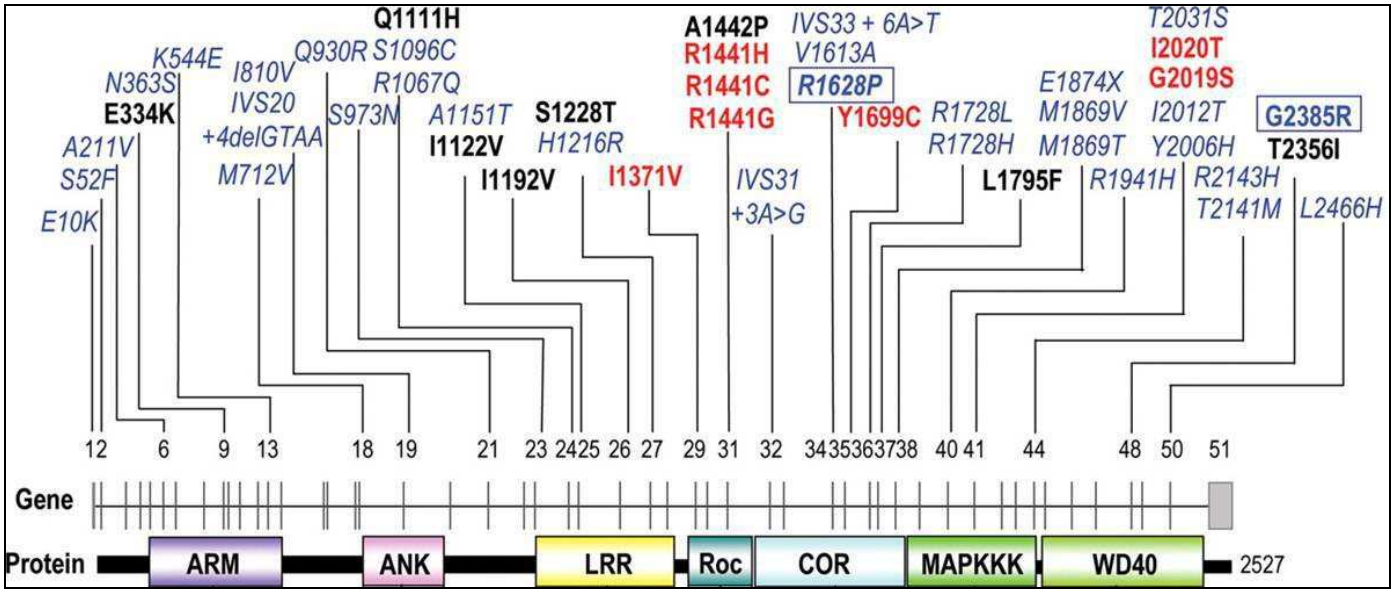

Figure 1.6: A schematic representation of the functional domains and genetic variation in the *LRRK2* gene. The 51 exons of *LRRK2* encode 2527 amino acids, and the functional domains which are conserved comprise of: Armadillo (ARM), Ankyrin repeat (ANK), leucine rich repeat (LRR), Ras of complex proteins: GTPase (Roc), C-terminal of Roc (COR), mitogen activated kinase kinase kinase (MAPKKK) and WD-40 domains. The exons and the variants identified in them are numbered above the gene line. The variants in red and bold represent recurrent proven pathogenic mutations, whereas the potentially pathogenic mutations (which display cosegregation), are highlighted in bold. Risk factors are shown in blue and in hatched box. Variants of unknown significance are represented in blue and in italics. This figure is adapted from (Lesage & Brice, 2009).

The multi-domain complex of LRRK2 allows two distinct enzymatic activities, namely, GTPase and kinase. The ROC domain of LRRK2 shares homology with the Ras related GTPase superfamily, responsible for regulating diverse cellular processes, such as mitogenic signalling (Guo et al. 2006). The activation of the Ras related GTPase requires a conversion of the GDP-bound state to the GTP-bound conformation. The GTPase binding domain of LRRK2 is necessary for the protein's kinase activity as it is predicted to stimulate LRRK2 autophosphorylation. Mutations R1441C/G in the GTPase domain, disrupt GTP hydrolysis which subsequently alters the downstream enzymatic activity of the protein (Lewis et al. 2007; Li et al. 2007) . A crystal structure of the LRRK2 ROC domain (in complex with GDP-$Mg^{(2+)}$) was recently predicted to display a dimeric fold which is stabilised by complex interactions and extensive domain-swapping of two monomers (Deng et al. 2008). Pathogenic mutations (R1441 and I1371) disrupt the ROC dimer resulting in decreased GTPase activity. This led the authors to conclude that the ROC domain regulates LRRK2 kinase activity as a dimer, possibly via the COR domain acting as a molecular hinge (Deng et al. 2008).

The kinase domain of the protein remains inactive until a change in the confirmation of the activation segment within the large C-terminal lobe is induced by phosphorylation (auto- or exogenous) (Mata et al. 2006a). This enables substrate access and catalysis. The activation segment is found between conserved tripeptide motifs DF/YG and APE, and the *LRRK2* mutations, G2019S and I2020T lie at the N-terminal boundary of this segment (Mata et al. 2006a). By using myelin basic protein (MBP) as a test substrate, West and colleagues (2005) measured the activity of LRRK2 protein, and determined that it possesses mixed-lineage kinase (MLK) activity (West et al. 2005). LRRK2 protein has also been demonstrated to undergo autophosphorylation, where the intrinsic GTP binding activity modulates downstream kinase activity (Smith et al. 2006; West et al. 2007). Other regulatory sequences suggested to modulate the kinase activity of LRRK2, include the N and C-termini. The N-terminus of LRRK2 has been suggested to have an inhibitory effect (Greggio et al. 2008), and C-terminal tail is

required for full kinase activity (Jaleel et al. 2007) (reviewed in (Greggio & Cookson 2009)).

A knockdown of LRRK2 in a DAergic neuroblastoma cell line induced using RNA interference (RNAi), identified a transcriptional downregulation of genes involved in various functions, namely, axonal guidance, nervous system development, cell cycle, cell growth, cell differentiation, cell communication, MAPKKK cascade, and Ras protein signal transduction (Häbig et al. 2008). This suggests that LRRK2 might have an important physiological role. The presence of Ras/GTPase and kinase domains provide support for the LRRK2 protein being involved in upstream regulation of intracellular signalling, such as the MAP kinase pathways. These pathways are evolutionary conserved three-tiered signalling cascades where each kinase activates the subsequent kinase (Mata et al. 2006a). Activation of MAPKKK by Ras starts a chain of events, whereby, the extracellular signal from receptor is relayed to cytosolic kinases by phosphorylation and subsequent activation of MAPKK (MAPK/ERK kinase), which in turn phosphorylates and activates MAPK (Guo et al. 2006). Substrates of MAPK activation include transcription factors, mitochondrial and cytosolic proteins and nuclear substrates for various cellular functions. Investigation of LRRK2 substrates and interacting partners would help define the regulatory pathways it participates in. Studies have already reported on the potential LRRK2 interactors that can be grouped into proteins that induce a chaperone-mediated response, proteins associated with the cytoskeleton and trafficking, and phosphorylation and kinase activity (Dächsel et al. 2007a). For example, LRRK2 has been shown to phosphorylate moesin, an actin- binding ERM (ezrin, radixin and moesin) protein that has been implicated in neurite outgrowth (Jaleel et al. 2007). The substrates for LRRK2 have been identified using the *in-vitro* kinase assays, and still remain to be tested for physiological relevance in *in-vivo* kinase assays. *In-vivo* kinase assays are technically demanding, but Imai and colleagues (2008) have identified what could be an authentic *in-vivo* substrate for LRRK2 (Imai et al. 2008). The authors showed that 4E-BP, a repressor of protein translation that is affected by oxidative stress and other stimuli, is prime

phosphorylated by LRRK2, and that drosophila LRRK2 (dLRRK2) modulates the maintenance of DAergic neurons by regulating protein synthesis in this pathway.

1.6.2 LRRK2 and neurodegeneration

LRRK2 protein has been shown to have a cytoplasmic localisation, and occurs in a soluble state in the normal brain (Giasson et al. 2006). Studies have been published evaluating the morphological expression of LRRK2 mRNA and protein in post-mortem human brain (discussed in later chapters). Differences in the transcriptional activity of LRRK2 in post-mortem human brains have been reported, although there is only limited information available on this. LRRK2 protein has been shown to localise to LBs, however, this is heavily dependent on the antibody used for immunohistochemical studies and currently remains a contentious issue.

The centromeric region for PARK8 locus also mapped onto dementia with late onset familial Alzheimer's disease (Scott et al. 2000). A G2019S mutation carrier with frontotemporal lobar degeneration (FTLD) was identified with ubiquitinated intranuclear neuronal inclusions, but due to the reduced penetrance of the mutation, it cannot be said whether the mutation is an underlying cause of the disease (as a disease modifier) or purely co-incidental (Dächsel et al. 2007b). The possibility of LRRK2 being involved in other neurodegenerative diseases was further demonstrated in the brains of frontotemporal dementia with parkinsonism-17 (FTDP-17) and MSA diagnosed patients (Miklossy et al. 2007; Huang et al. 2008). Miklossy and colleagues demonstrated that LRRK2 is associated with tau-positive neuronal and oligodendroglial inclusions (coiled bodies) in the brains of frontotemporal dementia of the pallido-ponto-nigral degeneration type linked to the chromosome 17 (FTDP-17/PPND) (Miklossy et al. 2007). As mentioned previously, *LRRK2* variants produce clinical and pathological features reminiscent of other parkinsonian entities (see section 1.5.2.1.7). This favours a possible role for LRRK2 in tauopathies, despite a lack of genetic variants.

Identification of G2019S mutation in a patient diagnosed with frontotemporal lobar degeneration with ubiquitinated neuronal intranuclear inclusions (FTLD-U/NII), lends support to the notion that LRRK2 might be involved in the UPS

system, and like ubiquitin might play a central physiological role in neurodegeneration (Dächsel et al. 2007b). LRRK2 was reportedly identified in glial cytoplasmic inclusions (GCIs) of MSA patients, which typically contain α-synuclein (Huang et al. 2008). Interestingly, LRRK2 protein has been shown to phosphorylate α-synuclein *in-vitro* (Qing et al. 2009). The wild-type LRRK2 protein has been shown to form cytoplasmic aggregates which are greatly ubiquitinated upon interaction with parkin (Smith et al. 2005a).

The interaction of LRRK2 with other PARK loci (dominant and recessive), and its implication in both synucleino- as well as tauopathies, suggests that it might play an important role in various pathways. However, the extent to which LRRK2 might contribute to these pathways, common or otherwise, remains to be seen.

1.6.3 *LRRK2* G2019S mutation in PD

The G2019S (6055G->A) mutation occurs in exon 41 of *LRRK2* and substitutes glycine to serine. It accounts for 3-6% of FPD and 1-2% of IPD cases in Europeans (Gilks et al. 2005; Nichols et al. 2005; Di Fonzo et al. 2005). G2019S associated PD is asymmetrical, tremor-predominant parkinsonism with bradykinesia and rigidity that responds to dopamine replacement (Hernandez et al. 2005; Goldwurm et al. 2006).

1.6.3.1 LRRK2 G2019S mutation and 'gain- of function'

In-vitro kinase assays using full length recombinant LRRK2 protein have shown an increase in the kinase activity of mutant (G2019S) LRRK2 in comparison to the wild-type protein (Smith et al. 2005a; West et al. 2005). G2019S mutation has also been shown to form inclusion bodies, and cause neuronal degeneration in SH-SY5Y neuroblastoma cells and mouse primary cortical neurons (Smith et al. 2005a). Replacing the kinase domain with a 'kinase-dead' version blocks inclusion body formation and delays cell death, thereby supporting the notion that increased kinase activity results in neuronal toxicity (West et al. 2005; Greggio et al. 2006). Over-expression of wild-type and mutant (G2019S) LRRK2 has been shown to reduce the neurite length and branching in primary neuronal cell cultures, whereas LRRK2 deficiency results in increased neurite length and branching (MacLeod et al. 2006). Neurite shortening has also been reported in

differentiated SH-SY5Y transfected with G2019S mutant- LRRK2, which was also shown to exhibit an increase in autophagic vacuoles (Plowey et al. 2008). This observation in addition to the sequence similarity of LRRK2 to receptor interaction protein kinase (RIPK) family, led the authors to hypothesize that LRRK2 is involved in MAPK/ERK signalling. This hypothesis was later confirmed in two cellular models (HEK293 and SH-SY5Y), whereby the authors demonstrated that wild-type LRRK2 protein is involved in the activation of the ERK pathway, and also confers protection in response to hydrogen peroxide mediated oxidative cellular stress (Liou et al. 2008).

This 'gain-of-function' mechanism for G2019S- linked pathogenesis is not limited to cellular models, and has to some extent been recapitulated in an animal model too. Adult-onset loss of DAergic neurons, locomotor dysfunction, and early mortality associated with expression of wild-type and G2019S mutant LRRK2 protein has been reported in transgenic *D. melanogaster* (Liu et al. 2008). Expression of wild-type and mutant LRRK2 protein in photoreceptor cells resulted in retinal degeneration, and L-dopa treatment improved locomotor impairment but did not prevent the loss of DAergic cells in the mutant flies. The G2019S mutant-LRRK2 protein was observed to cause a more severe parkinsonism-like phenotype than the wild-type protein in the drosophila model. This is in contrast to the clinical findings observed by the International *LRRK2* Consortium who reported that *"LRRK2 G2019S PD is less severe than IPD and requires dopamine replacement treatment later than IPDs, and were less prone to drug induced dyskinesia"* (Healy et al. 2008).

Based on the *in-vitro* 'gain-of-function' studies, LRRK2 kinase inhibitors have been suggested as potential therapeutics for *LRRK2*-linked PD. However, the core clinical and pathological phenotypic features for PD subjects with G2019S mutation are indistinguishable from IPD, and there is no difference in the symptoms of homozygous or heterozygous carriers of the G2019S mutation (Ishihara et al. 2006). No difference was observed in striatal dopamine transporter binding [^{123}Ioflupane] analysis of G2019S mutation carriers and IPD patients (Isaias et al. 2006). Moreover, no specific biochemical differences in the phosphorylation and levels of signal transduction proteins were reported in

leukocyte extracts of G2019S PD versus IPD subjects (White et al. 2007). However, identification of physiological substrates and interactors of LRRK2 is needed in order to better understand the *in–vitro* and *in-vivo* kinase activity of wild-type and mutant LRRK2.

1.6.3.2 G2019S penetrance

Typically associated with late onset PD symptoms (mean age of onset of 57.5 years) (Healy et al. 2008), rare cases of G2019S mutation carriers with early onset (<50 years) PD have also been reported (Bras et al. 2005; Clark LN et al. 2006; Punia et al. 2006; Ferreira et al. 2007). The penetrance of G2019S mutation has increasingly come into question as reports have identified G2019S mutation carriers who do not develop parkinsonian symptoms well into their 80s, and in some instances remain unaffected throughout their lifetimes (Kay et al. 2005; Eblan et al. 2006; Saunders-Pullman et al. 2006). The penetrance levels of G2019S mutations were initially estimated to be 17% at the age of 50, increasing to 85% at the age of 80 years (Kachergus et al. 2005). Another study estimated the G2019S penetrance in a selected autosomal dominant series from North Africa and Europe (probands included in the analysis) to be 33% at age 55, and 100% at 75 (Lesage et al. 2005b). A lower estimation of G2019S penetrance (17% at 50 years, 54% at 70 years) in a family of Italian origin has been reported (Goldwurm et al. 2007). This variability in penetrance (lifetime penetrance of 32% (at age 80), among families, albeit estimated using different study designs (including multiple affected members versus single), suggests that other genetic or environmental factors play a part in modifying the penetrance of G2019S mutation and its function in PD development.

The International *LRRK2* Consortium pooled worldwide data to address many important clinical questions related to *LRRK2* mutations but also to assess the age-specific cumulative risk of PD for G2019S mutation carriers in a sample size of 19,376 unrelated PD patients from various populations (Healy et al. 2008). They estimated that a G0219S mutation carrier has a 28% risk of developing PD at the age of 59 which increases to 51% at 69 years, and 74% at the age of 79, and this did not differ according to gender or ethnicity (Healy et al. 2008). This revised but reduced penetrance explains the high prevalence of *LRRK2* mutations in PD, and

its occasional occurrence in controls. They also estimated that 8% of *LRRK2* mutation carriers developed PD symptoms before the age of 40 years but symptoms were rare in G2019S mutation carriers before the age of 40.

1.6.3.3 Worldwide frequency of LRRK2 G2019S mutation

The frequency of G2019S mutation is highly population specific but a worldwide carrier rate of 1% in IPDs (n=14,253), and 4% in patients with hereditary PD (n= 5,123) has been estimated (Healy et al. 2008). The highest frequency of G2019S mutation related PD cases has been reported in North African Berbers and Ashkenazi Jews with proportions of up to 30-40% and 18-30%, respectively (Ozelius et al. 2006; Lesage et al. 2006; Healy et al. 2008).

Amongst European populations, low frequencies of this mutation are observed in FPD patients from Northern Europe (~1%), intermediate frequency (1.9%) in selected Italian populations, and high frequency in Southern Europe (2.9% in Northern Spain; 3.4% in Catalonia and 4.9% in Portugal) (Aasly et al. 2005; Bras et al. 2005; Berg et al. 2005; Hernandez et al. 2005; Gaig et al. 2006; Mata et al. 2006b, Goldwurm et al. 2006). This led to the suggestions that G2019S mutation frequency displays a European north-south gradient. However, a low frequency of G2019S mutation in southern European populations of Greek and Italian origins refutes this (Spanaki et al. 2006; Cossu et al. 2007; Xiromerisiou et al. 2007; Kay et al. 2006; Squillaro et al. 2007; De Rosa et al. 2009). Therefore, a north-south gradient of G2019S mutation in the Iberian Penninsula might be a more appropriate term to use, excepting the already known genetically distinct Basque population (Cavalli-Sforza & Piazza 1993), which displays a higher frequency of the R1441G *LRRK2* mutation (Gorostidi et al. 2009; Mata et al. 2009a). The G2019S mutation has also been identified in the southern American countries of Chile, Brazil, Peru and Uruguay, which were colonized by European settlers mainly from the Iberian Peninsula (Perez-Pastene et al. 2007; Mata et al. 2009b; Pimentel et al. 2008; Munhoz et al. 2008; Santos-Rebouças et al. 2008).

In Eastern Europe, a frequency of 5.9-7.7% has been reported amongst FPD and 0.5-0.7% in IPD patients from Russia (Illarioshkin et al. 2007; Pchelina et al. 2008). Although this mutation is rare in Central Asia and the far East, isolated

cases have been reported in Japan and India (Lu et al. 2005; Tan et al. 2005a; Zabetian et al. 2006b; Fung et al. 2006b; Punia et al. 2006; Tomiyama et al. 2006; Tan et al. 2007a; Cho et al. 2007; Shojaee et al. 2009). Homozygous carriers of G2019S mutation are rare in Europe, but have frequently been reported in North African populations, such as Tunisia and Algeria where consanguineous marriages are common (Lesage et al. 2006; Ishihara et al. 2007; Warren et al. 2008; Lesage et al. 2008; Hulihan et al. 2008). Although there is no difference in clinical phenotypes, or the age of onset of first PD symptom in heterozygous (ranging from 30 to 82 years) or homozygous (ranging from 28 to 86 years) carriers of the mutation, a higher penetrance for G2019S homozygous carriers has been reported (Ishihara et al. 2006; Lesage et al. 2006; Ishihara et al. 2007; Hulihan et al. 2008; Healy et al. 2008).

Reports of elderly and apparently healthy G2019S mutation carriers, adds a caveat to the potential genetic testing, and as such appropriate framework of pre- and post-test counselling is required for this mutation with such a variable penetrance (Goldwurm et al. 2007). An accurate estimation of population specific frequency of G2019S mutation is essential for the correct and cost-effective use of genetic testing and counselling of PD patients and asymptomatic carriers.

	Population	IPD (N)	FPD (N)	Control (N)
North Africa	*Arab Berbers*	***39%*** *(56)*	***36%*** *(143)*	***<1%*** *(739)*
Jews	*Ashkenazi Jews*	***10%*** *(259)*	***28%*** *(78)*	***1%*** *(410)*
Iberian Peninsula	*Portuguese*	***4%*** *(317)*	***14%*** *(85)*	***0%*** *(100)*
	Spanish	***3%*** *(806)*	***4%*** *(283)*	***0%*** *(544)*
	Basque	***0%*** *(117)*	***0%*** *(41)*	***0%*** *(425)*
Southern Europe	*Italian and Sardinian*	***2%*** *(2516)*	***4%*** *(633)*	***<1%*** *(1040)*
	Greek	***<1%*** *(235)*	***0%*** *(0)*	***0%*** *(0)*
	Cretan	***0%*** *(174)*	***1%*** *(92)*	***0%*** *(0)*
Central and	*French*	***2%*** *(300)*	***3%*** *(174)*	***0%*** *(348)*
Northern Europe	*German and Austrian*	***<1%(***803)	***1%*** *(231)*	***0%*** *(436)*
	British	***1%*** *(1145)*	***2%*** *(192)*	***0%*** *(1786)*
	Irish	***<1%*** *(236)*	***3%*** *(35)*	***0%*** *(212)*
	Swedish	***2%*** *(200)*	***0%*** *(127)*	***0%*** *(200)*
	Norwegian	***1%*** *(371)*	***1%*** *(64)*	***0%*** *(572)*
Eastern Europe	*Polish*	***0%*** *(153)*	***0%*** *(21)*	***0%*** *(190)*
	Serbian	***0%*** *(47)*	***4%*** *(51)*	***0%*** *(161)*
	Russian	***1%*** *(157)*	***0%*** *(10)*	***0%*** *(126)*
Other European	*North American*	***1%*** *(2606)*	***3%*** *(1450)*	***<1%*** *(4934)*
	South American (Chilean)	***3%*** *(137)*	***3%*** *(29)*	***0%*** *(153)*
	Australian	***<1%*** *(578)*	***2%*** *(252)*	***0%*** *(0)*
Asia	*Indian*	***<1%*** *(718)*	***0%*** *(82)*	***0%*** *(1200)*
	Chinese	***0%*** *(1360)*	***<1%*** *(973)*	***0%*** *(938)*
	Japanese	***<1%*** *(526)*	***2%*** *(60)*	***<1%*** *(372)*
	Korean	***0%*** *(436)*	***0%*** *(17)*	***0%*** *(0)*

Table 1.2: World-wide carrier rate of *LRRK2* G2019S mutation in PD subjects and unaffected controls, according to the International *LRRK2* consortium (Healy et al. 2008). This table displays the percentage carrier rates of G2019S mutation in various populations. IPD= idiopathic PD; FPD= familial PD; (N) = the total number of samples genotyped.

1.7 Objectives and Principal questions addressed in the thesis

Variation in gene expression has been demonstrated to be a major driving force of the phenotypic evolution. Many factors work together in *cis* or *trans* to regulate gene expression and as such produce the phenotypic diversity so readily observed amongst different species. In any study of the disease aetiology, it is essential to establish the effects of auxiliary mechanisms that might not necessarily be the primary cause of the disease, but nevertheless have an impact on the eventual product of the gene, and thereby contribute to the clinical and pathological understanding of the disease. The Queen Square Brain Bank (QSBB) houses an excellent resource for post-mortem PD tissue with detailed clinical summaries, and studying a measurable phenotype such as gene expression in human tissue that has experienced disease pathogenesis would further our understanding of PD pathogenesis.

It is widely acknowledged that the impact of genetic variation on quantitative traits such as gene expression can have an effect on the overall phenotype. As such, the effects of genetic variation (coding and non-coding) on *LRRK2* expression remains a central and primary theme of this thesis.

The exonic *LRRK2* mutation, G2019S is reported to be pathogenic, and biochemical studies have proposed an *in-vitro* 'gain of function' for the mutation. However, the clinical (and pathological) phenotype displayed by G2019S mutation carriers remains indistinguishable from IPD subjects that are reportedly negative for this mutation. Therefore, studying the gene expression in PD brains that suffered from idiopathic forms of the disease versus those of the G2019S mutational insult would allow us to ascertain potential differences or identify overlapping pathogenic events between the two forms of PD.

Therefore, the overall hypothesis of this thesis was that differences in the LRRK2 expression profile between unaffected controls and PD subjects could contribute to the development of PD, and both the coding and non-coding genetic variation in the *LRRK2* gene could play a major role in this.

The major aims used to test the hypothesis are summarised as follows:

- To estimate the carrier rate frequency of the common *LRRK2* G2019S mutation in unaffected subjects from populations that might have contributed to the genetic origins of G2019S mutation.

- To determine the distribution of LRRK2 mRNA and protein in the human brain, and to assess whether there is a deviation from the normal pattern in cases of IPD and those with G2019S mutation.

- To establish any potential dysregulation in the mRNA transcriptional levels, and to assess how this might contribute to PD pathogenesis.

- To ascertain if common genetic variation in *LRRK2* upstream regions can affect the transcriptional ability of the gene.

Chapter 2

2 Methods and Materials

2.1 QSBB Tissue

Frozen post-mortem brain tissue was obtained from the Queen Square Brain Bank (QSBB) after acquiring ethical approval from National Hospital of Neurology and Neurosurgery (NHNN), Local Research Ethics Committee (LREC) (Reference: 06/Q0512/11) and Research and Development department of University College Hospital London (UCLH) (Reference: 06L 306). Informed consent had been acquired by the QSBB. All the tissue used in this study was pathologically proven to be IPD.

2.1.1 Paraffin embedded tissue

Formalin fixed brain tissue and spinal cord were processed as shown in Table 2.1. The processed tissue was the embedded in paraffin wax and stored until required.

Reagent	3 Day Time
70% Alcohol	6.00 hours
90% Alcohol	6.00 hours
90% Alcohol	6.00 hours
Absolute Alcohol	6.00 hours
Absolute Alcohol	6.00 hours
Absolute Alcohol	6.00 hours
Absolute Alcohol	6.00 hours
Chloroform	6.00 hours
Chloroform	6.00 hours
Wax	6.00 hours
Wax	6.00 hours
Wax	6.00 hours

Table 2.1: Reagents and times used for paraffin processing of post-mortem tissue.

2.1.2 Frozen tissue

In order to preserve the integrity of the post-mortem tissue, it was frozen using polished brass plates, which were pre-cooled to -70^0C. The tissue was subsequently stored at -70^0C prior to use. The pH value of the tissue was routinely recorded for each subject.

2.2 Nucleic acid extraction

2.2.1 DNA extraction

Genomic DNA was extracted from human brain (pathology proven), blood (clinical), or buccal swab (where specified) samples using the wizard genomic DNA purification kit (Promega, U.K.) described as follows. 960µl 0.5M ethylendiaminetetraacetate (EDTA) was added to 4ml nuclei lysis solution and chilled on ice. 4.8ml of this mixture was added to a frozen piece of brain approximately $1cm^3$ in size. 140µl proteinase K (at 20 mg/ml) was then added and the tube incubated at 55ºC for 16 hours until the brain was completely digested. 24µl RNAse solution was added to the nuclear lysate and mixed in by inversion. The tube was incubated at 37ºC for 30 minutes, and then allowed to cool to room temperature for 5 minutes. 200µl of protein precipitation solution was added, and the tube vortexed vigorously for 20 seconds. The tube was chilled on ice for 5 minutes, and then centrifuged at 13,000 rpm at room temperature for 4 minutes. The supernatant was carefully transferred (leaving the protein pellet behind) to a tube containing 4.8ml of propan-2-ol (Sigma, UK). The tube was gently mixed by inversion to precipitate the DNA and then centrifuged at 13,000 rpm at room temperature for 1 minute. The supernatant was carefully decanted and 4.8ml of 70% ethanol (Sigma, UK) added. The tube was gently mixed by inversion (to wash the DNA pellet) and then centrifuged at 13,000 rpm for 1 minute at room temperature. The ethanol was carefully aspirated and the pellet air-dried (sealed over with perforated parafilm to avoid contamination). The pellet was resuspended in 800µl DNA rehydration solution and incubated at room temperature for 16 hours. The DNA solution was stored at 4ºC. The DNA concentration (assayed at 260 nm) and quality was measured using the NanoDrop

ND-1000 (NanoDrop Technologies, U.S.A.), enabling the identification of samples contaminated with protein or other organic compounds.

2.2.1.1 DNA samples obtained through external collaborations

For chapter 3, DNA samples from unaffected subjects of various ethnicities were obtained from Dr. Neil Bradman (The Centre for Genetic Anthropology, UCL) and have been described in previous studies (Weale et al. 2001; Thomas et al. 2002; Behar et al. 2003; Ingram et al. 2007; Veeramah et al. 2008). For chapter 6, DNA samples from unaffected subjects were obtained from Prof. Steve Humphries (Rayne Institute, UCL) and have been described in a previous study (Miller et al. 1996).

2.2.2 RNA isolation and extraction

The quality and quantity of isolated RNA is essential for successful analysis of gene expression. The RNA must be pure and intact and free of contaminants such as DNA and other potential inhibitors, for example, RNAses (released from membrane bound-organelles upon cell disruption). As RNA is highly susceptible to degradation, it is essential that endogenous RNAse activity is rendered non-functional by using strong denaturants in order to ensure successful RNA isolation. Therefore, a sterile technique should be employed at all times when handling reagents and equipment used for RNA isolation.

The tissue was homogenised in 1ml of Trizol, a monophasic solution of phenol and guanidine isothiocyanate (Invitrogen, UK) in tissue grind tubes (Kontes glass company, UK). The homogenate was transferred to sterile eppendorf tubes. To separate different phases, 200µl of chloroform (Sigma, UK) was added to the homogenate and shaken vigorously to mix. The mixture was incubated at room temperature for 2-3 minutes followed by centrifugation at 13,000 rpm for 15 minutes. The centrifugation separated the mixture into three phases, and the upper aqueous phase which contains that RNA was transferred to a separate tube and the organic phase discarded. The RNA was then precipitated using 500µl of isopropyl alcohol (Sigma, UK) from the aqueous phase and incubated at room temperature for 10 minutes followed by centrifugation at 13,000 rpm for 10 minutes. The supernatant was removed. The RNA pellet was washed with at least 1ml of 75%

ethanol. The sample was then mixed by vortexing and centrifuging at 7,500 rpm for 5 minutes. The ethanol was removed and the pellet air dried for up to half an hour or until dry (sealed over with perforated parafilm to avoid contamination).

The RNA was then dissolved in RNAse free water (70-100µl). RNA concentration (assayed at 260 nm) and quality was measured using the NanoDrop ND-1000 (NanoDrop Technologies, U.S.A.).

2.3 Genotyping

2.3.1 Polymerase chain reaction (PCR)

Polymerase chain reaction (PCR) was routinely used to determine genotypes. PCR was developed by Kary Mullis in 1983, and has since become a common and an indispensable technique in molecular biology. It is a relatively simple technique that amplifies a DNA template to produce millions of copies of specific DNA fragments *in vitro*. However, to produce such specific fragments some prior knowledge of the sequence is required. This information is then used to design oligonucleotide primers which are usually a stretch of approximately 20 nucleotides corresponding to the sequence of interest. The primers bind to the complementary DNA sequence (one to the strand running from 5' to 3' direction and the other to the strand running in 3' to 5' direction) of the denatured template DNA. In the presence of a heat-stable DNA polymerase and the four deoxynucleoside triphosphates (dNTPs, namely, dATPs; dGTPs; dCTPs and dTTPs), the primers initiate synthesis of new DNA strands that are complementary to the DNA strands of the target DNA segment. Each newly synthesized strand then act as a template for further DNA synthesis in subsequent cycles, thereby doubling the amount of template each cycle. After about 25 cycles of DNA synthesis, the PCR product will include up to 10^5 copies of the initial target sequence.

2.3.2 PCR components

Genomic DNA (50 ng/µl) was amplified using Taq DNA polymerase kit (Qiagen, UK). The PCR components included 2µl 10X buffer; 4µl Q-solution; 2µl each primer (100nM each); 2µl deoxynucleoside triphosphates (dNTPs; 10mM each),

0.16µl Taq polymerase and double distilled water (ddH_2O) to make up a total volume of 20µl. The dNTPs were obtained from Invitrogen (UK) and the primers were designed using online tools available at http://www.cybergene.se/. The primers were blasted against NCBI database to check for specificity and were obtained from Sigma Genosys, UK. Standard cycling conditions were used: 94° C for 5 minutes; and 30 cycles of 94° C for 30 seconds, 55-65°C for 30 seconds and 72° C for 45 seconds; 72° C for 7 minutes. Annealing temperatures were dependent on the primers. The thermal cycler used for the PCR reaction was GeneAmp PCR system 9700 (Applied Biosystems, UK).

2.3.3 Restriction Fragment length polymorphisms

Restriction digestion of amplified genomic DNA was carried out in a total volume of 15µl, containing 1.5µl of appropriate reaction buffer, 10µl PCR product, 1-2 units of the restriction enzyme, and the rest of the volume was made up with ddH_2O. However, the volume of water was adjusted accordingly upon the addition of 100X bovine serum albumin (BSA) and each assay was incubated overnight according to manufacturer's instructions. All the restriction enzymes were provided by New England Biolabs, UK. The digested product was then genotyped using agarose gel electrophoresis.

2.3.4 Agarose gel Electrophoresis

Agarose gels used for analysing and genotyping DNA fragment sizes were made by melting agarose powder (Roche, UK) in 1X Tris-Borate- EDTA (TBE) buffer (121.1g Tris, 61.8g anhydrous boric acid, 7.4g EDTA in 10 litres of ddH_2O) in a microwave oven. The gels were routinely made between 1 to 2.5% of the volume. The gels were cast with the addition of 10µg/ml of ethidium bromide (EtBr). In order to be analysed, 5µl of digested PCR product was mixed with 1µl of Orange G loading dye (prepared in equal volumes of glycerol and water) and run along a 1 kb DNA ladder. The Orange G loading dye and the 1 kb DNA ladder were obtained from Sigma, UK and Promega, respectively. The samples were subjected to electrophoresis for approximately 30 to 60 minutes at 80 to 120mV. The DNA samples in the gel were visualised under a UV transilluminator.

2.3.5 Taqman assays

The taqman assay by design service for SNP genotyping assays provided by Applied Biosystems was occasionally used to design probes for specific assays. These probes were dye-labelled with FAM and VIC. The allelic discrimination PCR reaction consisted of: taqman universal PCR master mix (2.5µl), 40X assay mix (0.125µl), genomic DNA (5-20ng) in a total volume of 5µl made up with ddH_2O. The reaction was run on ABI7900 (Applied Biosystems, UK) and the cycling conditions were optimised to the specific probe. SDS2.1 software (Applied Biosystems, UK) was used for allelic discrimination.

2.4 PCR based mRNA expression studies

Many techniques have been developed to measure the relative and absolute levels of gene expression in tissue. Traditionally, gene expression levels were measured using northern blot analysis; RNAse protection assays or *in situ* hybridisation. All of these methods have their advantages. For example, northern blot analysis can provide information about mRNA size, alternative splicing and the quality of the RNA samples; RNAse protection assays can map transcript initiation and termination sites, and intron-exon boundaries; *in- situ* hybridisation is a complex technique but the only one that allows identification of anatomical or cellular localisation of a specific transcript. The major disadvantage common to all these techniques is the lack of sensitivity when measuring transcripts that are expressed at low levels. However, recently more high throughput, sensitive and accurate methods have been developed. Microarrays and quantitative PCR based methods are now routinely used to measure gene expression levels. Quantitative PCR based methods are especially sensitive in detecting low level RNA expression, and was the technique most routinely used to measure mRNA expression levels for the purpose of this thesis.

2.4.1 Reverse-Transcriptase (RT-PCR)

DNA templates are required for thermostable DNA polymerases used in the PCR process, therefore in theory, limiting the technique to DNA studies. However, this technique could also be applied to the analyses of RNA populations by reverse transcribing RNA to complementary DNA (cDNA). This reverse transcription

provides the necessary DNA template for the thermostable DNA polymerases to perform the PCR. Either random primers, oligo(dT) primers or sequence specific primers can be used for reverse-transcription. However, the quality and purity of starting RNA template are essential for a successful RT-PCR reaction and any subsequent analysis. After the initial reverse transcription step, where the RNA has been converted into cDNA, basic PCR can be performed to amplify the target sequence many-fold.

RNA was reverse transcribed to form cDNA using the First-Strand cDNA synthesis Superscript II RT (Invitrogen, UK) kit. The reaction constituted 2µg of total RNA, 1µl random hexamers, 1µl dNTP mix (10mM each) and 8µl sterile ddH_2O. The mixture was heated to 65° for 5 minutes, followed by a quick chill on ice. The contents were then centrifuged and the remaining cDNA synthesis mixture was added which included 4µl of 5X First-Strand Buffer, 2µl of 0.1 M dithiothreitol (DTT), followed by 1µl of RNAse OUT. The contents were then mixed and incubated at 25°C for 2 minutes. 1µl (200 units) of SuperScript II RT was added and the mixture was incubated at 42°C for 50 minutes, followed by 70°C for 15 minutes to inactivate the reaction. The cDNA was further diluted 1 in 10 in Diethyl pyrocarbonate (DEPC) treated water (Ambion, UK) to make up a working stock.

2.4.2 Quantitative real Time PCR (qPCR)

Quantitative real-time polymerase chain reaction (qPCR) is a technique that quantitates the fluorescence emitted each PCR cycle (in real time). Methods used to detect and quantitate a PCR product, involve fluorescently labelled oligonucleotide probes or DNA-binding fluorescent dyes, for example, SYBR green that intercalates with double stranded DNA as it is being synthesized.

The DNA binding fluorescent dyes are easy to use and do not require the oligonucleotide primers to be labelled, however, they can also generate non-specific products. In order to check the amplicon homogeneity, thermal melt curves can be generated that allow the product to form a double-stranded DNA at a lower temperature of 60°C (fluorescence is quenched when the product is double-stranded). The temperature is slowly ramped up to 95°C to be denatured. Any potential peaks with different melting temperatures and/or broad peaks in the

melt curve are indicative of multiple products or non-specific amplification. This serves as a good quality control during routine use of this particular application of PCR.

Fluorescence values are recorded during every cycle, however, the first significant increase in the florescent signal (above the background noise) is measured at the threshold cycle (Ct). The Ct values directly correlate to the initial amount of target template, that is, the amount of RNA in the sample. This Ct value is recorded during the exponential phase of amplification, and is fundamental to qPCR. It works on the premise that a sample with high concentrations of starting template will require fewer amplification cycles to cross the critical threshold cycle where the fluorescent will be quantitated (Bustin et al. 2005). However, if there is little template to start off with, then many rounds of amplification would be required to reach that critical threshold cycle. As the Ct value is inversely proportional to the initial copy number, a standard curve can be generated by plotting the Ct values against the logarithm of initial copy numbers. The linear regression of the standard curve allows the target Ct to be directly compared to the Ct of the standard calibrator, resulting in the quantitation of the original amount of the template, which could be recorded as having more or less mRNA than the standard.

Factors like fluctuations in the efficiency of the reaction, small initial quantities of the target RNA, non-specific priming, and slow degradation of the reaction mix add to the disparities associated with qPCR (Bustin et al. 2005). Therefore, it is essential that the assay is well optimised and reproduces with same efficiency across the plates. Multiple Ct values should be determined by performing the reaction in triplicates for each sample.

The qPCR in this thesis was performed on ABI7500 (Applied Biosystems, UK) using SYBR-green dye mix that releases fluorescence during the critical threshold, allowing for an accurate quantitation of the initial RNA starting template. The 25µl reaction required 5µl of cDNA (50ng/µl), 12.5µl SYBR-green, 2.25µl primers (900nM) and 3µl ddH_2O. The SYBR-green dye mix and the

MicroAmp Optical 96-well reaction plates were both supplied by Applied Biosystems.

2.4.2.1 Primer sequences and conditions

The cDNA primers were designed so as to have at least one of the primers on an exon-exon boundary. This minimises any contamination through the amplification of genomic DNA. They were designed so as to amplify the predicted transcripts for that gene. The cycling conditions, apart from the annealing temperatures were similar for all the target genes: 50° C for 2 minutes; 95° C for 10 minutes; and 35 cycles of 95° C for 15 seconds, 55-65°C for 30-45 seconds and 72° C for 45 -60 seconds. A dissociation curve was added at the end of each reaction to determine that a single specific PCR product was being formed by the primers: 95°C for 15 seconds; 60°C for 1 minute and 99°C for 15 seconds. A single peak for all the samples at the same temperature ensures all the product is dissociating at the same temperature ensuring only one product. The qPCR products were also checked on agarose gels to ensure the presence of a single product.

2.4.2.2 Standard curve v/s Ct

Triplicate reactions were run for each sample. The plates for each gene were calibrated using the same sample to ensure that the Ct values remained consistent across the plates. The samples were quantitated against a standard curve generated from reactions containing serial dilutions of human brain for each target gene. Six-fold serial dilutions of a calibrator template were used for the relative quantitation, with the highest dilution being 500 fold of the lowest. The dilutions were as follows: 500, 100, 20, 4, 2 and 1 fold of the lowest. The Ct values of these serial dilutions were used to construct the standard curve, which was generated using the SDS2.0 software (Applied Biosystems, UK).

2.4.2.3 Normalisation

The normalisation of target gene expression is essential to account for any inherent variations between and within cDNA samples. This is achieved by the use of an endogenous reference gene. This reference gene should be expressed invariantly in all tissues of an organism. The use of reference genes corrects for any potential sample variations and increases the reliability of qPCR by taking

into account the amount of starting materials, inherent variation in RNA and cDNA sample loading variation between the samples etc (Gutala & Reddy 2004).

2.4.2.3.1 Endogenous reference genes and normalisation factor

In this study, four endogenous reference genes were used to normalise the expression of our gene of interest, and are mentioned as follows: Ribosomal Protein L13a (*RPL13A*) (Jesnowski et al. 2002); Hypoxanthine Phosphoribosyl-transferase 1 (*HPRT1*), (Meldgaard et al. 2006); TATA binding protein (TBP), and Glucose 6 –phosphate-1-dehydrogenase (G6PD) (Ohl et al. 2005). The relative abundance values for the reference genes were calculated for each experimental sample.

2.4.2.3.2 Calculation of normalisation factor

The data produced by qPCR can give rise to spurious results if an appropriate normalisation factor is not calculated. Despite using four endogenous reference genes it was important to determine which of these reference genes behaved in a dissimilar pattern in affected and unaffected tissue. It is also possible that different reference genes have varied expression levels in different anatomical regions. Therefore, it was important to use more than one reference gene to calculate a normalisation factor. The software, NormFinder employs a model based approach to identify the reference genes that present the least amount of variation in the dataset (Andersen et al. 2004). The algorithm used in this software requires the use of a minimum of three reference genes. It then estimates the variation in the reference genes in cases as well as control samples, and selects the reference gene with the best stability value or a combination of two best reference genes. A geometric mean of these two best reference genes is calculated (to account for any outliers) for each sample, giving rise to a virtual reference gene. Therefore, when affected and unaffected subjects were compared the NormFinder software was used to identify the reference genes with the least amount of variation.

In order to normalise each target gene sample, the relative value obtained for the target gene was divided by the value of the virtual reference gene. Since a large number of samples were used in the study and a triplicate for each sample was included, it was not possible to perform the reaction for all the samples on a single

plate. Therefore, in order to normalise the samples across the different plates the following steps were used:

Step 1, normalisation of individual samples to its reference gene:

$$\text{Internal normalisation of each sample, } X = \frac{\text{Gene of interest}}{\text{Virtual reference gene}}$$

(where X is the sample)

Step 2, calculation of a normalisation factor:

$$\text{Final normalisation factor, } N_f = \frac{1}{N}\left[X_1 + X_2 + X_3 \ldots\ldots X_i\right]$$

(where N refers to the total number of subjects, i refers to the sample number and N_f is essentially a mean of all the samples that have been normalised in step 1)

Step 3, use of the normalisation factor from step 2 to normalise the samples across the different plates:

$$\text{Final normalised value for each sample} = \frac{X_i}{N_f}$$

2.5 Histochemical techniques

2.5.1 *In situ* hybridisation protocol

PCR based methods are highly sensitive at detecting low levels of mRNA, however, these methods cannot distinguish between different cellular populations. Laser-capture microdissection techniques can be used to isolate single cells of specific population, and quantitative PCR can be performed on RNA isolated from these specific populations. The RNA yield from such a technique can be low and this limits the number of experiments that can be performed. There are various techniques that can quantitate mRNA expression. However, *in situ* hybridisation (ISH) remains the only method that enables the morphological demonstration of specific mRNA or indeed DNA sequences in tissue sections, individual cells, or chromosomal localisation. Therefore, *in situ* hybridisation studies were used to determine the cellular localisation of LRRK2 mRNA and to complement the qPCR study.

As ISH can be used to identify the localisation of a specific RNA or DNA sequence in a hetrogenous cell population, it is possible to determine whether a gene is being expressed at low levels in all the cells or at a high level in a few cells. This is especially useful if cerebral tissue sections are being used, as many regions of the brain are composed of different cellular populations. ISH works on the principle that under appropriate conditions, stable hybrids can be formed by hybridising labelled, single-stranded fragments of RNA (or DNA) containing complementary sequences (probes) to the target RNA (or DNA) of interest. These stable hybrids can then be visualised using a detection system. ISH is technically demanding and can be complicated by non-specific binding that can increase the background noise, thereby reducing the signal to background ratio. Hence, an extensive optimisation of the protocol is required.

Different methods were used to look at the expression profile of LRRK2 in post-mortem human tissue. The oligonucleotide probes were labelled using both radioactive (^{35}S) and non-radioactive (digoxigenin) label. Both procedures have

their advantages and the following sections will discuss the protocol used for the LRRK2 ISH study discussed in this thesis.

ISH is a procedure that requires careful handling of tissue sections and reagents prior to hybridisation as any contamination could have drastic effects on the development of the mRNA signal. The tissue sections should be handled in an RNAase-free environment right up until the time they have been hybridised and washed. It was essential that all glassware was baked at 400°C and only sterile plastic was used. The reagents were made in diethyl pyrocarbonate (DEPC)-treated or sterile water, as appropriate. Any unbaked glassware or non-sterile plastic was rendered RNAase-free by washing in 0.1M NaOH and subsequently with sterile water.

2.5.1.1 Tissue samples

Flash frozen tissue was removed from -80°C freezer and placed in a cryostat (Bright) at -20°C for two hours in order for the temperatures to equilibrate prior to cutting. The frozen sections were cut at 12µm, and depending on the size of the section collected they were mounted onto either superfrost slides (BDH, UK) or vectabond coated slides (Vector, UK). The blade was cleaned with three changes of absolute alcohol to avoid any cross contamination of mRNA between different samples. The sections were allowed to dry on a hot plate for 30 minutes and then stored at -80°C until further use.

2.5.1.2 Labelling method

The probes used for the ISH procedure were labelled using ^{35}S (radioactive) and digoxigenin (non-radioactive) labelling methods. Appropriate positive controls were used for the study

2.5.1.2.1 Radioactive labelling and probe purification

Oligonucleotides were 3' end-labelled with [^{35}S] dATP 1000Ci/mmol (Perkin Elmer, UK). This was done using terminal deoxynucleotide transferase at 500-1000 units/ml in cacodylate buffer at 37^0C for 60 minutes, according to the manufacturer's protocol (Promega, UK). Reactions were stopped by addition of TE buffer (10mM Tris, 1mM EDTA) at pH 8.0 to a total volume of 100µl. Unincorporated bases were separated from the labelled probe on G50 sephadex

columns, which were equilibrated in TE pH 8.0. These columns were prepared to 2ml by volume in 2.5ml sterile syringes and plugged with baked glass wool. The column was washed gently with 2 x 1ml TE pH 8.0. The radioactively labelled probe in TE was added to the top of the column and the column was further washed in 3 x 200µl TE; 2 x 400µl TE (these fractions should contain about 50-70% of the probe), and final washes of 3 x 200µl TE. These were collected as separate fractions. Elution characteristics of each batch of G50 sephadex were determined prior to the probe purification by taking 2µl aliquots from each fraction and measuring them for radioactive peaks using scintillation counter.

24µl of tRNA (8.33 mg/ml in water, from Brewer's yeast), 42µl sodium acetate (3.0M, pH 5.2) was added to the fractions that gave the highest radioactive peaks. 950 µl of ethanol at -20 °C was added to the mix and incubated at -70°C for 120 minutes or -20°C overnight. The tubes were spun at 13,000 rpm, for 30 minutes at 4^0C. The supernatant was decanted and precipitated with cold ethanol. The tubes were allowed to dry and the precipitates were combined by quantitative transfer in 100µl of 10mM Tris, 1mM EDTA, pH 7.6, 10mM dithiothreitol (DTT) and stored at 4°C.

2.5.1.2.2 Digoxigenin labelling

The probes were labelled at a total concentration using the Digoxigenenin 3' end labelling kit (Roche, UK). A total of 100pmol of the probe was labelled using 4µl of the reaction buffer; 4µl of cacodylate buffer; 1µl of terminal transferase and 1µl of dATP, with the rest being made up to 20µl double distilled RNAse free water. The reaction was incubated at 37°C for 1 hour and 2µl of 0.8M sterile EDTA was added to stop the reaction. The labelling efficiency was measured by blotting serial dilutions of the labelled probe, along with a known control probe supplied with the kit. The visualisation procedure was carried out according to the manufacturer's instructions.

2.5.1.3 Tissue preparation

The sections were prepared using the following steps in an RNAase free environment. The slides were allowed to thaw, flat and face-up for 10 minutes, and were then fixed in 4% paraformaldehyde in PBS (w/v) at room temperature for 5 minutes. The slides were then washed twice in PBS, 2 minutes and 1 minute per wash, followed by a wash in physiological saline for 1 minute. The sections were then dehydrated by immersion in 70%, 80% and 95% ethanol in DEPC-treated water for 2 minutes each and allowed to air-dry for a minimum of 30 minutes

2.5.1.4 Hybridisation

The hybridisation buffer (Sigma, UK) was warmed to room temperature. The radioactively labelled probe was diluted at 10µl/ml in hybridisation buffer. DTT was added to hybridisation buffer to a final concentration of 1mM. The digoxigenin labelled was probe was diluted at 250fmol/µl and no DTT was added to this. Diluted probe was evenly layered over slides and covered with parafilm coverslips (75-100µl per small section and 150-200µl for the larger ones). The slides were then incubated at 42°C overnight.

2.5.1.5 Washing

The water bath was heated to 55°C. All solutions for post-hybridisation steps were made in non-sterile distilled water. Four glass troughs were filled with about 1 litre of 1x SSC (Sigma, UK) each and allowed to heat to 55°C in the water bath. The coverslips were floated off, dipped into 1 x SSC rinse solutions three times and then stored in 1 x SSC prior to the first 55°C wash. The coverslips that were used for radioactive sections were stored and dealt appropriately for radioactive disposal. The slides were washed 4x 15minutes in 1 x SSC at 55°C, followed by 2 x 30 minutes at room temperature. The sections were then washed twice in distilled water (to remove remaining salts), followed by washes in 70% and 95% ethanol. The slides were then transferred to plastic stands and allowed to air-dry for 30 minutes.

2.5.1.6 Visualisation procedures

2.5.1.6.1 Radioactive Autoradiography

After hybridisation, film autoradiographs were prepared by exposing slides to Hyperfilm (Amersham, UK) for 15-20 days. These were developed using automated X-Ray film processing. Emulsion autoradiographs were prepared by dipping slides in K5 nuclear track emulsion (Ilford Imaging, UK) diluted 1:1.5 in distilled water and exposing for 4-6 weeks. Emulsion-dipped slides were developed in phenisol (1:4 in distilled water) for 3.5 minutes at 20°C, washed in stop bath (diluted 1:20 in distilled water) for 1 minute and fixed in hypam (1:4 in distilled water) 3.5 minutes. The phenisol, stop bath and hypam were all obtained from Ilford Imaging, UK. Slides were subsequently washed in distilled water (30 minutes), counterstained, dehydrated through graded ethanols, cleared and mounted in DPX mountant (BDH, UK).

2.5.1.6.2 Digoxigenin

After the appropriate washings were done with 1X SSC in order to remove any non-specific hybridisation, the sections were prepared for a visualisation procedure. The sections were first blocked in 10% non-fat milk in phosphate buffered saline (PBS) for 30 minutes, and then sections were incubated with a primary anti-DIG antibody (Roche, UK) at a dilution of 1:250 at 4°C overnight. The sections were then washed in 1 X PBS several times before a secondary biotinylated anti-mouse antibody (Dako, UK) was added at a dilution of 1:200 for 30 minutes at room temperature. The following steps were conducted at room temperature. The sections were rinsed in 1X PBS and a combination of ABC stain (Vector, UK) followed by biotinylated tyramide signal amplification (TSA) solution (Pierce Biotechnology, UK) was applied. The ABC and TSA were applied to the sections for 30 minutes each and this step was performed twice. This step increases the signal amplification and is instrumental during visualisation procedure for low copy-number mRNAs. After this incubation the sections were then again rinsed with 1 X PBS and incubated in 0.1M PBS for 30 minutes.

2.5.1.6.2.1 Glucose oxidase nickel DAB (G.O.D) method

The digoxigenin ISH sections were washed in 0.1M PBS for 30 minutes, rinsed in 0.1M ammonium acetate buffer (pH 6.0) and incubated in the following reaction solution: 0.1 M acetate buffer (pH 6.0), 0.05% diaminobenzidine (DAB), 0.04% ammonium chloride, 2.5% ammonium nickel sulphate, 0.25% β- D- glucose and 0.001% glucose oxidase. The sections were incubated in the solution for around 15 minutes, and placed in 1X PBS to stop the reaction. If darker precipitation was desired the sections were returned to the G.O.D. solution for a longer period.

2.5.1.6.3 Histological counterstaining

To assist with microscopic examination, tissue sections were counterstained. Destaining of K5 silver emulsion for radioactive sections was achieved by immersion in 70% alcohol, for up to 20 minutes. These sections were then counterstained using toulidine blue (BDH, UK), depending on the intensity of the stain required. The sections for digoxigenin ISH were dipped in Mayers haemotoxylin (BDH, UK) for ~10 seconds and then washed with water to remove any excess staining.

The sections were mounted by sequential dehydration in graded alcohols 70%, 80% and 95%, followed by xylene, a non-polar solvent that is used in fixation of animal tissues. The sections were mounted and visualised under a microscope to observe cellular localisation of mRNA signal.

2.5.2 Immunohistochemistry

2.5.2.1 Paraffin embedded tissue

Paraffin embedded tissue sections were cut at 8μm using a Leica microtome and placed onto 30% alcohol solution and floated out onto warm water. The sections were then picked up on vectabond coated slides (Vector, UK), and left to dry at 37°C for at least 48 hours. The sections were then incubated at 60°C overnight, prior to immunohistochemistry (IHC). A minimum of two sections were cut for each sample, one for IHC and the other for a haemotoxylin and eosin (H & E) stain (BDH, UK).

2.5.2.2 Tissue processing

Sections were de-paraffinised using three changes of xylene for 10 minutes, followed by rehydration using graded alcohols (100%, 90% and 70%). Any endogenous peroxidase activity was blocked using 0.3% hydrogen peroxide (H_20_2) in methanol for 10 minutes followed by washing in distilled water. Depending on the antibody used, the sections were subjected to various treatments for antigen retrieval. 10% non-fat milk in PBS was used to block any non-specific protein binding for 30 minutes at room temperature. Primary antibodies diluted in 1X PBS were then spread onto the section and allowed to incubate for 1 hour at room temperature. This was followed by three washes in PBS and the relevant secondary antibody was then applied onto the section. The sections were washed in PBS and incubated in avidin-biotin complex (ABC) (Vector, UK) for 30 minutes at room temperature followed by washes in PBS.

2.5.2.3 Visualisation procedures

The chromogen diaminobenzidine (DAB) (Sigma, UK) was used to visualise the antigen-antibody reaction. Sections were placed in 500µg/100ml PBS DAB solution that was activated using 32µl of H_2O_2 (30% solution, BDH, UK) for up to 4 minutes and the colour intensity checked. The sections were replaced in the DAB solution if darker colour intensity was required.

2.5.2.4 Histological counterstaining

Sections were counterstained with Mayer's haemotoxylin for 20-30 seconds and washed in distilled water. Finally, the sections were dehydrated through 70%, 90% and absolute alcohol and then cleared in three changes of xylene and permanently mounted with DPX (BDH, UK). Sections adjacent to the ones that had undergone tissue processing as described in 2.5.2.2 were stained for H & E, allowing a morphological assessment of the anatomical regions being assessed.

2.5.2.5 Pretreatments used for paraffin embed tissue

Tissue fixation or processing can sometimes result in antigens being obscured which can be retrieved by different treatments. For the purpose of antigen retrieval in this study, various pre-treatments were used with the different antibodies as appropriate and are described below:

Formic Acid- sections were placed in formic acid for ten minutes, followed by several washes in distilled water.

Pressure cooking- sections were placed in boiling citrate buffer (pH 6.0) for ten minutes after the maximum pressure had reached, followed by several washes in distilled water.

Formic Acid + Pressure cooking: sections were placed in formic acid for ten minutes, followed by several washes in distilled water, and then placed in boiling citrate buffer (pH 6.0) for 10 minutes as described above.

2.6 Western blot and immunoabsorption assay

Post-mortem frozen tissue was homogenised in ice-cold 1X Tris-buffered saline (Sigma, UK) containing protease inhibitor cocktail (Roche, UK) and spun at 12,000X g for 10 minutes to remove cellular debris. Protein was measured by the bicinchoninic acid (BCA) method (Biorad, UK). Resulting protein was solubilised in Laemmli buffer (4% SDS, 20% glycerol, 10% 2-mercaptoethanol, 0.004% bromophenol blue and 0.125 M Tris HCL, overall pH 6.8), and loaded onto 12% Tris-glycine gels (Biorad, UK). The gel was run in Tris-glycine-SDS running buffer for 3 hours at 125V. The proteins were transferred to hybond-P nylon membranes (GE Healthcare, UK) by electroblotting. Duplicate membranes were blocked with 5% marvel in 1X PBS-Tween 20 (0.1% v/v).

For antibody pre-absorption, the primary antibody was incubated with the corresponding peptide used to raise the antibody at a molar ratio of 1: 200 sequentially at 37°C for 1 hour and then overnight at 4°C. The solution was spun at 10,000 X g and the supernatant was used to probe the duplicate blot. Both blots were incubated overnight at 4°C followed by washing 3 X 5min washes in 1 X PBS. The blots were then probed with horseradish peroxidase (HRP)-conjugated anti-rabbit secondary antibody (Dako, UK) at 1:1000 dilution. The blots were visualised using enhanced chemiluminesence (Pierce Biotechnology, UK) and captured onto Biomax autoradiography film (Kodak, UK).

2.7 Procedures testing transcriptional regulation

Eukaryotic transcriptional regulation is a highly complex procedure where a multitude of different mechanisms occur simultaneously. Functional transcriptional assays under the influence of luciferase reporter genes are a good way of determining the transcriptional activity of the gene. Assays that identify accurate DNA:protein interactions are also an important step towards determining the role of genetic variation on the transcriptional behaviour of the gene.

2.7.1 SH-SY5Y cells and nuclear lysates

The SH-SY5Y human neuroblastoma cell line was obtained from the European collection of cell cultures (ECACC), and seeded from a split sub-confluent culture at 1x1,000-1x10,000 cells/cm² as recommended by ECACC. The culture medium used for plating and incubating cells was DMEM High Glucose with L-glutamine (Sigma, UK containing FBS (Gold Heat inactivated EU approved, PAA Laboratories) and penicillin/streptomycin antibiotics (Sigma, UK). The cells were incubated at 37°C in 100% relative humidity and 5% carbon dioxide ($CO_{2)}$. The culture medium was changed approximately every two days.

Cells were propagated and allowed to reach a confluency of 70-80%, prior to being sub-cultured at a ratio of 1:5, using the following protocol. The process involved aspirating existing culture medium from the cells and addition of 10ml of warm HBSS (without Ca^{2+} and Mg^{2+}, PAA laboratories) to each plate which was then aspirated after the cells had been rinsed. The cells were dislodged using 2ml of 0.25% Trypsin EDTA solution (Sigma, UK) and incubated in 5% CO_2 at 37°C for 5 minutes. The plate was then tapped to dislodge the cells, and 5ml of culture medium was then added to the plate. The media was then triturated to break up the cell clumps and transferred to a 15ml falcon. The plate was then rinsed with further 5ml of culture medium which was then transferred to the 15ml falcon already containing the cells. The cells were then centrifuged at 1,200 rpm for 5 minutes and the supernatant was removed and discarded. The cells were then resuspended in 5ml of culture medium, diluted accordingly for seeding and growth in subsequent culture flask. Alternatively, the cells were resuspended in lysis buffer to extract nuclear lysates. Protease inhibitors (Roche, UK) were added from a concentrated stock to the lysis buffer as recommended by the

manufacturers. It should be noted that this procedure is for growing cells in a 10 cm plate or a T75 flask. Therefore, for preparation of nuclear lysates, cells were propagated in 3 X T175 flasks, with appropriate scale-up of reagent volumes.

A packed cell volume of up to 50µl (100mg) was needed to extract nuclear lysates using the NE-PER nuclear and cytoplasmic extracting reagents from Pierce Biotechnology (UK). Please see the manufacturer's instructions for using the kit. The lysate concentration was measured using the BCA assay kit (Pierce Biotechnology, UK), against a standard curve generated by serial dilutions of 10mg/ml bovine serum albumin (BSA). The nuclear lysates were aliquoted and stored at -80°C until further use.

2.7.2 Electrophoretic mobility shift assay (EMSA)

Electrophoretic mobility shift assays (EMSAs) can determine the binding between DNA and proteins within regulatory regions. The assay is based on the premise that compared to unbound DNA, complexes of DNA and protein migrate through a gel much slowly. The migration rate of the bound DNA further slows down if an additional protein binds to the multi-protein complex.

2.7.2.1 Probe annealing

In order to investigate DNA:protein interactions, nuclear proteins (e.g. transcription factors) need to bind to double stranded DNA. For this purpose, complementary nucleic acids (oligonucleotide probes) need to be annealed together. Stocks of oligonucleotide probes were prepared at a concentration of 1-100 pmol/µl in a Tris buffer containing salt (10mM Tris, 1mM EDTA, 50mM NaCl) at pH 8.0. The oligonucleotide probes (labelled with biotin) were mixed and annealed in 1:1 ratio at a concentration of 1pmol/µl at 95°C for 5 minutes. A thermocycler was used for this procedure, and was programmed so as to gradually reduce the heat (-1°C/cycle), until the annealed probes reached room temperature. This minimises the formation of secondary structures. The annealed probes were aliquoted and stored at -20°C until further use.

2.7.2.2 EMSA procedure

The LightShift Chemiluminescent EMSA Kit (Pierce Biotechnology, UK) was used to detect DNA:protein interactions. The annealed probes with binding site of interest labelled with biotin were incubated with the SH-SY5Y nuclear extract as per the manufacturer's instructions. The reaction was then subjected to gel electrophoresis on a 6% TBE gel (Invitrogen, UK) in 0.5 % TBE buffer and transferred onto a nylon membrane (BioBond plus nylon membrane, Sigma, UK) at 60 V over 1-2 hours, or as instructed by the manufacturer. The membrane was cross-linked for 10-15 minutes (face down) on a transilluminator at 6 J/cm^2. The biotin end-labelled DNA was detected using the streptavidin-horseradish peroxidase conjugate and the chemiluminescent substrate. This was exposed onto an X-ray film for 2-5 minutes depending on the signal intensity required.

2.8 Bioinformatics and other web based resources

2.8.1 Ensembl, NCBI and UCSC

The Ensembl genome browser (http://www.ensembl.org/) and the National Centre for Biotechnology information (NCBI) (http://www.ncbi.nlm.nih.gov) are publicly available resources for genetics and molecular biology. Nucleotide sequences, population frequencies, and also transcript sequences are some of the many invaluable data that can be retrieved from these resources. They also contain web based bioinformatics programs such as basic local alignment search tool (BLAST), that are essential in searching and retrieving homologous sequences to the gene of interest.

The University of California Santa Cruz genome browser (UCSC) (http://www.genome,ucsc.edu) is also a publicly available web resource that provides the reference sequence and working draft assemblies for a large collection of genomes. It is especially useful for annotating information such as the locus position, genetic variation, polymorphic repeats, cross-species conservation and structural variation.

2.8.2 HapMap

High-density SNP genotype data in a total of 270 individuals from four different populations was used to create the International HapMap project (HapMap). The populations include 30 CEPH (Centre Humain d'Etude du Polymorphisme) trios (families from Utah, US of Western European origin), 45 unrelated Chinese individuals, 30 trios from the Yoruba people of Nigeria and 45 unrelated individuals from Japan. This is a web based resource (http://www.hapmap.org/) that allows the population genotype data to be analysed for haplotypic diversity of the population of interest. This resource was routinely used to identify tag SNPs for candidate gene association studies.

2.8.3 Transcription factor binding site (TFBS) prediction

TRANSFAC is a repository that contains data on transcription factors, their experimentally-proven binding sites, and regulated genes. The online tool PROMO predicts DNA:protein interaction using the TFBS predicted in TRANSFAC database to construct specific binding site weight matrices for TFBS prediction (Messeguer et al. 2002). The PROMO algorithm can be accessed at:

http://alggen.lsi.upc.es/cgi-bin/promo_v3/promo/promo.cgi?dirDB=TF_8.3&calledBy=alggen

2.8.4 Image processing

Image J is a free web-based image processing program developed by National Institute of Health (NIH). This program was routinely used to mark the total area of section in order to convert the image pixels into area per mm^2.

2.9 Statistical analysis in population genetics studies

2.9.1 Hardy-Weinberg Equilibrium

Hardy-Weinberg equilibrium (HWE) is the stable frequency distribution of genotypes in a population if mating is assumed to be random. In the absence of mutation, migration, natural selection or random drift, the allelic frequencies for a bi-allelic polymorphism with alleles A and a, will be p and q, which equal to 1. The stable frequency of genotypes will be p^2, 2pq and q^2. In a case-control association study, the expected numbers for HWE can be calculated and compared to observed genotypes of the population. Deviations from HWE can be identified

through a chi-squared test. Determination of HWE deviations in case and control populations was routinely made using an online tool (FINETTI) offered by the Institute of Human Genetics, Technical University Munich, Germany. The statistical significance was set at $P < 0.05$ for significant deviations. The statistical tests Pearson chi-square (χ^2) goodness -of –fit, Log likelihood ratio chi-square (Llr) and an Exact test are used to test deviations from expectations (HWE) in FINETTI, and these tests for association are adapted from a previous study (Sasieni 1997). The online program is available at http://ihg2.helmholtz-muenchen.de/cgi-bin/hw/hwa1.pl.

2.9.2 Linkage disequilibrium analysis and tagging SNPs

Linkage disequilibrium (LD) is a non random association of two or more loci in a haplotype block, where they segregate more frequently than would be expected by chance alone. Two measures have been proposed to evaluate the marker pairwise LD value: D' and r^2. An association probability of D' value 0.0 between two markers shows independent allele assortment whereas a value of 1.0 shows complete linkage between the two. Therefore, genotyping one would accurately predict the allelic state of the other. However, the other pairwise LD measure of r^2 takes the allele frequency of each locus into account and to obtain a LD value of 1.0 using r^2, the allele frequency of the two locus' should also be the same. For the purpose of creating LD maps in this study, the more stringent pairwise measure of r^2 was used. The LD plots were routinely obtained from a Caucasian data dump available through the International HapMap Project web page (www.hapmap.org) and Ensembl (www.ensembl.org). The bioinformatics software Haploview functions as a SNP haplotype analysis suite that can analyze LD patterns in genetic data and estimate haplotype frequencies. This software was used to select the SNPs that could 'capture' up to 95% of the common genetic variation across the region (r^2= 0.80), termed tag SNPs (tSNPs), and is available at: http://www.broadinstitute.org/haploview/haploview.

2.9.3 Odds ratio

The odds ratio (OR) is a way of comparing whether the probability of a certain event is the same for two groups. In terms of case-control association studies, this is interpreted as the ratio of odds of having a particular allele (or genotype) in the case group divided by the odds of having the allele (or genotype) in the control group. The 95% confidence interval (CI) for the OR's are always estimated as the OR calculation is based purely on a sample of the population. For interpretation, an OR of 1 implies that the allele (or genotype) is equal in both groups; an OR > 1 (and lower bound of CI no less than 1) implies significant risk in the case group; whereas an OR < 1 (and upper bound of CI less than 1) implies protection of the allele (or genotype) towards the case group. The OR and 95% CI's were calculated using the same online tool (FINETTI) as was used for HWE http://ihg2.helmholtz-muenchen.de/cgi-bin/hw/hwa1.pl.

2.9.4 Statistical packages used

2.9.4.1 Data analysis

SPSS (version 14) and STATA^{tm} $_{10.0}$ (StataCorp, USA) software were routinely used to perform parametric, non-parametric analyses and frequency probability tests. Specific tests are described in the individual chapters. GraphPad PRISM software (USA) was also occasionally used for the production of graphs.

2.9.4.2 Corrections for multiple comparison of tests

During hypothesis testing, the null hypothesis (H_0) assumes that there is no difference between the factors. Any difference between the factors is attributable to chance, and a significance test will indicate a 'statistically significant' association between the factors with a probability of α, which is the cut off value for significance and usually placed at 0.05. Therefore, if n is the independent associations (or number of comparisons) that are examined for statistical significance, then the probability that at least one of them will be found statistically significant is $1 - (1 - \alpha)^n$, if all n of the null hypothesis are true (Rothman 1990). For example, if n is 20 and α is 0.05, then the probability of finding at least one statistically significant comparison is 0.64.

Increasing the number of comparisons also increases the number of potentially 'significant' results that negate an otherwise correct null hypothesis. Therefore, correcting for multiple comparisons is essential to avoid false-positives or type I errors. Traditionally, the Bonferroni procedure has been used to correct for false-positives in multiple comparisons. However, this procedure is considered to be ultra-conservative on true statistical significance. Therefore, improved procedures based on Bonferroni have now been introduced, and include methods such as the step-up Simes' threshold (Simes 1986).

The step- up Simes' algorithm examines the *P*-values in order, from largest to smallest, and sets a threshold cut off. Once a *P*-value is found that is small according to the criterion based on α (0.05) and the *P*-value's position in the list, then that *P* -value and all smaller *P*-values are rejected. The step- up Simes' algorithm was used to correct for multiple comparisons in this thesis where statistical significance was observed.

Chapter 3

3 Screening of G2019S mutation in sub-Saharan African, Middle- Eastern and Eastern European populations

3.1 Introduction

The *LRRK2* G2019S mutation has a population specific frequency, and the highest carrier rates for the mutation have been reported for North African Berber subjects at a frequency of 34% (95% CI 25.8-42.5) for idiopathic PD (IPD) and 41% (95% CI 21.5-64.3%) for familial PD (FPD) subjects (Lesage et al. 2005a; Lesage et al. 2006). This is followed by Ashkenazi Jews who report a frequency of 18.3% (95% CI 11.9 – 26.4%) in IPD and as high as ~30% in FPD subjects (Ozelius et al. 2006). As detailed in Table 1.2 of chapter 1, a high frequency of the G2019S mutation is also found amongst populations from the Iberian Peninsula.

The worldwide incidence rate of PD has been suggested to vary by ethnicity, and differences in the frequency of PD-related mutations or other common genetic variation has been suggested to play a role in this (Van Den Eeden et al. 2003; Djarmati et al. 2004; Tan et al. 2004; Li et al. 2005). For example, the G2019S mutation has been found to be most common in North Africa where a crude incidence rate of PD at 4.5 per 100,000 (Libya) is much lower in comparison to the crude incidence rate in Europeans which can vary from 10-26 per 100,000 (Twelves et al. 2003) (see Table 1.2 for worldwide frequencies). This has led to the suggestions that "*The identification of populations with low and high mutation prevalence may allow future clinical trials to focus on neuroprotection or possibly disease prevention in LRRK2 carriers"* (Papapetropoulos et al. 2008). As such, estimating the precise frequency of G2019S mutation in unaffected subjects from populations at risk would permit for a genetic test better suited to the needs of a particular ethnicity, and therefore, allow for a better disease management.

A worldwide G2019S carrier rate frequency in unaffected subjects has been estimated at <1% (N= 14, 886) (Healy et al. 2008) (see Table 1.2 in chapter 1), but a higher proportion of unaffected carriers have been reported in North African Berbers and

Ashkenazi Jews. Amongst the North African populations, a frequency of 1-2% has been reported in control subjects from Algeria (Lesage et al. 2006; Hulihan et al. 2008). A more comprehensive screening of G2019S mutation in various North African populations identified an overall carrier rate of 2.18% (95% CI 0 - 3.35) amongst healthy North African Arab subjects (N= 597), in comparison to European populations (1 in 1550) (N= 3100) (Change et al. 2008) (see Table 3.1). The study also reported an elevated proportion of 3.31% (1 in 46) (95% CI 0.46- 6.17%) in unaffected subjects of Moroccan Berber origin whereas non- Berber Moroccans were identified as having a slightly lower proportion at 1.96% (95% CI- 0- 4.65%). Amongst the other North African populations, the reported proportions were 2.13% (95% CI 0-4.51%) in Algerians, 1.57% (95% CI 0 – 3.74%) in Tunisians, and 1.32% (95% CI 0-3.88%) in Libyans (Change et al. 2008). See Table 3.1 for a summary of these G2019S mutation frequency in North African populations.

Another population that has a high frequency of the G2019S mutation is the Jewish population, specifically the Ashkenazim among them. Ozelieus et al. (2006) reported a frequency of 1.3% (95% CI 0.34- 3.2%) in their Ashkenazi Jewish control population. Subsequent studies have demonstrated a G2019S mutation frequency of 1.4- 2.4% amongst the unaffected Ashkenazim (see

Table 3.2), (Ozelius et al. 2006; Clark et al. 2006; Eblan et al. 2006; Orr-Urtreger et al. 2007; Healy et al. 2008). Amongst the non- Ashkenazi Jewish population, a lower carrier rate of 0.4%-1.4% has been suggested, with no G2019S mutation carriers being reported for Yemenite and Iraqi Jews (Orr-Urtreger et al. 2007; Change et al. 2008). However, a relatively high frequency of 2.55-2.7% (CI 0.34 - 4.76% CI) in Sephardi Jews originating from Morocco and Djerba-Tunisia has been identified, which is comparable to the carrier rates of Ashkenazi Jews (2.2%) and even non-Jewish subjects of Moroccan (not Berber) and Tunisian origins (1.96% and 1.57%, respectively) (Eblan et al. 2006; Orr-Urtreger et al. 2007; Change et al. 2008). See

Table 3.2 for a summary of the G2019S mutation frequency in different Jewish ethnicities.

	Population	*IPD (N)*	*FPD (N)*	*Controls*
(Lesage et al. 2005a; Lesage et al. 2006)	*North Africa*	41% (49)	37% (27)	*1% (151)*
(Ishihara et al. 2007)	*Tunisia*	*N/A*	42% (91)	*N/A*
(Lesage et al. 2007)	*Algeria*	*N/A*	*14% (6)*	*N/A*
(Warren et al. 2008)	*Tunisia*	*N/A*	42% (91)	*N/A*
(Lesage et al. 2008)	*North Africa*	34% (119)	41% (17)	1.5% (66, Algerians)
(Hulihan et al. 2008)	*Tunisia*	30% (238)	*N/A*	2% (371)
(Change et al. 2008)	*Total North Africa* *(Moroccan Berbers* *Morocco* *Algeria* *Tunisia* *Libya)*	*N/A*	*N/A*	2.18% (597) 3.31% (151) 1.96% (102) 2.13% (141) 1.57% (127) 1.32% (76)

Table 3.1: Summary of G2019S carrier rates in populations from North Africa. IPD: idiopathic PD; FPD: familial PD; (N): the total number of samples genotyped for the G2019S mutation in the study; N/A= not available. Unless otherwise stated all the samples used for the G2019S mutation frequency for controls were unaffected subjects.

	Population	*IPD (N)*	*FPD (N)*	*Controls or non-PD patients*
(Ozelius et al. 2006)	*Ashkenazi Jews*	13.3% (83)	29.7% (37)	1.3% (317)
(Saunders-Pullman et al. 2006)	*Ashkenazi Jews*	*N/A*	*N/A*	1.4% (143) Dementia patients
(Clark et al. 2006)	*Ashkenazi Jews*	7.7% (155)	26.1% (23)	2% (98)
(Eblan et al. 2006)	*Ashkenazi Jews*	*N/A*	*N/A*	2.2% (45) Gaucher disease patients
(Deng et al. 2006)	*Ashkenazi Jews*	*10.7% (28)*	*N/A*	*N/A*
(Pchelina et al. 2006)	*Ashkenazi Jews*	*0.6%*	*3.9%*	*0%*
(Orr-Urtreger et al. 2007)	*Ashkenazi Jews* *Total non-Ashkenazi Jews: (Bulgaria, Syria, Morocco & Iraq)*	*14.8% (344)* *2.7% (112)*	*N/A*	*2.2% (500)* *0.4% (957)* *(1.6% (125 Bulgarian)* *0.25% (400 Morocco)* *0% (300 Iraq))*
(Djaldetti et al. 2008)	*Ashkenazi Jews* *Yemenite Jews*	*12.7% (96)* *0% (63)*	*N/A*	*N/A*
(Change et al. 2008)	*Sephardi Jews (Morocco & Djerba-Tunisia)*	*N/A*	*N/A*	1.4% (361) 2.55% (196)

Table 3.2: Summary of G2019S carrier rates in Jewish populations. IPD: idiopathic PD; FPD ; familial PD; (N) :the total number of samples genotyped in the study; N/A= not available. Unless otherwise stated all the samples used for the G2019S mutation frequency for controls were unaffected subjects.

3.1.1 Haplotypic studies and origins of G2019S mutation

The presence of G2019S mutation in various populations over the world has resulted in many studies attempting to describe its origins through haplotypic analysis. A common ancestral haplotype known as the European- Middle Eastern North African (MENA) has been identified in North African, Jewish and European populations, and has been shown to contain the G2019S mutation (Lesage et al. 2005b; Kachergus et al. 2005; Goldwurm et al. 2005; Warren et al. 2008; Bar-Shira et al. 2009).

The high frequency of G2019S mutation in Ashkenazi Jews (13.3% IPD and 29.7% FPD), and North African Arabs (40.8% IPD and 37% FPD) has led to the hypothesis that the common founder originated in the Middle East (Lesage et al. 2006; Ozelius et al. 2006). A likelihood- based haplotype approach in the study of 6 families of North African and European origins identified a minimal haplotype of 60 kb, and estimated that the families shared a common ancestor back in the 13th century (Lesage et al. 2005a). However, due to a high carrier rate of G2019S mutation in Ashkenazi Jews, this timeframe seemed unlikely as the historical migration patterns suggest that the Ashkenazim and Arab populations had already separated a long time ago (Colombo 2000b; Niell et al. 2003; Zabetian et al. 2006a). Therefore, in order for these populations to share a common ancestor for G2019S mutation, the event must have taken place long before the estimated 13th century.

Zabetian and colleagues (2006) were able to replicate the findings that G2019S mutation originated in a common founder of European-MENA populations, by typing 22 families of European and Ashkenazi Jewish ancestry (Zabetian et al. 2006a). They also showed that the initial estimate of 60 kb (as predicted by Lesage and colleagues, 2005b) for the ancestral haplotype was too short, and reasoned that the use of unstable marker(s) contributed to this. These subjects were tested for 25 markers spanning 9 Mb across the LRRK2 region, and two ancestral haplotypes were identified. Haplotype 1 (European-MENA haplotype) was shown spanning 243 kb, and a distinct haplotype 2 spanned 6Mb. Haplotype 2 could be differentiated from the

minimal core region of the haplotype 1 (European-MENA) by using five intragenic and one extragenic marker. The European-MENA haplotype 1 was predominant in the Ashkenazi Jewish and European families (total of 19 families), whereas the geographic origin of haploytpe 2 was suggested to be from Western Europe (3 families). Using the likelihood method, Zabetian and colleagues were able to estimate that families with the common European-MENA haplotype shared a common ancestor ~2,250 (95% CI 1,375-2,600) years ago, when Jewish and Arab populations lived in close proximity.

This estimated timeframe also coincides with the Jewish exile from the Middle East in 586 BCE to 70 CE. Warren *et al*., also identified a haplotype in 38 Tunisian and 2 North American families with the G2019S mutation, and confirmed it as being consistent with European-MENA haplotype (Warren et al. 2008). Using a 25 year intergenerational interval, they estimated that the families shared a common founder 2,600 years ago (95% CI- 1950- 3850). These timeframes have resulted in the speculation '*that G2019S might be of Phoenician origin, rather than Arabic, dating from the founding of ancient Carthage in 814 BC*' (Farrer et al. 2008). A recent study estimated that Ashkenazi Jewish carriers of European-MENA haplotype share a common ancestor who lived 61 generations ago (95% CI 52 - 72), and at a 25 year intergenerational interval this would approximate to 1,525 years (95% CI- 1,300 - 1,800 years) ago (Bar-Shira et al. 2009). Amongst Jewish peoples, the G2019S mutation has been identified in Ashkenazim and Sephardim, but so far has not been reported in Yemenite or Iraqi Jews. Yemenite Jews form a distinct ethnic Jewish group, and Iraqi Jews are descendents of the original Babylonian Jews (586 BCE) (Motulsky 1995). This suggests that the mutation was acquired by Sephardim and what were to become Ashkenazim after the initial divergence of Jewish groups. However, the G2019S European-MENA founder haplotype has also been shown in non-G2019S mutation carriers of Han Chinese origins (Tan et al. 2007c).

Another haplotype has been reported in a subset of G2019S positive PD patients in Russia, suggesting that the *LRRK2* G2019S mutation in the Russian subjects had arisen independently on different chromosomes (Illarioshkin et al. 2007). However,

this haplotype differed from the European-MENA founder haplotype at one SNP only which is indicative of a mutational event. A distinct founding haplotype associated with the G2019S mutation has also been reported in a Japanese family that fails to share alleles with the European-MENA haplotype, suggesting separate founding effects for this mutation in the Japanese (Zabetian et al. 2006b). Interestingly, a recent study reported a G2019S affected PD patient from Turkey carrying the haplotype identified in the Japanese (Pirkevi et al. 2009). Taking into account the long migrations of the Turkic people into and possibly beyond Central Asia, led the others to suggest common ancestry for the Japanese-Turkic haplotype. However, only a single PD Turkish patient was identified with the Japanese haplotype, and a larger and genetically heterogenous Turkish PD cohort is needed before strong recommendations of common ancestry for the Japanese-Turkic haplotype can be made.

3.1.2 Populations chosen for this study and the rationale behind it

The presence of G2019S mutation with such varying frequencies in different geographical locations would suggest that the spread of this mutation is strongly associated with human migration patterns (Tomiyama et al. 2006). Despite rare instances of *de novo* occurrence of the mutation and haplotypes associated with it, the current literature supports a Middle-Eastern, and more specifically a North African Berber origin for the *LRRK2* G2019S mutation.

North African Berbers belong to the coastal Mediterranean regions of the African continent, and modern populations of Mediterranean origins are the remnants of genetic and cultural impact of contact amongst different civilisations over centuries (e.g. Phoenicians, Carthaginians, Greeks, Romans and more recently the Arabs) (Bosch et al. 2000; Bosch et al. 2001; Zalloua et al. 2008). Genetic relationships between populations from Africa and the Arabic sub-continent would be informative of population movements and its impact on the Mediterranean demography. For this purpose, the chapter reports an investigation into sub-Saharan African, Arabian and

Eastern Mediterranean populations that might have contributed to the genetic makeup of the G2019S founding populations.

3.1.2.1 Sub-Saharan Africa

Chaabani and Cox reported that the Berbers are native to North Africa and "*that Berber ancestors could have presented a geographical and genetic intermediate population between European and sub-Saharan populations*" (Chaâbani & Cox 1988). A south to north migration from sub-Saharan into Northwest Africa, and from North Africa into the Iberian Peninsula would have resulted in a substantial gene flow between the populations (Flores et al. 2000; Esteban et al. 2004). This would explain the relatively high frequency of G2019S mutation in the Iberian Peninsula compared to other European regions. The frequency of G2019S mutation has been explored in healthy subjects of North African Berbers, Mediterranean and many European origins but has not been thoroughly investigated in the sub-Saharan populations, although small numbers of PD samples (N= 57) and controls (N= 51) from Nigeria have been screened for *LRRK2* mutations (Lesage et al. 2005a; Okubadejo et al. 2008a). The prevalence of PD in sub-Saharan Africa (Nigeria 10 per 100,000; Ethiopia 7 per 100,000) is much lower than in Arabs (27-43 per 100,000), and is also in contrast to the prevalence rates reported in North Africa (North East Libya 31.4 per 100,000) (Ashok et al. 1986; Osuntokun et al. 1987; al Rajeh et al. 1993; Twelves et al. 2003; Okubadejo et al. 2006). The prevalence rates of PD in African Americans has been reported as being similar to the Caucasian population (Copiah County, Mississipi), but almost fivefold higher than in Nigerians after adjustment for age (Schoenberg et al. 1988; Okubadejo 2008b). However, a meta-analysis of PD prevalence in populations of African ancestry identified a lower prevalence in Africans and African Americans compared to Caucasians, but concluded that additional work was needed before making any speculations on ethnic differences in PD (McInerney-Leo et al. 2004). Since age still remains the biggest risk factor for PD, the low crude prevalence of PD in Western and Eastern African countries could be attributed to a life expectancy of less than 57 years of age (Okubadejo et al. 2006). G2019S positive carriers are reportedly rare in Asia, but the identification of the common European-

MENA haplotype amongst Han-Chinese population, suggests that the haplotype itself is much older than the G2019S mutation (Tan et al. 2007c). Estimating the G2019S mutation frequency in sub-Saharan African populations would add to the genetic data associated with the Berber origins of this mutation. Additionally a high carrier rate of mutation in African populations would also be indicative of the mutation being more ancient than the current prediction of ~2,250 years by Zabetian and colleagues.

3.1.2.2 Middle Eastern/Semitic populations

Middle-East is a vast region that includes the Arabian sub-continent as well as the Arab countries of North Africa. Arabian sub-continent on the other hand, refers to the Arabian Peninsula as well as the regions of Eastern Mediterranean Basin/Asian Minor. Therefore, the populations mentioned in this section will be described as such.

3.1.2.2.1 Arabian Peninsula

Berbers are considered to be the original inhabitants of North Africa, and have historically come into contact with various other communities as a result of population expansion, invasions and trade navigations. Invasions from the Arabian Peninsula which started in 7th century CE, eventually led to the consolidation of Islamic rules, religion, language and culture in North Africa around the 11th century (Esteban et al. 2004). The large geographical area of Arabic countries stretches over two continents, and ethnic groups such as Berbers, Kurds and selected African communities form part of the Arabic society (estimated at 315 million) (Benamer et al. 2008). Despite the term "Arab-Berber" used by Tunisians/North African Berbers to define their ethno-cultural identity, Berbers are thought to have retained their own languages and culture and tend to practice endogamy (Benamer 2008). Therefore, it would be imprudent to assume that the Arabs and Berbers in North Africa are a genetically homogenous population. The majority of G2019S mutation data relating to Arabic populations have been limited to the Arab-Berbers of the North African coast, and these frequencies cannot account for a vast majority of Arabic people that might not share an immediate genetic identity with the Berbers. Therefore, a precise estimate of the G2019S mutation frequency in populations from the Arabian

Peninsula is important for two reasons. Firstly, it would allow the design of appropriate pre-symptomatic genetic testing in Arab populations which has a PD prevalence rate of 27-43 per 100,000 (Benamer et al. 2008). Secondly, the possible contribution of Arabs to the origins of G2019S mutation in the Berber genetic pool, if any at all could be addressed.

3.1.2.2.2 Eastern Mediterranean Basin/ Asia Minor

Regions in Eastern Mediterranean Basin, such as Syria, Jordan, and Israel/Palestine are also included in the Arabian sub-continent, and various civilisations have contributed to the complex genetic makeup of the ethnicities around the Mediterranean Basin (Zalloua et al. 2008). As mentioned previously, the G2019S mutation has a high carrier rate amongst Ashkenazi Jews and North African Berbers, with isolated cases identified amongst Sephardi Jews along the Mediterranean (Morocco, Syria, Bulgaria and Turkey) (Orr-Urtreger et al. 2007). Similarly, mutations in the MEFV gene that cause Familial Mediterranean Fever (FMF) also show a non-uniform distribution around the Mediterranean Sea. This disease is prevalent amongst ethnically diverse populations of Mediterranean origins, but the highest incidence is reported in non-Ashkenazi Jews, Armenians, Arabs (not from the Peninsula) and Turks (Touitou 2001; Yilmaz et al. 2001; Papadopoulos et al. 2008). Incomplete penetrance of MEFV mutations has been suggested as a possible cause for a milder phenotype observed in other populations from the Mediterranean basin, such as Syrians, Ashkenazi, Iraqi and Iranian Jews (Gershoni-Baruch et al. 2001; Mattit et al. 2006; Papadopoulos et al. 2008). The mutation V726A shows a high prevalence in Ashkenazi (7.4%), Iraqi Jews (12.8%) and Arabs (7.3%) but is absent in Moroccan Jews, and the mutation M694V is absent in Ashkenazi Jews but is present in the other ethnicities (Moroccan Jews 11.1%, Iraqi Jews 2.9% and Arab 0.6%) (Gershoni-Baruch et al. 2001). Both these mutations, like the G2019S mutation in *LRRK2* are associated with specific haplotypes in populations that have been separated for many centuries (Aksentijevich et al. 1999). The Jewish diaspora, the dispersal of Armenian nation, the Byzantine Empire, Arab conquests, and the Ottoman dominance have been suggested to have had an impact (unclarified as yet)

on the historical background of MEFV (Papadopoulos et al. 2008). Taking into account the geographical distribution of the G2019S mutation, it is feasible that it follows a pattern similar to the MEFV mutations.

Farrer and colleagues (2008), recently hypothesised that the high frequency of G2019S mutation in populations of Mediterranean heritage is due to a Phoenician origin of the mutation (Farrer et al. 2008). Phoenicians or Canaanites were ancient coastal dwelling people, and like the Hebrews (founders of Jewish population) and Arabs are considered to be of ancient Semitic roots. The Phoenician civilisation was centred in the ancient Canaan, with its heartland along the coastal regions of Lebanon and Syria, and also comprising Israeli/Palestinian territories. Phoenicians had a sea-faring and trading culture, and being the dominant sea power established many cities in the Mediterranean Basin (Farrer et al. 2008). For example, Carthage was an ancient city established by Phoenicians in Tunisia, and G2019S mutation is observed at a high frequency in Tunisians. Therefore, assessing the G2019S mutation carrier rate in other populations with Phoenician heritage would add to the current hypothesis of the mutation being Phoenician. For this purpose, populations from the Eastern Mediterranean/Asia Minor that historically lived in close proximity, and were ethno-culturally similar to the predicted founding populations were also included in this study.

3.1.2.3 Jewish diaspora: Middle-East and Eastern Europe

Jewish people have their origins in the Middle East, but the extensive geographical movement (and instances of extreme genetic isolation) associated with the Jewish diasporas have resulted in different Jewish communities. According to Risch and colleagues, three founder events in the Jewish population history have contributed to different Jewish ethnicities, and if a generation is defined as 25 years then the ancestral Jewish population of middle-east was founded >100 generations ago; the second founder effect resulted in Jewish populations of Central Europe ~ >50 generations ago, and the third founder effect ~12 generations ago gave rise to the

eastern European Jewish community, commonly termed as the Ashkenazim (Risch et al. 2003).

The Jewish diaspora which refers to the settling of scattered colonies of Jews outside the areas of Jerusalem and vicinity, began in 6th century BCE (563 BCE) whereupon the Jews of the ancient Kingdom of Judah were exiled to Babylon (modern day Iraq and Iran). The descendents of these Babylonian Jews and other surrounding regions came to be known as the Oriental Jews (Motulsky 1995). Upon conquest of Jerusalem in 301 BCE, Jews moved towards Egypt, and by 63 BCE Jewish communities had also settled in the present day areas of Syria, Turkey, Greece, Italy and North Africa. The destruction of the second temple in ~70 CE ensured that the Jewish diaspora continued, and the Bar Kokhba revolt in 135 CE led to a significant destruction of Jewish communities in Egypt and North Africa, resulting in Jews moving up north to southern Europe, and settling primarily in Spain. These Jews of Spain who came to be known as Sephardi Jews, were later exiled from Spain in 1492, when many resettled along the North African coast, and in Italy, Egypt, Palestine and Syria (Motulsky 1995; Colombo 2000a). Although it is not clear when Jews first arrived in Europe, there are records of Jews in France and Germany dating from the 4th century CE, and it is only from 10th century CE that the group destined to become Ashkenazim moved from Southern Europe into Rhineland (France/Germany) (Motulsky 1995). These Central European Jewish ancestors of the Ashkenazi community faced increasing persecution in Western and Central Europe, and began to flee to Eastern Europe in the 11th century. By the 18th century, most Eastern European Jews were exiled to particular districts which became known as the 'Pale of settlement' and included much of the present day Lithuania, Belarus, Ukraine, Poland and parts of Western Russia.

Currently, 80% of the world Jewry is of Ashkenazi descent, and this community also reports the highest frequency of G2019S mutation amongst Jewish groups (Motulsky 1995; Ozelius et al. 2006). Few studies have investigated the G2019S mutation frequency in Oriental Jews, and so far no carriers have been reported amongst this specific Jewish ethnicity (Orr-Urtreger et al. 2007; Djaldetti et al. 2008). Isolated

non-Ashkenazi Jewish cases have been identified in Morocco, Bulgaria, Turkey and Syria (Orr-Urtreger et al. 2007). This observation along with the high levels in Northern African Berbers has led to the suggestions that G2019S mutation was acquired by the Jewish community after the split from the Babylonian Jews. In comparison to Ashkenazi Jews (18-30%) fewer G2019S mutation carriers amongst Sephardi Jews (2.7%) have been reported, despite them having lived in a closer proximity to the North African Berbers for a longer period of time, than the Ashkenazi ancestors.

The high prevalence of G2019S mutation and shared haplotypic region in North African Berbers and Ashkenazi Jews, indicates admixture between the different populations. Although rare, G2019S mutation has been shown to occur *de novo.* Haplotypes distinct from the common European-MENA ancestral haplotype have also been identified in European populations (Zabetian et al. 2006a; Zabetian et al. 2006b; Illarioshkin et al. 2007). The high frequency of G2019S related PD in Ashkenazi Jews compared with non-Ashkenazi Jews does raise the issue of whether this mutation was present in the Ashkenazi ancestral population (European Jews 9^{th}-13^{th} century), and later spread to various European populations, or whether it was an original European mutation introduced into the Ashkenazi Jewish population whilst living in the eastern 'Pale of Jewish settlement'.

3.1.3 Hypothesis and specific aims

In this chapter, I wished to investigate the hypothesis that the G2019S mutation might have arisen in the neighbouring populations of North African Berber and Ashkenazi Jews. The specific questions addressed in this chapter were whether G2019S mutation is common in: a) sub-Saharan Africa, and as such is older than the currently predicted estimate; b) populations from the Arabian peninsula, and whether they were responsible for introducing the mutation into the Berber genetic pool; c) Mediterranean/Asia Minor populations with Phoenician heritage that either lived in close proximity or shared a similar diaspora distribution to Jewish populations. d) Eastern European populations, and whether G2019S mutation in Ashkenazim arose prior to or after its establishment as an ethnic Jewish group in Eastern Europe?

To address these questions, healthy subjects from various populations were screened for the G2019S mutation. Subjects from sub-Saharan African communities of Ethiopia and Bantu speaking tribes were genotyped in order to address the question of whether the mutation is older than the current estimates. Populations from the Arabian Penninsula, including Kuwaiti Arabs and Bedouins from Jordan and Saudi Arabia, would have had a considerable impact on the North African Arab Berber culture during the Islamic conquest of the region in 7th century CE, and as such were included in the study. Estimating the carrier rate in a diverse spread of ethnic mixes around the Eastern Mediterranean Basin and Asia Minor such as Syrians, Druze, Israeli and Arab Palestinians, and Armenians would allow us to estimate the frequency of G2019S mutation in ethnic groups that lived in close proximity to Jewish populations prior to the diaspora and would allow us to address the question of Phoenician origin for the mutation. Screening non-Ashkenazi Jewish subjects (Morocco, Iraq and Iran), and non-Jewish eastern European subjects (Ukraine and Belarus) would also address the question of whether G2019S mutation was introduced into the Ashkenazim prior to or after their establishment, respectively.

3.2 Methods and Materials

3.2.1 DNA source- collaborative study

The DNAs of a total of 2,450 healthy subjects (non- Parkinsonian when examined) from 13 different ethnicities were included in this study to test for the presence of G2019S mutation. These DNAs were obtained as part of a collaborative study with Dr. Neil Bradman (The Centre for Genetic Anthropology, UCL). The individuals were unrelated at the paternal grandfather level, and were involved in previous genetic and anthropological studies at The Centre for Genetic Anthropology (Thomas et al. 2002; Behar et al. 2003; Ingram et al. 2007; Veeramah et al. 2008). Table 3.3 reviews the numbers in the ethnically diverse mix of populations. A total of 731 samples from sub-Saharan Africa, with 366 samples from the Bantu speaking tribes (Cameroon, Ghana, Democratic Republic of Congo, Malawi and Mozambique), and 365 from Ethiopia were genotyped for the mutation. From the Arabian Peninsula, a total of 214 Arabs were obtained from Kuwait, and 108 Bedouins from Jordan, Saudi Arabia and Israel. From the Eastern Mediterranean Basin/Asia Minor, 75 Syrians, 39 Druzes, 141 Israeli Arabs and 19 Palestinian Arabs and 308 Armenians were genotyped. The number of non-Ashkenazi Jewish subjects studied was 337 of Moroccan (186), Iraqi (46) and Iranian (105) Jewish origins, and were obtained from Sheba Medical Centre, Israel. 270 healthy subjects were genotyped from Ukraine and 248 from Belarus.

3.2.2 DNA extraction and Taqman genotyping

Genomic DNA was extracted from buccal swab (at The Centre for Genetic Anthropology) using standard DNA extraction protocols. Refer to section 2.2.1 in chapter 2 for DNA extraction procedure. The *LRRK2* G2019S (6055G >A) mutation was detected using a pre-designed Taqman Assay C_63498123_10 probe (NCBI Reference rs34637584) (section 2.3.5). The context sequence for Taqman probes for wild-type (G) allele: 5’ [FAM]CAT CAT TGC AAA GAT TGC TGA CTA C**[G]**G CAT TGC TCA GTA CTG CTG TAG AAT; and mutant (A) allele 5’[VIC] CAT CAT TGC AAA GAT TGC TGA CTA C**[A]**G CAT TGC TCA GTA CTG CTG TAG AAT

Figure 3.1: A schematic representation of the populations used in this study.

Non-Ashkenazi Jews; Arabian Peninsula; Asia Minor; Eastern Europe; Africa- Sub-Saharan and Bantu speaking tribes.

3.2.3 Statistical analysis

The *P*-value of a hypothesis test is the probability (calculated assuming null hypothesis is true) of observing any outcome as extreme or more extreme than the observed outcome, with extreme being the direction of the alternative hypothesis. An exact hypothesis test (for binomial random variables) was performed to estimate the true probability of success using a one-sided test of null hypothesis (H_0) versus the alternative hypothesis (H_A): $p< 0.01$. In other words, the probability of the observed frequency given the assumed frequency under the null hypothesis (H_0) is 0.01 (at 1% level).

The 95% confidence intervals (CIs) for the observed proportions were estimated, and Fisher's exact test was also performed to examine any significant association between the populations and the number of G2019S mutation carriers identified in them. All these tests were performed using the STATA^{tm} $_{10.0}$ (StataCorp, USA) software for statistical analysis.

3.3 Results

The results in this chapter demonstrate that *LRRK2* G2019S mutation carriers are rare amongst selected populations of sub-Saharan African, non-Jewish Middle Eastern (Arabian Peninsula, Eastern Mediterranean Basin and Asia Minor), non-Ashkenazi Jewish and Eastern European ancestry. Only 2 positive G2019S heterozygous carriers were identified out of a sample of 2,485 subjects from these populations (see Table 3.3). No G2019S mutation carriers were observed in over 700 subjects from the sub-Saharan Africa, thereby indicating that the mutation might have arisen after the human migrations out of Africa. The mutation was also not identified in 379 unaffected subjects from the Arabian Peninsula, but the two positive G2019S mutation carriers are of Middle Eastern origin. This observation along with a lack of G2019S mutation in over 500 subjects from Eastern Europe, remains neutral on the Middle-Eastern origin for the mutation as has been previously predicted.

3.3.1 Proportion of G2019S positive carriers in the Middle- East

3.3.1.1 Non-Jewish Middle East

A G2019S positive heterozygote carrier was observed in the Syrian population (1 in 75), and a proportion of .0133 (exact binomial 95% CI .00033- .07206) was calculated. A one-sided exact hypothesis test was performed to test whether the observed sample proportion is different to a hypothesised proportion of 1% (0.01).

N	Observed k	Expected k	Assumed *p*	Observed *p*
75	1	0.75	0.01	0.01333

(N = number of observations, K= events, *p* = frequency)

Pr (k <= 1) = 0.827092 (one-sided test).

Under an exact hypothesis test, (H_0) is $p = 0.01$ versus (H_A): $p < 0.01$, i.e. the probability of observing one or fewer events assuming the H_0 is true (i.e. $p = 0.01$). The *P* - value for this proportion is 0.827. Therefore, the null hypothesis cannot be

rejected, and implies that the observed proportion (p = 0.01333) is either similar to the assumed proportion of 0.01, or the sample size is too small.

When the other two other populations in the Eastern Mediterranean Basin (Druze and Israeli/Palestinians Arabs) are also taken into account (n = 271), the proportion of G2019S positives is calculated at .00369 (exact binomial 95% CIs 0.0000934 - 0.0203870). This proportion is not different from the hypothesised proportion of 0.01 (H_A: $p < 0.01$; P value 0.245, one sided test), indicating that frequency of G2019S mutation in Eastern Mediterranean Basin could be 1%. However, when all the non-Jewish Middle Eastern populations are taken into account (n = 901), the proportion of 0.0011093; (exact binomial 95% CIs: 0.0000281- 0.0061682) under the hypothesis testing is significantly different to 1% (H_A: $p < 0.01$; P value 0.0012, one sided test).

3.3.1.2 Non- Ashkenazi Jewish Middle East

Amongst the non-Ashkenazi Jewish population, only one subject from Morocco (N= 186) was identified as being heterozygous for the G2019S mutation. Using the hypothesis test for a sample size of 186 (Moroccan Jews), the proportion is 0.0053763 (exact binomial 95% CIs 00013 - .02959). This proportion was similar to the hypothesised proportion at the 1% level (H_A: $p < 0.01$; P value 0.444, one sided test). When the Iraqi and Iranian Jews were included in the analysis (total n = 335), similar results were obtained for the observed proportion (.0029851; exact binomial 95% CIs .0000756 - .0165187; H_A: $p < 0.01$; P value 0.151, one sided test).

Fisher's exact test for comparisons between non-Ashkenazi Jewish (n = 335) and Eastern Mediterranean Basin/Asia Minor (n = 582) identified no major difference between these two Middle-Eastern sub-populations (P -value- 0.597, one sided).

3.3.1.3 Middle – East

The other populations from the Middle-East included in this study were from Arabian Peninsula (n = 322) and Armenia (n = 308). For the populations from the Peninsula no G2019S mutation carriers were observed, and under the hypothesis test, this proportion (0-.0113908- one sided, 97.5% CI) was found to be significantly different

from the assumed frequency of 1% (H_A: $p < 0.01$; *P* value 0.0039, one sided test). A similar result was observed for the population from Armenia (0 - 0119054- one sided, 97.5% CI; H_A: $p < 0.01$; *P* value 0.0045, one sided test).

The proportion of G2019S mutation carriers in all Middle- Eastern populations genotyped in this study (2 in 1,236) was calculated at .00162 (exact binomial 95% CI 0.000196 - 0.0058329). This proportion (p <0.01) was significantly different from 1% (H_A: $p < 0.01$; *P* value 0.00368, one sided test). A small sample size of the two populations with G2019S positive carriers in comparison to the sample size of other Middle-Eastern populations could have contributed to the observed frequency of < 1%.

3.3.2 No G2019S mutation carriers in sub-Saharan African and Eastern European populations

No G2019S mutation carriers were observed in sub-Saharan African and Eastern European populations either, and the proportions (p <0.01) tested significant at *P* - values of 0.0006 and 0.0055, respectively, indicating that G2019S is not common in either of these populations. Fisher's exact test to compare all the sub-populations of Middle-Eastern origins (n = 1,236) to the sub-Saharan African populations (n = 731), also indicated no differences between these populations either. Since the G2019S mutation is only occasionally observed in the Middle-Eastern populations investigated in this study, a larger sample size would be needed for a conclusive result.

The rarity of this mutation demonstrates that *LRRK2* G2019S mutation is not common in selected Middle Eastern populations amongst whom North African Berbers and Jews have lived. The lack of this mutation in sub-Saharan Africa and Arabian Peninsula also suggests that the mutation was not acquired by the Berbers from the sub-Saharan African or the Arabian genetic pool. It is also not prevalent in selected Eastern European populations amongst whom Ashkenazi Jews lived.

	Population	Country	Sample numbers (*n*)	G2019S mutation carriers
Sub-Saharan Africa	**1**	Bantu speaking	366	0
	2	Ethiopia	365	0
	Total		***731***	
Middle- East				
Arabian Peninsula	**3**	Kuwait	214	0
	4	Bedouin	108	0
	Total		***322***	
Eastern Mediterranean Basin	**5**	Syrians	75	1
	6	Druze	36	0
	7	Israeli/Palestinian	160	0
	Total		***271***	
Asia Minor	**8**	Armenia	***308***	0
Non-Ashkenazi Jewish	**9**	Morocco	186	1
	10	Iraq	46	0
	11	Iran	103	0
	Total		***335***	
Eastern Europe	**12**	Ukraine	270	0
	13	Belarus	248	0
	Total		***518***	

Table 3.3: The LRRK2 G2019S mutation is not common in selected populations used in this study. The table represents the number of G2019S positive healthy heterozygous carriers identified in 2,485 samples in over 13 populations representing sub-Saharan Africa, Middle-East, and Eastern Europe.

3.4 Discussion

The G2019S mutation has been identified as a major genetic cause of autosomal dominant PD in Europeans, Ashkenazi Jews and populations of North African Berber origins (Healy et al. 2008). The highest frequency of this mutation has been reported in North African Berbers and Ashkenazi Jews. The coastal geographical location inhabited by the North African Berbers, and the extended diaspora of the Jewish people has meant that both these groups have come into contact with various other ethnicities, and as such have developed a rich genetic and cultural legacy. For this purpose, the main objectives of this chapter were to estimate the carrier rate frequency of G2019S mutation in populations that have contributed to the genetic makeup of Berbers or Ashkenazi Jews either through having lived in close proximity, or being ethno-culturally similar. The G2019S carrier rate frequency was estimated in the populations to address the specific questions of whether this mutation a) is associated with sub-Saharan African population, b) or whether it is associated with Semitic populations from the Arabian sub-continent (Peninsula and Eastern Mediterranean Basin/Asia Minor), c) whether the mutation in Ashkenazim arose prior to or after its establishment in Eastern Europe?

A total of 2,485 samples were screened for G2019S mutation from populations obtained from sub-Saharan Africa (Ethiopia and Bantu speaking), Arabian Peninsula (Kuwait and Bedouins), Eastern Mediterranean Basin/ Asia Minor (Israel/Palestine, Jordan, Syria and Armenia), non-Ashkenazi Jews (Morocco, Iraq and Iran), and Eastern Europe (Ukraine and Belarus).

The lack of G2019S positive carriers in a relatively large sample size of sub-Saharan African (n = 731), is indicative of the mutation (in North African Berbers) not being acquired from sub-Saharan Africa, and suggests that it arose after the earlier human migrations out of Africa. G2019S mutation was also not observed in subjects from the Arabian Peninsula (n = 322) either, although two heterozygote carriers of Middle Eastern ancestry were identified. One of the positive samples was of Syrian descent and the other sample was identified as Moroccan Jewish. Based on such few positive

samples, it cannot be conclusively said whether the mutation was brought over to the West (North Africa) by invading Arabs, and as such we cannot dispute the proposed North African Berber origins for G2019S mutation in the literature. This study also demonstrates that G2019S mutation is not common in selected Eastern European populations amongst which the ancestors of modern day Ashkenazim lived, nor is it prevalent in selected non- Jewish groups that followed a similar diaspora to the Jewish population (Armenia, *n* = 307). The identification of G2019S mutation in a Moroccan Jew, indicates that the mutation was present in the ancestral Ashkenazi community, prior to settlement in the 'Pale'. The study demonstrates that G2019S mutation is not common amongst healthy subjects in these selected populations but the two positive subjects lend support to the published data of a Middle-Eastern origin for G2019S mutation, and it being acquired by Jewish communities whilst living amongst other Middle Eastern populations. Unfortunately, a lack of parental DNA for these two G2019S positive subjects meant that the haplotype phase could not be resolved. Therefore, no haplotype analysis could be performed to determine whether these subjects contained the common European-MENA haplotype.

Semitic origins of G2019S mutation

Orr-Urtreger and colleagues, screened PD patients (*n* = 23) of Moroccan Jewish origin and did not identify any G2019S positive carriers. However, a recent study looking at the spread of G2019S mutation in healthy subjects from Sephardic Jewish population reported a proportion of 1/37 amongst Moroccan Jews (total *n* = 147). The higher proportion of G2019S mutation carriers in the Sephardi Jewish populations as reported by Change and colleagues could be due to an unidentified Ashkenazi ancestry of those samples. Only one Moroccan Jew was identified as having the mutation in this study, and in such a small sample set (*n* = 186), it is not unlikely that this positive could be due to statistical fluctuation. Regardless of this, the presence of G2019S mutation in healthy carriers amongst Sephardi Jewish populations supports a Middle-Eastern origin for the mutation. No G2019S positive carriers were identified in healthy Jewish subjects from Iraq and Iran. This is in agreement with a previous

study that also did not observe G2019S mutation in PD (*n* = 19), or in healthy Jewish subjects of Iraqi origin (*n* =300) (Orr-Urtreger et al. 2007). This is not surprising as the Iraqi and Iranian Jews are thought to be descendents of the original Babylonian Jews who settled in Iraq and Iran after the destruction of first temple, and therefore, could represent a different gene pool to the Jewish communities that settled in the Iberian Peninsula and North Africa (Sephardi) or Eastern Europe (Ashkenazi) (Motulsky 1995; Colombo 2000a).

The other G2019S positive samples reported in this study is of Syrian origin and a previous study identified a PD affected Syrian Jew who was also positive for G2019S mutation (Orr-Urtreger et al. 2007). Therefore, it cannot be discounted that the one positive Syrian subject in this study is a migrant into the general Syrian population and does indeed have Jewish heritage. However, a lack of information regarding the ancestral heritage of the positive Syrian sample in this study does not allow us to address this question. The G2019S mutation has recently been hypothesised to be of Phoenician origin, and for that purpose populations around the Eastern Mediterranean Basin (Syrians, Israeli/Palestinians, and Druze), were screened for the mutation. Even though one positive carrier was identified amongst Syrians, due to the overall low number of Syrians (*n* = 75), the data presented in this chapter remains inconclusive on this matter.

The two samples identified in this chapter both belong to coastal Mediterranean regions that were probably frequented by Phoenician navigators and traders. The observed proportion of positive samples was identified as not being different from 1% for their respective ethnicities, (Syrian and Moroccan Jews). However, the small sample size (Syrian, *n* = 75; Moroccan Jews, *n* = 186) should be taken into account. In contrast, these proportions were found to be < 1% when other populations from the Middle-Eastern group were included. Also no difference was observed in the proportions of G2019S mutation carriers in either of these sub-groups using a Fisher's exact test. Estimating the G2019S carrier rate in a larger sample set in Syrian and Moroccan Jews would address the questions of the true proportion in these ethnicities, and also the differences between the two groups. Screening samples from

Lebanon and Palestine for G2019S mutation would also add to the genetic data of the Phoenician origin for this mutation.

Amongst European populations, the highest carrier rate of G2019S mutation has been reported in the regions of Iberian Peninsula (excluding Ashkenazi). However, nothing has so far been reported in the Southern Spanish regions (Andalusia) or in Gibraltar. These regions were under North African Moroccan dominion for a considerable amount of time and a bidirectional genetic admixture between these populations has been demonstrated (Bosch et al. 2001). Therefore, it is feasible that the mutation could have arrived in the Iberian Peninsula prior to the invasion by North Africans in 711 CE. The coastal surroundings of these regions make it likely that they presented important trading routes across the Mediterranean coast for sea-faring peoples like the Phoenicians. In order to achieve an accurate carrier rate of G2019S mutation in the Iberian Peninsula, and to further provide evidence for the Phoenician origins of the mutation, populations from Andalusia and Strait of Gibraltar, and other populations with Phoenician heritage, (for example, Syrians, Lebanese and Palestinians) should be screened for the G2019S mutation

G2019S mutation in Ashkenazi versus non-Ashkenazi Jews: selective heterozygotic advantage or founder effect?

The G2019S carrier rates in various Jewish ethnicities have been described as high in the Ashkenazim, followed by Sephardim. So far no incidences for the G2019S mutation have been reported in Yemenite or Iraqi/Iranian Jews. The highest frequency of G2019S mutation amongst unaffected Ashkenazi Jews has been reported at 2.4%, and an overall carrier rate of 1.4% was reported for unaffected Sephardim, but a frequency comparable to Ashkenazi was reported in Sephardi subjects specifically from Djerba Tunisia (2.55%) (Change et al. 2008).

There has been some debate as to the stability of certain microsatellite makers used in the estimation of the common ancestral haplotype (Zabetian et al. 2006a). However, current data in the literature suggests an ancient founder for the G2019S mutation in

the Middle-East, a result of which has been the identification of this mutation in various ethnicities of the Middle-East.

Founder effects can either result from the establishment of a new population from individuals derived from a much larger population (true founder event), or a population bottleneck which is an extreme reduction in size. In either case, certain alleles maybe found at a higher frequency than they were originally present at prior to the founder event or bottleneck, and small population sizes under strong genetic drift can also result in these alleles achieving an even higher frequency. One way of achieving high frequency by chance (genetic drift) is the rapid growth of a population from a limited group of founders, and Ashkenazi Jewish populations have gone through severe bottlenecks and growth periods in its history (Risch et al. 1995). The demographic history, extreme population contractions and rapid expansions, (and endogamous culture) have resulted in many genetic diseases that are unique to the Ashkenazi Jewish population. For example, Tay-Sachs; Niemann-Pick type C (NPC); mucolipidosis type IV and Gaucher disease are all common to the Ashkenazim, and result from a defect in sphingolipid storage (Zlotogora et al. 1988). Initially the high frequency of these autosomal recessive diseases was attributed to selective heterozygote advantage, where selection was considered to have favoured heterozygous carriers of alleles affecting lipid metabolism and storage (possibly protecting or atleast providing resistance to tuberculosis) (Motulsky 1995). However, founder effects and genetic drift on the alleles rather than heterozygote advantage have now been shown to account for the lipid storage diseases in the Ashkenazi population (Risch et al. 1995; Risch et al. 2003). *LRRK2* related PD results in autosomal dominant form of the disease like idiopathic torsion dystonia, breast cancer type 1 and 2 in Ashkenazi Jews, and the heterozygote advantage applied for recessive disorders is not applicable here (Risch et al. 1995; Risch et al. 2003; Slatkin 2004). Therefore, specific founder effects resulting from the dynamics of population contractions and growth in the Eastern European Jewish population, could explain the high frequency of this mutation in the Ashkenazim versus the other Jewish

ethnicities, and future studies investigating specific founder-effect hypothesis in Ashkenazi Jews needs to be performed (Slatkin 2004).

Furthermore, the G2019S mutation has been identified in Jewish subjects with dementia and Gaucher's disease (Saunders-Pullman et al. 2006; Eblan et al. 2006). In addition to the kinase, GTPase and multi-protein complex activities, LRRK2 protein may also have an affinity for lipids or lipid-associated proteins, and has been recently to regulate synaptic vesicle endocytosis (Biskup et al. 2006; Hatano et al. 2007; Shin et al. 2008). This has led to the suggestion that LRRK2 protein may play a role in the regulation of membranous intracellular structures. Even though the *LRRK2* G2019S has shown not to be associated with Gaucher disease patients (Eblan et al. 2006), it would nevertheless be interesting to investigate whether this mutation plays a role in other neurological lipid associated disorders that might be common among the Ashkenazi Jews.

Conclusion

This report shows that G2019S mutation is not present in selected populations of sub-Saharan Africa, and Arabian Peninsula. Therefore, this data remains neutral on the predicted North African Berber origin for G2019S mutation. The data also suggests that G2019S mutation in Ashkenazi Jews has not been acquired from the local populations amongst whom the ancestors of modern day Ashkenazim lived, but supports the published data of the mutation being acquired prior to the beginning of Jewish diaspora. The identification of two positive G2019S mutation carriers: a Moroccan Jew and non-Jewish Syrian also support the published data of Middle-Eastern origin for the mutation. However, it should be noted that both of these samples are from the coastal regions of the Mediterranean Basin, therefore, a Phoenician or a Carthaginian origin of the mutation cannot be conclusively ruled out as yet.

Chapter 4

4 A morphological study of LRRK2 mRNA and protein expression in the human brain

4.1 Introduction

In order to understand the effects of LRRK2 dysfunction on PD pathogenesis, it is necessary to establish its cellular expression (both transcriptional and translational). LRRK2 mRNA and protein expression in CNS, lungs, kidney, spleen and leucocytes, has led to the suggestion that this gene plays an important physiological role (Zimprich et al. 2004b; Giasson et al. 2006, Biskup et al. 2006; Li et al. 2007; Westerlund et al. 2008a). Mouse embryonic development studies have suggested that *LRRK2* is not an essential gene for development, and *in-situ* hybridisation (ISH) studies have shown that LRRK2 mRNA in the mouse embryonic brain is first detected at postnatal day 8 (P8), and is expressed in striatum at constant levels during aging (Westerlund et al. 2008a). However, immunoblot assays have shown that the LRRK2 protein is detectable at E17 (Biskup et al. 2007), rises continuously and eventually peaks at the post-natal age of P60 (Li et al. 2007). This apparent discrepancy in the time course of the detection of mRNA and protein has led to the suggestions that LRRK2 mRNA is present in low quantities in the brain.

4.1.1 LRRK2 mRNA expression

The mRNA expression of LRRK2 was initially suggested to have a specific localisation to the dopamine innervated areas in the nigrostriatal dopamine system with a definitive distribution in the medium spiny neurons of striatum (Galter et al. 2006; Melrose et al. 2006). Lack of mRNA in dopaminergic (DAergic) neurons of the substantia nigra (SN) led the authors to conclude that the gene was expressed in the dopamine innervated neurons as opposed to dopamine synthesising neurons. However, a comprehensive regional study investigating the cellular localisation of LRRK2 mRNA in rodent brain found that it did indeed localise to the SN in addition to various other regions in the brain (Simón-Sánchez et al. 2006). The localisation of LRRK2 mRNA to the SN and cortex was confirmed in post-mortem human brain and

also in subsequent mouse studies (Taymans et al. 2006; Higashi et al. 2007a; Higashi et al. 2007b). Studies examining the cellular expression of LRRK2 mRNA are summarised in Table 4.1.

The use of oligonucleotide probes versus riboprobes for ISH studies could be the major cause in the discrepant results observed in relation to LRRK2 mRNA distribution (Galter et al. 2006; Melrose et al. 2006; Simón-Sánchez et al. 2006; Taymans et al. 2006; Higashi et al. 2007a; Higashi et al. 2007b). Owing to the length of the riboprobes (up to 200 bp), a stronger and a more specific hybridisation to mRNA molecules is formed in comparison to the oligonucleotide probes which are traditionally less than 50 bp. Initial studies that used oligonucleotide probes did not identify LRRK2 mRNA in SN, whereas the studies that used riboprobes demonstrated LRRK2 mRNA presence in dopamine synthesising and innervated areas (Galter et al. 2006; Melrose et al. 2006; Simón-Sánchez et al. 2006; Taymans et al. 2006). Subsequent studies identified LRRK2 mRNA in SN and striatal regions using radioactive oligonucleotide probes in rodents and post-mortem human brain (Higashi et al. 2007a; Higashi et al. 2007b). However, an exposure time of 10 weeks was needed to identify LRRK2 mRNA signal, further indicating that it might be present as a low copy number mRNA in the post-mortem human brain (Higashi et al. 2007b).

Study reference	Tissue Type	mRNA quantitation	Regional mRNA expression established
(Galter et al. 2006)	Rat Human	Radioactive oligonucleotide	High expression in medium spiny neurons of STR (none in cholinergic); moderate to weak in CTX and negative in SN.
(Melrose et al. 2006)	Mouse	Radioactive oligonucleotide and qRT-PCR	High expression in STR, CTX and OT, moderate in CBM and ON; weak in HIP and SBM; negative in the MB and BTM (but qRT-PCR revealed low mRNA expression in these regions).
(Simón-Sánchez et al. 2006)	Mouse	Digoxigenin riboprobe	High expression in STR, CTX, HIP, AMG, SN; moderate to low in OT, THA, brainstem, granule cell layer (CBM); negative in GP and PrN (CBM).
(Taymans et al. 2006)	Rat and mouse	Digoxigenin riboprobe	High expression in STR, CTX, OT, HIP, AMG, PrN, moderate in THA, HT and BTM; weak in SN, GP, LC and granule cell layer (CBM).
(Miklossy et al. 2006)	Human cells	qRT-PCR	Primary cultured human oligodendrocytes, astrocytes and microglia. LRRK2 expression was also found in human neuroblastoma cell lines.
(Higashi et al. 2007a)	Mouse	Radioactive oligonucleotide	High expression in CTX and STR; moderate in HIP and CBM; weak in HT, THA and SN.
(Westerlund et al. 2008a)	Mouse Human	Radioactive oligonucleotide	Expression in STR, HIP and CTX. In mice, LRRK2 mRNA was also identified in sensory and sympathetic ganglia. SN not included in study.
(Higashi et al. 2007b)	Human	Radioactive oligonucleotide	High expression levels detected in SN, STR and CTX.

Table 4.1: Summary of studies investigating LRRK2 mRNA localisation in the brain. AMG: amygdala, BTM: brainstem, CBM: cerebellum, CTX: cortex, GP: globus pallidus, HIP: hippocampus, HT: hypothalamus, LC: locus coeruleus, MB: midbrain, OT: olfactory tubercle, ON: olfactory nuclei, SBM: subiculum, PrN: Purkinje neurons, SN: substantia nigra, STR: striatum, THA: thalamus.

Such contradictions in the literature could be attributed to the inherently sensitive and fragile nature of mRNA molecules. In addition, post-mortem studies performed on human tissue may be compromised by the peri-mortem changes that affect the integrity of mRNA expression. Post-mortem delay has been shown not to critically affect the quality and preservation of mRNA for long term storage (Barton et al. 1993; Kingsbury et al. 1995; Ervin et al. 2007). Ante-mortem events, on the other hand, can have a huge impact on mRNA preservation in the tissue, and agonal state has been reported to be influential in post-mortem preservation of mRNA molecules (Kingsbury et al. 1995). Hypoxia caused due to respiratory distress (or longer terminal phase), results in anaerobic glycolysis within the brain, leading to an increasing lactate concentration in the tissue (Harrison et al. 1991). This lowers the pH of the tissue leading to a detrimental effect on mRNA preservation. Tissue pH has therefore, come to be regarded to as an important marker for terminal hypoxia in the absence of detailed clinical information for agonal state (Kingsbury et al. 1995). A combination of degraded post-mortem tissue and possible insensitive ISH probes could have contributed to the previous discrepancies reported in cellular localisation of LRRK2 mRNA in the human brain, thereby warranting further investigation.

4.1.2 LRRK2 protein expression

LRRK2 protein has consistently been demonstrated to have a constitutive neuronal expression in the mammalian brain. Regional quantitative differences in LRRK2 protein levels using immunoblot assays have been demonstrated in the rodent brain (Biskup et al. 2006; Taymans et al. 2006; Melrose et al. 2007). Immunohistochemical studies have corroborated regional variation in the LRRK2 protein levels in the human brain too (Miklossy et al. 2006; Higashi et al. 2007b; Alegre-Abarrategui et al. 2008). LRRK2 protein has been shown to localise not only to neuronal populations in the brain, but also weakly to astrocytes and microglia (Miklossy et al. 2006). The presence of LRRK2 in Lewy bodies (LBs) has also been frequently described, although the inconsistencies in the reports have made LRRK2 localisation to LBs a controversial issue (reviewed in (Santpere & Ferrer 2009)).

Just as the inconsistencies relating to LRRK2 mRNA localisation can be attributed to the type of hybridisation probe and the quality of tissue used, the discrepancies in LRRK2 localisation to LBs can also be attributed to the antibody used in the study. Polyclonal antibodies have been produced that recognise the LRRK2 protein, and despite recognising a ~250 kDa band for the protein in mammalian brain homogenates (Biskup et al. 2007), variations have been reported in LRRK2 immunoreactivity between the antibodies (reviewed in (Santpere & Ferrer 2009)). It has been widely reported that for identifying the presence of LRRK2 in LBs, the best results are achieved with the antibodies raised against the C- and N- termini, and antibodies raised against the central domains of LRRK2 do not detect the protein in LBs (see Table 4.2 for a summary on the antibodies that have been used to localise LRRK2 in LBs). The possibility of LRRK2 functional domains folding in a complex manner in LBs could result in antigen retrieval treatments not being able to expose the epitopes sufficiently enough to be recognised by the antibodies raised against the core functional domains. Zhu et al (2006) used four antibodies to identify LRRK2 in LBs and reported immunoreactivity with all of them (some better than others), whereas Melrose and colleagues, used six different antibodies and did not find consistent immunoreactivity in LBs or Lewy neurites (apart from with NB300-268) (Zhu et al. 2006a; Zhu et al. 2006b; Melrose et al. 2007). Recent investigations have established that only NB300-268 antibody stains the core of perikaryal LBs, and others recognise the halo region of about 10% of LBs (Alegre-Abarrategui et al. 2008; Santpere & Ferrer 2009). Despite the fact that the presence of LRRK2 as a major component of LBs remains a contentious issue, a new C-terminal raised antibody (EB06550) has been shown to produce robust immunohistochemical results in post-mortem human brain (Alegre-Abarrategui et al. 2008).

Antibody	Epitope	Immunolabelling of α-synuclein-positive inclusions
Ab7099b, Abgent	1246-1265 Rabbit	No immunolabelling of α-synuclein immunoreactive inclusions identified in G2019S positive PD cases; sporadic PD, DLB and MSA cases (Giasson et al. 2006; Zhu et al. 2006a; Zhu et al. 2006b; Covy et al. 2006; Santpere & Ferrer 2009).
NB300-267, Novus Biological	900-1000 Rabbit	Immunolabels the halo around a proportion of LBs in sporadic PD, DLB, MSA and DLBD cases. No lewy neurites or cortical LBs observed (Zhu, Babar et al. 2006; Zhu, Siedlak et al. 2006; Covy et al. 2006; Miklossy et al. 2006; Higashi, Biskup et al. 2007; Melrose et al. 2007; Alegre-Abarrategui et al. 2008; Santpere & Ferrer 2009).
NB300-268, Novus Biological	2500-2527, Rabbit;	Immunolabels intraneuritic and perikaryal brainstem, limbic and neocortical LBs in sporadic PD, DLB, MSA and DLBD cases. Lewy neurites were also strongly stained (Zhu, Babar et al. 2006; Zhu, Siedlak et al. 2006; Covy et al. 2006; Miklossy et al. 2006; Higashi, Biskup et al. 2007; Melrose et al. 2007; Alegre-Abarrategui et al. 2008; Santpere & Ferrer 2009).
AT106, Alexis	1838-2133 Rabbit	No immunoreactivity to LBs or LNs in sporadic PD, DLB and MSA cases (Covy et al. 2006).
Ab04/11 PA0362-	2507-2527 Rabbit	No robust or consistent immunoreactivity to LBs or LNs in DLBD brains (Melrose et al. 2007). Antibody developed in- house.
AB9704 AB9682 Chemicon	*Rabbit *Sheep	No robust or consistent immunoreactivity to LBs or LNs in DLBD brains (Melrose et al. 2007). *Epitope sequences are proprietary.
JH5514 JH5517 JH5518	2500-2515 334-347 527-537 all rabbit	JH5517 stains the halo structure of brainstem LBs but is not associated with cortical LBs or LNs in sporadic PD and DLB cases (Higashi et al. 2007b). Antibody developed in-house.
EB06550, Everest Biotech	2015- 2026 Goat	Stained the halo of a minority of perikaryal and intraneuritic LBs in PD and DLB cases. (Alegre-Abarrategui et al. 2008)

Table 4.2: Summary of antibodies used for determining LRRK2 in Lewy bodies.

As described in chapter 1, LRRK2 mutations exhibit a highly complex neuropathological phenotype, and as such this protein has been suggested to play a role in synucleopathies as well as tauopathies. The prevalent G2019S mutation occurs in the kinase domain, and is associated with pure nigral degeneration and classic LB pathology (in the brainstem). Autopsy of three G2019S mutation carriers revealed nigral degeneration accompanied with nigral LBs, leading to the question of selective vulnerability of catchecolaminergic neurons to degeneration in LRRK2 mutation carriers despite the widespread expression of the protein (Giasson et al. 2006). Two of these patients showed LBs in limbic cortex, and the third had neocortical senile plaques and occasional NFTs which could be associated with the pathology of normal aging.

The G2109S mutation has been shown to increase the kinase activity of LRRK2 and enhance autophosphorylation and phosphorylation of generic substrates in *in-vitro* kinase assays, although the *in-vivo* effects of this mutation remain to be established. Even though the clinical and pathological phenotype associated with the G2019S mutation is indistinguishable from the idiopathic PD, reports have not been published detailing the expression profile of LRRK2 mRNA or protein in G2019S mutation carriers. If as the *in-vitro* data suggests that G2019S mutation increases LRRK2 autophosphorylation, it would be interesting to assess whether the mutation has a qualitative or quantitative effect on the expression profile of IPD and G2019S positive PD subjects. Any differences, subtle or otherwise in the brains of these subjects would not only highlight the mechanistic pathways but also allow for a better interpretation of the *in-vitro* and in future *in-vivo* data relating to this protein.

4.1.3 Hypothesis and specific aims

In this chapter, I wished to investigate the hypothesis that a disease phenotype could result in an anatomical and cellular expression profile of LRRK2 that is different in control and PD subjects. The specific questions addressed in this chapter were: a) what is the anatomical distribution of LRRK2 mRNA and protein in human brain; b) are there any differences in the morphological distribution of LRRK2 mRNA and protein expression in control, IPD and G2019S positive PD subjects; c) is LRRK2 protein a major component of LBs?

To address these questions, a morphological expression profile of LRRK2 mRNA and protein was determined using *in-situ* hybridisation (ISH) and immunohistochemistry (IHC), respectively. The anatomical distribution was determined using post-mortem tissue from medulla, brainstem, basal ganglia (deep grey nuclei), cerebellum, medial temporal lobe, and neocortical regions obtained from QSBB. Radioactive and non-radioactive methods were employed for the ISH procedure. A recently reported antibody EB06550 was used to determine LRRK2 immunoreactivity in post-mortem human brain, and also to establish the presence of LRRK2 in LBs.

4.2 Methods and materials

4.2.1 Tissue used

Following removal at autopsy, samples of brain tissue which had been flash frozen and stored at -80ºC or formalin fixed and paraffin embedded were obtained for *in-situ* hybridisation (ISH) and immunohistochemical (IHC) studies, respectively. The tissue was obtained from the Queen Square Brain Bank (QSBB) archive. All tissue at the QSBB is collected using ethically approved protocols, and is stored under a licence issued by the Human Tissue Authority. See Table 4.3 for a summary of subjects used in the study.

4.2.2 *In-situ* hybridisation

Frozen tissue sections from 2 controls, 1 IPD and 3 G2019S positive PD cases are summarised in Table 4.4. The tissue sections were cut at 12µm as per instructions in section 2.5.1.1 of chapter 2. Both the radioactive and digoxigenin labelled probes were prepared as described in section 2.5.1.2 (of chapter 2). The tissue preparation, hybridisation, washing and visualisation procedures are described in sections 2.5.1.3 to 2.5.1.6 of chapter 2.

Table 4.5 summarises the oligonucleotide probes used in this study. During the optimisations probes 1-4 were used for both the radioactive and non-radioactive ISH, but the digoxigenin labelled probe 3 which binds to the kinase domain of the LRRK2 gene produced the best results, and was therefore used to produce non-radioactive ISH data. Previously published oligonucleotide probes for aldolase- C and *BRI2* (Kingsbury et al. 2001; Lashley et al. 2008) were labelled using ^{35}S and digoxigenin, respectively to be used as positive controls for the ISH method being used. A dot blot was performed according to the manufacturer's instructions (Roche, UK) to determine the labelling efficiency of the digoxigenin labelled probes.

	Sex	Age	PM delay (hours)	pH	Cause of death	Pathological diagnosis	ISH study	IHC study
Con1	M	76	39.5	N/A	Cancer	Control	√	N/A
Con2	M	93	89	N/A	Old age	Control	√	N/A
Con3	F	78	23.3	6.07	N/A	Control	N/A	√
Con4	F	84	28.5	6.13	Cancer	Control	N/A	√
Con5	F	91	98.5	6.41	Old age	Control	N/A	√
Con6	F	88	11.1	5.67	Myocardial infarct	Control	N/A	√
IPD1	F	77	80	6.53	Congestive heart failure	IPD	√	N/A
IPD2	F	62	46.8	5.88	Gradual deterioration	IPD	N/A	√
IPD3	F	81	24.25	N/A	Congestive heart failure	IPD	N/A	√
G2019S-1	F	81	15.00	6.53	Bronchopneumonia	IPD (G2019S)	N/A	√
G2019S-2	F	84	32.3	5.79	Congestive heart failure	IPD (G2019S)	√	√
G2019S-3	F	80	44.4	6	Advanced PD	IPD (G2019S)	√	√
G2019S-4	F	72	24.55	N/A	Pulmonary embolism	IPD (G2019S)	√	√

Table 4.3: Summary of subjects used for in-situ hybridisation (ISH) and immunohistochemical (IHC) studies. This tissue was obtained from QSBB. Con- control, M- male, F-female, PM delay- post-mortem delay. N/A: not available.

		Con 1	Con 2	IPD 1	G2019S 2	G2019S 3	G2019S 4
Medulla	X nerve nucleus	√	N/A	N/A	N/A	N/A	N/A
	XII nerve nucleus	√	N/A	N/A	N/A	N/A	N/A
	Inferior olive	√	√	√	N/A	N/A	√
Pons	Locus coeruleus	N/A	N/A	N/A	N/A	√	√
	Pontine base	√	√	√	√	√	√
	Tegmentum	√	N/A	N/A	N/A	√	√
Midbrain	Substantia nigra	√	√	√	√	N/A	√
	IIIrd nerve nucleus	√	N/A	N/A	√	N/A	√
	Red nucleus / tegmentum	√	√	√	√	N/A	√
	Tectum	√	√	N/A	√	N/A	√
Deep grey nuclei	Caudate	√	√	√	N/A	√	√
	Putamen	√	√	√	N/A	√	√
	Globus pallidus	√	N/A	√	N/A	N/A	√
	Thalamus	N/A	N/A	√	N/A	N/A	N/A
Medial temporal lobe	Dentate fascia	√	√	N/A	N/A	N/A	√
	CA1-4	√	√	N/A	N/A	N/A	√
	Subiculum	√	√	N/A	N/A	N/A	√
	Entorhinal cortex	N/A	√	N/A	N/A	N/A	√
	Transentorhinal	√	√	N/A	N/A	N/A	√
Cerebellum	Dentate nucleus	√	N/A	√	N/A	√	N/A
	Purkinje cells	√	√	√	√	√	√
	Granule cells	√	√	√	√	√	√
Neocortices	Frontal	√	√	√	√	√	√
	Parietal	√	√	√	√	√	N/A
	Temporal	√	√	N/A	√	N/A	√
	Fusiform gyrus	√	√	N/A	N/A	N/A	N/A
	Insular cortex	√	N/A	N/A	N/A	N/A	√
	Cingulate gyrus	√	N/A	N/A	N/A	√	N/A

Table 4.4: Summary of anatomical regions obtained from controls, IPD and G2019S positive subjects for in-situ hybridisation. This tissue was obtained from QSBB. N/A: not available.

ISH Probes	Sequence 5'to 3'	Corresponding nucleotides
LRRK2 Probe 1	GTTGATAGTCAGGCTGAACAATGTCCAG LRRK2 cDNA BLAST accession: AY792511	54 –81 N-terminal
LRRK2 Probe 2	CAGGCTGTTAAGACAAGAGCTTGTGGTGCTTTGCCACCTC LRRK2 cDNA BLAST accession: AY792511	5742-5781 Kinase domain
LRRK2 Probe 3	CCGCTGATGGCAAGTTAGCAATTTTTGAAGATAAGACT LRRK2 cDNA BLAST accession: AY792511	6800 – 6838 WD40 domain
LRRK2 Probe 4	TTGTCAGTGATTGGACTGAAGACCTTAGATCTCC LRRK2 cDNA BLAST accession: AY792511. Previously published probe (Higashi et al. 2007b)	133- 144 N-terminal
Aldolase-C	CGACGCAGGGCAGTGACAGTTGCCATGGC cDNA BLAST accession: AK296053 (Kingsbury et al. 2001)	2837-2866 Positive control for radioactive ISH
BRI2	CCGCTCTTGGGCTCGTCCTTCTTGGCCTCCTTCTGGGCCAC cDNA BLAST accession: BF941808.1 (Lashley et al. 2008)	28 – 68 Positive control for nonradioactive ISH

Table 4.5: Oligonucleotide probes used for radioactive and non-radioactive ISH.

4.2.3 Immunohistochemistry

Immunohistochemistry was performed on paraffin embedded tissue sections from 4 controls, 2 IPD and 4 PD cases positive for the G2019S mutation (see Table 4.3). The antibody and pre-treatments used in this study are listed in Table 4.6. The anatomical regions cut are summarised in Table 4.7. The sections were cut at 8µm and processed as described in section 2.5.2 of chapter 2.

The anti-LRRK2/PARK8 antibody- EB06550 obtained from Everest Biotech (UK) was raised against the peptide with sequence CELAEKMRRTSV in goat. The peptide sequence of this polyclonal antibody corresponds to a region near the C terminus of the LRRK2 protein sequence according to NP_940980.2. Immunoabsorption of this antibody has been reported previously in an immunohistochemical study (Alegre-Abarrategui et al. 2008). The visualisation procedure was carried out as described in section 2.5.2.3 of chapter 2 using goat immunoglobulins (Dako, UK) at a dilution of 1:200 and choromogen diaminobenzidine.

Antibody	Source	Host	Dilution for IHC	Pre-treatments required
Anti-LRRK2/ PARK8-EB06550	Everest Biotech, Oxfordshire, UK	Goat	1 : 150	pressure cooking chapter2: section 2.5.2.5

Table 4.6: Dilution and pre-treatments used for LRRK2 EB06550 antibody in this study.

4.2.4 Western blot analysis and antigen absorption assay

In order to confirm the specificity of the EB06550 antibody, a western blot analysis using an antigen absorption assay was conducted as described in section 2.5.3 of chapter 2. Post-mortem frozen tissue from medulla was homogenised, and 10µg and 20µg of the homogenised protein was used for the assay.

		Con 3	Con 4	Con 5	Con 6	IPD 2	IPD 3	G2019S 1	G2019S 2	G2019S 3	G2019S 4
Medulla	X nerve nucleus	√	√	√	√	√	√	√	N/A	√	√
	XII nerve nucleus	√	√	√	√	√	√	√	N/A	√	N/A
	Inferior olive	√	√	√	√	√	√	√	√	√	√
Pons	Locus coeruleus	√	√	√	√	√	√	√	√	N/A	√
	Pontine base	√	√	√	√	√	√	√	√	√	√
	Tegmentum	√	√	√	√	√	√	√	√	√	√
Midbrain	Substantia nigra	√	√	√	√	√	√	√	√	√	√
	IIIrd nerve nucleus	√	√	√	√	N/A	√	N/A	√	√	√
	Red nucleus/ tegmentum	√	√	√	√	√	√	N/A	√	√	√
	Tectum	√	√	N/A	√	√	√	N/A	√	N/A	√
Deep grey nuclei	Caudate	√	√	√	√	√	√	N/A	√	√	√
	Putamen	√	√	√	√	√	√	√	√	√	√
	Globus pallidus	N/A	√	√	√	√	√	√	√	N/A	√
	Thalamus	N/A	N/A	√	√	N/A	√	√	√	N/A	N/A
	Subthalamic nucleus	N/A	N/A	√	√	N/A	√	N/A	√	√	N/A
Medial temporal lobe	Dentate fascia	√	√	√	√	√	√	√	√	√	√
	CA1-4	√	√	√	√	√	√	√	√	√	√
	Subiculum	√	√	√	√	√	√	√	√	√	√
	Entorhinal cortex	√	√	√	√	√	√	√	√	√	√
	Transentorhinal	√	√	√	√	√	√	N/A	√	√	√
	Amygdala	√	√	√	√	√	√	√	√	√	√
Cerebellum	Dentate nucleus	√	√	√	√	√	√	√	√	√	√
	Purkinje cells	√	√	√	√	√	√	√	√	√	√
	Granule cells	√	√	√	√	√	√	√	√	√	√
Neocortical regions	Frontal	√	√	√	√	√	√	√	√	√	√
	Parietal	√	√	√	√	√	√	N/A	√	√	√
	Temporal	√	√	√	√	√	√	√	√	√	√
	Fusiform gyrus	√	√	√	√	√	√	√	√	√	√
	Insular cortex	√	√	√	√	√	√	√	√	√	√
	Cingulate gyrus	√	√	√	√	√	√	√	√	N/A	N/A

Table 4.7: Summary of anatomical regions obtained from control (con), IPD and G2019S PD subjects for LRRK2 immunohistochemistry.

This tissue was obtained from QSBB**.** N/A: not available.

4.3 Results

4.3.1 LRRK2 mRNA expression

4.3.1.1 Radioactive ISH

During the course of the study, two different ISH methods were used to construct an anatomical profile of LRRK2 mRNA expression in human brain. The radioactive ISH technique was initially employed to detect the mRNA levels in this study. Emulsion autoradiography using silver stain emulsion was used for the assessment of cellular localisation of LRRK2 mRNA in post-mortem human tissue. The preliminary experiments conducted using radioactively labelled LRRK2 oligonucleotide probes produced high levels of background labelling. However, the aldolase-C (*ALD-C*) probes which served as the positive control for radioactive ISH consistently demonstrated robust ALD-C mRNA localisation (see Figure 4.1). After numerous attempts, radioactive emulsion autoradiography was rendered unfeasible to reliably detect the LRRK2 mRNA signal in post-mortem human brain tissue. Therefore, in order to generate LRRK2 mRNA expression profile a non-radioactive approach using a digoxigenin labelled oligonucleotide probe was employed for the ISH study.

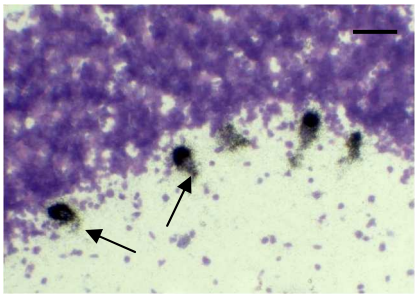

Figure 4.1: Radioactive ISH demonstrating the localisation for the positive control in the human brain. The arrows in the figure represent the localisation of radioactively labelled aldolase C (ALD-C) probe to the Purkinje neurons of the cerebellum in the human brain. The robust signal intensity was consistently observed for the ALD-C probe, whereas this level of intensity could not be achieved for any of the LRRK2 probes without significantly increasing the background levels. The scale bar represents 39µm.

4.3.1.2 Non-radioactive ISH

The findings related to the LRRK2 mRNA distribution were similar in control, IPD and G2019S positive PD subjects, and are therefore described collectively. LRRK2 mRNA was identified as having a widespread expression in a number of neuronal populations in the brain regions examined (Table 4.8). LRRK2 mRNA was found to be expressed, but not limited to the brainstem nuclei affected by α-synuclein pathology in early stages of PD progression which include the Xth nerve nucleus, locus coeruleus (LC) and DAergic neurons of the SN (see images A-D in Figure 4.2). The other brainstem nuclei where LRRK2 mRNA was shown to be localised, include the XIIth nerve nucleus and the inferior olive of the medulla oblongata, the pontine base and tegmentum, and the IIIrd nerve nucleus (Figure 4.2G), tegmentum and tectum of the midbrain (summarised in Table 4.8). The dopamine-innervated regions of caudate nucleus (Figure 4.2E) and putamen stained for LRRK2 mRNA, which was also identified in the globus pallidus and thalamus. Neurons in all regions of the hippocampal formation were found to express LRRK2 mRNA (Figure 4.2H and K), and the neuronal populations of the cortical regions examined in this study also demonstrated LRRK2 mRNA localisation (Figure 4.2F and summarised in Table 4.8). In the cerebellum, granule cell layer did not express LRRK2 mRNA, whilst clear mRNA expression was identified in the cytoplasm of Purkinje neurons (Figure 4.2I) and in the dentate nucleus (Figure 4.2J). LRRK2 mRNA expression was consistently observed in the vascular smooth muscle of blood vessels of different sizes (Figure 4.2L). LRRK2 mRNA hybridisation signal was successfully reduced by diluting the labelled probe with unlabelled excess at different concentrations (Figure 4.2N), thereby confirming the specificity of the oligonucleotide probe used in this study. The positive control for the BRI2 mRNA also allowed us to check the integrity of mRNA preservation for each subject (Figure 4.2M).

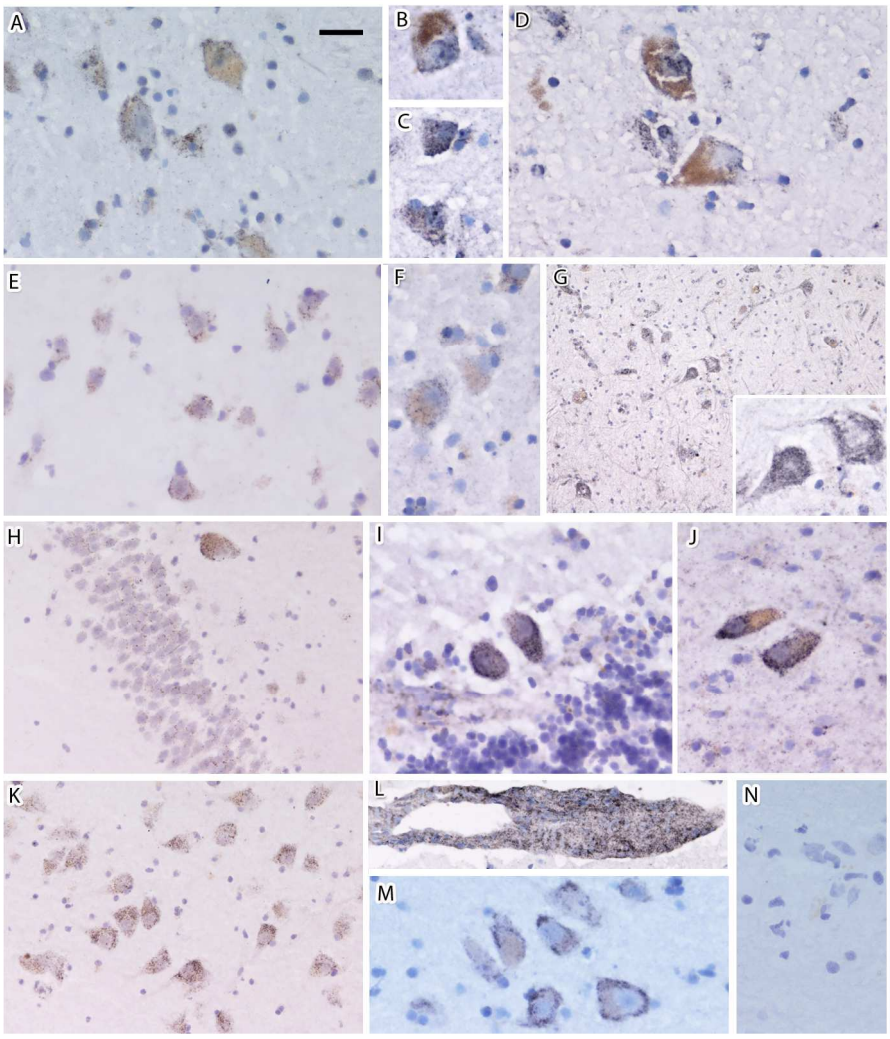

Figure 4.2: Anatomical localisation of LRRK2 mRNA using non-radioactive ISH. Neuronal expression of LRRK2 mRNA in controls and G2019S positive PD cases is represented. Regions particularly vulnerable to α-synuclein pathology and neurodegeneration in PD are represented in images A- E; A) Xth nerve nucleus of the medulla (control), B) and C) neurons of the LC (G2019S), and D) melanised DAergic neurons of the SN (control) E) caudate nucleus (G2019S). LRRK2 mRNA was also detected in F) neocortical regions (represented by parietal cortex) (control), G) IIIrd nerve nucleus of the midbrain (and inset) (control), H) dentate fascia (G2019S), I) Purkinje neurons (control), and J) dentate nucleus of the cerebellum (control) and K) CA4 neurons of the hippocampal formation (G2019S). In addition, LRRK2 mRNA expression was observed in L) smooth muscle (G2019S). M) Neuronal localisation of BRI2 mRNA was treated as positive control. N) Negative control for the LRRK2 mRNA. The scale bar in A represents 20µm in images A, B –D, E, F, inset in G, I, J, L and M; 39µm in images H, K and N; 78µm in G.

4.3.2 Distribution of LRRK2 protein in the brain

The distribution of the LRRK2 protein was demonstrated using the commercially available polyclonal antibody EB05660 (raised against the c-terminus of the protein). Prior to the IHC, the specificity of the antibody was investigated using an antigen absorption assay (Figure 4.3).

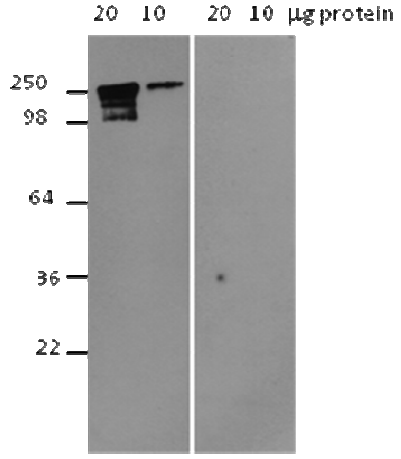

Figure 4.3: Western blot analysis showing specificity of LRRK2 EB06550 antibody and antigen absorption by >10 fold molar ratio of the peptide. Lysates were prepared from post-mortem human tissue from the (medulla). The first panel shows EB06550 accurately identifying ~ 250 kDa LRRK2 protein at 10 µg and 20µg of protein loading. This signal is obliterated when a molar excess of the antigen is added to the antibody prior to incubation with the blot.

An IHC study was performed on four controls, two IPD cases and four PD cases with the LRRK2 G2019S mutation. The LRRK2 protein like the mRNA was also found to be expressed in anatomical regions of the brain examined in this study (summarised in Table 4.8). Since no difference was observed in the morphological distribution of the LRRK2 protein amongst the three groups, the results are therefore described collectively.

Region	Sub- Regions	LRRK2 mRNA	LRRK2 protein
Medulla	Xth nerve nucleus	√	√
	XIIth nerve nucleus	√	√
	Inferior olive	√	√
Pons	Locus coeruleus	√	√
	Pontine base	√	√
	Tegmentum	√	√
Midbrain	Substantia nigra	√	√
	IIIrd nerve nucleus	√	√
	Red nucleus/ Tegmentum	√	√
	Tectum	√	√
Deep grey nuclei	Caudate nucleus	√	√
	Putamen	√	√
	Globus pallidus	√	√
	Thalamus	√	√
	Subthalamic nucleus	N/A	√
Medial temporal lobe	Dentate fascia	√	√
	CA2/3/4 neurons	√	√
	CA1 neurons	√	√
	Subiculum	√	√
	Entorhinal cortex	√	√
	Transentorhinal cortex	√	√
	Amygdala	N/A	√
Cerebellum	Dentate nucleus	√	√
	Purkinje neurons	√	√
	Granule cell layer	X	√
Neocortical regions	Frontal cortex	√	√
	Parietal cortex	√	√
	Temporal cortex	√	√
	Insular cortex	√	√
	Fusiform gyrus	√	√
	Cingulate gyrus	√	√

Table 4.8: Summary of LRRK2 mRNA and protein distribution in post-mortem human brain tissue. LRRK2 mRNA was not identified in the granule cell layer of the cerebellum, however, LRRK2 protein localisation was observed in this region. N/A: not available.

The protein displayed a cytoplasmic localisation in the neurons often extending into the apical dendrites. Localisation in the nuclear envelope was not clearly identified as a consistent finding. The strongest staining for LRRK2 was found in the medulla with particularly strong staining in the Xth nerve nucleus, the XIIth nerve nucleus and the inferior olive (Figure 4.4A-C). In the pons, the noradrenergic pigmented neurons of the LC (Figure 4.4D) showed weak LRRK2 staining compared to the neurons of the pontine base (Figure 4.4E). The melanised DAergic neurons of the SN (Figure 4.4F) also showed weaker LRRK2 protein expression in comparison to other midbrain regions (Figure 4.4G). The weakest neuronal staining for LRRK2 was consistently recorded in the caudate and putamen (Figure 4.4H) with only occasional neurons showing weak immunoreactivity. However, diffuse neuropil staining was observed in the striatum. Moderate to high LRRK2 levels were observed in the subthalamic nucleus (Figure 4.4I), globus pallidus (Figure 4.4J) and thalamus. Strong staining of the LRRK2 protein was routinely identified in the white matter tracts of the internal capsule (Figure 4.4K and L). Vascular smooth muscle also expressed LRRK2 protein (Figure 4.4M).

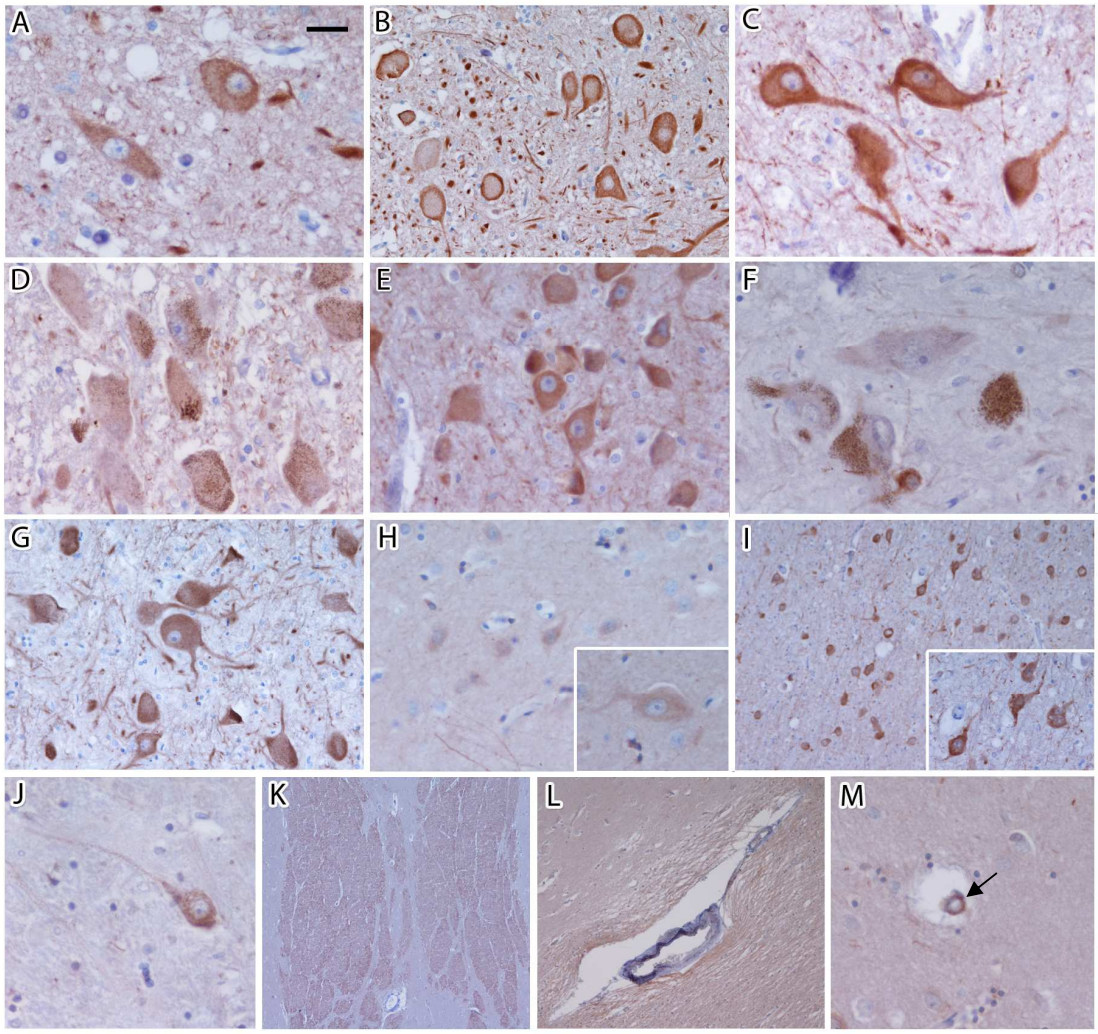

Figure 4.4: LRRK2 immunoreactivity in brainstem and basal ganglia. LRRK2 protein localises to neurons in the medulla which are represented in A) Xth nerve nucleus (control), B) XIIth nerve nucleus (control), C) inferior olive (IPD). LRRK2 was detected in the pons as represented in D) locus coeruleus (IPD) and E) pontine neurons (IPD). LRRK2 immunoreactivity was weak in the DAergic neurons of F) substantia nigra (control), but stronger staining was detected in other midbrain regions, such as G) the IIIrd nerve nucleus (G2019S). H) Neurons in the putamen (control), consistently demonstrated weak LRRK2 immunoreactivity, whereas strong staining was observed in the neurons of I) subthalamic nucleus (control), and J) globus pallidus (G2019S). LRRK2 immunoreactivity was observed in the white matter tracts in the internal capsule, K) (control) and L) (G2019S), and M) smooth vasculature staining with LRRK2 (arrow). The scale bar in A represents 20µm in image A, C-F, J, M and inset in H; 39µm in B, G, H, L and inset in I; 78µm in I and K.

The regions of the medial temporal lobe also displayed varying levels of LRRK2 protein immunoreactivity (see Figure 4.5). LRRK2 staining of the hippocampal formation highlighting the regions of CA1-4 of Ammon's horn, and the granule cell layer of the dentate fascia are represented in Figure 4.5A. The pyramidal neurons of CA2-4 (Figure 4.5B) showed moderate to strong staining for LRRK2 while the CA1 neurons showed only weak staining. A consistently weak to moderate LRRK2 immunoreactivity was observed in the amygdala (Figure 4.5C), whereas the neurons in subiculum, entorhinal (Figure 4.5D) and transentorhinal cortex displayed moderate staining. Neurons in the neocortical regions also exhibited moderate to strong immunoreactivity for the LRRK2 protein (Figure 4.5E and F), with pyramidal and stellate neurons in the molecular layers III-V showing the strongest LRRK2 immunoreactivity. Within the pyramidal neurons of the hippocampal formation and neocortical regions, LRRK2 immunoreactivity was observed in the neuronal perikarya and also axonal fibers and dendrites. Strong labelling of LRRK2 protein was observed within the neurons of the dentate nucleus and in Purkinje neurons (Figure 4.5G), where staining clearly extended into the dendritic tree of the cerebellum. Golgi cells in the cerebellar granule layer also showed moderate staining although this varied from case to case (Figure 4.5H). LRRK2 was also observed in glial cells that displayed astrocytic morphology (Figure 4.5I).

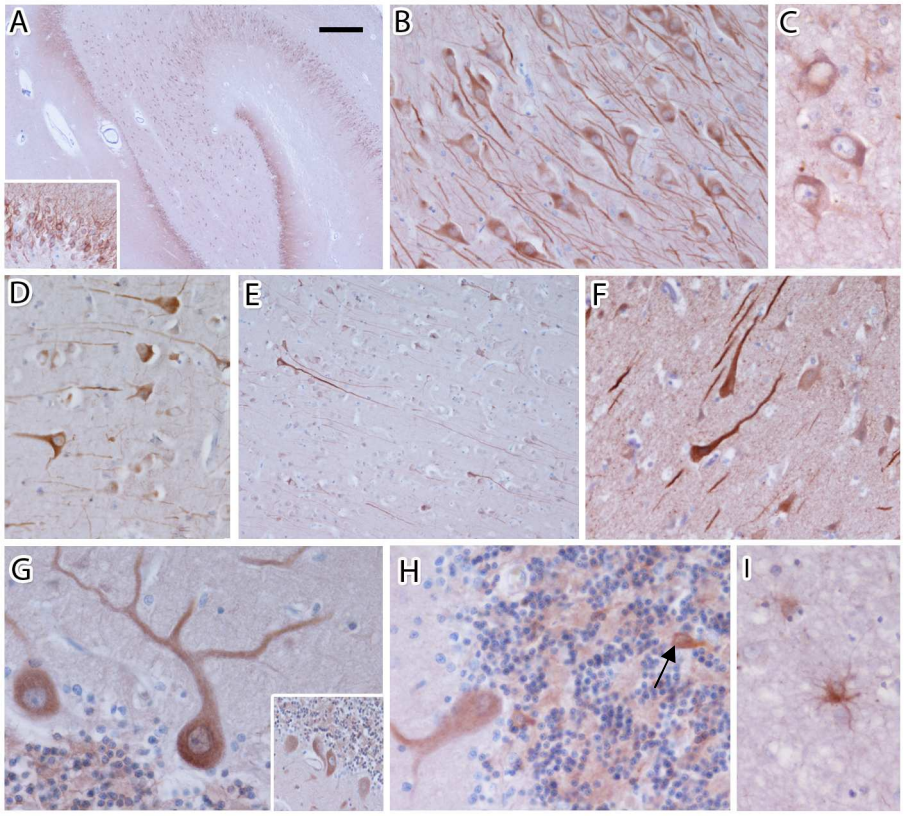

Figure 4.5: LRRK2 immunohistochemistry in medial temporal lobe and cortical regions. IHC staining demonstrated that LRRK2 immunoreactivity varied in intensity in medial temporal lobe structures. In the hippocampal formation, neurons of the A) dentate fascia (G2019S) and B) CA2-1 (G2019S) were positively stained. Neurons in the C) amygdala consistently showed low to moderate staining for LRRK2 (IPD). Moderate staining for LRRK2 was observed in the neurons of neocortical regions D) entorhinal cortex (G2019S), E) temporal cortex (G2019S) F) cingulate gyrus (control). G) Purkinje neurons of the cerebellum were consistently found to have moderate to strong staining for LRRK2 protein which also extended into the dendritic tree (control), (inset–IPD). H) Golgi cells (see arrow) of the cerebellum also showed weak LRRK2 immunoreactivity (IPD). LRRK2 protein distribution was not limited to neurons and the protein was also detected in I) reactive astrocytes (IPD). The scale bar in A represents 410µm in image A; 78µm in image E, 39µm in the inset in G; 20µm in the inset in A and images B – D and F-I.

4.3.3 A semi-quantitative analysis of LRRK2 protein expression in control, IPD and G2019S positive PD subjects

In order to ascertain whether a difference in LRRK2 protein levels could contribute to the PD pathogenesis, we decided to perform a semi-quantitative analysis on the regional LRRK2 protein variation in control, IPD and G2019S positive PD subjects. The four tiered grading system included: 0 - no staining, + - weak staining, ++ - moderate staining and +++ - strong staining. The regional levels of LRRK2 protein in the control, IPD and G2019S positive PD subjects are summarised in Table 4.9.

There was no quantitative difference in the immunoreactivity for LRRK2 protein between control, IPD and G2019S positive PD subjects, although a consistent variation in regional expression was recorded across the groups. Regions implicated in PD pathogenesis showed extensive variability in the LRRK2 protein staining. The Xth nerve nucleus of the medulla (Figure 4.6A-C) was identified as having some of the highest levels of LRRK2, while the melanised neurons of LC (Figure 4.6D-F) and SN (Figure 4.6G-I), displayed low to moderate levels of the protein in all three groups. The dopamine-innervated areas of caudate nucleus and putamen were consistently found to have the lowest LRRK2 protein levels of all the regions examined (Figure 4.6J-L). However, other regions in midbrain (IIIrd nerve nucleus, red nucleus/tegmentum and tectum) and basal ganglia (globus pallidus, thalamus and subthalamic nucleus) were demonstrated as having much higher levels of LRRK2 protein in comparison to the nigrostriatal dopamine system (see Table 4.9).

Overall some of the highest LRRK2 protein levels were recorded in medulla, and some of the lowest in striatum and amygdala (irrespective of the disease status). Similarly, in the medial temporal lobe, moderate LRRK2 protein levels were observed in the dentate fascia and the CA2-4 neurons, while the CA1 neurons consistently showed weak staining in the three groups of subjects. The dentate nuclei and Purkinje neurons of the cerebellum were consistently found to have high and moderate LRRK2 immunoreactivity, respectively. This was found to be consistently similar in control, IPD and G2019S positive PD subjects (Table 4.9). The moderate staining for LRRK2 in the neocortical regions examined in this

study was also comparable in the subjects, irrespective of the disease status (Table 4.9). Therefore, taking into account all the regions and subjects examined in this study, a marked difference in LRRK2 protein levels was not found between control, IPD and G2019S positive PD subjects, but consistent regional differences were recorded within the groups.

Region	Sub- Regions	Control	IPD	G2019S
Medulla	Xth nerve nucleus	++ - +++	++ - +++	++ - +++
	XIIth nerve nucleus	+++	+++	++ - +++
	Inferior olive	++ - +++	++ - +++	++ - +++
Pons	Locus coeruleus	+	+ - ++	++
	Pontine base	++ - +++	+++	+ - ++
	Tegmentum	++	++ - +++	+ - ++
Midbrain	Substantia nigra	+	+ - ++	+
	IIIrd nerve nucleus	++ - +++	+++	++ - +++
	Red nucleus/ Tegmentum	+ - +++	++ - +++	+ - ++
	Tectum	+ - ++	+	+
Basal Ganglia	Caudate nucleus	0 - +	0 - +	0 - +
	Putamen	0 - +	0 - +	0 - +
	Globus pallidus	+ - ++	++	+ - ++
	Thalamus	+++	+++	++ - +++
	Subthalamic nucleus	+ - +++	+++	+ - +++
Medial temporal lobe	Dentate fascia	++	++	+ - +++
	CA2/3/4 neurons	+ - ++	+ - ++	+ - +++
	CA1 neurons	0 - +	0 - +	0 - +++
	Subiculum	+ - +++	+ - ++	+ - +++
	Entorhinal cortex	+ - ++	+ - ++	+ - ++
	Transentorhinal cortex	+ - ++	+ - ++	+ - ++
	Amygdala	+	+	+
Cerebellum	Dentate nucleus	++ - +++	++ - +++	+ - +++
	Purkinje neurons	++	+ - ++	+ - ++
	Granule cell layer	+ - ++	++	+
Neocortical regions	Frontal cortex	+ - ++	++	++
	Parietal cortex	+ - ++	++	++
	Temporal cortex	+ - ++	++	++
	Insular cortex	+ - ++	++	+ - ++
	Fusiform gyrus	+ - ++	++	+ - ++
	Cingulate gyrus	++ - +++	+++	++

Table 4.9: A semi-quantitative analysis of LRRK2 protein in post-mortem control, IPD and G2019S positive PD brain tissue. The four tiered grading system includes: 0- no staining, +- weak staining, ++- moderate staining and +++ strong staining. This data was collected using four control, two IPD and four G2019S positive PD subjects, and indicates the range of staining intensity observed in each region.

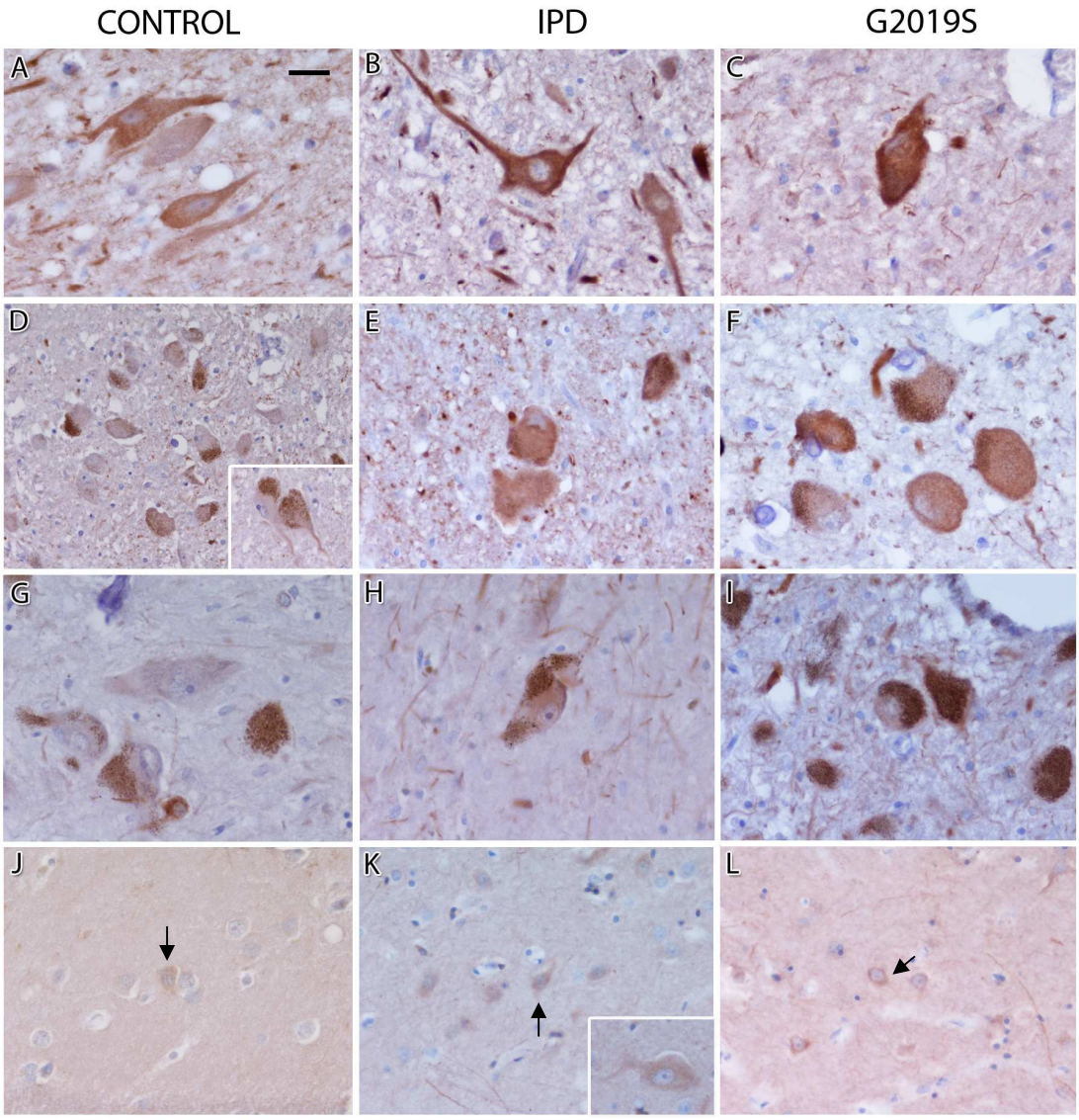

Figure 4.6: Morphological distribution of LRRK2 protein in control, IPD and G2019S positive PD subjects. Neurons of the Xth nerve nucleus do not show a significant difference in the intensity of LRRK2 immunoreactivity of A) control, B) IPD, and C) G2019S positive PD subjects. LRRK2 staining intensity was also similar in the noradrenergic neurons of LC of all three groups (D-F). Similarly, the melanised DAergic neurons of the SN showed no difference in the three groups (G–I). LRRK2 immunoreactivity was consistently recorded as being the weakest in striatal neurons (see arrows), irrespective of the disease status (J–L, putamen). The scale bar in A represents 20µm in images A – C and E – I, and insets in D and K; 39µm in images D and J – L.

4.3.4 LRRK2 in Lewy bodies

LRRK2 protein was found in the halo of a small proportion of LBs (around the periphery). The LRRK2 immunoreactive LB inclusions were identified in nigral neurons (Figure 4.7A- E), neurons of the locus coeruleus (Figure 4.7F), and also in the amygdala (Figure 4.7G). Cortical LBs were not immunoreactive for LRRK2. Lewy neurites also stained for LRRK2 protein (Figure 4.7C). The staining of LBs with LRRK2 remained very selective with some LBs showing extensive staining (Figure 4.7F), whilst others demonstrating pale staining (Figure 4.7A).

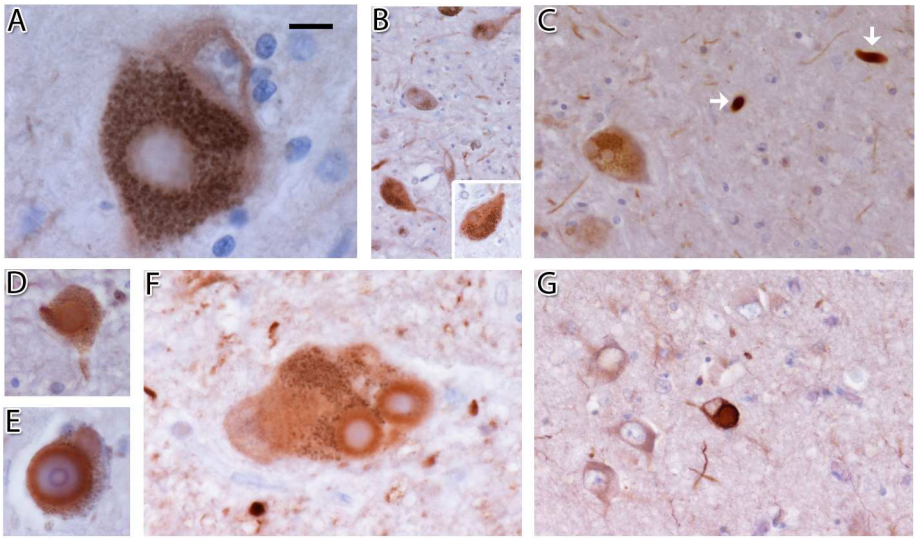

Figure 4.7: LRRK2 protein is present in a proportion of Lewy bodies. This figure illustrates LRRK2 staining the halo of a small proportion of LBs in the brainstem and also in the amygdala. Panels A –E display varying intensities of LRRK2 staining in nigral LBs. C) Lewy neurites were also shown to contain LRRK2 (arrows). F) Strongly stained LBs in locus coeruleus, G) a small proportion of LBs were also stained in amygdala. The scale bar in A represents 8µm in A and F; 20µm in C, D, E, G and inset in BG; 39µm in B.

4.4 Discussion

This study demonstrates that LRRK2 mRNA and protein have a ubiquitous neuronal expression in the human brain that was not limited to the neuroanatomical regions most severely affected by α-synuclein pathology in PD pathogenesis. LRRK2 mRNA and protein was identified in the melanised neurons of the Xth nerve nucleus, LC, SN and the dopamine-innervated areas of striatum. However, the lowest LRRK2 protein levels were consistently recorded in the nigrostriatal dopamine system. IHC studies confirmed the previously described neuronal cytoplasmic distribution of the LRRK2 protein, and also identified the protein in the apical dendrites, axonal fibers and the neuropil of the striatum (Biskup et al. 2006; Higashi et al. 2007a; Higashi et al. 2007b; Melrose et al. 2007). This study also demonstrates that LRRK2 localises to a small proportion of LBs and Lewy neurites in the brainstem and amygdala.

LRRK2 mRNA has a ubiquitous neuronal expression in the human brain

The ISH study in this chapter was designed with a view to addressing the major inconsistencies that have been reported in the distribution of LRRK2 mRNA in the brain. As described in section 4.1.1, the original studies reported low levels of LRRK2 mRNA in the SN but high levels in the striatum. These were subsequently contradicted when widespread LRRK2 mRNA expression was demonstrated in the mammalian brain using modified ISH techniques. The ISH data presented in this chapter demonstrates that LRRK2 mRNA is localised not only throughout the nigrostriatal dopamine system but is also present in a number of other anatomical regions in the brain. These findings contradict the original studies that did not detect LRRK2 mRNA in dopamine-synthesising areas in rodents and humans (Galter et al. 2006; Melrose et al. 2006), but instead supports the subsequent studies that demonstrated widespread expression of LRRK2 mRNA in the human brain (Simón-Sánchez et al. 2006; Higashi et al. 2007b).

Dependent on the type of hybridisation probe, labelling methods, and quality of tissue used, different regional distribution and levels of LRRK2 mRNA signals have previously been reported (summarised in Table 4.1). Even though a ubiquitous expression for the LRRK2 mRNA in human brain has been

demonstrated in this study using a digoxigenin labelled probe, multiple amplification steps were needed to detect the LRRK2 mRNA signal. These low levels of LRRK2 mRNA in the human brain did not enable us to use radioactively (^{35}S) labelled oligonucleotide probes to perform emulsion autoradiography without producing significant background staining. Therefore, quantitation of LRRK2 mRNA in the human brain could not be undertaken by counting silver emulsion grains, and was instead achieved by a PCR based technique described in chapter 5 of this thesis.

The results presented in this study concur with those of others suggesting a low copy number of LRRK2 mRNA in the mammalian brain (Simón-Sánchez et al. 2006; Higashi et al. 2007b). Such an expression profile could be due to the fact that the LRRK2 mRNA is either a) unstable, b) has a short half-life, c) is transported to distal sites where local translation occurs in response to external stimuli or, d) or has an efficient translational machinery that allows for a low copy number of LRRK2 mRNA molecules to produce enough protein for the region. The stability of LRRK2 mRNA has not been explored, and future experiments assessing the half-life of LRRK2 mRNA could provide valuable insight into its stability and also shed light on any potential regional variation. Overall this study supports a widespread but a low copy number expression of LRRK2 mRNA in the human brain that is not limited to the nigrostriatal system.

LRRK2 protein has a ubiquitous but a variable regional expression in the human brain

In this chapter, I present data demonstrating widespread LRRK2 immunoreactivity in neuronal cell bodies, apical dendrites and axons. Like the mRNA, LRRK2 protein was also found to have a ubiquitous expression in the anatomical regions examined. The highest levels of the LRRK2 protein were consistently recorded in the neurons of the medulla, and the nigrostriatal dopamine system consistently displayed low levels of the protein, irrespective of the disease status. The pigmented neurons in the SN showed weak to moderate immunoreactivity for LRRK2 protein, but the neuronal populations of caudate nucleus and putamen exhibited the lowest immunoreactivity with occasional small

numbers of labelled neurons being identified, although there was strong LRRK2 immunoreactivity in striatal neuropil confirming previous reports (Higashi et al. 2007b; Melrose et al. 2007). Higashi and colleagues showed extensive LRRK2 immunoreactivity in the striatal neurons (Higashi et al. 2007b), but a previous study that also used EB06550 antibody reported low to moderate staining of LRRK2 in striatal neurons, thereby demonstrating the reproducibility of EB06550 antibody used in this study (Alegre-Abarrategui et al. 2008). These variations in LRRK2 immunoreactivity between studies could be attributed to disparities in tissue fixation. However, the variations are more likely to be due to the difference between the antibodies used, as we demonstrated an extensive and consistent neuropil staining of LRRK2 and weak neuronal staining in striatum of all the subjects used in this study with the EB06550 antibody. Western blot assays have suggested high LRRK2 levels in mammalian striatum (rodents), but crude tissue lysates cannot distinguish between different cellular compartments, and may therefore be compatible with our findings (Biskup et al. 2006; Taymans et al. 2006; Melrose et al. 2007). This data demonstrates that neuronal perikaryal expression of LRRK2 is weakest in striatum when EB6550 antibody is used.

It is interesting that in both the midbrain and basal ganglia, regions such as the IIIrd nerve nucleus, red nucleus/tegmentum and tectum (in midbrain), and globus pallidus, thalamus and subthalamic nucleus (in basal ganglia), that are not the primary targets of degeneration in PD pathogenesis have much higher levels of LRRK2 protein compared to the nigrostriatal dopamine system (see Table 4.9). This could suggest a possible high turnover, and an important role for the LRRK2 protein in regions critical to PD pathogenesis. Extensive LRRK2 immunoreactivity was especially evident in the thalamus, a region which receives modulatory input from the motor nuclei in the cerebellum and relays excitatory sensory signals to the cortex (Melrose et al. 2007). The presence of LRRK2 in a region such as thalamus which is essential to the basal ganglia circuitry, further establishes the importance of this protein in ensuring normal neuronal function to execute movement. LRRK2 was also shown to be present in numerous brain regions such as the hippocampus, and amygdala which are key structures of the limbic system. This suggests that LRRK2 may play a physiological role in not

only the motor but also in certain cognitive elements associated with the PD pathogenesis, or perhaps even normal aging. LRRK2 has also been reported in neurofibrillary tangles (NFTs) and the pleomorphic pathology related to LRRK2 mutations certainly suggest an important upstream role for this gene in other neurodegenerative disorders associated with cognitive decline (Giasson et al. 2006; Miklossy et al. 2006). Overall, the findings demonstrate that the LRRK2 protein, like the mRNA is ubiquitously present in neuronal populations of the brain and is not limited to the regions susceptible to α-synuclein pathology in PD. The IHC findings presented here also corroborate well with a previous study investigating LRRK2 protein levels (western blot) in distinct regions of rat brain, and confirmed the presence of high levels of LRRK2 in the hippocampus, followed by cortex and the least amount in putamen (Biskup et al. 2006).

Melrose and colleagues previously reported a lack of LRRK2 mRNA, but a considerable immunoreactivity for the LRRK2 protein in the thalamus. (Melrose et al. 2007). This chapter demonstrates the presence of both the LRRK2 mRNA and protein in the thalamus of the human brain. However, I was able to demonstrate regions that did not have LRRK2 mRNA signal but were positive for LRRK2 immunoreactivity. LRRK2 mRNA signal was not identified in the cerebellar granule cell layer (Figure 4.1I), but golgi cells in this layer displayed moderate LRRK2 immunoreactivity (Figure 4.5H). The lack of LRRK2 mRNA expression in the granule cells could be due to small quantities of cytoplasm in these cells. Alternatively, LRRK2 mRNA could be present as a low copy number mRNA which cannot be detected using the digoxigenin labelled probe in the granule cells of cerebellum.

Similarly, we were not able to identify LRRK2 mRNA in the glial population, despite a previous report showing LRRK2 mRNA in cultured glial cells using a sensitive PCR based method (Miklossy et al. 2006). A low copy number of the LRRK2 mRNA or differences between physiological and cultured glial cells could have prevented the result being replicated using the digoxigenin ISH method reported in this chapter. LRRK2 immunoreactivity has previously been documented in human glial cells, (Miklossy et al. 2006; Melrose et al. 2007), but not in mouse glial population (Biskup et al. 2006; Higashi et al. 2007b). Although

we were able to confirm LRRK2 immunoreactivity in the reactive astrocytes, this was not a common occurrence.

The localisation of LRRK2 to axons, apical dendrites and the neuropil network lends further support to LRRK2 being involved in axonal transport or vesicular trafficking system (reviewed in (Greggio & Cookson 2009). For example, LRRK2 has been suggested to bind to lipid rafts in synaptic terminals which play an important role in signal transduction, cytoskeletal organisation (Hatano et al. 2007), and was recently shown to regulate synaptic membrane trafficking (Shin et al. 2008). Furthermore, immunoblots have previously demonstrated the presence of LRRK2 in lung, kidney, liver, heart, skeletal muscle, and spleen of rodents (Giasson et al. 2006; Biskup et al. 2006), and a previous IHC study also showed vasculature staining with LRRK2 protein (Zhu et al. 2006a). I confirm the presence of LRRK2 mRNA and protein expression in smooth muscle which supports a wider role for the protein involvement in the physiology.

No difference in the LRRK2 mRNA and protein expression profile in control, IPD and G2019S positive PD subjects

This chapter demonstrated a similar morphological distribution of LRRK2 mRNA and protein expression in control, IPD and G2019S positive PD subjects. Although the semi-quantitative analysis on the LRRK2 immunoreactivity showed no quantitative regional differences in the protein levels between the three groups, the only region where variable intensity of LRRK2 immunoreactivity was recorded in the three subject groups was the CA1 sub-region of the hippocampus. These neurons have been given a higher score in the G2019S positive PD subjects in comparison to control and IPD cases, and this is most likely due to the vulnerability of these cells to hypoxic damage immediately prior to death.

Stronger labelling of LRRK2 protein in neuronal cell bodies and axons of PD subjects has previously been reported (Zhu et al. 2006a), and another report recorded a decrease in LRRK2 immunoreactivity in the SN of PD brains compared to controls (Higashi et al. 2007b). These apparent contradictions in the literature and our findings could be attributed to the use of different antibodies (see Table 4.2 for the antibodies used by these authors). The issue of quantitative

differences between unaffected and diseased subjects could be further addressed by the development of a sensitive ELISA technique.

The overall low intensity of LRRK2 immunoreactivity in dopamine producing and dopamine innervated regions (irrespective of the disease status) could be indicative of a high turnover of the molecules in regions critical to PD pathogenesis. There was no apparent difference in the morphological expression profile of LRRK2 protein in the SN and striatal neurons between control, IPD and G2019S positive PD subjects. Since LRRK2 has been suggested to be involved in neuronal maintenance of DAergic neurons (Imai et al. 2008), it is possible that the disease pathogenesis results in increased LRRK2 protein in the surviving neurons. This could result in similar intensity of LRRK2 immunoreactivity across different subject groups. Nigral degeneration with LBs is a pathological phenotype of both IPD and G2019S positive PD subjects. The G2019S mutation is supposed to alter the function of wild-type LRRK2, but there is a distinct lack of difference in the expression profile of IPD and G2019S positive PD subjects in this study. It is possible that an overlap in or indeed a shared auxiliary mechanism is contributing to the pathogenesis in PD subjects with G2019S mutant LRRK2 and PD subjects without the G2019S mutant LRRK2.

It is evident from this study that LRRK2 expression is not limited to nigrostriatal system and has a widespread expression both in terms of mRNA and protein levels, but what remains to be seen is whether LRRK2 dysfunction causes nigral degeneration or nigral degeneration itself affects LRRK2 function at a cellular or systems level?

LRRK2 is present but is not an obligate component of LBs

My results also demonstrate the presence of LRRK2 in the halo region of the LBs in the brainstem and amygdala of IPD cases, confirming previous reports using C-terminal LRRK2 antibodies (see Table 4.2). The labelling of LBs in the pigmented neurons of the SN and LC with the EB06550 antibody was variable and not all LBs labelled with the same intensity, also confirming previous reports (see Table 4.2 for a summary). Intense staining of Lewy neurites was also observed with the EB06550 antibody, in contrast with other reports in which

Lewy neurites were not labelled with LRRK2 antibodies (Miklossy et al. 2006; Higashi et al. 2007b). LRRK2 positive LBs were not identified in the neocortical regions, confirming the findings of others using the NB300-268 antibody. In contrast to the NB300-268 antibody which labels the core of LBs as well as immunostains neocortical LBs (see Table 4.2), the EB06550 antibody used in this study demonstrated LRRK2 protein localisation only to the halo of the brainstem and amygdala LBs with varying intensities. The discrepancies between antibodies could be explained by differences in the affinity and avidity of the LRRK2 antibodies, and also the possibility that routine IHC techniques are not able to expose the antigen within the densely packed insoluble fibrils of LBs. Conformational and post-translational modifications (truncated LRRK2 isoforms) of the neuronal LRRK2 protein could also prevent some LRRK2 antibodies from staining LBs. It should be noted that NB300-268 is the only antibody to have reportedly identified 60 – 80 % of LRRK2 stained LBs (Zhu et al. 2006a; Zhu et al. 2006b; Miklossy et al. 2006; Alegre-Abarrategui et al. 2008). Even though the NB300-268 antibody has been suggested to demonstrate sufficient specificity for detecting endogenous human LRRK2 and human LRRK2 overexpressed in (HEK-293T) transfected cells, this antibody did not exhibit specificity for endogenous or overexpressed mouse LRRK2 (Biskup et al. 2007). It was also shown to be cross-reactive to many other species that appear near the expected size of LRRK2 protein in wild-type and LRRK2 deficient mouse brain lysates (Biskup et al. 2007). Furthermore, the hyaline type LB inclusions have been suggested to bind to a wide range of unrelated antibodies, in particular rabbit antibodies (Melrose et al. 2007). This challenges the specificity of NB300-268 which has also been shown to localise to a wide range of other neurodegenerative pathologies (Giasson et al. 2006; Miklossy et al. 2006). The EB06550 antibody used in this study has not been tested in knockout mice but did identify a ~250 kDa band on lysate prepared from human brain homogenate, and the specificity of the signal was tested by obliterating the signal using a >10 fold molar excess of the corresponding antigen (Figure 4.3). Our findings of variation and low fraction of LRRK2 staining in LBs and Lewy neurites, in addition to a distinct lack of LRRK2 in cortical LBs with EB06550 antibody is in agreement with previous studies, and suggests that LRRK2 protein is not a principal component of LBs.

LRRK2 has been shown to be present in α-synuclein immunopositive glial cytoplasmic inclusions (GCIs) in multiple system atrophy (MSA), and LRRK2 immunoreactivity was also increased in the early stages of myelin sheath disruption and degradation in MSA (Huang et al. 2008). α-synuclein is also a major component of GCIs and was recently shown to be phosphorylated by LRRK2 *in-vitro* (Qing et al. 2009). An *in-vivo* phosphorylation of α-synuclein by LRRK2 remains to be determined but it has been shown to co-localise with α-synuclein in brainstem and limbic LBs (not in cortical LBs or Lewy neurites) of PD and DLBD brains (Miklossy et al. 2006; Higashi et al. 2007b; Perry et al. 2008). Recently, the mRNA for both α-synuclein and LRRK2 were suggested to be co-regulated in rodent striatum (Westerlund et al. 2008b). LRRK2 has been suggested to play an important role in signal transduction mechanisms (White et al. 2007; Greggio & Cookson 2009), and it is feasible that LRRK2 is involved in an upstream (possibly regulatory) role in the initial formation of LBs either through irregular protein phosphorylation and subsequent aggregation, and/or protein misfolding as has been observed in *in-vitro* studies (Smith et al. 2005a; West et al. 2005; Smith et al. 2006; Greggio et al. 2006). Even though no work has yet been published on the presence of LRRK2 in pale bodies, presence of LRRK2 in these inclusions would help elucidate the potential role of LRRK2 during different developmental stages of LBs.

Conclusion

This study describes several aspects of LRRK2 mRNA and protein expression in the human brain. The ubiquitous identification of LRRK2 expression in the cytoplasm of neurons, axons, apical dendrites, neuropil network, and smooth muscle vasculature supports an important physiological role for this protein. No difference was observed in the expression profile of LRRK2 mRNA and protein in control, IPD and G2019S positive PD subjects. However, any subtle differences would have to be quantitated using more sensitive assays. One of the major findings of this study was the consistently low immunoreactivity for the LRRK2 protein in the nigrostriatal dopamine system, suggesting a high turnover for the protein in the regions critical to PD pathogenesis. If LRRK2 does indeed have a major role in neuronal maintenance as recommended by some, then any

dysregulation in its expression, quantitative or qualitative could have drastic effects on this role and contribute to nigral degeneration that is observed in PD subjects. Since no apparent difference was observed in the expression profiles of PD subjects with wild-type or G2019S LRRK2, it does raise the possibility of a shared auxiliary mechanism contributing to the indistinguishable phenotype of IPD and G2019S positive PD subjects. This concept is investigated in the next chapter. The data presented here confirms that LRRK2 epitopes are present in LB of three distinct anatomical regions in the brain (i.e. LC, SN and amygdala). However, the variable intensity of LB immunoreactivity with LRRK2 suggests that is not an obligate component of LBs, but may play an upstream role in the formation of LBs as the major pathological marker of PD.

Chapter 5

5 A quantitative study of LRRK2 mRNA expression in the human brain

5.1 Introduction

Like most complex diseases, PD manifests a genetic heterogeneity which is not easily explained by a simple mendelian mode of inheritance. Even though mutational screening of the PARK loci in PD subjects, and assessing the functional impact of identified mutations has contributed vastly to our knowledge behind the genetic aetiology of the disease, majority of PD cases cannot be explained by mutational screening. Thereby, indicating that other mechanisms might contribute substantially to the PD pathogenesis. Auxiliary mechanisms that ensure an accurate production of the protein from a gene sequence have long been of interest to biologists. One such mechanism is the transcriptional activity of a gene, which is a carefully regulated procedure that dictates not only the accurate structure and production of the protein but also the levels of protein expression.

Microarray platforms have been used to assess differences in whole genome transcription across the nigrostriatal system in post-mortem tissue of PD and control subjects (Grünblatt et al. 2004; Miller et al. 2004; Zhang et al. 2005; Mandel et al. 2005; Hauser et al. 2005; Miller et al. 2006; Vogt et al. 2006; Duke et al. 2006; Moran et al. 2006; Simunovic et al. 2008; Bossers et al. 2009). These whole genome expression studies have identified novel genes and pathways that include genes related to protein processing (degradation - UPS system and trafficking - chaperones), signal transduction, oxidative and mitochondrial stress, apoptosis, vesicle trafficking, cytoskeletal stability and maintenance, and axonal transport. Transcriptional profiling has also been used to describe regional and gender specific differences in PD (Miller et al. 2006).

In addition to identifying novel genes that might play a role in PD pathogenesis, these studies have also elaborated on the role of PARK loci in PD cases (Hauser et al. 2005; Moran et al. 2006; Moran et al. 2007; Gründemann et al. 2008). A recent study has described a down- regulation for the PARK genes in the dopaminergic (DAergic) neurons of PD cases (Simunovic et al. 2008), but there is limited

information as to the transcriptional profile of LRRK2. A combination of northern blot analysis (Paisán-Ruíz et al. 2004), *in-situ* hybridisation (ISH) (Simón-Sánchez et al. 2006; Higashi et al. 2007b), and quantitative PCR (qPCR) (Zimprich et al. 2004b; Melrose et al. 2006; Simunovic et al. 2008) have been used to identify quantitative differences in the regional expression of LRRK2 mRNA, although these data were produced using a small number of subjects.

Mutations in the *LRRK2* gene are a common genetic cause of PD, and also exhibit the most heterogeneous neuropathology (Zimprich et al. 2004b, Wszolek et al. 2004; Ross et al 2006). Establishing differences in the transcriptional activity of the gene could highlight shared mechanisms in the pathogenic process(es) displayed by the idiopathic cases versus the PD phenotype resultant from G2019S mutation, which interestingly exhibits a clinical and a pathological phenotype indistinguishable from IPD (Aasly et al. 2005). Ubiquitous expression of LRRK2 mRNA in the brain is demonstrated in the previous chapter of this thesis, although no difference was observed in the morphological distribution of LRRK2 mRNA in unaffected, IPD and G2019S positive PD subjects. A more sensitive PCR based technique would be capable of identifying subtle differences in mRNA expression that an *ad-hoc* analysis by chromogenic ISH cannot. Quantitative analysis describing regional variations in LRRK2 mRNA in not only these two forms of PD (IPD and G2019S mutant) but also in unaffected controls is needed to further elucidate the role of *LRRK2* gene in contributing to the molecular pathogenesis of PD.

LBs are the pathological hallmark of PD, and the presence of LRRK2 protein has been demonstrated in a small proportion of LBs in the previous chapter, thereby supporting published reports in the current literature. α-synuclein is the major component of LBs (Spillantini et al. 1997), and extensive *in-vitro* phosphorylation of α-synuclein results in its oligomerisation which has been shown to promote aberrant aggregation of the protein as LB inclusions in both PD and DLBD cases (Fujiwara et al. 2002; Iwatsubo 2003; Smith et al. 2005b). It has been suggested that these inclusions initially form in order to sequester toxic effects that might result from an increased α-synuclein activity in the DAergic neurons, but eventually become cytotoxic (reviewed in (Goldberg & Lansbury 2000)).

Recently, the mRNA for both α-synuclein and LRRK2 was suggested to be co-regulated in rodent striatum (Westerlund et al. 2008b), and a co-localisation of the two proteins was also shown in PD brains (Perry et al. 2008). Decreased LRRK2 mRNA levels and increased α -synuclein mRNA levels in DAergic neurons of SN have recently been reported (Simunovic et al. 2008; Gründemann et al. 2008). Even though the physiological substrates for LRRK2 still remain to be confirmed, α -synuclein was recently shown to be phosphorylated by LRRK2 *in-vitro* (Qing et al. 2009). As such it is feasible that LRRK2 might be involved in modulating upstream phosphorylating events of excessive α-synuclein resulting in the formation of LB inclusions. Establishing a correlation between LRRK2 mRNA and LB levels in brain regions prone to these inclusions would elucidate the mechanistic pathway that might link together two highly important PARK loci.

5.1.1 Hypothesis and specific aims

In this chapter, I wished to investigate the hypothesis that auxiliary mechanisms, such as dysregulation of LRRK2 mRNA could contribute to the PD pathogenesis. The major aims of this study were a) to provide a quantitative map of the LRRK2 mRNA expression in the human brain; b) to investigate regional variations in the LRRK2 mRNA levels between unaffected, IPD and G2019S positive PD subjects; and c) to investigate if there is a correlation between LRRK2 mRNA and the levels of LB inclusions observed in IPD and G2019S positive PD subjects?

To address these questions, a quantitative expression profile of LRRK2 mRNA in post-mortem tissue from controls, IPD and G2019S PD subjects was determined using qPCR. Post-mortem tissue from selected brain regions (medulla, putamen, amygdala, cingulate gyrus, cerebellum, frontal, parietal and entorhinal cortices) was used to establish the LRRK2 mRNA expression profile. In order to investigate a correlation between LRRK2 mRNA and LB levels in the PD subjects, α-synuclein immunoreactivity was used to determine the LB levels in the medulla, putamen, amygdala, cingulate gyrus, frontal, parietal and entorhinal cortices brain regions.

5.2 Materials and Methods

5.2.1 Tissue Selection

Post-mortem tissue that had been frozen at -70°C was obtained from Queen Square Brain Bank (QSBB) as detailed in chapter 2 (section 2.1). A preliminary study was conducted using the cerebellum tissue from 121 IPD cases and 36 unaffected controls. A summary of these subjects is provided in the Appendix. 20 unaffected and 20 IPD subjects were selected from the tissue used in the preliminary study, and additional tissue from four G2019S positive PD subjects was also obtained from QSBB. The PD subjects were identified as neocortical or transitional LB disease according to the McKeith criteria (McKeith et al. 2005). Clinical and pathological details of the subjects are described in Table 5.2, Table 5.3 and Table 5.5. In order to investigate the anatomical expression profile of LRRK2 mRNA, a detailed analysis was conducted using tissues from medulla, putamen, amygdala, cingulate gyrus, entorhinal, frontal and parietal cortices from these subjects. The anatomical regions available from these subjects are described in Table 5.4 and Table 5.6.

5.2.2 mRNA quantitation

The procedures for RNA extraction, cDNA synthesis and qPCR and normalization are described in detail in chapter 2 sections 2.2.3 and 2.4. The oligonucleotides used in the study are described in Table 5.1.

5.2.3 qPCR data analysis

qPCR data was processed using the SDS 2.0 software (Applied Biosystems, UK) as described in chapter 2 (section 2.4.2.2). Four endogenous reference genes (*HPRT1, RPL13A, G6PD* and *TBP*) were measured for all the samples, and an appropriate normalisation factor was calculated using the software NormFinder as described in chapter 2 (section 2.4.2.3).

Primer	Sequence 5'-3'	Tm	Fragment size
***LRRK2* Forward**	TGTTGTGGAAGTGTGGGATAA	60°C (30 sec)	295 bp
***LRRK2* Reverse**	CATTTTTAAGGCTTCCTAGCTG		
***RPL13A* Forward**	GATATAATTGACACTGGCAA	55°C (30 sec)	89 bp
***RPL13A* Reverse**	AGCAAGCTTGCGACCTTGA		
***HPRT1* Forward**	TGAACGTCTTGCTCGAGAT	55°C (30sec)	188 bp
***HPRT1* Reverse**	GGTCATTACAATAGCTCTTC		
***TBP* Forward**	TAATCCCAAGCGGTTTGCTG	60°C (45 sec)	112 bp
***TBP* Reverse**	CTGTTCTTCACTCTTGGCTC		
***G6PD* Forward**	CCACCATCTGGTGGCTGTTC	62°C (45 sec)	113 bp
***G6PD* Reverse**	GAAGGGCTCACTCTGTTTGC		

Table 5.1: The oligonucleotide primers used for qPCR study. The primer design is described in section 2.4.2.1. Tm: annealing temperature; sec: seconds. The cycling conditions were 50° C for 2 minutes; 95° C for 10 minutes; and 35 cycles of 95° C for 15 seconds, 55-65°C for 30-45 seconds and 72° C for 45 -60 seconds. With the exception of LRRK2 the extension time (72°C) for all other probes was 45 seconds and for LRRK2 probes was 1 minute. A dissociation curve was also added at the end of the reaction; 95°C for 15 seconds; 60°C for 1 minute and 99°C for 15 seconds, to determine that a single specific PCR product was being formed by the primers.

	Sex	Age	PM delay	pH	Cause of death	Pathological diagnosis	LB status
IPD1	M	77	77.00	6.73	Heart failure	IPD	neocortical
IPD2	M	73	11.20	6.32	N/A	IPD	neocortical
IPD3	F	62	46.20	5.88	Gradual deterioration	IPD	neocortical
IPD4	F	78	75.45	6.46	Advanced PD	IPD	neocortical
IPD5	F	87	47.45	6.62	IPD, slow deterioration	IPD	transitional
IPD6	F	81	24.25	N/A	IPD, congestive heart disease	IPD	transitional
IPD7	M	81	103	6.15	Bronchopneumonia	IPD	transitional
IPD8	M	73	20.30	6.22	PD, Malignant melanoma, 2 in lung	IPD	transitional
IPD9	F	66	125.30	6.2	Advanced PD	IPD	neocortical
IPD10	F	77	~80	6.53	Congestive heart failure	IPD	neocortical
IPD11	F	88	11.30	6.38	Chest infection	IPD	transitional
IPD12	M	70	61.20	6.29	Chest infection	IPD	transitional
IPD13	M	55	8.00	6.37	Progressive degenerative PD disorder	IPD	neocortical
IPD14	M	71	40.45	6.1	Chest infection	IPD	neocortical
IPD15	M	79	27.25	5.88	Sudden death	IPD	neocortical
IPD16	M	71	81.30	6.76	N/A	IPD	neocortical
IPD17	M	70	71.30	6.17	Coronary artery atheroma	IPD	transitional
IPD18	M	91	31.45	5.81	Congestive heart failure	IPD	neocortical
IPD19	F	81	57.30	N/A	Heart failure	IPD	neocortical
IPD20	M	70	51.20	6.29	Gradual deterioration	IPD	neocortical
G2019S-1	F	81	15.00	6.53	Bronchopneumonia	IPD (G2019S)	N/A
G2019S-2	F	84	32.3	5.79	Congestive heart failure	IPD (G2019S)	N/A
G2019S-3	F	80	44.4	6	Advanced PD	IPD (G2019S)	N/A
G2019S-4	F	72	24.55	N/A	Pulmonary embolism	IPD (G2019S)	transitional

Table 5.2:.Summary of IPD and G2019S positive PD cases used in this study. M: male; F: female; PM delay: Post-mortem delay (hours); IPD: idiopathic PD; N/A: not available. Mean age at death = 75.05 years; mean PM delay= 49.48 hours, mean pH= 6.29. LB status refers to transitional or neocortical Lewy body status as described by the McKeith criteria.

	Age at onset	*Age at death*	*Duration of disease*	*Sex (1M/0F)*	*Duration of l-dopa use (yrs)*	*Maximum dose l-dopa (mg/day)*	*dyskinesia after 1st 2 years of disease onset*	*mths to dyskinesia post l-dopa initiation*
IPD1	73.1	77.7	4.6	1	1.6	435.5	0	N/A
IPD2	65.2	73.8	8.6	1	6.3	500	0	N/A
IPD3	55.8	65.1	9.3	0	N/A	N/A	0	N/A
IPD4	***49.4***	***78.7***	***29.3***	***0***	***26.8***	***N/A***	***1***	***54***
IPD5	73.9	88.2	14.3	0	12	500	0	N/A
IPD6	***59***	***81.5***	***22.5***	***0***	***20.6***	***1300***	***1***	***205.2***
IPD7	64.4	81	16.6	1	12.1	N/A	1	N/A
IPD8	58.4	73.2	14.8	1	12.8	N/A	1	N/A
IPD9	***36.5***	***66.5***	***30***	***0***	***25.2***	***660***	***1***	***21.6***
IPD10	***53.1***	***77.1***	***24***	***0***	***23.5***	***580***	***1***	***222***
IPD11	77.2	89	11.8	0	11	250	0	N/A
IPD12	45.9	70.1	24.2	1	13.4	750	0	N/A
IPD13	56.5	65.2	8.7	1	3.4	1000	0	N/A
IPD14	67	72.2	5.2	1	0.9	N/A	0	N/A
IPD15	73.8	79.9	6.1	1	3.9	N/A	0	N/A
IPD16	***57.1***	***71.2***	***14.1***	***1***	***9.1***	***625***	***1***	***98.4***
IPD17	***50.4***	***73.3***	***22.9***	***1***	***21.6***	***1500***	***1***	***12***
IPD18	82.4	92.1	9.7	1	4.9	750	0	N/A
IPD19	***52.9***	***81.1***	***28.2***	***0***	***24.6***	***770***	***1***	***55.2***
IPD20	***59.5***	***70.5***	***11***	***1***	***10***	***870***	***1***	***54***
G2019S-1	***64.6***	***81***	***16.4***	***0***	***14.9***	***1000***	***1***	***90***
G2019S-2	N/A	84.9	N/A	0	N/A	N/A	N/A	N/A
G2019S-3	***52***	***80.9***	***28.9***	***0***	***28***	***2000***	***1***	***37.2***
G2019S-4	***57.1***	***72.9***	***15.8***	***0***	***14***	***600***	***1***	***72***

Table 5.3: A clinical summary of IPD and G2019S positive PD cases used in this study. This tissue was obtained from QSBB and the data was collected by Dr. Sean O Sullivan at QSBB. l-dopa: levodopa; yrs: years; mths: months; N/A: not available. Only the italicised samples in bold red letters were used for the L-DOPA induced dyskinesia correlation analysis described in section 5.3.4.

	Cerebellum	Medulla	Putamen	Amygdala	Entorhinal Ctx	Cingulate gyrus	Frontal Ctx	Parietal Ctx
IPD1	√	√	√	√	√	√	√	√
IPD2	√	N/A	√	√	√	√	√	√
IPD3	√	√	√	√	√	√	√	√
IPD4	√	√	√	√	√	√	√	√
IPD5	√	√	√	√	√	√	√	√
IPD6	√	N/A	√	√	√	√	√	√
IPD7	√	√	√	√	√	√	√	√
IPD8	√	√	√	√	√	√	√	√
IPD9	√	N/A	√	√	√	√	√	√
IPD10	√	√	√	√	√	√	√	√
IPD11	√	√	√	N/A	√	√	√	√
IPD12	√	√	√	√	√	√	√	√
IPD13	√	√	√	√	√	√	√	√
IPD14	√	√	√	√	√	√	√	√
IPD15	√	√	√	√	√	√	√	√
IPD16	√	√	√	√	√	√	√	√
IPD17	√	√	√	N/A	√	√	√	√
IPD18	√	√	√	√	√	√	√	√
IPD19	√	N/A	N/A	√	√	√	√	√
IPD20	√	√	√	√	√	√	√	√
IPD21	N/A	√	N/A	N/A	N/A	N/A	N/A	N/A
G2019S-1	√	N/A	N/A	N/A	N/A	N/A	N/A	√
G2019S-2	√	N/A	N/A	√	√	√	√	√
G2019S-3	√	N/A	N/A	N/A	√	N/A	N/A	√
G2019S-4	√	N/A	N/A	√	√	√	√	√

Table 5.4: Summary of the anatomical regions collected for IPD and G2019S positive PD cases. This tissue was obtained from QSBB, and the table provides a detail for the frozen post-mortem tissue used for the qPCR study and the availability of the anatomical regions. Ctx: cortex; N/A: not available.

	Sex	Age	PM delay (hours)	pH	Cause of death
Con1	F	77	23.00	5.60	Cancer (colon)
Con2	F	86	46.50	6.17	Cancer
Con3	F	84	81.45	6.28	Cancer, heart failure
Con4	M	85	43.35	6.68	Cancer (Oesophagus)
Con5	M	86	53.00	6.65	Bronchopneumonia, heart failure
Con6	M	86	23.30	6.55	Myocardial infarction
Con7	M	81	40.00	6.48	N/A
Con8	F	53	29.50	6.64	Intra-cerebral haemorrage
Con9	M	91	48	6.54	Bronchopneumonia
Con10	F	88	49.25	6.23	Chronic obstructive airway disease
Con11	F	85	34.00	6.31	Cancer (breast)
Con12	F	89	77.3	6.49	Pneumonia
Con13	M	83	117.05	6.81	Heart attack
Con14	M	79	56.40	6.60	Cancer (prostate)
Con15	M	75	64.50	6.18	Pulmonary embolism
Con16	F	81	13.50	6.39	Cancer (colon)
Con17	M	63	42.00	6.23	Congestive heart disease
Con18	M	57	78.5	6.03	Adenocarcinoma
Con19	F	78	23.30	N/A	N/A
Con20	M	71	38.5	N/A	Mesolithioma
Con21	F	83	20.00	6.55	Bowel resection with complications
Con22	F	78	51.30	6.24	Cancer (colon)

Table 5.5: Summary of unaffected subjects used in this study. This tissue was obtained from QSBB. Con: control; M: male; F: female; PM: post-mortem; N/A: not available. Mean age at death: 79 years, mean PM delay: 47.89 hours, mean pH: 6.38.

.

	Cerebellum	Medulla	Putamen	Amygdala	Entorhinal Ctx	Cingulate gyrus	Frontal Ctx	Parietal Ctx
Con1	√	√	N/A	√	√	√	√	√
Con2	√	√	√	√	√	√	√	√
Con3	√	N/A	√	√	√	√	√	√
Con4	√	√	√	√	√	√	√	√
Con5	√	N/A	N/A	√	√	√	√	√
Con6	√	N/A	√	√	√	√	√	√
Con7	√	√	√	N/A	√	√	√	√
Con8	√	√	√	√	√	√	√	√
Con9	√	√	√	N/A	√	√	√	√
Con10	√	N/A	√	N/A	√	√	√	√
Con11	√	N/A	√	√	√	√	√	√
Con12	√	√	√	√	√	√	√	√
Con13	√	√	N/A	√	√	√	√	√
Con14	√	√	√	√	√	√	√	√
Con15	√	N/A	√	N/A	√	√	√	√
Con16	√	N/A	√	√	√	√	√	√
Con17	√	√	√	√	√	√	√	√
Con18	√	N/A	√	√	√	√	√	√
Con19	√	√	√	√	√	√	√	√
Con20	√	√	√	√	√	√	N/A	√
Con21	N/A	√	N/A	N/A	N/A	N/A	N/A	N/A
Con22	N/A	√	N/A	N/A	N/A	N/A	N/A	N/A

Table 5.6: Summary of anatomical regions collected from unaffected controls. This tissue was obtained from QSBB. This table provides a detail for the frozen post-mortem tissue used for the qPCR study and the availability of the anatomical regions. Ctx: cortex; N/A : not available.

5.2.4 Immunohistochemistry

Immunohistochemistry (IHC) was performed on paraffin embedded tissue sections from IPD and PD cases positive for G2019S mutation as described in section 2.5.2. The subjects used are summarised in Table 5.2. The anatomical regions obtained were: medulla, putamen, amygdala, cingulate gyrus, entorhinal, frontal and parietal cortices. The sections were cut at 8µm and processed as described in section 2.5.2 of chapter 2. The tissue processing and visualisation procedure was carried out as described in sections 2.5.2.2–2.5.2.4 of chapter 2. The widely used monoclonal α-synuclein antibody (VP-A106, Vector Laboratories) was used as the primary antibody for the IHC procedure in this study. For visualisation with secondary antibody, mouse immunoglobulins (Dako, UK) were used at a dilution of 1:200. A corresponding haemotoxylin and eosin stain was performed for all the sections. The antibodies and pre-treatments used in this study are listed in Table 5.7. The α-synuclein immunohistochemistry for cingulate gyrus, entorhinal, frontal and parietal cortices was performed by Dr. Tammaryn Lashley (QSBB).

Antibody	Source	Host	Dilution for IHC	Pre-treatments required
α-synuclein	DAKO	Mouse (monoclonal)	1 : 75	pressure cooking and formic acid treatment (Chapter 2, section 2.5.2.5)

Table 5.7: Antibody used for expression of α-synuclein immunohistochemistry.

5.2.5 LB counts and image processing

Upon α-synuclein immunoreactivity, the LBs within the neurons were counted for medulla, putamen, amygdala, cingulate gyrus, entorhinal, frontal and parietal cortices. All the extra-cellular inclusions that displayed α-synuclein positive immunoreactivity were ignored. The area containing LB inclusions was identified under an Olympus BX50 microscope and a photograph of the section was taken using a Nikon Eclipse E800. Image J (NIH) was used to mark the total area of the section to obtain the pixels which were then converted into area per mm^2 (see section 2.8.4). The total number of LBs was then divided by area per mm^2 to obtain LBs per mm^2. The LB

counts for cingulate gyrus, entorhinal, frontal and parietal cortices were performed by Dr. Tammaryn Lashley (QSBB)

5.2.6 Statistical analysis

The qPCR data was analysed using the statistical package SPSS version 14.0. Parametric tests (student's t-test) were conducted for data that was normally distributed and non-parametric tests (Kruskal-Wallis and Mann-Whitney or Spearman's correlation where stated) were used for the data that did not exhibit normal distribution.

Outliers were identified using a box and whiskers plot, and any data point that was more than three standard deviations from the mean was excluded from the subsequent analysis. If tissue was available for all three subject groups (i.e. control, IPD and at least three G2019S positive PD subjects), and the data did not demonstrate normal distribution, then non-parametric test of Kruskal-Wallis (K-W) was used to determine any significant difference. Any significance observed for the K-W test was further refined by using a Mann-Whitney (M-W) test between two groups at a time, i.e. control- IPD, control- G2019S, and IPD- G2019S. This allowed us to determine the combination of subject groups that might contribute to the significance observed in the K-W test.

The LB levels for each region were counted twice on independent occasions and an inter-class correlation was performed to assess the consistency between the two sets of LB counts. For a correlation analysis between LRRK2 mRNA levels and clinical data or LB levels in the brain, Spearman's non-parametric test was used. Outliers were identified using a scatter plot, and a bivariate correlation was performed using the Spearman's rho which was set at 0.500 for a positive correlation and -0.500 for negative correlation between the parameters.

The tests were corrected using the step up Simes' threshold algorithm for multiple comparisons as described in section 2.9.4.2. The graphs were plotted either in SPSS version 14.0 or in Graphpad PRISM (for dot blots).

5.3 Results

5.3.1 LRRK2 mRNA expression study in cerebellum of unaffected and IPD subjects

A study was conducted using qPCR to measure the LRRK2 mRNA expression levels in post-mortem human brain cerebellum tissue of 121 IPD cases and 36 unaffected controls. The mRNA expression data was normalised using two endogenous reference genes, *HPRT1* and *RPL13A.* A geometric mean of the two reference genes was also used to normalise the mRNA expression data. The data was checked for normal distribution, and any outliers (three standard deviations from the mean) were excluded prior to using student's t-test to compare any potential differences between control (n= 35) and IPD (n = 115) subjects.

The analysis revealed a significant difference in mRNA expression levels of *LRRK2* in IPD cases and unaffected controls when the data was normalised individually to the two endogenous reference genes, *HPRT1* and *RPL13A*, (p = 0.001 and 0.003, respectively), or with the geometric mean of the two reference genes (p = 0.001). For the purpose of simplicity, only data normalized to the geometric mean is presented in Figure 5.1 (control LRRK2 mRNA mean = 1.187 and IPD LRRK2 mRNA mean = 0.847, a mean difference of 0.340 in the LRRK2 mRNA levels, 95% CI: 0.149881 and 0.530573).

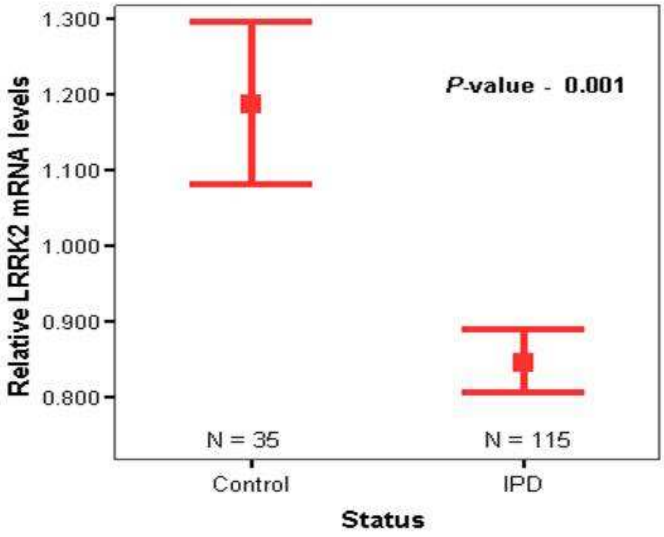

Figure 5.1: A preliminary study showing differences in LRRK2 mRNA levels in the cerebellum of unaffected controls and IPD cases. The data was checked for any outliers (three standard deviations from the mean) using a box and whiskers plot and removed prior to the statistical analysis using a t-test. The data presented here reflects the LRRK2 mRNA levels normalised using the geometric mean of the two endogenous reference genes (*HPRT1* and *RPL13A*). The dots show the mean of LRRK2 mRNA levels, and the error bars around them represent standard error of the mean (+/- 1 SEM). Mean LRRK2 mRNA levels for controls is 1.187 and for IPD subjects is 0.847. The mean difference in the LRRK2 mRNA values for controls and IPD subjects is 0.340 (95% confidence interval of. 0.149881 – 0.53057). The decrease in the cerebellum LRRK2 mRNA of IPD cases versus unaffected controls is significant ($p = 0.001$).

Following on from the results obtained from the preliminary study in cerebellum, post-mortem tissue was collected from other brain regions to determine a quantitative regional map of LRRK2 mRNA levels in the human brain. The data in following sections was produced using tissue from a maximum of 20 controls, 20 IPDs and four G2019S positive PD subjects. Four endogenous reference genes were measured for all the samples, and the data was analysed using non-parametric tests.

5.3.2 Regional variation in LRRK2 mRNA levels in control human brain

A quantitative regional map of LRRK2 mRNA expression levels was determined to complement the LRRK2 ISH results in chapter 4. The data in this particular section was only produced using LRRK2 mRNA levels from unaffected controls (a maximum of 20 samples). These samples were also normalised using a geometric mean of the four endogenous reference genes. Figure 5.2 represents the relative LRRK2 transcript levels and demonstrates that in this data set medulla has the highest mRNA levels of LRRK2, followed by entorhinal cortex, cerebellum and amygdala. The cortical regions of cingulate, frontal and parietal are slightly higher than putamen, but overall Kruskal-wallis (K-W) test revealed no regional differences in LRRK2 mRNA levels.

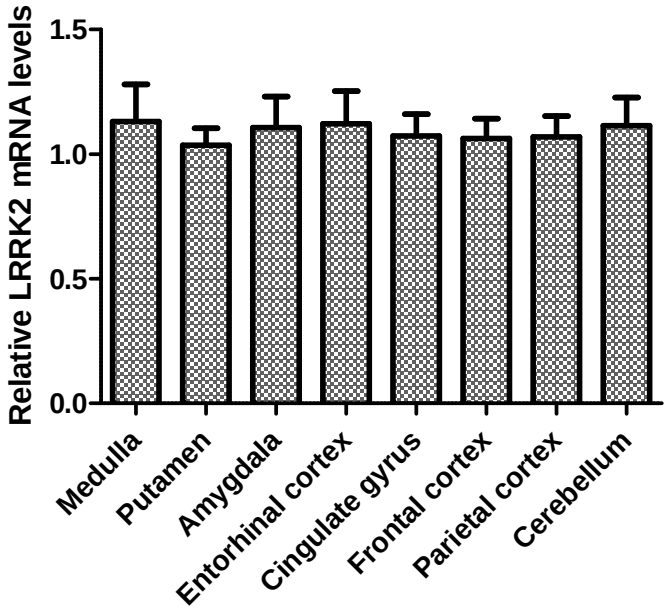

Figure 5.2: Regional expression of LRRK2 mRNA in the normal human brain. The mean LRRK2 mRNA levels were normalised to the geometric mean of the four corresponding endogenous references genes. The bars represent the standard error of the mean, and indicate that overall regional levels of LRRK2 mRNA are not significantly different from each other. Although a slight decrease in LRRK2 mRNA levels is observed in the putamen, overall the LRRK2 mRNA levels were comparable across the regions.

5.3.3 Differential LRRK2 mRNA expression in multiple brain regions of control, IPD, and G2019S positive PD subjects

Differences in LRRK2 mRNA levels were investigated in a maximum of 20 unaffected controls, 20 IPD cases and four G2019S positive cases for various regions across the brain. Due to limited tissue availability, anatomical regions for all the G2019S positive PD subjects were not obtained (please refer to Table 5.4 and 5.6)

Insufficient number of G2019S positive PD subjects in medulla (n =0), putamen (n = 0), amygdala (n = 2), cingulate gyrus (n = 2), and frontal cortex (n = 2) meant that only controls and IPD subjects were included in the statistical analysis (Mann-Whitney (M-W)) for these regions. However, the trend of LRRK2 mRNA levels in G2019S positive PD samples are represented in Figure 5.3.

G2019S positive PD subjects were included in the statistical analysis for entorhinal cortex (n = 3), cerebellum and parietal cortex (both n = 4). Therefore, K-W test was performed for these three regions to assess differences between controls, IPDs and G2019S positive PD subjects. If a statistical significance was achieved with the K-W tests, then M-W tests were performed as described in section 5.2.6.

A general widespread decrease was observed in the LRRK2 mRNA levels in IPD cases compared to unaffected controls in a majority of the regions. This was significant in amygdala, cingulate gyrus, frontal and parietal cortices and cerebellum (see Figure 5.3). Medulla on the other hand, showed an increase in the LRRK2 mRNA levels in IPD subjects. Figure 5.3 represents the box and whiskers plot detailing the interquartile ranges and minimal and maximal points of the data. Any point that was three standard deviations away from the mean was considered an outlier and not included in the analysis. A detailed spread of the individual points, mean and standard error of the mean are represented in Figure 5.4, Figure 5.5, and Figure 5.6.

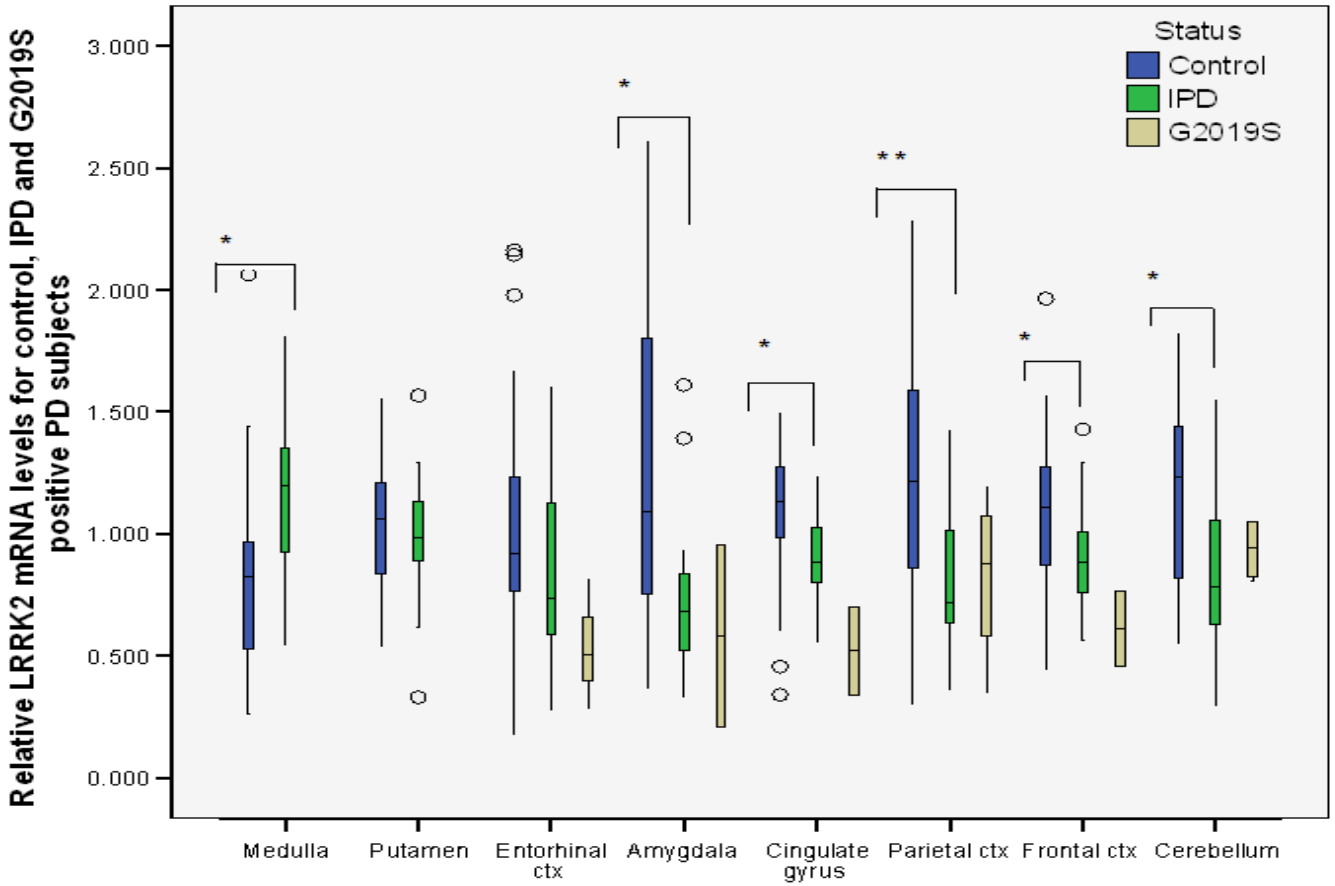

Figure 5.3: Differential expression in LRRK2 mRNA levels in unaffected and IPD subjects. The median in the box plot is represented by the horizontal line inside the box and the interquartile range (IQR) is between the 25th and 75th percentiles which are represented by the horizontal borders of the box. The whiskers show the minimal and maximal values of the main data. *P < 0.05 and **P < 0.01. Statistical tests for G2019S positive PD subjects are not shown on this graph.

5.3.3.1 LRRK2 mRNA levels are increased in the medulla of IPD cases but remain unaffected in the putamen.

Mann-Whitney (M-W) tests were performed for medulla and putamen, and a significant increase was observed in the LRRK2 mRNA levels in the medulla of IPD cases when compared to the controls (p = 0.027). No difference was observed in LRRK2 mRNA levels in putamen of the two subjects groups, although there was a trend towards a decrease in the LRRK2 mRNA levels of IPD cases when compared to the controls. The differential expression observed in medulla and putamen is represented in Figure 5.3, and the figure below (Figure 5.4) represents the spread of the individual points (control and IPD subjects only) using standard error of the mean.

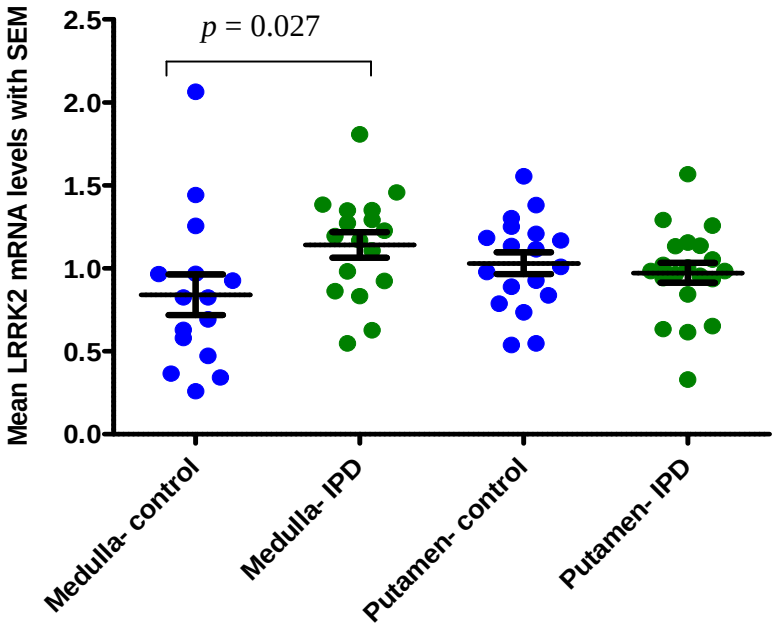

Figure 5.4: Mean LRRK2 mRNA levels in medulla and putamen of unaffected and IPD subjects. This figure represents the spread of individual points, the mean and standard error of the mean (SEM). The number of samples (n) used for this study were: medulla- controls, n = 15 and IPDs, n = 16 and for putamen- controls, n = 18 and IPDs, n = 20. A significant increase in the LRRK2 mRNA levels in IPD cases was observed in the medulla (p = 0.027).

5.3.3.2 LRRK2 mRNA levels are decreased in the medial temporal regions and neocortical regions of IPD cases

No significant difference was observed in the LRRK2 mRNA levels of controls, IPD and G2019S positive PD subjects for entorhinal cortex, although there was a trend towards a decrease in the LRRK2 mRNA levels in PD subjects. Due to the low number of G2019S positive PD cases in amygdala (n = 2), only controls and IPD subjects were included in the statistical analysis for this region. The M-W test revealed a significant decrease in the LRRK2 mRNA levels of IPD cases in amygdala in comparison to unaffected controls (p = 0.014). The differential expression observed in entorhinal cortex and amygdala is represented in Figure 5.3.

LRRK2 mRNA levels were also obtained for a maximum of 20 IPD and 20 unaffected controls for the cortical regions of cingulate gyrus; frontal cortex; parietal cortex and cerebellum. Statistical analysis demonstrated a decrease in the LRRK2 mRNA levels of IPD subjects in comparison to the unaffected controls in cingulate gyrus and frontal cortex. This was significant at the 5% level, p = 0.012 for cingulate gyrus, and p = 0.035 for frontal cortex (see Figure 5.3).

The preliminary cerebellum data was only normalised using, *HPRT1* and *RPL13A* (Figure 5.1). Therefore, to provide consistency the other two reference genes (*G6PD* and *TBP*) were also measured in cerebellum of 20 controls, 20 IPDs and 4 G2019S positive PD cases. A significant decrease in the LRRK2 mRNA levels of IPD subjects was again observed in comparison to the unaffected controls in cerebellum (p = 0.01). However, the most significant decrease in the LRRK2 mRNA levels of IPD subjects was observed in the parietal cortex at a significance level of 1% (p = 0.004) (see Figure 5.3). The spread of the individual points (control, IPD and G2019S positive PD subjects) using standard error of the mean is represented in Figure 5.6.

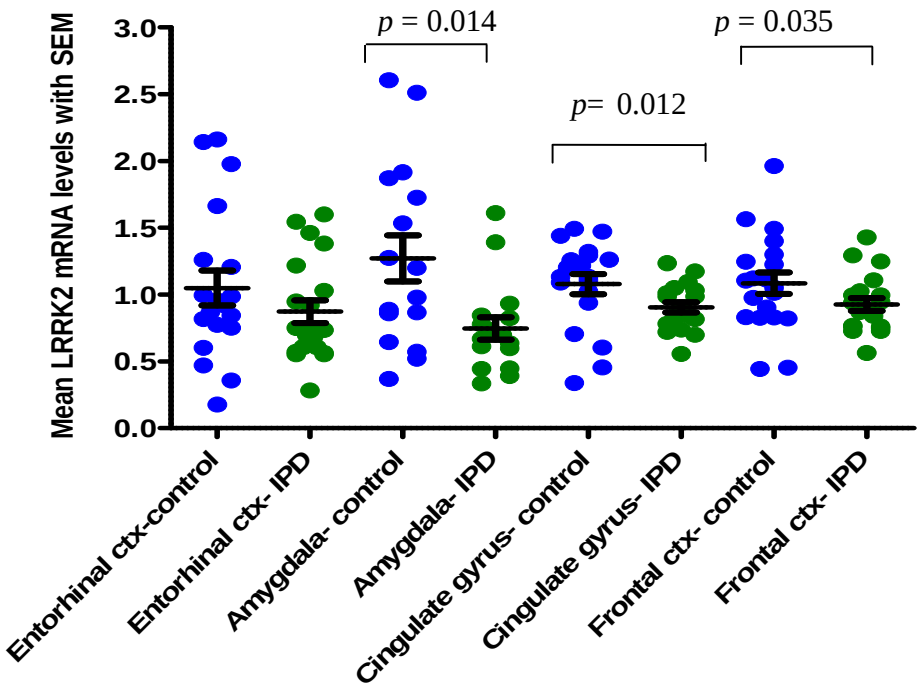

Figure 5.5: LRRK2 mRNA levels are decreased in the medial temporal regions and frontal cortices of IPD cases. This figure represents the spread of individual points, the mean and standard error of the mean (SEM). The number of samples (*n*) used for this study were: entorhinal cortex- control, *n* = 19 and IPD, *n* = 20; for amygdala- control, *n* = 18 and IPD, *n* = 20; for cingulate gyrus- control, *n* = 19 and IPD, *n* = 20; and for frontal cortex,- control, *n* = 19 and IPD, *n* = 20.

5.3.3.3 Is there any difference between LRRK2 mRNA levels of IPD and G2019S positive PD cases?

There was a trend towards a generalised decrease in the mRNA levels of LRRK2 in G2019S positive PD cases compared to the IPDs in the medial temporal lobe regions of amygdala and entorhinal cortex, and the neo-cortical regions of cingulate gyrus and frontal cortex (Figure 5.3). The G2019S positive PD subjects were not included in statistical analysis for these regions (apart from entorhinal cortex), lest their low number skewed the results. Despite no statistical significance, the slight increase in

the LRRK2 mRNA levels of G2019S positive PD cases in comparison to IPD cases for both cerebellum and parietal cortex is an interesting observation (see Figure 5.6. However, when the individual samples are plotted (Figure 5.6), the increase in LRRK2 mRNA levels of G2019S PD compared to IPD subjects is only slightly evident. However, the LRRK2 mRNA levels remain lower than the unaffected controls in both set of PD subjects. It should be noted that cerebellum and parietal cortex are the only two regions where post-mortem tissue from all the four G2019S cases was available. Therefore, any trends where fewer G2019S positive PD cases were used should be interpreted with caution.

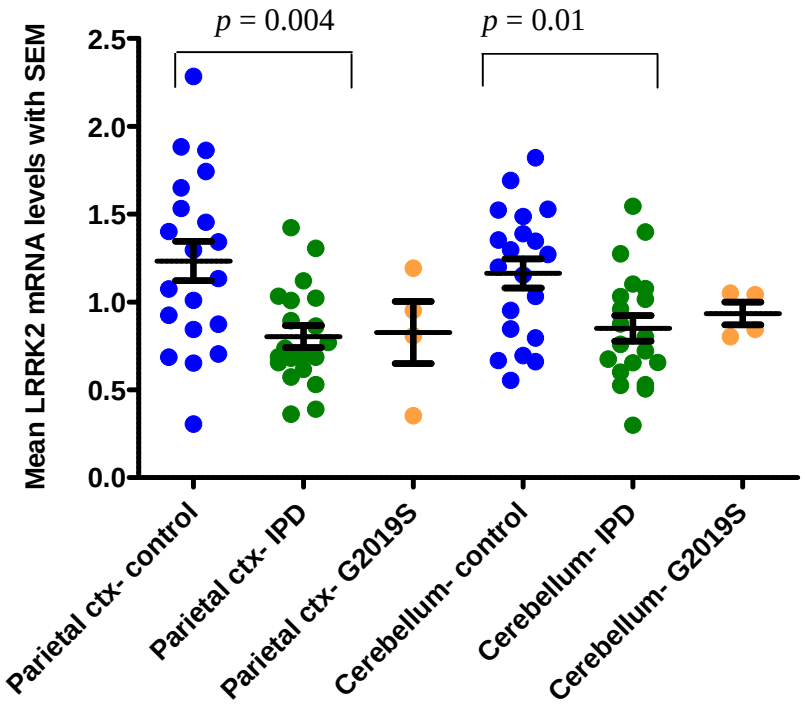

Figure 5.6: Relative LRRK2 transcript levels in cerebellum and parietal cortex of controls, IPDs and G2019S positive PD subjects. This figure represents the spread of individual points, the mean and standard error of the mean (SEM). The number of samples (*n*) used for this study were: parietal cortex - control, *n* = 20; IPD, *n* = 20 and G2019S, *n* = 4. For cerebellum: control, *n* = 20; IPD, *n* = 20 and G2019S, *n* = 4.

5.3.3.4 Multiple test Correction

During hypothesis testing, even if all the null hypotheses are true, there is a 1 in 20 chance that at a significance level of $\alpha = 0.05$, a statistically significant finding will be observed, thereby increasing the risk of false-positives (see 2.9.4.2 for details). Therefore, in order to avoid spurious results (i.e not to reject a correct null hypothesis), it is essential that all the data is corrected for multiple comparisons.

The comparisons being carried out in this particular study related to regional differences in LRRK2 mRNA levels of unaffected, IPD and G2019S positive PD subjects. As described in section 5.3.3, K-W test was performed when samples were present for all three groups (3 tests: entorhinal cortex, cerebellum and parietal cortices). M-W test was performed for two groups at a time (12 tests). Taking into account the initial student's t-test performed for the preliminary cerebellum data set, this puts the total number of comparisons up to 16. The data was corrected using the step-up Simes' algorithm for multiple testing by ranking the *P* -values from the 16 tests in an ascending order, and setting a threshold *P*-value depending on its position within the order. As described in section 2.9.4.2, the step-up Simes' algorithm is an extension of the Bonferroni procedure, although it is a little less conservative on the data.

The *P* -value obtained using the student's t-test for the preliminary cerebellum ($p = 0.001$) data survived the step-up Simes' threshold for multiple testing. Table 5.8 shows the multiple test correction for all the regions that had 20 unaffected, 20 IPD and G2019S positive PD subjects. As can be seen in Table 5.8, the differences observed between IPD and unaffected subjects for parietal cortex, cerebellum, cingulate gyrus, amygdala, frontal cortex and medulla remained significant after being corrected for multiple testing with the step-up Simes' threshold.

	Kruskal-Wallis Test for IPD-G2019S-Control	*step-up Simes' threshold*	*Simes' outcome threshold < 0.05, reject* H_0*, threshold > 0.05, accept* H_0	*Mann-Whitney Test- IPD-Control*	*step-up Simes' threshold*	*Simes' outcome threshold< 0.05, reject* H_0*, threshold > 0.05, accept* H_0
Parietal cortex	**0.012**	**0.022**	**Reject** H_0	**0.004**	**0.011**	**Reject** H_0
Cerebellum	**0.031**	**0.044**	**Reject** H_0	**0.011**	**0.016**	**Reject** H_0
Cingulate gyrus	X	X	X	**0.012**	**0.027**	**Reject** H_0
Amygdala	X	X	X	**0.014**	**0.03**	**Reject** H_0
Medulla	X	X	X	**0.027**	**0.038**	**Reject** H_0
Frontal cortex	X	X	X	**0.035**	**0.05**	**Reject** H_0
Entorhinal cortex	0.126	0.061	Accept H_0	X	X	X
Putamen	X	X	X	0.579	0.077	Accept H_0

Table 5.8: *P*- values corrected using step-up Simes' threshold. Kruskal-wallis was performed for parietal cortex, cerebellum and entorhinal cortex only. The preliminary cerebellum study (student's t-test) is not represented here but was included in the overall multiple comparisons. A significant *P*-value for K-W test meant that the groups (control, IPDs and G2019S PD subjects) were then compared to each other using M-W test. In order for the null hypothesis to be rejected, the threshold value set up by the step-up Simes' correction had to be < 0.05. Only the *P* -values for the M-W tests between control and IPD subjects are shown in this table. H_0 : null hypothesis.

5.3.4 LRRK2 mRNA expression and clinical data

LRRK2 mRNA levels were correlated with gender and duration of illness for IPD and G2019S positive PD subjects. Spearman's correlation revealed no association of LRRK2 mRNA levels with either of the parameters.

Subjects with clinical history reporting levodopa (L-DOPA) induced dyskinesia were identified amongst the IPD group (n = 8) and G2019S subjects (n = 3) (see Table 5.3 for details on the subjects). The effects of L-DOPA induced dyskinesia on regional LRRK2 mRNA levels were then investigated. Spearman's correlation was performed to investigate association between regional LRRK2 mRNA levels and maximum L-DOPA dose (mg/day) or with cumulative L-DOPA dosage during the duration of the illness for these subjects. No correlation was observed for maximum dose of L-DOPA and LRRK2 mRNA levels, but positive trends were observed for amygdala (Spearman's rho= 0.657; p= 0.156) and medulla (Spearman's rho= 0.800; p = 0.200). Weak correlations were observed for cumulative dose of L-DOPA and LRRK2 mRNA levels in cingulate gyrus (Spearman's rho 0.714, p = 0.047) and entorhinal cortex (Spearman's rho 0.683, p =0.042) of subjects with L-DOPA induced dyskinesia. Even though the effects of L-DOPA induced dyskinesia on LRRK2 mRNA levels would have been most relevant to the putamen, no correlations were observed with maximum L-DOPA or cumulative dose in putamen.

5.3.5 LRRK2 mRNA expression and LB pathology count

A correlation between LRRK2 mRNA levels and the collective LB load described as transitional or neocortical (according to the McKeith criteria) was performed and no association was observed. The LB counts per mm^2 (see section 5.2.5) in medulla, putamen, amygdala, entorhinal cortex, cingulate gyrus, frontal and parietal cortices were also correlated to the normalised LRRK2 mRNA levels of the corresponding regions. No correlation was observed between the number of LB inclusions and LRRK2 mRNA levels for any of the regions.

5.4 Discussion

This study demonstrates a widespread dysregulation in the LRRK2 mRNA levels between unaffected and IPD subjects in various anatomical regions across the brain. Trends towards decreased LRRK2 mRNA levels were also observed in G2019S positive PD subjects in comparison to the unaffected subjects. This overall decrease in LRRK2 mRNA levels in PD subjects used in this study suggests a shared mechanism is contributing to the PD pathogenesis experienced by IPD and G019S positive PD subjects. Following on from the identification of LRRK2 protein in LBs (as demonstrated in chapter 4), the effects of LRRK2 mRNA on the eventual LB load in different anatomical regions were also investigated.

A preliminary study comparing LRRK2 mRNA levels in the cerebellum of 115 IPD cases and 35 unaffected controls suggested a marked decrease in LRRK2 mRNA in IPD cases. This was of interest since a decrease in the mRNA levels of the PARK9 (*ATP13A2*) locus in the cerebellum has previously been reported (Vilariño-Güell et al. 2008), despite cerebellum not being immediately affected in the PD pathogenesis like the brainstem. Therefore, further quantitation of LRRK2 mRNA levels was performed in regions more directly implicated in PD, namely, medulla, putamen, cingulate gyrus, frontal cortex, entorhinal cortex and parietal cortex. 20 unaffected cases, 20 IPD cases, and where available, tissue from four G2019S positive PD cases were chosen for this purpose.

A total of four endogenous reference genes were measured for each sample and for every anatomical region. Whilst performing a quantitation of the regional mRNA expression of LRRK2 in unaffected subjects, the geometric mean of all the four endogenous reference genes was used to normalise LRRK2 mRNA data. However, a slightly different methodology was taken to normalise the data when the affected and unaffected were compared. This was done because the normalisation by endogenous reference genes works on the premise that they do not differ between the affected and unaffected. However, it cannot be assumed for certain that the reference genes themselves are not affected during the disease pathogenesis. Therefore, to account for

this anomaly, the software NormFinder was used to select a combination of the reference genes with the least amount of estimated variation in unaffected and affected subjects for each region. Once these were selected, a normalisation factor was calculated using the geometric mean of the reference genes recommended by NormFinder, and this factor was then used to normalise the LRRK2 mRNA levels for affected and unaffected before any further analysis could be undertaken.

Regional expression of LRRK2 mRNA in normal human brain

This chapter demonstrates a quantitative regional description of LRRK2 mRNA in a maximum of 20 unaffected subjects, which to our knowledge is the largest number of samples examined to estimate the LRRK2 transcript levels in post-mortem human brain. Overall there was no statistically significant difference in the regional levels of LRRK2 mRNA, but as demonstrated in Figure 5.2, the highest LRRK2 mRNA levels were identified in medulla and cerebellum. This correlates well with the semi-quantitative results for LRRK2 protein in chapter 4 of this thesis where medulla followed by cerebellum was consistently shown to have high LRRK2 protein levels. Similarly, the medial temporal regions of amygdala and entorhinal cortex, and neocortical regions of cingulate gyrus, frontal and parietal cortices had slightly lower levels of LRRK2 mRNA compared to medulla and cerebellum which also correlates well with the LRRK2 protein data in chapter 4. The moderate to high LRRK2 mRNA and protein (chapter 4) levels in the limbic regions of amygdala, entorhinal cortex and cingulate gyrus, indicates that this protein might play a role in other neurodegenerative diseases or possible late stage cognitive decline associated with PD.

The lowest LRRK2 mRNA levels in this study were recorded for putamen, however, these mRNA levels were still comparable to other regions, and no significant difference was observed as is demonstrated by the error bars in Figure 5.2. This is of interest as in chapter 4 the lowest LRRK2 protein levels were consistently recorded for the striatal neurons. Previous studies have reported higher LRRK2 mRNA levels in striatal putamen as compared to substantia nigra (SN) (Zimprich et al. 2004b; Melrose et al. 2006), but due to a lack of nigral tissue we were not able to make such a comparison,

and this obviously remains a limitation of our study. However, a quantitation of LRRK2 mRNA levels in the putamen as presented in this chapter coupled with data from chapter 4, lends further support to the recommendation that LRRK2 protein has a high turnover in the striatal regions, and as such could play an important role in the nigrostriatal dopamine system.

Widespread reduction of LRRK2 mRNA in IPD cases

As demonstrated in the results section (Figure 5.3), with an exception of an increase in the medulla, LRRK2 mRNA levels were shown to have a generalised decrease in all other anatomical regions of IPD cases examined in this study. Apart from putamen and entorhinal cortex, these trends of decrease in LRRK2 mRNA were statistically significant and all survived the step up Simes' threshold for multiple comparisons.

Taking the Braak staging into account, medulla is the first region to be vulnerable to α-synuclein PD pathology in comparison to the other regions examined in this study. The increase in the LRRK2 mRNA levels in the medulla of IPD cases is different from the generalised decrease observed in the other regions (Figure 5.3 and Figure 5.4). Tissue effect on genetic control of transcript isoform variation has previously been reported in human osteoblasts (Kwan et al. 2009). It is feasible that the LRRK2 mRNA increase in the medulla of IPD cases is due to an upregulation of a region specific isoform(s) of LRRK2 transcript as a compensatory mechanism during initial stages of PD progression in the medulla. However, this is purely speculative and further experiments aimed at measuring not only the region specific isoforms of LRRK2 transcripts, but also their half-lives are needed before inferring that this increase in the LRRK2 mRNA levels of medulla might be an early compensatory mechanism in response to PD progression.

The putamen shows no significant change in LRRK2 mRNA levels despite there being a widespread decrease in all other regions. This is in agreement with previous studies that also reported no difference in the striatal LRRK2 levels in IPD cases and unaffected controls (Melrose et al. 2006; Hurley et al. 2007), although a trend in

decreased levels was observed in IPD cases as was recorded by Galter and colleagues (Galter et al. 2006). The loss of dopamine depletion in the striatum results in a clinical phenotype which is treated using L-DOPA replacement therapy. L-DOPA replacement therapy was administered to the IPD cases (all but one) used in this study and L-DOPA induced dyskinesia was also reported in some IPD and G2019S positive PD subjects (see Table 5.3). Previously L-DOPA induced dyskinesia has been suggested to increase striatal LRRK2 mRNA levels in marmosets (Hurley et al. 2007). Clinical history detailing L-DOPA induced dyskinesia was only available for half of the cases and no correlation between LRRK2 mRNA levels with maximum L-DOPA dose and cumulative dose was observed in putamen. Although a previous study that reported increased LRRK2 mRNA levels in marmosets (Hurley et al. 2007), it should be noted that a detailed retrospective analysis of dyskinesia levels in post-mortem human tissue is not possible. Moreover the clinical data for L-DOPA induced dyskinesia was only available for a minority of cases, therefore not allowing for an accurate correlation analysis between L -DOPA induced dyskinesia and putamen LRRK2 mRNA levels.

Pallor of substantia nigra (SN) is a pathological phenotype associated with both IPD and G2019S positive PD cases. The absence of SN is a limitation of this study, but the data resultant from whole nigral tissue that might be severely degenerated in affected subjects cannot be easily interpreted. This is because a decrease in the mRNA could be associated with extensive cell loss, and a lack of change (or an increase) could be due to compensatory mechanisms which might result in a transcriptional upregulation in the surviving neurons in a region that is critical to PD pathogenesis. The best way to capture transcriptional profile for SN is to obtain individual DAergic neurons using laser capture microdissection, which we were unable to do. Thus, no whole nigral tissue was involved in this study, but a recent study has showed a decrease in LRRK2 mRNA levels of laser capture microdissected DAergic neurons from IPD patients (Simunovic et al. 2008), raising the question of whether LRRK2 is essential for the survival of DAergic neurons or whether reduction in mRNA levels is just an effect of the overall cell loss in SN?

LRRK2 expression in numerous brain regions such as the hippocampus and amygdala which are the key structures of the limbic system has led to suggestion that LRRK2 plays a physiological role not only in the motor but also in certain cognitive elements associated with the PD pathogenesis and/or normal aging (Giasson et al. 2006). The presence of LRRK2 has been reported in neurofibrillary tangles (NFTs) and the pleomorphic pathology related to LRRK2 mutations certainly suggests an important upstream role for this gene in other neurodegenerative disorders (Giasson et al. 2006). It would have been interesting to correlate LRRK2 mRNA levels in these regions to mini mental state examination (MMSE) scores of the patients used in this study. However, a lack of detailed information of MMSE scores for these subjects used in this study, made a correlation analysis unfeasible. Nonetheless, the significant quantitative difference reported in the LRRK2 transcript levels in amygdala and cingulate gyrus, both of which form an important part of the limbic system does lead to the suggestion that LRRK2 might also play a role in the cognitive related decline in PD.

The reduction of LRRK2 mRNA in the cortical regions is also of interest, as even though the biggest impact of PD is felt on the functions of the nigrostriatal dopamine system, PD is a systemic disease of the nervous system. Whether this reduction in cortical regions represents an end-stage involvement remains to be determined but various metabolic defects such as mitochondrial abnormalities, oxidative stress, protein aggregation and abnormal gene regulation have been suggested to result in the early involvement of cerebral cortex in PD (reviewed in (Ferrer 2009)). The multi-domains of LRRK2 have been suggested to play a role in signal transduction, apoptosis, vesicle trafficking, neuronal maintenance, and axonal transport (reviewed in (Greggio & Cookson 2009)). As such a reduction in the LRRK2 mRNA levels could have drastic effects on any number of these functions resulting in various metabolic defects that might contribute to PD progression.

Could dysregulation of a shared auxiliary mechanism contribute to the indistinguishable phenotype of IPD and G2019S positive PD subjects?

The LRRK2 mRNA levels were also investigated in the anatomical regions for the four G2019S positive PD cases obtained from the QSBB archive. Despite the low number of G2019S positive PD subjects, there was a consistent trend towards low LRRK2 mRNA levels in G2019S positive PD subjects in comparison to the unaffected subjects. This is interesting as the dysregulation of LRRK2 mRNA in G2019S positive PD subjects is in the same direction as observed in IPD cases without the G2019S mutation.

For a majority of the regions (cingulate gyrus, amygdala, frontal and entorhinal cortices), lower levels of LRRK2 mRNA were recorded in G2019S positive PD subjects in comparison to IPD subjects. However, the only regions where the trends in LRRK2 mRNA levels of G2019S positive PD subjects were comparable to IPD subjects were in the cerebellum and parietal cortex. This is because cerebellum and parietal cortex are the only two areas where tissue was available for the maximum number of G2019S positive PD subjects (n = 4) in this study. It should be noted that the sample G2019S-2 that was available for all the regions (not including medulla and putamen) also displayed low levels of mRNA for the endogenous reference genes, indicating that tissue from this subject might not be well preserved. Therefore, all the regions that display low mRNA levels in G2019S positive PD samples in comparison to IPD cases (Figure 5.3) could have been skewed by this particular sample. Regardless of this, LRRK2 mRNA levels were decreased in all G2019S positive PD subjects when compared to the unaffected controls.

A previous study that examined the phosphorylation activity of LRRK2 in leucocytes of unaffected, IPD and G2019S positive PD subjects reported a reduced LRRK2 protein activity in G2019S positive PD and IPD subjects in comparison to controls, but a slight increase in LRRK2 phosphorylation activity of G2019S positive PD in comparison to IPD subjects (White et al. 2007). There is also a slight increase in the LRRK2 mRNA levels of the G2019S positive PD cases compared to the IPDs in this

study (as presented in cerebellum and parietal cortices, Figures 5.3 and 5.6), but the low numbers of G2019S positive PD subjects in this study does not allow us to make any statistical inferences. Therefore, tissue from a larger numbers of G2019S positive PD subjects is needed in order to accurately assess this question.

In addition, chapter 4 of this thesis demonstrated no difference in the morphological profile of LRRK2 mRNA and protein in IPD and G2019S positive PD subjects. Collectively, these data suggest that the widespread decrease in LRRK2 mRNA levels of IPD as well as G2019S positive PD cases (in comparison to unaffected subjects) might be a shared auxiliary mechanism that contributes to the purely idiopathic PD as well as PD resultant from the mutational insult of G2019S.

No correlation between LRRK2 mRNA and α-synuclein immunoreactivity to LBs

In-vivo substrates of LRRK2 have not yet been identified, but it was recently shown that LRRK2 phosphorylates α -synuclein *in-vitro* (Qing et al. 2009). Moreover, LRRK2 has also been shown to phosphorylate ERK (Liou et al. 2008) which itself has been implicated in a MAPK pathway phosphorylating increased levels of α-synuclein in response to MPP+ administration in a neuroblastoma cell line (Gómez-Santos et al. 2002). Increased levels of α-synuclein have shown to be toxic in DAergic neurons both in MPTP administered *in-vitro* and *in-vivo* models neurons (reviewed in (Goldberg & Lansbury 2000)). Increased mRNA levels of α-synuclein in DAergic neurons of PD patients have been identified, (Gründemann et al. 2008), and more recently a decrease in LRRK2 mRNA levels of DAergic neurons were also reported (Simunovic et al. 2008). Taking the current literature into account, one could make a conceptual argument that LRRK2 is an active member of the MAPKKK pathway that might play a part in the modulation of α-synuclein by phosphorylation.

The presence of LRRK2 protein in a small proportion of LBs was confirmed in chapter 4 of this thesis, and as such a correlation was performed to investigate the effect of LRRK2 mRNA levels on the number of LB inclusions, if any at all. No

correlation was observed between the levels of LRRK2 mRNA and LB inclusions in IPD or G2019S positive PD subjects. However, the number of IPD (20) and G2019S positive PD (4) subjects in this study could be low for an accurate correlation analysis. Therefore, a higher number of samples are needed for a robust correlation analysis between the levels of LRRK2 mRNA levels and LB inclusions in IPD and G2019S positive PD subjects.

A major contribution to this investigation would have been an accurate quantitative measurement of both LRRK2 and α-synuclein proteins. However, current lack of a robust ELISA assay for LRRK2 makes it hard to perform accurate quantitative analysis for the LRRK2 protein levels. Alternatively, if LRRK2 does indeed modulate phosphorylation of α-synuclein in LBs, assessing the levels of phospho-α-synuclein in the LBs might provide a better parameter for a correlation with the LRRK2 mRNA and protein levels in IPD and G2019S positive PD subjects.

Conclusion

This study describes a quantitative regional expression of LRRK2 mRNA in the human brain. The widespread reduction of LRRK2 mRNA levels in various limbic and neocortical regions across the brains of IPD and G2019S positive PD subjects in comparison to the unaffected controls, suggests that auxiliary mechanisms might make an important contribution to PD pathogenesis.

Although the function of LRRK2 remains debatable, the multiple domains it contains suggest a possible involvement in various upstream signalling events. Subtle quantitative changes in the LRRK2 transcription could affect its kinase activity (amongst other functions), and have unfavourable consequences on subsequent signalling pathways. It is feasible that the broad decrease in LRRK2 mRNA levels in the brains of IPD subjects is an indication of how complex interactions between many cells types across different regions might be affected in addition to the characteristic loss of nigral neurons, thereby resulting in PD progression. Alternatively, if LRRK2 is indeed involved in neuronal maintenance, then a reduction of LRRK2 mRNA

levels in PD brains, providing that it results in a reduction of LRRK2 protein levels might contribute to the characteristic loss of nigral neurons in both IPD and G2019S positive PD subjects.

Chapter 6

6 The effects of cis-acting variation on *LRRK2* mRNA levels

6.1 Introduction

Differences in interspecies gene (transcription) expression profile suggest that the regulation of the transcriptome has been an essential driving force for the phenotypic evolution of humans (Gilad et al. 2006). Despite sharing 98.7% of their genomic sequence, marked variations in the gene expression of human and chimpanzees have been reported, especially in the central nervous system (Enard et al. 2002). The human genome has a lower number of protein encoding genes than previously expected, and the precise regulation of these has been suggested to result in the physiological complexity of humans (Pastinen & Hudson 2004).

The process of transcription, where DNA is transcribed into mRNA is a carefully regulated mechanism that results in a quantitative phenotype. This mechanism can be affected by *cis*-acting (genetic variation) factors, or by *trans*-acting regulatory elements, such as transcription factors that regulate gene expression by inducing DNA-protein interactions (reviewed in (Knight 2003). The *cis*-acting genetic variation can be present in regulatory regions, such as promoters and enhancers, or as exonic (or intronic) variants that alter transcript splicing and stability, and thereby produce various alternatively spliced isoforms of the mRNA. Genetic variation also has the ability to act in *trans*, if present on a different chromosome. All these regulatory factors can affect the delicate process of transcription, and result in altered levels of the nascent mRNA (reviewed in (Knight 2003).

Genetic variation that is involved in regulation of gene expression (mRNA transcription) is difficult to identify, as it can be located within the promoter, the 5' upstream region (5'-UTR), the transcript, or the introns. Enhancers or silencers, upstream or downstream of the transcribed region also contain regulatory sequences. Thus, accurate identification of putative regulatory sequences is highly dependent on how well the genomic sequence has been annotated. However, large scale genome wide expression studies have demonstrated that altered gene expression due to

genetic variation is a common phenomenon, and many linked loci work together in *cis* to exert regulatory influences (Morley et al. 2004; Buckland 2004a; Cheung et al. 2005; Dixon et al. 2007; Göring et al. 2007; Stranger et al. 2007). Variations in gene expression have been extensively demonstrated in the human brain (Bray et al. 2003; Buckland et al. 2004b). Studies suggest that quantitative trait loci for expression (eQTL) are correlated with the transcript abundance, and could work together to have a cumulative effect on gene expression (Myers et al. 2007). These large scale studies that correlate global gene expression levels to genetic variation have identified a regulatory role for a significant proportion of the non-coding variation.

A popular hypothesis about risk of common, complex diseases is that the causation is due to a small collection of variant loci (eQTL), each of which contributes a little to the ultimate complexity of the disease phenotype (Myers et al. 2007). Investigation of common genetic variation that might produce a regulatory effect on the gene expression is fast becoming an approach that can help with the understanding of disease pathogenesis when a mutational insult is not always apparent. This phenomenon has already been shown to have an effect on the catechol-o-methyl transferase (COMT) expression in schizophrenia patients (Bray et al. 2003), and apolipoprotein E (APOE) expression in Alzheimer's disease (Bray et al. 2004). Therefore, the concept that gene expression differences are influenced by variants in regulatory elements has become increasingly popular in investigation of complex disorders (Pastinen & Hudson 2004; Pastinen et al. 2006).

Whole genome expression studies provide the most information for the transcriptome profile. However, the effects of *cis*-genetic variation on inter- and intra-individual differences in the gene expression can also be detected using technologies that measure the relative abundance of mRNA transcripts containing each allele. These technologies include a single base extension (SBE) method (Yan et al. 2002), an oligo array method (Lo et al. 2003), RT- coupled 5'nuclease assays (Zhu et al. 2004), haploCHIP assays (Knight et al. 2003), or purely mathematical algorithms (Teare et al. 2006). However, these methods usually focus on heterozygous individuals, as it is assumed that in the absence of any *cis*-acting variation, both the alleles of a gene will

be equally expressed. Therefore, if an individual is heterozygous for a variant that regulates expression in *cis* then the mRNA from each allele will be differentially expressed. Such allelic imbalances, known as differential allelic expression (DAE) are a widespread occurrence and can be used to identify *cis*-acting factors that modify disease risk. These can then be functionally assessed using a variety of techniques, such as in-*vitro* promoter luciferase assays.

The effects of *cis*-acting variation on mRNA levels have previously been documented in PARK loci associated with autosomal dominant and recessive forms of PD. Variation in the 5'UTR regions of *SNCA* and *PRKN* have been shown to affect the transcriptional activity of these genes. The polymorphic microsatellite repeat NACP-Rep1 is located 10 kb upstream of *SNCA* transcription start site, and its alleles have frequently been show to produce differing risks of PD by modulating the transcription of *SNCA* (Chiba-Falek & Nussbaum 2001; Maraganore et al. 2006). The variant -258T/G in the core *PRKN* promoter has been demonstrated to affect the expression of the gene by binding to nuclear protein in substantia nigra (SN) *in-vitro*, (West et al. 2002). The wild type allele -258T was shown to have an *in-vitro* increase in the transcriptional activity of the *PRKN* gene under oxidative stress or proteasomal inhibition (Tan et al. 2005b). Furthermore, the variant -258G allele was shown to be significantly associated with PD risk in Caucasian and Chinese populations (West et al. 2002; Tan et al. 2005). These results demonstrate the importance of investigating non-coding genetic variation and their regulatory role in PD pathogenesis.

Thus far no reports have been published on genetic variation in 5' UTR of *LRRK2* affecting its transcriptional activity. A widespread reduction of *LRRK2* mRNA in the brains of IPD cases versus unaffected subjects has been demonstrated in chapter 5. Therefore, the study described in this chapter was designed with a view to investigating whether LRRK2 mRNA expression, like the PARK loci, *SNCA* and *PRKN*, can also be regulated by genetic variation in its 5'UTR sequence.

6.1.1 Hypothesis and specific aims

In this chapter, I wished to investigate the hypothesis that the alterations in *LRRK2* mRNA expression between IPD cases and controls as demonstrated in chapter 5 of this thesis is a quantitative phenotype that can be attributed to *cis*-acting genetic variation in putative regulatory elements of the *LRRK2* gene.

To address this question, a study was designed with a view to investigating the regulatory variation in the regions upstream of the *LRRK2* gene. A 10 kb region upstream of the *LRRK2* transcription start site was investigated for genetic variation and four tag SNPs (tSNPs) were identified. An *in-silico* analysis with the genotype information and the results of the qPCR study for the cerebellum (section 5.3.1, chapter 5) was then performed to identify whether any of the four tSNPs were involved in the mRNA regulation of the *LRRK2* gene. Assays were then designed to ascertain whether differences in DNA:protein interaction due to the variation in the putative regulatory sequence could modulate LRRK2 mRNA levels. A genetic association study was also performed to identify the risk posed by the tSNP in question.

6.2 Methods and Materials

6.2.1 LD analysis and tagging SNPs

A LD map 10 kb upstream (38,895,080-38,905,350) of the *LRRK2* transcription start site was generated to select SNPs that were representative of the common genetic variation in that region. Caucasian HapMap Data release 21/phase II Jul06, on NCBI B35, dbSNP b125, available through International HapMap Project (www.hapmap.org) was used to calculate the LD metrics. Haploview was used to select the SNPs that could 'capture' up to 95% of the common genetic variation across the region (r^2= 0.80). These are termed tag SNPs (tSNPs). The 'tagger' function in Haploview generated four tSNPs for the 10 kb 5'-UTR of *LRRK2*. The tSNPs identified were rs10878224, rs2708435, rs1472117 and rs7294619 (see Figure 6.1). All of these four tSNPs were shown to be conserved in the primates, and rs1472117 and rs7294619 were also conserved in other mammals (see Figure 6.2).

6.2.2 Genotyping

Genomic DNA was genotyped either using standard PCR and RFLP assays or the taqman technology as described in section 2.3 of chapter 2. The DNA for section 6.3.1 was obtained from tissue acquired by the QSBB (see appendix 1 for a clinical summary of these samples). The mean age of the IPD subjects was 77 years and for the control subjects was 78.4 years. The DNA for the 2800 unaffected controls in section 6.3.1.3 was obtained through collaboration with Prof. Steve Humphries (Rayne Institute, UCL). These controls were all male with a mean age of 56 years and an age range of 49-64 years. These samples have been described in a previous study (Miller et al. 1996).

6.2.2.1 Restriction fragment length polymorphism

Following on from chapter 5, the genomic DNAs for 115 IPD cases and 35 controls (cerebellum tissue used in the preliminary RNA studies) was obtained as described in section 2.2.1 of chapter 2. The primers for the four tSNPs, annealing temperatures

and restriction enzymes used to genotype genomic DNA are summarised in Table 6.1.

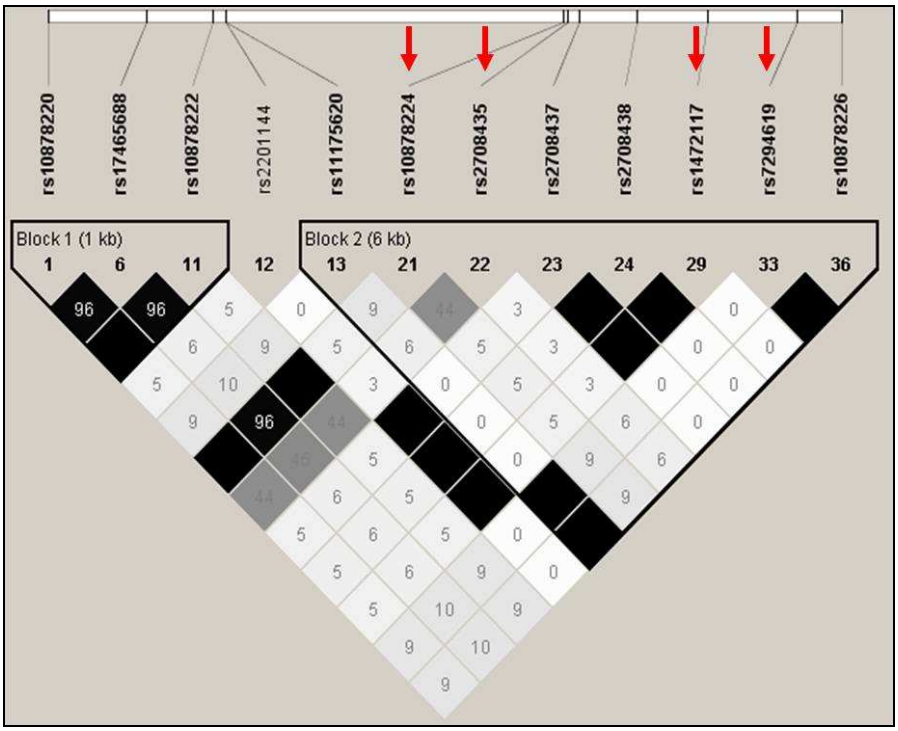

Figure 6.1: Graphical representation of LD map for a 10 kb region upstream of the *LRRK2* gene. The r^2 parameter is used to calculate the pairwise LD values with black boxes showing complete LD (r^2=1.0) between the two loci. The lighter shading denotes a lower LD value ($r^2 < 1.0$), and the numbers in the boxes represent the LD measure of r^2. Red arrows represent the tSNPs chosen by Haploview to represent 95% of the common genetic variation across the region ($r^2 \geq 0.80$).

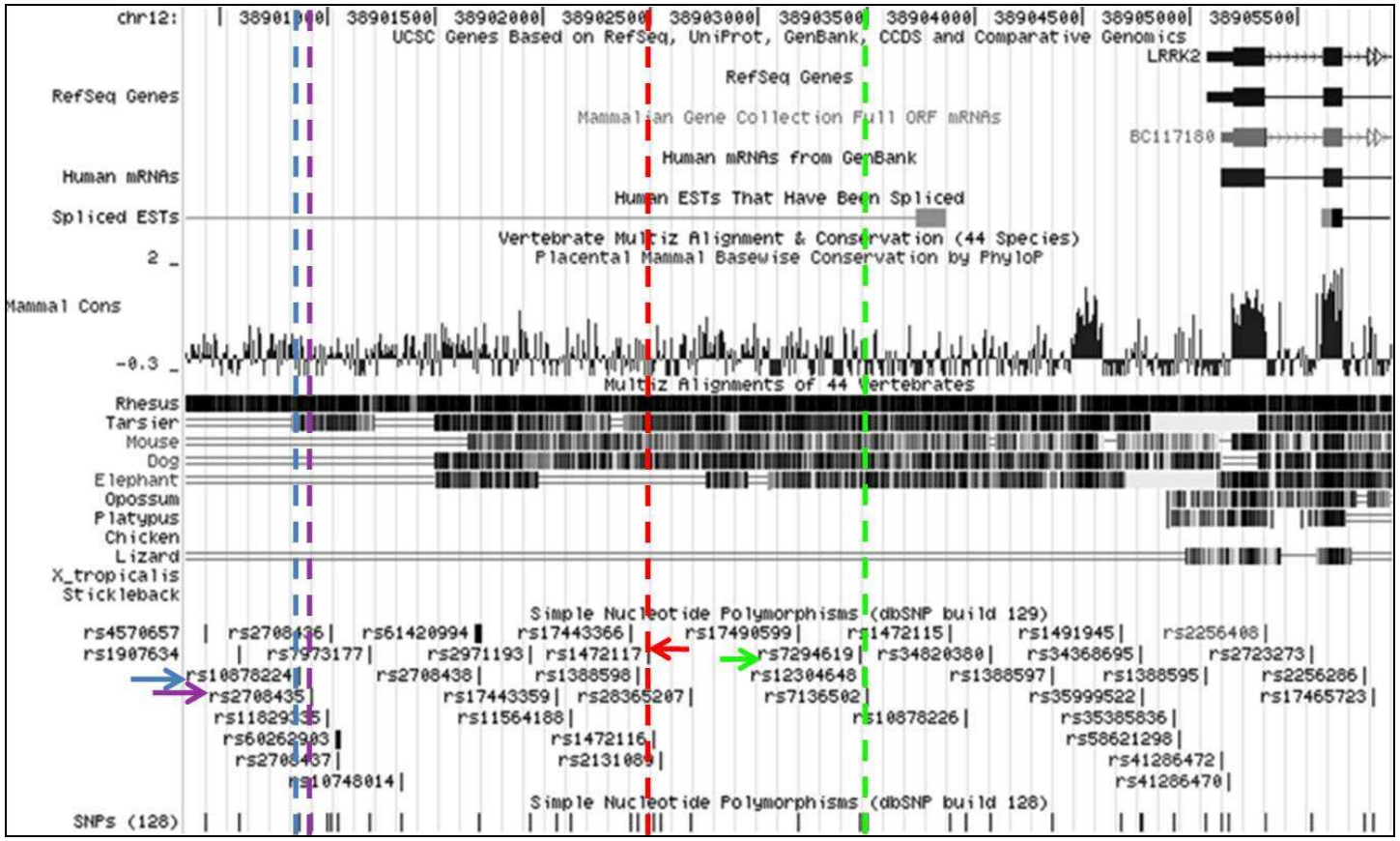

Figure 6.2: Variation in upstream regions of *LRRK2* and the levels of conservation. This was obtained using UCSC Genome browser on Human March 2006 assembly of chr12:38,900,340-38,905,940. The blue arrow indicates tSNP1 rs10878224, purple arrow indicates tSNP2 rs2708435, red arrow indicates tSNP3 rs1472117 and green arrow indicates tSNP4 rs7296419.

tSNP	Position	Primer sequence 5'-3'	Amplicon size (bp)	Tm	Alleles & MAF	Restriction Enzyme	Type
tSNP1: rs10878224	38,900,868	F: CTTCCAGCCTATGGTCATC R: GGAGTTATAGGTTACACTGAGC	263	58°C	T/C C=0.35	Sml1	Common variant cutter
tSNP2: rs2708435	38,900,923	F: CTTCCAGCCTATGGTCATC R: GGTGGGAGGCTTACTTGAGG	361	58°C	G/A A= 0.35	HinF1	Rare variant cutter
tSNP3: rs1472117	38,902,484	F: TCACTCATGTTTAGGAACAC R: GAAACTAGAAGTCAAACGGC	239	55°C	G/A A= 0.067	BstN1	Common variant cutter
tSNP4: rs7294619	38,903,469	F: CATATTATCTTCAACAATgA R: GTTGAAATGGTTAGGATTTC'	118	48.3°C	T/C C= 0.103	DpnII	Artificial site for common variant cutter

Table 6.1: PCR primer sequences and restriction enzymes used for genotyping genomic DNA. Tm: Annealing temperature at 30 seconds; tSNP: tag SNP; bp: base pair; MAF = minor allele frequency. Since the tSNPs for *LRRK2* were genotyped using restriction assays, an artificial restriction site was created for *LRRK2* rs7294619 by changing a base on the forward primer (highlighted 'g'). All the restriction enzymes were provided by New England Biolabs.

6.2.2.2 Taqman

The taqman assay-by-design service for SNP genotyping assays (Applied Biosystems, UK) was used to design probes for the intronic SNP rs4567538. The probes were dye-labelled with FAM and VIC;

5'AGGAGTTCAGATATATCTTTGATATACTGATGTTCTTTTTTTGGNTATAT ACCCAG**[C/T]**GATGAGATTACTGGATCATATGAAAATTCTCTTTTTAGTTT TTTAAGATACCTCCA 3'

The allele discrimination PCR components are described in section 2.3.5 of chapter 2 and the PCR cycling conditions used were as follows:

95º for 10 minutes,

(92º for 15 seconds, 60ºfor 1 minute) X 40 cycles

4º ∞

6.2.3 LRRK2 mRNA quantitation

LRRK2 mRNA levels from section 5.3.1 of previous chapter was used to assess any correlations between the LRRK2 tSNP genotypes and mRNA levels in the cerebellum. It should be noted that unlike chapter 5 where the NormFinder software was used to estimate the variation in the endogenous reference genes, the same could not be done to this data. NormFinder needs data from more than three reference genes to estimate variation, and only two reference genes were measured in this relatively large number of samples for cerebellum (see section 5.3.1). Therefore, the LRRK2 mRNA data presented in this chapter was either normalised to two independent reference genes, *HPRT1* and *RPL13A*, or normalised to the factor calculated using a geometric mean of the two reference genes.

6.2.4 Statistical analysis

The statistical significance was set at $P < 0.05$, and one way ANOVA analysis was used to determine differences between genotypes and LRRK2 mRNA levels. Please refer to sections 2.4.2.3 and 2.4.2.4 of chapter 2 for data normalisation with the endogenous reference genes. Any sample that was not within three standard deviations (SD) of the overall mean was regarded as an outlier and subsequently

omitted from the analysis. Any deviations from the Hardy Weinberg equilibrium (HWE) in the case and control populations were tested through a chi-squared test. For the genetic association study, calculations of HWE, genotype-specific Odds ratio (OR), and 95% CI were carried out using an online tool, FINETTI (section 2.9.1 and 2.9.3 of chapter 2).

6.2.5 Transcription regulation procedures

The virtual laboratory software PROMO (refer to section 2.8.3) was used to identify putative transcription factor binding sites (TFBS) in a 25mer DNA sequences around the SNP of interest in the *LRRK2* upstream region. A dissimilarity margin of less or equal than 5 % was indicated for the predicted factors.

6.2.5.1 Electrophoretic mobility shift assay (EMSA)

Please refer to section 2.7.1 for details on preparation of nuclear lysates from SH-SY5Y neuroblastoma cell line. The oligonucleotide probes used for EMSAs are detailed in Table 6.2. The procedure for the annealing of these probes to generate double stranded DNA (dsDNA) as well as the EMSA protocol is described in section 2.7.2 of chapter 2.

SNP rs2708435	**EMSA double stranded probe sequences (5' – 3' direction)**
A allele	
Forward	Biotin-CACAG**TGGAATCAAGTGATCC**ACAG
Reverse	CTGTGGATCACTTGATTCCACTGTG
G allele	
Forward	Biotin-CACAG**TGGGATCAAGTGATCC**ACAG
Reverse	CTGTGGATCACTTGATCCCACTGTG

Table 6.2: Oligonucleotide sequences for EMSAs. The oligonucleotide probes representing the forward strands were labelled with biotin at the 5' end. The bases highlighted in yellow represent the alleles A and G. Prior to the EMSA the biotinylated probes were annealed to their complementary strands as described in section 2.7.2.1 to generate dsDNA.

6.3 Results

6.3.1 LRRK2 mRNA expression and genotypes

The IPD and unaffected subjects were genotyped for four tSNPs. These tSNPs were selected from a 10 kb upstream region of the *LRRK2* start site that was shown to be conserved in the primates (see Figure 6.2). The results for these genotypes were checked for deviations from HWE are summarised in Table 6.3.

tSNPs	**tSNP1-rs1087224** ***n***	**tSNP2-rs2708435** ***n***	**tSNP3-rs1472117** ***n***	**tSNP4-rs7294619** ***n***
Cases				
Wild-type Homozygote	*23*	*65*	*115*	*102*
Heterozygote	*70*	*47*	*13*	*24*
Rare Homozygote	*32*	*13*	*0*	*1*
***P*-value**	*0.16*	*0.31*	*0.54*	*0.75*
Deviation from HWE	*No*	*No*	*No*	*No*
Controls				
Wild-type Homozygote	*9*	*12*	*29*	*18*
Heterozygote	*21*	*18*	*1*	*9*
Rare Homozygote	*2*	*2*	*0*	*3*
***P*-value**	***0.03***	*0.16*	*0.93*	*0.27*
Deviation from HWE	***Yes***	*No*	*No*	*No*

Table 6.3: Genotype information for the four tSNPs upstream of *LRRK2* transcription start site. *n* represents the number of samples genotyped. IPD cases and unaffected controls were genotyped for the four tSNPs using restriction enzymes, and the deviation from HWE was assessed. Apart from the control genotype data for tSNP1 (rs1087224), all other data displayed HWE.

An *in-silico* analysis was then performed to determine whether this genotype information could affect the LRRK2 mRNA expression data from the cerebellum of IPDs (n =115) and controls (n =35) as described in section 5.3.1 of chapter 5. The reference genes, *HPRT1* and *RPL13A* were measured for this large set of cerebellum post-mortem tissue (section 5.3.1). A significant difference was not observed for the *LRRK2* tSNP genotypes and mRNA expression. There was a trend (a marginal significance) towards a difference in genotypes for tSNPs rs10878224 and rs2708435 and mRNA levels (p = 0.042 and 0.057, respectively) when the data was normalised to the housekeeper *RPL13A*.

The mRNA expression levels for the rare variant genotype (CC) for tSNP1 rs10878224 showed a decrease (p= 0.042) when compared to the wild-type homozygote and the heterozygote (see Table 6.4). Due to the deviation of rs1087224 control genotype data from HWE, this result was interpreted with caution and was not included in further analysis. The variant genotype (AA) for tSNP2 rs2708435 showed a trend towards increased LRRK2 mRNA levels in comparison to the other groups (p=0.057). Nothing significant was observed for tSNP3 (rs1472117) and tSNP4 (rs7294619) (see Table 6.4).

LRRK2 tSNPs	Genotype	*n*	Mean LRRK2 mRNA levels	Standard deviation	*P*-value
rs10878224_H	TT	26	1.001	0.510	0.424
	TC	82	0.919	0.517	
	CC	30	0.831	0.348	
rs10878224_R	TT	26	1.110	0.578	**0.042**
	TC	80	0.928	0.551	
	CC	29	0.758	0.278	
rs2708435_H	GG	69	0.870	0.425	0.238
	GA	58	0.892	0.522	
	AA	11	1.135	0.593	
rs2708435_R	GG	68	0.859	0.411	**0.057**
	GA	56	0.912	0.589	
	AA	12	1.247	0.642	
rs1472117_H	GG	127	0.909	0.473	0.794
	GA	13	0.946	0.606	
rs1472117_R	GG	124	0.919	0.525	0.682
	GA	13	0.981	0.504	
rs7294619_H	TT	103	0.904	0.501	0.988
	TC	30	0.897	0.437	
	CC	4	0.938	0.423	
rs7294619_R	TT	102	0.911	0.514	0.642
	TC	29	0.885	0.496	
	CC	4	1.141	0.494	

Table 6.4: Effects of *LRRK2* tSNPs on mRNA levels. This table represents the effects of *LRRK2* 5'-UTR tSNPs genotypes (rs10878224, rs2708435, rs1472117 and rs7294619) on the mean *LRRK2* mRNA levels in the post-mortem cerebellum tissue. No 'AA' samples were identified for rs1472117. These descriptive statistics were calculated using one way ANOVA. tSNP_H and tSNP_R refers to the LRRK2mRNA data normalised using the reference genes *HPRT1* and *RPL13A*, respectively. Dissimilar genotype numbers (*n*) for the same tSNP are due to different outliers being excluded during the analysis of the LRRK2 mRNA levels.

The effects of rs2708435 genotypes on the LRRK2 mRNA levels were also normalised using the geometric mean of the two reference genes. A similar trend as displayed in Table 6.4 was observed with AA genotypes displaying increased LRRK2 mRNA levels in the subjects, and GG or GA genotypes showing decreased LRRK2 mRNA levels.

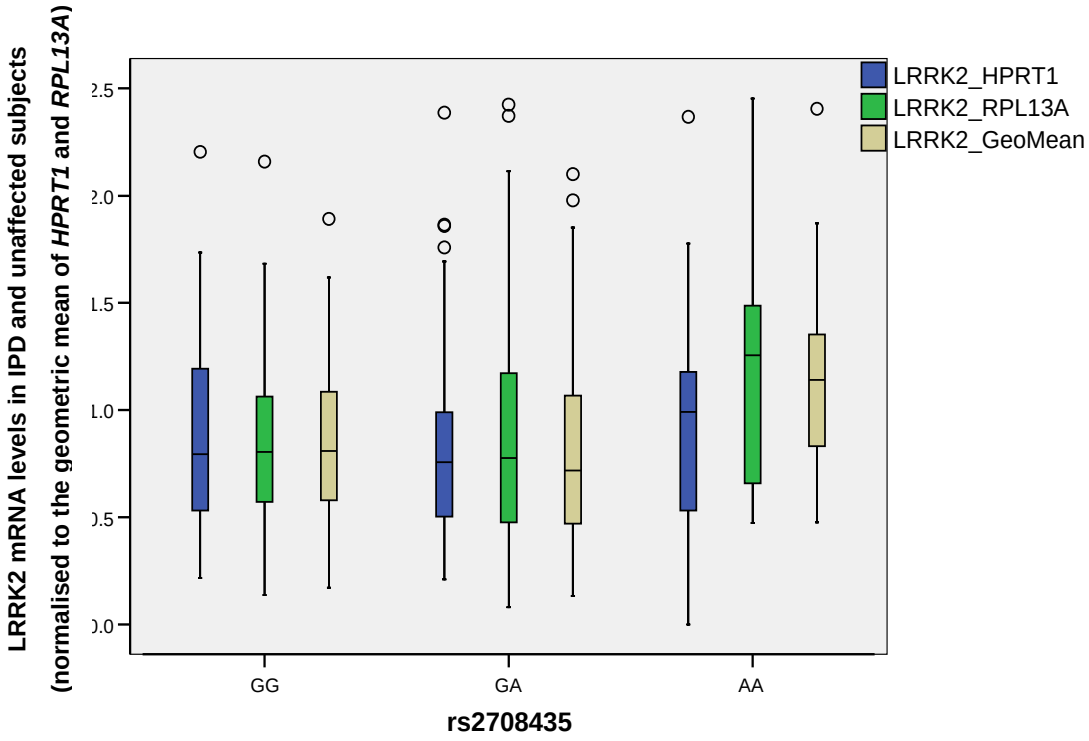

Figure 6.3: The effects of rs2708435 genotypes on LRRK2 mRNA expression in cerebellum. This figure represents a trend towards higher LRRK2 mRNA expression levels in subjects with the AA genotype in comparison to GG or GA genotype. The LRRK2 mRNA levels were normalised using the reference gene *HPRT1* (blue bars), *RPL13A* (green bars), and a geometric mean of the two reference genes (yellow bars). This box and whiskers plot was determined using the data from the unaffected and IPD subjects. The median in the box plot is represented by the horizontal line inside the box and the interquartile range (IQR) is between the 25th and 75th percentiles which are represented by the horizontal borders of the box.

6.3.1.1 A 5′- UTR SNP regulating LRRK2 mRNA expression

As can be seen in Figure 6.3, only weak trends were observed for the rs2708435 genotypes and LRRK2 mRNA expression levels. However, this data was analysed in both unaffected and IPD subjects. Therefore, in order to determine whether the disease pathogenesis itself has an effect on the rs2708435 genotypes and subsequently on the LRRK2 mRNA levels, IPD and unaffected subjects were analysed separately using the Mann-Whitney test. Since the genotypes GG and GA were showing a trend in the same direction, these subjects were combined to observe any potential allelic effects.

	Reference gene normalisation	**Genotypes**	***n***	**Mean rank**	**Significance (2-tailed)**
IPD	*LRRK2_HPRT1*	GG+GA	102	55.81	0.241
		AA	11	68	
	LRRK2_RPL13A	GG+GA	98	52.79	**0.029**
		AA	11	74.73	
	*LRRK2*_Geometric Mean	GG+GA	102	54.99	**0.047**
		AA	11	75.64	
Control	*LRRK2_HPRT1*	GG+GA	30	16.50	1.00
		AA	2	16.50	
	LRRK2_RPL13A	GG+GA	31	16.61	0.417
		AA	2	23	
	*LRRK2*_Geometric Mean	GG+GA	30	16.27	0.629
		AA	2	20	

Table 6.5: rs2708435 genotypes have an effect on the LRRK2 mRNA levels in IPD subjects. *n* refers to the number of samples, and the mean rank relates to a mean of the LRRK2 expression levels in these subjects as calculated by the Mann-Whitney tests. The 2-tailed significance in this test shows that there is a marked difference in the mean values of LRRK2 mRNA levels in subjects who have the GG or GA genotype versus the AA genotypes in IPD subjects when normalised according to the reference gene *RPL13A* or to the geometric mean of *HPRT1* and *RPL13A*.

As can be seen in Table 6.5, the rs2708435 genotypes GG and GA are associated with decreased levels of LRRK2 mRNA, whereas the genotype AA increases the LRRK2 mRNA levels in IPD subjects. This result was significant at the 5% level when the mRNA data was normalised to RPL13A (p = 0.029), and also when the data was normalised to the geometric mean of the two reference genes (p = 0.047). The spread of the data is represented in Figure 6.4. However, for the purpose of clarity only LRRK2 mRNA data normalised to the geometric mean of the two reference genes is displayed.

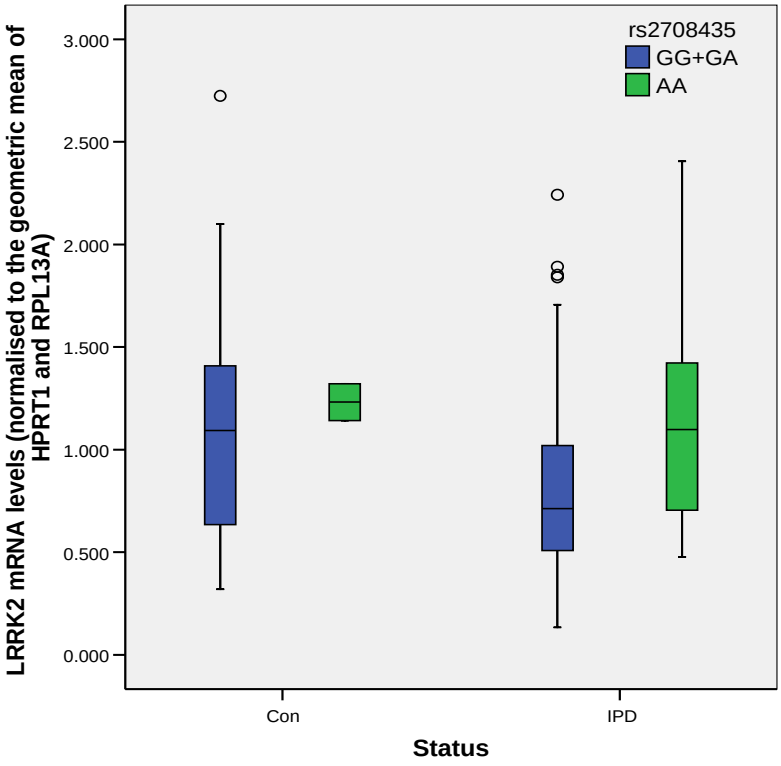

Figure 6.4: The rs2708435 variant genotype AA is associated with higher LRRK2 mRNA levels in the cerebellum of IPD subjects. The box and whiskers plot demonstrates the effects of rs2708435 genotypes on LRRK2 mRNA levels normalised to the geometric mean of the two reference genes. The median in the box plot is represented by the horizontal line inside the box and the interquartile range (IQR) is between the 25th and 75th percentiles which are represented by the horizontal borders of the box. The difference in the mRNA levels for the AA genotype versus the GG+GA genotype is marginally significant at the 5% level (p = 0.047).

6.3.1.2 Functional significance of rs2708435

The difference in the rs2708435 genotypes and their effects on the LRRK2 mRNA expression in the cerebellum of IPD subjects was perceived to be an interesting result. Therefore, further investigations were carried out to determine what might contribute to this differential allelic expression.

The SNP rs2708435 has been shown to be conserved in primates (rhesus monkey, see Figure 6.2). Its position in the upstream sequence of *LRRK2* transcription site, in addition to the data in 6.3.1.1 suggests a possible regulatory role for this tSNP. Analysis of 25mer DNA sequence around the rs2708435 predicted TFBS for this particular DNA sequence. The PROMO database predicted that the 'A' allele of the variant creates a putative transcription factor binding site (TFBS) that interacts with the transcription factor GR-beta, a glucocorticoid receptor, whereas the presence of the ancestral allele 'G' was suggested to obliterate this DNA:protein interaction.

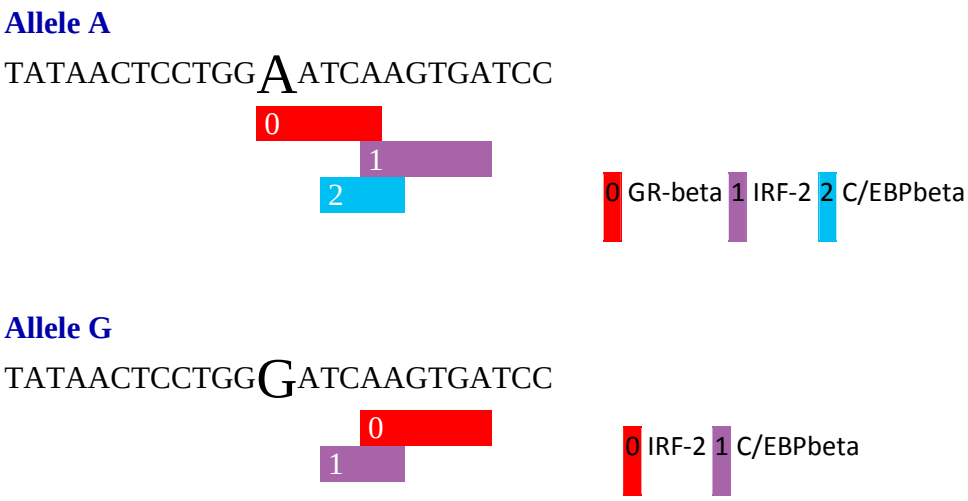

Figure 6.5: Prediction of putative transcription factor binding sites in 25mer DNA region surrounding rs2708435 by PROMO. Using a matrix dissimilarity rate of < 5%, the region is predicted to bind to the transcription factors IRF-2 and C/EBPbeta. The allele 'A' is predicted to create a TFBS for GR-beta, whereas the 'G' allele lacks this DNA:protein interaction.

In order to establish whether rs2708435 was indeed a TFBS as predicted by PROMO, and as such could regulate LRRK2 mRNA levels, EMSAs were performed on nuclear lysates from SH-SY5Y cells. Figure 6.6 demonstrates a common DNA:protein interaction for both 'G' and 'A', but an extra interaction can be observed for the 'A' allele as was predicted by PROMO (Figure 6.5). Although initially promising, these results could not be reproduced or tested on nuclear lysates stressed with PD mimetics.

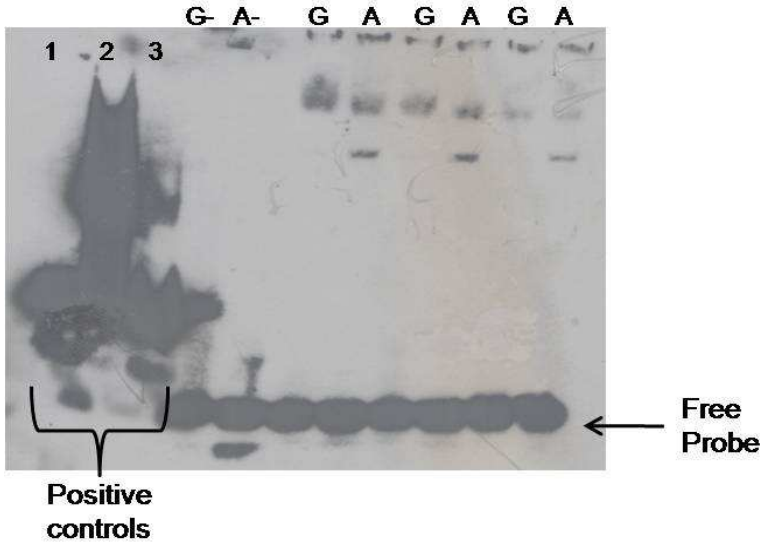

Figure 6.6: EMSA results with a set of rs2708435G/A biotinylated probes. Positive controls are 1) Biotin + control DNA; 2) Biotin + control DNA + control extract; 3) Biotin + control DNA + control extract + 200 fold molar excess of unlabeled control DNA. The positive control 1 demonstrates that there is no protein extract for DNA to bind and therefore no shift is observed whereas control 2 contains sufficient target protein for biotin-control DNA. Control 3 shows a shift resultant from a specific DNA:protein extraction, and demonstrates that the signal shift observed in control 2 can be prevented by competition from an excess of unlabeled DNA. The free probe at the bottom of the blot shows equal loading of the probes representing the two alleles. The negative controls (G- and A-) did not contain nuclear extract, and as such no shift was observed. The blot demonstrates that the DNA probe containing the **'A'** allele undergoes an extra DNA:protein interaction compared to the **'G'** allele in three independent reactions.

6.3.1.3 Is rs2708435 representing an eQTL that might be a risk factor for PD

A genetic association study was performed to determine whether the 5'UTR SNP rs2708435 represents non-coding common genetic variation. An appropriate taqman assay was not available for rs2708435. Therefore, an assay was instead designed for a surrogate SNP that displayed strong LD with rs2708435 (D' =1 and r^2= 0.98). The surrogate SNP was rs4567538 at position 38,908,171 (intronic) in the *LRRK2* gene. Genotype data from 109 subjects for both rs2708435 and rs4567538 was compared to establish the LD pattern between the two. Haploview was used to generate the LD metrics, and an r^2 of 0.95 was obtained after taking into account the minor allele frequencies of the two SNPs (rs2708435 and ts4567538) (see Figure 6.7).

A)

SNP	Position	Obs. HET	Pred. HET	HWpval	MAF	Alleles
rs2708435	38900923	0.376	0.405	0.5471	**0.282**	G : A
rs4567538	38908171	0.368	0.393	0.5897	**0.269**	C : T

B)

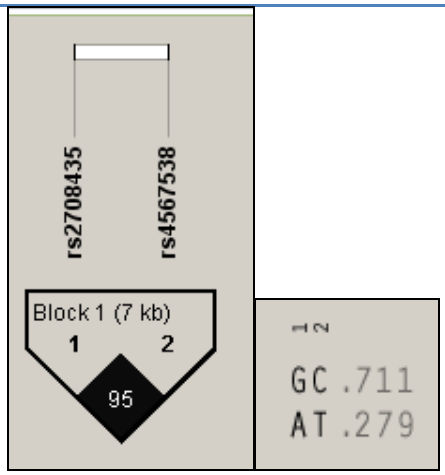

Figure 6.7: LD structure between rs2708435 and rs4567538 as constructed by Haploview. A) In the table, Obs.HET and Pred.HET refer to observed and predicted heterozygosities for 109 subjects. HWpval describes deviations from HWE and MAF refers to minor allele frequency of the two SNPs. 'A' is the minor allele for rs2708435 and 'T' is the minor allele for rs4567538. B) The LD pattern between the two SNPs provides an r^2 of 0.95. The frequencies of haplotypes GC and AT within these dataset are established at 0.711 and 0.279, respectively.

The taqman assay for rs4567538 was used to genotype 614 IPD cases and 2800 unaffected controls (collaboration with Prof. Steve Humphries, Rayne Institute, UCL). The case-control associations were assessed using FINETTI (see 6.2.4 for a description of the statistics used). However, in a case control association study it is reasonable to only use controls when checking for consistency with HWE proportions, as under the assumption of a rare disease controls represent the population well. If genotypes are associated with different disease risks then genotypes of cases may not be in HW equilibrium. The test statistics show that the controls (Pearson's goodness of chi-square fit, p = 0.148), and cases (Pearson's goodness of chi-square fit, p = 0.058) are in HWE (see Figure 6.8).

The odds ratio (OR) tests were performed to see whether this SNP acts as a risk factor to the disease. The most important OR tests in order are the allele OR; Homozygous OR; and Heterozygous OR (see Figure 6.8). Allele OR informs whether the SNP is a risk factor for disease or not (95% CI boundaries must not cross the null line of 1), with OR < 1 – giving protective and OR > 1- providing risk. In this instance, a *P* value of 0.00112 would suggest that the SNP rs4567538 is a risk factor for the disease. Depending on the genetic model this value could be improved with either the 1) Homozygous OR (recessive) or 2) Heterozygous OR (dominant). For allele 1 (major allele), the OR improves with the homozygous test ([22] <-> [11]), p = 0.030, and for allele 2 (minor allele) the OR improves with the heterozygous test ([11] <-> [12]), p = 0.0018. In other words, the major allele is acting as a risk to disease recessively, or perhaps additively, and allele 2 (minor allele) is acting dominantly as a protective factor (OR heterozygous P = 0.00184 > OR homozygous, p = 0.03017).

The allele positivity test is also a useful test for functional variants. An OR of < 1 under a dominant model for allele 2 (minor allele) gives a significant *P*-value of 0.00063, suggesting that the minor allele for the SNP might function as a protective factor against IPD.

Tests for deviation from Hardy-Weinberg equilibrium		Tests for association (C.I.: 95% confidence interval)				
Controls	**Cases**	**allele freq. difference**	**heterozygous**	**Homozygous**	**allele positivity**	**Armitage's trend test**
		Risk allele 2 'Minor allele'				
n11=1310 (1293.36) **n12=1186** (1219.28) **n22=304** (287.36) f_a1=0.68 +/- 0.006 **p=0.148662** (Pearson) **p=0.149699** (Llr) **p=inf** (Exact)	**n11=334** (324.69) **n12=225** (243.61) **n22=55** (45.69) f_a1=0.73 +/- 0.013 **p=0.058347** (Pearson) **p=0.061297** (Llr) **p=0.066623** (Exact)	**[1]<->[2]**	**[11]<->[12]**	**[11+]<->[22]**	**[11]<->[12+22]**	**common odds ratio**
		Odds_ratio=0.796 C.I.=[0.694-0.913] chi2=10.61 **p=0.00112** (P)	Odds_ratio=0.744 C.I.=[0.618-0.897] chi2=9.70 **p=0.00184**	Odds_ratio=0.710 C.I.=[0.520-0.969] chi2=4.70 **p=0.03017**	Odds_ratio=0.737 C.I.=[0.619-0.878] chi2=11.69 **p=0.00063**	Odds_ratio=0.817 chi2=10.24 **p=0.00138**
		Risk allele 1 'Major allele'				
		[2]<->[1]	**[22]<->[12]**	**[22]<->[11]**	**[11+12]<->[22]**	**common odds ratio**
		Odds_ratio=1.256 C.I.=[1.095-1.442] chi2=10.61 **p=0.00112** (P)	Odds_ratio=1.049 C.I.=[0.761-1.445] chi2=0.08 p=0.77173	Odds_ratio=1.409 C.I.=[1.032-1.924] chi2=4.70 **p=0.03017**	Odds_ratio=1.238 C.I.=[0.916-1.673] chi2=1.93 p=0.16466	Odds_ratio=1.220 chi2=10.24 **p=0.00138**

Figure 6.8: rs4567538 an LD partner of rs2708435 represents a risk factor for IPD. The statistical package FINETTI was used to assess deviations from HWE and also to test for case-control association for rs4567538. The package can be accessed from http://ihg2.helmholtz-muenchen.de/cgi-bin/hw/hwa2.pl and uses association tests adapted from Sasieni PD (1997) which include the Pearson's goodness-of-fit chi-square (P), Log Likelihood ratio chi-square (Llr) and the Exact test. Allele 1 is major and allele 2 is minor. 11: wild-type, 12 heterozygous and 22 homozygous rare variants and n (11), n (12) and n (22) represent the respective genotypic numbers; f_a1 is the frequency of allele 1 +/- standard deviation.

6.4 Discussion

A widespread reduction of the LRRK2 mRNA in the brains of IPD subjects was previously demonstrated in chapter 5 of this thesis. Following on from that, this chapter demonstrates that a SNP in the 5'- UTR region of the *LRRK2* gene could potentially act as a regulatory SNP for the LRRK2 mRNA levels in the cerebellum of IPD subjects.

A systematic search and LD analysis revealed four tSNPs; (rs10878224, rs2708435, rs1471127 and rs7294619) in a 10 kb region upstream of the *LRRK2* transcription start site. These tSNPs were genotyped in control and IPD subjects that were used to produce the preliminary cerebellum data for the differential expression in LRRK2 mRNA in section 5.3.1 of chapter 5. A marginal significance (*P*-value = 0.042) was observed for rs10878224 (tSNP1) variant genotype (CC) and decreased LRRK2 mRNA expression levels (when mRNA levels were normalised to the reference gene, *RPL13A*). However, the control genotype data for this tSNP was found to deviate from HWE. This could be a result of population stratification (differences in allelic frequencies in sub-populations). Due to the fact that it was the control population that deviated from HWE, this tSNP was not included in further analysis.

A trend towards increasing mRNA levels with the variant genotype AA was observed for rs2708435 (tSNP2) (p = 0.057). No significant effect on LRRK2 mRNA expression was observed for tSNP3 (rs1472117) and tSNP4 (rs7294619). Therefore, no subsequent analyses were performed on these SNPs. The tSNP3 (rs1472117) has previously been shown to be in LD with rs2201144, a SNP in the promoter region that has been predicted to create a transcription binding factor site depending on its allelic state (Paisán-Ruíz et al. 2006). However, the minor allele frequencies (MAF) frequencies for rs1472117 and rs7294619 were low (0.067 and 0.103, respectively), and this coupled with a small sample set could mask potentially regulatory influences on the LRRK2 mRNA expression levels.

rs2708435 genotypes affect LRRK2 mRNA expression levels in IPD subjects

The *in-silico* analysis revealed a marginal but promising trend for the tSNP2 (rs2708435) (*P*-value = 0.057). Therefore, IPD and unaffected subjects were split and analysed separately to determine whether the disease pathology itself could be having an effect on the LRRK2 mRNA levels. The GG and GA genotypes showed similar levels of LRRK2 mRNA levels, and were therefore, pooled together to identify potential allelic effects on the whole genotype. As can be seen in Table 6.5 and Figure 6.4, there was a difference in the LRRK2 mRNA levels of GG+GA genotype in comparison to AA in IPD subjects. This significance was observed for the reference gene *RPL13A* ($p = 0.029$) but not for *HPRT1* (although the trend was in the same direction). However, the difference was significant when the LRRK2 mRNA data was normalised to a geometric mean of *HPRT1* and *RPL13A* (*P*- value = 0.047). Such variation in data further establishes the need for a careful selection of endogenous reference genes whilst dealing with mRNA data obtained from post-mortem human tissue.

The difference in the LRRK2 mRNA levels of GG+GA and AA subjects was more pronounced in IPD subjects, although a similar trend was seen in the unaffected controls too. Alternatively, *trans*-acting or non-*cis* mechanisms (e.g., epigenetic events, chromatin condensation, or environmental factors) can also have an effect on the *cis*-variation (Pastinen et al. 2004). Therefore, it is likely that the significant difference in the genotypic impact on LRRK2 mRNA levels in the IPD subjects and not in the unaffected controls is a downstream effect of the disease pathogenesis, which in combination with other factors (environmental stresses or epigenetic events), results in decreased LRRK2 mRNA expression levels that have been well documented in the previous chapter. However, too few unaffected subjects, especially the AA genotypes could have masked any potential genotypic influence on the LRRK2 mRNA levels in unaffected controls. It should also be noted that this *in-silico* data was produced using a small number of homozygote variant (AA) samples in comparison to the wild-type homozygotes (GG) and heterozygotes (GA) samples.

This could skew a statistical artefact towards significance in the PD subjects. Therefore, further work testing the *in-vitro* effects of rs2708435 on LRRK2 transcriptional activity is warranted to firmly assess whether the results observed in this study are due to disease pathogenesis.

Does rs2708435 represent an eQTL that might also be a risk factor for IPD?

Support to the notion that rs2708435 might be acting as an eQTL or regulatory SNP for LRRK2 mRNA levels was provided by the genetic association study and the EMSA results. Unfortunately, a taqman assay could not be designed for rs2708435. Therefore, a genetic association study was carried out using a surrogate intronic SNP rs4567538. The study identified rs4567538 to be a risk factor for IPD cases, and demonstrated that the major allele (ancestral) was acting as a risk factor whereas the minor allele (variant) was protective against PD. Since rs4567538 displays strong LD with 5'- UTR SNP rs2708435 (r^2=0.95), it is not implausible that rs2708435 does indeed represent common genetic variation with a regulatory function.

Furthermore, the variant 'A' allele for rs2708435 was predicted to be a TFBS (*in-silico* analysis, see Figure 6.5). This was demonstrated as having an extra DNA:protein interaction not seen with the 'G' allele. This was an interesting result as the IPD subjects with the 'A' allele show increased LRRK2 mRNA levels in comparison to the IPD subjects with the ancestral 'G' allele. This suggests that a transcription factor binds to the variant 'A' allele and increases the LRRK2 mRNA levels. Although initially promising, the lack of reproducibility of the EMSA data was a major setback to this study. The crude sensitivity of the assay resulted in a number of technical difficulties, which meant that a) the data was not replicated consistently enough, b) could not determine the transcription factor that was actually responsible for the shift observed in EMSA blots, and c) could not determine whether the use of PD mimetics would produce an effect that was consistent with the LRRK2 mRNA data. A new method of multiplexing EMSAs has been developed, where assays containing different transcription factors are added to the nuclear lysates, and then selectively removed to determine the appropriate DNA:protein interaction(s)

(Smith & Humphries 2009). This is a promising approach that could be used in the future to determine the DNA:protein interaction(s) for the rs2708435 alleles.

Common genetic variation in *LRRK2* has been shown to increase the risk of IPD in the Chinese population (Skipper et al. 2005), but was found not to be associated with IPD risk in a German population (Biskup et al. 2005). Another case-control association study in Europeans (Finnish and Greek subjects) also did not produce any convincing associations for *LRRK2* and IPD, and the only SNP typed by them to have a moderately good LD with rs2708435 displayed an r^2 of 0.838 (Paisán-Ruíz et al. 2005). The two SNPs reported to have a mild association with IPD does not have strong LD with rs2708435 or to its LD partner rs4567538 (HapMap data, dbSNP build 125). The authors did observe that the LD distribution across the Greek and Finnish population varied considerably from that in the European populations used in the human diversity series for HapMap data (Paisán-Ruíz et al. 2005). A UK based cohort was genotyped in this chapter, and it is therefore likely that the result being observed is specific to the UK population. However, the result in this study needs to be replicated in another UK based cohort or possibly even in other European populations before it can be conclusively said that the intronic rs4567538 or its potentially regulatory LD partner rs2708435 is a risk factor for IPD.

Conclusion

This chapter demonstrates that the 'non-coding DNA' in 5' UTR of *LRRK2* gene harbours important regulatory elements in the form of eQTL that might affect the LRRK2 mRNA levels in IPD subjects. The notion that rs270435 represents an eQTL was supported by the EMSA results, and its LD partner rs4567538 was shown to be a risk factor in IPD. This suggests that rs2708435 might play a role in the PD pathogenesis. It is likely that rs2708435 is working cumulatively with other variants, to exert its regulatory effects on the LRRK2 mRNA levels. Future investigations into its role as a regulatory SNP for LRRK2 transcription are therefore warranted.

Chapter 7

7 General discussion

Parkinson's disease (PD) is a progressive neurodegenerative disorder that affects approximately 1-2 % of the population over the age of 65 years (Lees et al. 2009). Mutations in *LRRK2* gene, which resides in the PARK8 locus (Funayama et al. 2002; Zimprich et al. 2004b; Paisán-Ruíz et al. 2004) have been identified as a common genetic cause of familial and idiopathic PD (IPD) (Healy et al. 2008). G2019S is the most common *LRRK2* mutation, and results in a clinical and pathological phenotype indistinguishable from IPD cases (Di Fonzo et al. 2005; Gilks et al. 2005; Nichols et al. 2005; Aasly et al. 2005; Ross et al. 2006). The G2019S mutation has consistently been shown to increase the kinase activity of LRRK2 protein (Jaleel et al. 2007; Imai et al. 2008; Parisiadou et al. 2009; Gillardon 2009; Kumar et al. 2010), and has also been suggested to generate inclusion bodies and cellular toxicity *in vitro* (West et al. 2005; Smith et al. 2005a; Gloeckner et al. 2006; Greggio et al. 2006; Smith et al. 2006). Autopsy reports investigating LRRK2 protein localisation to pathological inclusions in G2019S PD cases have been published (Giasson et al. 2006), but the rarity of post-mortem tissue from G2019S PD cases means that the expression of LRRK2 mRNA and protein, both in terms of localisation and quantitation, have not been described in such individuals. The anatomical distribution of wild-type LRRK2 mRNA and protein in human and rodent brain has been published, but the literature is still lacking a broad evaluation of how *LRRK2* expression might be altered in response to idiopathic or *LRRK2* linked PD (Galter et al. 2006; Melrose et al. 2006; Simón-Sánchez et al. 2006; Miklossy et al. 2006; Taymans et al. 2006; Zhu et al. 2006a; Zhu et al. 2006b; Higashi et al. 2007a; Higashi et al. 2007b; Melrose et al. 2007; Westerlund et al. 2008a; Alegre-Abarrategui et al. 2008; Perry et al. 2008; Santpere & Ferrer 2009; Higashi et al. 2009). Hence, the central theme of this thesis focussed on the morphological and quantitative expression of LRRK2 mRNA and protein in the brains of control, IPD and G2019S affected PD cases, and on assessing the influence of genetic variation on *LRRK2* expression in these subjects. Additionally, G2019S mutation was also screened in PD unaffected members of various populations in sub-Saharan Africa, Middle East and Eastern Europe to

expand our understanding of the predicted origins of this mutation. The aim of the following discussion is to present a critical review of the different studies presented in this thesis.

7.1 Screening of G2019S mutation

The *LRRK2* G2019S mutation is common in Middle Eastern and European populations with the highest frequencies reported in North African Berbers and Ashkenazi Jews (Ozelius et al. 2006; Lesage et al. 2006; Healy et al. 2008). It has been predicted that the G2019S mutation arose in the Berbers, but there are suggestions that the mutation may have arisen independently on more than one occasion (Lesage et al. 2005b; Kachergus et al. 2005; Zabetian et al. 2006a; Warren et al. 2008; Bar-Shira et al. 2009; Pirkevi et al. 2009; Lesage et al. 2010). However, the carrier rate frequency of this mutation has not been investigated in detail in neighbouring populations, for example sub-Saharan Africa (Lesage et al. 2006). In chapter 3, I investigated the frequency of G2019S mutation in unaffected subjects from populations with a potentially higher chance of carrying the mutation, due to possible genetic admixture with North African Berbers and Ashkenazi Jews.

The G2019S mutation was screened in a sample set of 2,485 subjects without a clinical diagnosis of PD. These subjects were derived from populations of sub-Saharan African, Middle-Eastern, non-Ashkenazi Jewish, and Eastern European origins. Only two subjects were identified as positive for G2019S mutation, suggesting that the mutation is not common amongst members of the selected populations. The two samples that tested positive for G2019S mutation were of Syrian and Moroccan Jewish ancestry, respectively. According to the exact hypothesis test (for binomial random variables), the observed proportion is not different from the expected proportion (see 3.3.1; Syrian $p = 0.827$; Moroccan Jewish $p = 0.444$), but this is likely to represent a statistical fluctuation due to the small sample sizes of these two populations (Syria, $n= 75$; Moroccan Jew, $n= 186$). Therefore, these data do not clarify the current understanding regarding the origins of this mutation. No examples of G2019S mutation were observed in sub-Saharan

Africans in this study which suggests that it is not common amongst PD-unaffected members of the Bantu speaking and Ethiopian populations investigated, but the sample size is not large enough (n = 731) to evaluate whether the mutation arose after the early migrations out of Africa. Similarly, the data suggests that G2019S mutation is not common in Ukrainian and Belarusian populations in Eastern Europe, but does not allow us to comment on whether the G2019S mutation in Ashkenazi Jews could have been acquired from neighbouring populations.

The worldwide frequency of G2019S mutation in PD unaffected subjects has been suggested to be <1% (Healy et al. 2008), and whether the sample sizes available for this study had enough power to detect a mutation frequency of <1% is a matter of concern. For example, if worldwide frequency of G2019S mutation is set at 1%, then using an estimated proportion of 0.00080548 (2 out of 2485) for G2019S positive subjects in this study, suggests that a sample size of 731 for sub-Saharan Africans and 531 for eastern Europeans has >80% power, and a sample size of 335 for non-Ashkenazi Jews has >50% power to detect a frequency of 1% in this sample set. However, the negligible proportions estimated for G2019S positive subjects in this study (section 3.3.1), in addition to the predicted <1% worldwide G2019S mutation frequency (Healy et al. 2008) results in such extreme data that any estimation of power for the sample sizes used in this study may not be reliable. To the best of our knowledge, we could not find a method to reliably estimate power for these proportions that are close to zero. Overall, these data suggest that G2019S mutation is not common amongst PD unaffected members of the populations investigated in this study, but we cannot make any definitive statistical inferences as to the frequency of G2019S mutation in these subjects. A substantially large number of subjects are needed before we can definitively estimate G2019S carrier rate frequency in PD unaffected subjects of these populations. Expanding the study to include PD cohorts from the populations presented in this study would contribute to our understanding of the genetic origins of the mutation, and help us to assess whether the mutation in North African Berbers and Ashkenazi Jews could have resulted from admixture with their neighbours.

7.2 LRRK2 mRNA and protein expression in the human brain

Investigation of *LRRK2* expression in the brain is the major focus of the investigation recounted in this thesis, the hypothesis being that the anatomical and cellular expression profile of LRRK2 mRNA and protein may differ between control and PD cases. A combination of morphological and quantitative techniques was used to address this. The strength of this approach being that morphological techniques demonstrated the cellular expression of LRRK2 mRNA and protein in a large number of brain regions, whereas quantitative mRNA methods provided a more accurate indication of LRRK2 mRNA expression levels, albeit in a lower number of regions. LRRK2 protein levels were also compared using semi-quantitative immunohistochemistry (IHC) analysis in different brain regions. Post-mortem tissue from G2019S positive PD cases is limited; hence there are few descriptions of LRRK2 mRNA and protein localisation in such cases. In addition to investigating the morphological differences in LRRK2 mRNA and protein expression in control and IPD cases, this study took advantage of the rare resource at QSBB to describe the *LRRK2* expression profile in G2019S positive PD cases.

7.2.1 Morphological findings and regional quantitation of LRRK2 mRNA in the human brain

In chapter 4 of this thesis, *in-situ* hybridisation (ISH) study demonstrated ubiquitous neuronal LRRK2 mRNA expression in post-mortem brain tissue from 2 control, 1 IPD and 3 G2019S positive PD cases. The localisation of LRRK2 mRNA to dopamine synthesising as well as dopamine innervated regions of the brain is in contrast to the original studies performed in rodents and humans (Galter et al. 2006; Melrose et al. 2006). Our results concur with the subsequent findings of a more widespread evaluation of LRRK2 mRNA expression in the brain (Simón-Sánchez et al. 2006; Higashi et al. 2007a; Higashi et al. 2007b). The original findings reported by Galter and colleagues were based on a higher sample number (4 controls and 5 PD) than the 6 cases we have used, but PCR studies examining LRRK2 mRNA in dopaminergic (DAergic) neurons (Han et al. 2008; Simunovic et al. 2009) and

striatum (Zimprich et al. 2004b; Melrose et al. 2006; Dachsel et al. 2010) support the morphological findings in this study. ISH is a technically demanding procedure that is sensitive to various factors such as tissue preparation, tissue pH, probe labelling method (radioactive versus non-radioactive; choice of radioactive isotope) and hybridisation protocols, all of which can contribute to discrepant results between studies (Harrison et al. 1991; Barton et al. 1993; Kingsbury et al. 1995). For example, the original studies that investigated LRRK2 mRNA localisation using ^{33}P labelled oligonucleotide probes did not identify LRRK2 mRNA in DAergic neurons (Galter et al. 2006; Melrose et al. 2006), whereas the subsequent studies that used non-radioactive riboprobe (Simón-Sánchez et al. 2006); or ^{35}S labelled oligonucleotide probes reported a more widespread LRRK2 mRNA localisation (Higashi et al. 2007a; Higashi et al. 2007b). ISH is particularly challenging on post-mortem tissue due to variable RNA preservation, therefore to validate the ISH procedure in this study, the mRNA integrity was assessed using a positive control (BRI2 mRNA), and the specificity of the LRRK2 ISH probe was demonstrated using an excess of unlabelled probe, as previously described (Lashley et al. 2008).

Chromogenic digoxigenin ISH has previously been used to quantitate LRRK2 mRNA in the brain (Simón-Sánchez et al. 2006). However, unlike radioactive ISH where silver emulsion grains can be counted to provide mRNA quantitation, non-radioactive ISH cannot accurately measure mRNA signal. As described in section 4.3.1.1, the high background intensity associated with radioactive emulsion autoradiography required the use of non-radioactive ISH for LRRK2 mRNA localisation. Therefore, having demonstrated the distribution of LRRK2 mRNA in the brain using non-radioactive ISH, the mRNA levels were quantitated using a more sensitive qPCR based strategy utilising a large number of samples (Chapter 5, section 5.3.2). The qPCR results do not demonstrate regional variation in LRRK2 mRNA levels in control human brain (Figure 5.2). Although regional variations in LRRK2 mRNA levels in the human brain have previously been reported using a PCR based strategy, tissue from only one case was used to quantitate mRNA levels in these studies (Zimprich et al. 2004b; Dachsel et al. 2010). The LRRK2 mRNA quantitation data presented in chapter

5 are likely to be more robust as a sample number of 15-20 cases was used (Table 5.6), which to our knowledge is the largest number of samples examined to estimate relative LRRK2 transcript levels in post-mortem human brain. Having determined the cellular localisation and relative regional levels of LRRK2 mRNA, a future measurement of mRNA expression in laser capture microdissected (LCM) neurons would refine the quantitation of LRRK2 mRNA in specific cellular populations of the brain.

7.2.2 Morphological findings and regional semi-quantitation of LRRK2 protein in the human brain

Analogous to the morphological findings of LRRK2 mRNA, the IHC study in chapter 4 demonstrates a ubiquitous neuronal expression of LRRK2 protein in 4 control, 2 IPD and 4 G2019S positive PD cases. This confirmed not only the cytoplasmic distribution of the protein but also its extensive presence in the axons, apical dendrites and the neuropil (Biskup et al. 2006; Higashi et al. 2007b; Melrose et al. 2007; Alegre-Abarrategui et al. 2008). LRRK2 immunoreactivity was occasionally identified in reactive astrocytes (Figure 4.5I), but LRRK2 mRNA was not otherwise observed in glial cells, although the small amount of cytoplasm in oligodendrocytes could make it difficult to detect LRRK2 mRNA in these cells (Biskup et al. 2006; Miklossy et al. 2006). We also confirm the detection of LRRK2 mRNA and protein in vascular smooth muscle cells (Zhu et al. 2006a).

Using IHC, the presence of LRRK2 protein was demonstrated in the halo of a small proportion of Lewy bodies (LBs). However, identification of LRRK2 protein in LBs has been shown to be highly dependent on the antibody used, therefore it remains uncertain whether LRRK2 is an obligate component of these inclusions (Miklossy et al. 2006; Zhu et al. 2006a; Zhu et al. 2006b; Higashi et al. 2007b; Melrose et al. 2007; Alegre-Abarrategui et al. 2008; Perry et al. 2008; Santpere & Ferrer 2009; Higashi et al. 2009). Differences in tissue fixation, protein preservation and antigen retrieval procedures (not all antibodies recognise protein in native conformations) can result in variability in immunolabelling (Williams et al. 1997). For example, the only antibody that reportedly labels a large proportion of LBs in the brainstem and neocortical

regions is the commercial antibody NB300-268 (see Table 4.2), although previous observation in our group suggested that NB300-268 does not label LBs (Dr. Ann Kingsbury, unpublished findings), implying that the NB300-268 antibody may be sensitive to tissue fixation or protein preservation.

LRRK2 immunoreactivity in this study was demonstrated using the previously published polyclonal EB06550 antibody (Alegre-Abarrategui et al. 2008). The EB06550 antibody recognises LRRK2 amino acids 2015-2026 which also includes the site for the G2019S mutation (Santpere & Ferrer 2009). Since glycine and serine are both polar and hydrophilic, the extent to which this substitution changes the native conformation of LRRK2 in a way that might influence the antibody binding has not been documented in immunohistochemical detection. Although antibodies that recognise specific mutational isoforms have previously been reported (e.g. P102L substitution in the prion protein (Wadsworth et al. 2006)), they are technically demanding to produce, and it is unlikely that the polyclonal EB06550 is specific enough to discriminate between proteins that differ at a single amino acid site. The specificity of EB06550 has not been tested on a *LRRK2* knockout model, but it recognises a ~250KDa band corresponding to endogenous human LRRK2 protein in post-mortem tissue, (Figure 4.3), biopsy material (Alegre-Abarrategui et al. 2008), and also labels recombinant LRRK2 protein (Dr. Patrick Lewis, unpublished data) which covers the LRR-WD40 domain (previously described in Anand et al. 2009). The specificity of the EB06550 antibody was further demonstrated in this study by obliterating the signal using a pre-absorption assay (Figure 4.3).

An established 4-tiered grading method was used for semi-quantitation of regional LRRK2 immunoreactivity in post-mortem tissue from the 10 cases (Melrose et al. 2007; Alegre-Abarrategui et al. 2008). Variability in LRRK2 immunoreactivity between different brain regions was a consistent finding (Table 4.9), and confirmed the previously reported EB06550 findings in normal adult brain (Alegre-Abarrategui et al. 2008). It was of note that in the nigrostriatal dopamine system the cell bodies of striatal neurons were consistently recorded as displaying the weakest LRRK2 immunoreactivity. However, no difference had been observed in striatal LRRK2

mRNA levels compared to other regions (Figure 5.2). Nevertheless, the weak LRRK2 immunoreactivity in striatal neurons (Figure 4.4H) is in contrast to the intense striatal neuropil staining, suggesting that LRRK2 protein localises to neuronal processes rather than the cell body in this region (Figure 4.4K and L). This is supported by western blot data indicating high LRRK2 protein levels in striatum (Biskup et al. 2006; Taymans et al. 2006; Melrose et al. 2007) .

The LRRK2 immunoreactivity data reported in this study (Table 4.9) do not demonstrate an overall difference in LRRK2 immunoreactivity between the 4 control and 6 PD cases (2 IPD and 4 G2019S positive PD). Our results do not concur with a previous study that reported intense LRRK2 immunoreactivity in neuronal cell bodies and axons of PD cases (n = 6) compared to controls (n = 4) (Zhu et al 2006a). Additionally, we also did not observe a decrease in LRRK2 immunoreactivity in nigral neuronal processes in our PD cases as has been previously reported for a smaller number of PD cases (n = 2) when compared to controls (n = 2) (Higashi et al. 2007b). Differences in tissue fixation, protein preservation, and antibodies could have contributed to the discrepant results between the studies. For example, a recent study using a different antibody reported punctate staining of LRRK2 positive structures within cells (Higashi et al. 2009), whereas we observed a more diffuse pattern of LRRK2 immunoreactivity.

Western blots provide an alternative method to quantitate protein rather than the 4-tiered IHC grading system presented in this study. However, western blots are semi-quantitative in nature, and unlike IHC procedures, cannot determine the cellular localisation of a protein. It has been shown that western blotting with EB06550 antibody produces the best result on biopsy material compared with post-mortem tissue likely due to the superior protein preservation in biopsy material (Alegre-Abarrategui et al. 2008). A more accurate methodology to quantitate protein levels is an ELISA. However, lack of an available LRRK2 specific ELISA prevented the use of this method in my study. For this reason, a precise correlation between LRRK2 mRNA (Figure 5.2) and protein levels could not be performed, and this remains a major limitation of the current study, and an area for future development. Moreover,

EB06550, like a majority of other LRRK2 antibodies, is polyclonal, and future replication of this morphological data using specific monoclonal LRRK2 antibodies is warranted.

The morphological findings in this study describe the anatomical distribution of LRRK2 mRNA and protein in a substantial number of cases, in addition to presenting novel data relating to LRRK2 mRNA and protein localisation in the rarely available G2019S positive PD cases. The descriptive nature of the morphological data does not allow us to comment in detail on the physiological importance of the widespread *LRRK2* expression, but within the limitations of the methods used, suggests that there is no major variation in *LRRK2* expression resulting from the G2019S mutation. Future investigations into accurate quantitation of LRRK2 protein levels would address whether there are subtle variations in LRRK2 protein expression in PD compared to controls that cannot be assessed by the IHC technique used in this study.

7.2.3 An investigation into LRRK2 mRNA dysregulation in IPD cases compared to controls

Having quantitated LRRK2 mRNA levels in several regions of the normal human brain (Figure 5.2), qRT-PCR was further used to demonstrate statistically different LRRK2 mRNA levels in a number of cortical and subcortical regions of IPD cases compared to controls in chapter 5 of this thesis (Figure 5.3). The regions used in this study were chosen due to their selective vulnerability to α-synuclein pathology in PD (Braak et al. 2004). In order to determine whether changes in LRRK2 mRNA expression could also be identified in a brain region that is not vulnerable to α-synuclein pathology in PD, tissue from the cerebellum was included in the study.

Region specific expression of reference genes was taken into account by measuring four endogenous reference genes (*HPRT1*, *RPL13A*, *G6PD* and *TBP1*) for each sample. Variation in reference genes in the dataset was estimated using the NormFinder software (Andersen et al. 2004), and the geometric mean of the two most stable reference genes as predicted by the software was used to normalise the LRRK2 mRNA data (Bengtsson et al. 2005). The use of post-mortem tissue is associated with

many confounding factors, e.g. variability in cellular stress and loss, response to disease, cause of death, and medication (Kim & Webster 2009). Cases in this series were collected so as to minimise these limitations by considering factors such as age, gender, brain pH, post-mortem delay (Tables 5.2 and 5.4). Despite this approach a series of 20 IPD and 20 controls may be considered too small a number to accurately account for many of the variables associated with the study of post-mortem brain tissue (Harrison et al. 1991; Barton et al. 1993; Kingsbury et al. 1995; Kim & Webster 2009).

7.2.3.1 LRRK2 mRNA is reduced in limbic and several neocortical regions but increased in medulla of IPD cases in comparison to controls

Reductions of LRRK2 mRNA in parietal cortex, cerebellum, cingulate gyrus, amygdala and frontal cortex, and increases in LRRK2 mRNA in medulla were observed in IPD cases compared to controls but no difference was observed in entorhinal cortex or putamen (Figure 5.3). Although a difference of less than 0.5 fold in LRRK2 mRNA levels between IPD cases and controls is extremely modest, each sample was measured in triplicate and these differences in LRRK2 mRNA levels remained significant after multiple test correction (Table 5.8). Additionally, this level of < 0.5 fold reduction was also observed in a larger number of cerebellum samples (IPD, n = 115; control, n = 35; Figure 5.1), suggesting that in cerebellum at least, this observation is robust.

Furthermore, we also observed a reduction of LRRK2 mRNA levels in G2019S positive PD cases compared to controls (Figure 5.3) although, the small number of cases and restricted tissue availability of such samples does not allow us to make any statistical inferences. In view of the scarcity of G2019S PD cases coming to post-mortem, a collaborative international effort between brain banks would be needed to make available a larger cohort of G2019S positive PD cases, to confirm the suggested decrease in LRRK2 mRNA levels in G2019S positive PD cases compared to unaffected cases. This would provide an indication of a biochemical mechanism common to IPD and G2019S linked PD (White et al. 2007).

No change was observed for LRRK2 mRNA levels in putamen in IPD, and this concurs with a previous ISH study which also reported no significant differences in the striatal LRRK2 levels between IPD cases and unaffected controls (Galter et al. 2006). Previously, L-DOPA induced dyskinesia has been suggested to increase striatal LRRK2 mRNA levels in marmosets (Hurley et al. 2007). As clinical information detailing treatment, dosage and the occurrence of dyskinesia was only available for a small number of samples (Table 5.3), it was not possible to accurately correlate these data with LRRK2 mRNA levels. Recently, LRRK2 was suggested to be involved in striatal dopamine transmission (Li et al. 2010), and in this study unaltered striatal LRRK2 mRNA levels in PD brains are reported. This finding is in contrast to a reduction of LRRK2 mRNA in other regions of IPD brains, and may indicate that maintenance of LRRK2 mRNA is of some (as yet unidentified) significance in striatum where altered function plays a key role in contributing to the clinical symptoms in PD. LRRK2 mRNA was also reportedly reduced in DAergic neurons of a small number of IPD cases (Simunovic et al. 2009), however, it was not possible to address this in the current study as nigral tissue was unavailable.

Whole tissue lysates were used to quantitate LRRK2 mRNA levels, therefore we cannot be sure what cell type the observed changes might be associated with. However, the findings in chapter 4 demonstrate that LRRK2 mRNA and protein is largely found in neurons, therefore the quantitative reduction in LRRK2 mRNA is likely to reflect reduced expression by neurons. The widespread reductions could be attributed to neuronal loss in IPD cases, however, the reduction in LRRK2 mRNA was also observed in cerebellum which does not display overt neuronal loss in PD. Although four endogenous reference genes were used as internal controls, laser capture microdissection (LCM) of neurons is a more accurate method to account for neuronal loss. Replication of these data in a larger cohort of samples as well as refinement by LCM to analyse isolated neurons, would clarify how these results contribute to our knowledge of PD development. However, even the use of LCM cannot account for the biggest confounding factor when using diseased post-mortem tissue, which is the accurate interpretation of resultant data as to whether the changes

observed in mRNA levels contribute to the disease process or whether the disease itself results in mRNA expression dysregulation. Additionally, we do not know whether this LRRK2 mRNA dysregulation is specific to PD or neurodegenerative process in general. Investigation of LRRK2 mRNA in post-mortem tissue from neurodegenerative diseases, such as other α-synucleinopathies, Alzheimer's disease or progressive supranuclear palsy could ascertain whether the LRRK2 mRNA dysregulations observed in this study are indeed a PD specific phenomenon.

The autosomal dominant transmission of *LRRK2* mutations in familial PD cases, and the *in-vitro* mutant toxicity together suggest a '*gain-of-function'* model for *LRRK2*-linked PD (Funayama et al. 2002; Paisán-Ruíz et al. 2004; Zimprich et al. 2004b; Funayama et al. 2005; West et al. 2005; Gloeckner et al. 2006; Greggio et al. 2006; Smith et al. 2006; Liu et al. 2008). Additionally, a lack of phenotype in *LRRK2* knockout mouse models that report no major abnormalities, and an unaltered number of DAergic neurons (L. Wang et al. 2008; Andres-Mateos et al. 2009; Lin et al. 2009), further suggests that LRRK2 '*loss of function'* does not have a marked effect (although it is possible that *LRRK2* disruption in the developmental phase could be compensated for by another gene, for example *LRRK1*, in constitutive knock out models (Biskup et al. 2007; Westerlund et al. 2008a)). Therefore, in light of such data which recommends a '*gain of function'* model for *LRRK2*, and given that ablation of LRRK2 does not have a detectable effect, the modest reductions of LRRK2 mRNA levels in IPD cases observed in this study are perhaps indicative of a cellular response to PD as opposed to it being a causative factor.

In contrast to these reductions, our findings also suggest an increase in LRRK2 mRNA levels in the medulla of IPD cases (Figure 5.3). The dorsal motor nucleus of the vagus (DMNV) in the medulla is affected in the earlier stages of PD (Braak et al. 2004), and the disease duration of the subjects in this study (4.6-29.3 years, Table 5.3) suggests that we may be observing an end-stage effect in medulla. This could be supported by investigation of other CNS areas affected early in the disease process, such as olfactory bulb, locus coeruleus (Braak et al. 2004), and the intermediolateral nucleus of the thoracic cord (Kalaitzakis et al. 2008). The data presented are derived

from tissue containing various nuclear groups in medulla, such as the inferior olive that is not a target for α-synuclein pathology in PD. Further analysis by LCM to determine the contribution of different nuclei to the observed increase in LRRK2 mRNA is warranted. Interestingly, IPD cases belonging to this particular sample series, also exhibit increased levels of DJ-1 (PARK7) mRNA levels (Dr. R. Kumaran, unpublished findings). DJ-1 has been shown to have a neuroprotective role (Taira et al. 2004; Inden et al. 2006), but its physiological interaction with LRRK2 remains to be confirmed (Venderova et al. 2009; Heo et al. 2010). Additionally, a protective role for wild-type LRRK2 in cellular (Liou et al. 2008; Milosevic et al. 2009), transgenic worm (Wolozin et al. 2008; Saha et al. 2009; Ohta et al. 2010), and *Drosophila* models (Lee et al. 2007; D. Wang et al. 2008) has been proposed, but their contradictory phenotypes suggest that further validation of the protective role of LRRK2 is needed (Imai et al. 2008; Liu et al. 2008; Sämann et al. 2009; Venderova et al. 2009; Ng et al. 2009; Heo et al. 2010; Yao et al. 2010). Therefore, whether an increase in LRRK2 induces cell toxicity or a decrease affects cell protection or perhaps both events contribute to PD remains to be seen *in-vivo*.

LRRK2 has been suggested to be involved in various functions, such as cell signalling, cellular stress and neuronal maintenance, cytoskeletal dynamics, vesicle transport, apoptosis, mitochondrial dysfunction, and cellular scaffolding (reviewed in (Greggio & Cookson 2009)). Although physiological substrates of LRRK2 have been suggested, currently the most efficiently phosphorylated substrate of LRRK2 (apart from the generic substrate MBP) remains LRRK2 itself (West et al. 2005; Gloeckner et al. 2006; Smith et al. 2006; Greggio et al. 2006; Kumar et al. 2010). However, the potential pathological role of LRRK2 autophosphorylation is not well understood, but it is suggested to regulate LRRK2 GTPase activity which in turns regulates this protein's kinase activity (Greggio et al. 2008; Greggio et al. 2009). A dysregulation in LRRK2 protein levels could affect any of the above functions, but a lack of accurate quantitation of LRRK2 protein levels prevents us from commenting on how a dysregulation in LRRK2 mRNA might influence the protein levels. Although we present a semi-quantitation of LRRK2 protein levels in chapter 4, a more sensitive

technique detecting differences in LRRK2 protein levels between control and PD cases, subtle or otherwise, would elucidate the significance of LRRK2 mRNA dysregulation in these IPD cases, and could potentially lead to testable hypotheses that can be examined in model systems. We cannot comment on whether the modest LRRK2 mRNA dysregulations in selected cortical and subcortical regions of IPD cases in this study are a contributory factor or a cellular response to the disease, but these data describe a novel alteration in the LRRK2 mRNA expression profile of PD affected versus unaffected cases.

7.2.3.2 LRRK2 mRNA and Lewy bodies

Similar to the findings of others, we demonstrate that LRRK2 is present in the core of a small proportion of LBs in chapter 4 of this thesis (Figure 4.7) (Zhu et al. 2006a; Zhu et al. 2006b; Miklossy et al. 2006; Higashi et al. 2007b; Melrose et al. 2007; Alegre-Abarrategui et al. 2008; Santpere & Ferrer 2009). The infrequent presence of LRRK2 in brainstem LBs and absence in cortical LBs, much like the product of the PARK6 locus, PINK1 (Gandhi et al. 2006), suggests that LRRK2 is not an obligate component of the LBs. However, if LRRK2 is present upstream of α-synuclein in the PD pathway as a signalling molecule (Qing et al. 2009; Carballo-Carbajal et al. 2010; Hsu et al. 2010; Gloeckner et al. 2009), and is not directly involved in α-synuclein aggregation, then the lack of detection in LBs in not surprising. Additionally, the core of classical LBs is mainly composed of vesicle structures (Takahashi & Wakabayashi 2001). Electron microscopy would be required to detect whether the limited LRRK2 immunoreactivity in LBs is a result of its localisation to vesicular structures (Biskup et al. 2006; Hatano et al. 2007; Shin et al. 2008; Higashi et al. 2009).

LRRK2 has been shown to phosphorylate α-synuclein *in-vitro,* but the likelihood that there are other endogenous kinases in crude cell extracts indicates that this result should be treated with caution (Qing et al. 2009). Although α-synuclein-induced neuropathology was recently shown to be enhanced in a double mutant transgenic mouse overexpressing α-synuclein and LRRK2 (Lin et al. 2009), whether α-synuclein is a true physiological substrate of LRRK2 remains to be seen. We did not observe

any correlation between LRRK2 mRNA levels and LB loads in chapter 5 of this thesis. LB numbers were assessed in individual regions on independent occasions, and an inter-class correlation was performed to assess intra- and inter-observer variability (section 5.3.5). However, the number of cases (20 IPD and 4 G2019S positive PD cases) in this study is likely to be too small to permit an accurate correlation between LRRK2 mRNA and α-synuclein positive LBs.

7.3 Genetic variation in LRRK2 5′-UTR regions and its effect on LRRK2 mRNA levels

In chapter 6 of this thesis, I hypothesised that genetic variation in the 5'UTR region of *LRRK2* could influence LRRK2 mRNA levels. Cerebellum LRRK2 mRNA data (section 5.3.1) were chosen for this correlation due to the higher sample number of IPD (*n*=115) and control (*n*=35) subjects. The tag SNP (tSNP) rs2708435 upstream of *LRRK2* transcription start site (Figure 6.2) exhibited weak allele specific expression of the cerebellar LRRK2 mRNA levels in IPD cases (Table 6.5). Based on the *in-silico* data, EMSA was used to demonstrate that allele 'A' of rs2708435 undergoes an additional DNA:protein interaction in comparison to the 'G' allele (Figure 6.6). Variation at intronic tSNP rs4567538 which is in linkage disequilibrium (LD) with rs2708435 (r^2 = 0.95, Figure 6.7) demonstrated association with PD (Figure 6.8). Previous studies examining *LRRK2* variation have not observed this association (Biskup et al. 2005; Skipper et al. 2005; Paisán-Ruíz et al. 2006; Paisán-Ruíz et al. 2008; Sutherland et al. 2009b; Pankratz et al. 2009), and recent GWA studies have identified *LRRK2* SNPs that might be associated with PD, none of which are in LD with the tSNP rs4567538 genotyped in this study (Simón-Sánchez et al. 2009; Satake et al. 2009). Population specific differences and sample numbers can contribute to differing associations, but it is most likely that the association reported in this chapter is a false-positive result.

The initial statistical evidence presented for allele specific expression of rs2708435 was extremely weak (Tables 6.4 and 6.5), and using this result as a foundation for subsequent experiments (EMSA and association study) is a major criticism of my

work. The geometric mean of the reference genes (*HPRT1* and *RPL13A*), indicates that the association between variation at rs2708435 and LRRK2 mRNA levels in IPD cases is marginally-significant (p = 0.047, Table 6.5). However, individual analysis with the two endogenous reference genes both of which give different statistical values (*HPRT1*, p = 0.241 and *RPL13A*, p = 0.029, Table 6.5) does not clarify the effects of the tSNP on cerebellar LRRK2 mRNA levels. Although in chapter 5, four reference genes were measured for a subset of cerebellum IPD (n = 20) and control (n = 20) subjects, only two reference genes were measured for this larger set of cerebellum samples (IPD, n = 115; control, n = 35), and this is a big drawback of this particular study. Furthermore, analysis with ANOVA assumes homogeneity of variance, therefore it is likely that the marked variability in sample numbers (35 control and 115 IPD cases), may have contributed to the discrepant *P*-values for the two reference genes. Before performing the EMSA or the association study, it would have been preferable to confirm the weak finding of allele specific expression for rs2708435 (Tables 6.4 and 6.5) with a more robust assay. Although not reported in this thesis, various attempts were made to clone the 10kb 5'UTR region of *LRRK2* gene to a) assess whether rs2708435 alleles contributed to regulation of LRRK2 transcriptional activity *in-vitro*; and b) to define a minimal core promoter region for *LRRK2*. However, this was unsuccessful. Although this chapter was presented last, it was also the first to be undertaken, and transcriptome sequencing has since become a robust technology to assess differential allelic expression. Overall, due to the tenuous statistical evidence no inferences can be made about rs2708435 and its allelic specific expression on LRRK2 mRNA in IPD cases.

7.4 Future of LRRK2 and its role in PD

It has become increasingly evident that mitochondrial dysfunction may play a major role in PD pathogenesis (reviewed in (Büeler 2009)). Moreover autophagy, a catabolic process that results in degradation of cellular components through the endosomal-lysosomal machinery, has also been implicated in PD (reviewed in (Dagda et al. 2009)). The physiological function of LRRK2 is still far from understood, but its enzymatic activity and potential role in cell signalling events

has led to suggestions that it may play be involved in mitochondrial and autophagic dysfunction in PD (West et al. 2005; Gloeckner et al. 2006; Biskup et al. 2006; MacLeod et al. 2006; Iaccarino et al. 2007; Hatano et al. 2007; Shin et al. 2008; Plowey et al. 2008; Saha et al. 2009; Higashi et al. 2009; Alegre-Abarrategui et al. 2009; Ohta et al. 2010; Mutez et al. 2010). Although LRRK2 has been suggested to mediate mitochondrial kinase signalling via its interaction with extracellular signal regulated protein kinases (ERK) and c-Jun N-terminal kinases (JNK), it remains to be confirmed whether these are physiological substrates of LRRK2 (White et al. 2007; Plowey et al. 2008; Liou et al. 2008; Gloeckner et al. 2009; Carballo-Carbajal et al. 2010; Hsu et al. 2010). A lack of consensus regarding the physiological substrates of LRRK2 has created a bottleneck in our understanding of the true nature of the *in-vitro* and *in-vivo* effects of the intrinsic LRRK2 kinase activity (see (Yue 2009; Hu & Tong 2010) for review). Although LRRK2 kinase activity has been the major focus of investigation into *LRRK2* linked PD, there is increasing interest in the role of the kinase regulating GTPase domain in PD (West et al. 2007; Jaleel et al. 2007; Greggio et al. 2008; Greggio et al. 2009; Yao et al. 2010). The toxicity associated with mutations in other LRRK2 domains (LRR, COR and WD-40) (MacLeod et al. 2006; Iaccarino et al. 2007; Jaleel et al. 2007; Jorgensen et al. 2009) also suggests that *LRRK2* mediated toxicity might not be limited to its kinase activity, and perhaps requires dysregulation of the complex but finely balanced interactions between LRRK2 domains. Hence, before inhibition of LRRK2 kinase activity can be confidently postulated as a therapeutic target for PD (Covy & Giasson 2009; Hu & Tong 2010), identification of LRRK2 substrates and interactors, in addition to an extensive comparison of the pathogenic role of wild-type LRRK2 and PD linked mutations is needed in mammalian models. Furthermore, confirmation of LRRK2 interaction with the encoded proteins of other PARK loci that have been implicated in mitochondrial-related oxidative stress (reviewed in (Dagda et al. 2009), such as PINK1, parkin, DJ-1, and α-synuclein (Smith et al. 2005a; Venderova et al. 2009; Qing et al. 2009; Lin et al.

2009; Carballo-Carbajal et al. 2010)), would be an encouraging step towards elucidating a putative convergent pathway for different PARK loci and should contribute to the study of both familial and idiopathic PD.

Appendix

Summary of IPD and control subjects used for the cerebellum study in chapter 5 (section 5.3.1). Samples IPD1-IPD20 and Con1-Con22 have been previously described in Tables 5.2 and 5.5, respectively. M: male; F: female, PM: post-mortem delay.

	Sex	Age	PM delay	pH	Cause of death
IPD1	M	77	46.20	6.73	Heart failure
IPD2	M	73	11.20	6.32	CVA
IPD3	F	62	46.20	5.88	gradual deterioration
IPD4	F	78	75.45	6.46	Advanced PD
IPD5	F	87	47.45	6.62	IPD, slow deterioration
IPD6	F	81	24.25	N/A	IPD, congestive heart disease
IPD7	M	81	103	6.15	Bronchopneumonia
IPD8	M	73	20.30	6.22	PD, malignant melanoma,
IPD9	F	66	125.30	6.2	Advanced PD
IPD10	F	77	~80	6.53	Congestive heart failure
IPD11	F	88	11.30	6.38	Chest infection
IPD12	M	70	61.20	6.29	Chest infection
IPD13	M	55	8.00	6.37	progressive degenerative PD
IPD14	M	71	40.45	6.1	Chest infection
IPD15	M	79	27.25	5.88	Sudden death
IPD16	M	71	81.30	6.76	N/A
IPD17	M	70	71.30	6.17	Coronary artery atheroma
IPD18	M	91	31.45	5.81	Congestive heart failure
IPD19	F	81	57.30	N/A	Heart failure
IPD20	M	70	51.20	6.29	gradual deterioration
IPD21	M	68	39.35	N/A	N/A
IPD22	M	69	57.20	N/A	Left ventricular failure
IPD23	M	82	26.50	N/A	Bronchopneumonia
IPD24	M	83	66.00	N/A	Chest infection
IPD25	F	84	26.45	N/A	IPD
IPD26	M	78	79.33	N/A	IPD + dementia
IPD27	M	77	51.20	6.16	bronchopneumonia, heart and renal failure
IPD28	M	66	54.30	6.17	Cancer (prostate), chest infection
IPD29	M	72	25.45	N/A	IPD
IPD30	M	78	80.35	6.31	IPD + dementia
IPD31	M	77	40.30	N/A	Bronchopneumonia

	Sex	Age	PM delay	pH	Cause of death
IPD32	M	78	52.40	N/A	IPD
IPD33	F	73	18.00	6.11	PSP
IPD34	F	84	36.00	6.4	PD and trans-ischaemic disease
IPD35	M	78	38.35	6.2	PD, dementia and chest infection
IPD36	F	81	68.30	6.03	N/A
IPD37	F	79	27.20	6.68	IPD
IPD38	M	77	58.45		cardiac arrest
IPD39	F	71	36.00	6.25	N/A
IPD40	M	85	48.15	6.38	Chest infection
IPD41	F	79	24.20	6.39	PD, gradual death
IPD42	M	63	69.00	6.59	Heart failure
IPD43	F	71	50.10	6.38	Aspiration deterioration
IPD44	M	73	25.20	7.18	N/A
IPD45	F	73	70.00	6.63	PD, gradual decline
IPD46	F	79	49.30	6.07	pulmonary embolism
IPD47	M	66	56.00	6.49	heart attack
IPD48	F	80	27.10	5.62	PD/AD
IPD49	F	92	45.15	6.13	gradual deterioration
IPD50	M	76	51.15	5.77	bronchopneumonia
IPD51	F	73	40.15	6.44	bronchopneumonia
IPD52	M	84	47.00	6.11	bronchopneumonia
IPD53	F	69	52.45	6.14	bronchopneumonia
IPD54	M	87	76.10	6.01	bronchopneumonia
IPD55	F	68	77.35	6.05	bronchopneumonia
IPD56	M	79	22.05	6.27	bronchopneumonia
IPD57	F	86	43.45	6.27	gradual deterioration
IPD58	F	80	13.05	6.39	Haemo-pericardium
IPD59	F	73	45.00	5.86	multi organ failure
IPD60	M	76	35.3	N/A	N/A
IPD61	M	76	71.30	6.5	Chest infection
IPD62	M	66	21	N/A	N/A
IPD63	M	70	46.15	6.54	bronchopneumonia
IPD64	M	80	30	6.07	bronchopneumonia
IPD65	F	77	48	6.98	N/A
IPD66	M	77	23.35	6.26	bronchopneumonia
IPD67	F	73	50	6.44	bronchopneumonia
IPD68	F	81	29	5.59	N/A
IPD69	M	75	44.15	6.73	bronchopneumonia

	Sex	Age	PM delay	pH	Cause of death
IPD70	F	74	82.05	5.92	N/A
IPD71	M	79	71.15	6.5	bronchopneumonia
IPD72	F	74	35.05	6.11	pulmonary embolism
IPD73	F	89	47.1	6.47	Terminal PD
IPD74	F	77	N/A	N/A	N/A
IPD75	F	85	22.5	N/A	N/A
IPD76	F	71	34	6.37	N/A
IPD77	F	66	55.3	6.27	PD
IPD78	F	85	46.4	6.45	PD, Old age
IPD79	F	84	18	6.64	bronchopneumonia
IPD80	M	70	115	6.35	bronchopneumonia
IPD81	M	66	40	6.65	coronary artery disease
IPD82	M	69	N/A	N/A	N/A
IPD83	M	78	45.45	N/A	N/A
IPD84	M	76	4.5	6.32	Cancer (prostate), bronchopneumonia
IPD85	F	81	43	N/A	N/A
IPD86	M	71	28.5	6.23	N/A
IPD87	M	92	17.15	N/A	N/A
IPD88	F	69	46	N/A	N/A
IPD89	M	80	N/A	N/A	N/A
IPD90	M	76	38	N/A	N/A
IPD91	M	86	49.3	N/A	N/A
IPD92	M	74	32	N/A	N/A
IPD93	M	73	10	N/A	N/A
IPD94	M	71	7	N/A	N/A
IPD95	M	73	18	N/A	N/A
IPD96	M	75	17	6.44	lymphoma
IPD97	M	78	7.1	6.06	CVA
IPD98	M	79	2.55	N/A	N/A
IPD99	M	73	70	N/A	N/A
IPD100	M	75	4.3	N/A	N/A
IPD101	M	66	36.45	N/A	N/A
IPD102	M	84	6.55	N/A	N/A
IPD103	M	94	8.43	N/A	N/A
IPD104	M	71	N/A	N/A	N/A
IPD105	F	79	14.15	N/A	N/A
IPD106	F	83	1.38	N/A	N/A
IPD107	F	76	20	N/A	N/A
IPD108	F	81	23.3	N/A	N/A

	Sex	Age	PM delay	pH	Cause of death
IPD109	F	81	N/A	N/A	N/A
IPD110	F	83	73.15	N/A	N/A
IPD111	M	70	73	N/A	N/A
IPD112	F	79	14.15	N/A	N/A
IPD113	F	78	6.05	N/A	N/A
IPD114	M	62	34	N/A	N/A
IPD115	M	77	53.15	N/A	N/A
IPD116	F	84	24.13	N/A	N/A
IPD117	F	77	16.15	N/A	N/A
IPD118	F	90	26.15	N/A	N/A
IPD119	M	84	11.3	N/A	N/A
IPD120	M	73	55.55	N/A	N/A
IPD121	M	86	18.4	N/A	N/A
IPD122	M	75	23.15	N/A	N/A
IPD123	F	77	3.3	N/A	N/A
IPD124	M	74	12.3	N/A	N/A
IPD125	M	83	3.3	N/A	N/A
IPD126	F	82	24.3	N/A	N/A
IPD127	M	79	23.55	N/A	N/A
IPD128	M	79	28	N/A	N/A
IPD129	M	84	17.55	N/A	N/A

Summary of unaffected subjects used in cerebellum study in chapter 5.

	Sex	Age	PM delay	pH	Cause of death
Con1	Female	77	23	5.6	Cancer (Colon)
Con2	F	86	46.5	6.17	Cancer
Con3	F	84	81.45	6.28	Cancer and heart failure
Con4	M	85	43.35	6.68	Cancer (Oesophagus)
Con5	M	86	53	6.65	Bronchopneumonia, heart failure
Con6	M	86	23.3	6.55	Myocardial infarction
Con7	M	81	40	6.48	N/A
Con8	F	53	29.5	6.64	intra-cerebral haemorrage
Con9	M	91	48	6.54	bronchopneumonia
Con10	F	88	49.25	6.23	chronic obstructive airway disease
Con11	F	85	34	6.31	Breast cancer
Con12	F	89	77.3	6.49	Pneumonia
Con13	M	83	117.05	6.81	Heart attack
Con14	M	79	56.4	6.6	Cancer (prostate)
Con15	M	75	64.5	6.18	Pulmonary embolism
Con16	F	81	13.5	6.39	Cancer (Colon)
Con17	M	63	42	6.23	congestive heart disease
Con18	M	57	78.5	6.03	Adenocarcinoma
Con19	F	78	23.3	N/A	N/A
Con20	M	71	38.5	N/A	Mesolithioma
Con21	F	83	20	6.55	Bowel resection with complications
Con22	F	78	51.3	6.24	Colon cancer
Con23	F	64	79	5.88	Bowel and liver cancer
Con24	F	85	73.3	5.98	N/A
Con25	F	77	79.5	6.46	chronic obstructive airway disease
Con26	M	N/A	N/A	N/A	N/A
Con27	F	83	22	6.25	Cancer (lung)
Con28	M	67	22	6.55	Myocardial infarction
Con29	F	73	28	6.38	bronchopenumonia
Con30	F	80	28	6.08	myocardial infarction
Con31	M	72	13	6.16	N/A
Con32	M	74	5.5	6.51	left ventricular failure
Con33	M	76	16	6.71	ruptured thoracic aneurysm
Con34	F	77	18	6.7	N/A
Con35	F	73	15	6.68	congestive heart failure
Con36	M	71	17	6.74	ruptured thoracic aortic aneurysm
Con37	F	85	37.1	N/A	Liver and bone cancer
Con38	F	88	11.1	N/A	Myocardial infarction, respiratory failure

Bibliography

Aasly, J.O. et al., 2005. Clinical features of LRRK2-associated Parkinson's disease in central Norway. *Annals of Neurology*, 57(5), 762-5.

Abbas, N. et al., 1999. A wide variety of mutations in the parkin gene are responsible for autosomal recessive parkinsonism in Europe. French Parkinson's Disease Genetics Study Group and the European Consortium on Genetic Susceptibility in Parkinson's Disease. *Human Molecular Genetics*, 8(4), 567-574.

Abeliovich, A. et al., 2000. Mice lacking alpha-synuclein display functional deficits in the nigrostriatal dopamine system. *Neuron*, 25(1), 239-52.

Abeliovich, A. & Flint Beal, M., 2006. Parkinsonism genes: culprits and clues. *Journal of Neurochemistry*, 99(4), 1062-72.

Abou-Sleiman, P.M. et al., 2006. A heterozygous effect for PINK1 mutations in Parkinson's disease? *Annals of Neurology*, 60(4), 414-419.

Adam-Vizi, V., 2005. Production of reactive oxygen species in brain mitochondria: contribution by electron transport chain and non-electron transport chain sources. *Antioxidants & Redox Signaling*, 7(9-10), 1140-1149.

Aharon-Peretz, J., Rosenbaum, H. & Gershoni-Baruch, R., 2004. Mutations in the glucocerebrosidase gene and Parkinson's disease in Ashkenazi Jews. *The New England Journal of Medicine*, 351(19), 1972-1977.

Aksentijevich, I. et al., 1999. Mutation and haplotype studies of familial Mediterranean fever reveal new ancestral relationships and evidence for a high carrier frequency with reduced penetrance in the Ashkenazi Jewish population. *American Journal of Human Genetics*, 64(4), 949-62.

Alegre-Abarrategui, J. et al., 2008. LRRK2 is a component of granular alpha-synuclein pathology in the brainstem of Parkinson's disease. *Neuropathology and Applied Neurobiology*, 34(3), 272-83.

Alegre-Abarrategui, J. et al., 2009. LRRK2 regulates autophagic activity and localizes to specific membrane microdomains in a novel human genomic reporter cellular model. *Human Molecular Genetics*, 18(21), 4022-4034.

Andersen, C.L., Jensen, J.L. & Ørntoft, T.F., 2004. Normalization of real-time quantitative reverse transcription-PCR data: a model-based variance estimation approach to identify genes suited for normalization, applied to bladder and colon cancer data sets. *Cancer Research*, 64(15), 5245-5250.

Andres-Mateos, E. et al., 2009. Unexpected lack of hypersensitivity in LRRK2 knock-out mice to MPTP (1-methyl-4-phenyl-1,2,3,6-tetrahydropyridine). *The Journal of Neuroscience*, 29(50), 15846-15850.

Arai, T. et al., 1999. Argyrophilic glial inclusions in the midbrain of patients with Parkinson's disease and diffuse Lewy body disease are immunopositive for NACP/alpha-synuclein. *Neuroscience Letters*, 259(2), 83-86.

Ashok, P.P. et al., 1986. Epidemiology of Parkinson's disease in Benghazi, North-East Libya. *Clinical Neurology and Neurosurgery*, 88(2), 109-13.

Baker, M. et al., 1999. Association of an extended haplotype in the tau gene with progressive supranuclear palsy. *Human Molecular Genetics*, 8(4), 711-715.

Bandopadhyay, R. et al., 2004. The expression of DJ-1 (PARK7) in normal human CNS and idiopathic Parkinson's disease. *Brain*, 127(2), 420-430.

Bar-Shira, A. et al., 2009. Ashkenazi Parkinson's disease patients with the LRRK2 G2019S mutation share a common founder dating from the second to fifth centuries. *neurogenetics*, 10(4), 355-358.

Barton, A.J. et al., 1993. Pre- and postmortem influences on brain RNA. *Journal of Neurochemistry*, 61(1), 1-11.

Behar, D.M. et al., 2003. Multiple origins of Ashkenazi Levites: Y chromosome evidence for both Near Eastern and European ancestries. *American Journal of Human Genetics*, 73(4), 768-779.

Benamer, H.T.S. et al., 2008. Parkinson's disease in Arabs: a systematic review. *Movement Disorders*, 23(9), 1205-10.

Benamer, H.T.S., 2008. The ancestry of LRRK2 Gly2019Ser parkinsonism. *Lancet Neurology*, 7(9), 769-70; author reply 770-1.

Bengtsson, M. et al., 2005. Gene expression profiling in single cells from the pancreatic islets of Langerhans reveals lognormal distribution of mRNA levels. *Genome Research*, 15(10), 1388-1392.

Berg, D. et al., 2005. Type and frequency of mutations in the LRRK2 gene in familial and sporadic Parkinson's disease*. *Brain*, 128(12), 3000-11.

Betarbet, R., Sherer, T.B. & Greenamyre, J.T., 2002. Animal models of Parkinson's disease. *BioEssays: News and Reviews in Molecular, Cellular and Developmental Biology*, 24(4), 308-318.

Biskup, S. et al., 2005. Common variants of LRRK2 are not associated with sporadic Parkinson's disease. *Annals of Neurology*, 58(6), 905-908.

Biskup, S. et al., 2006. Localization of LRRK2 to membranous and vesicular structures in mammalian brain. *Annals of Neurology*, 60(5), 557-69.

Biskup, S. et al., 2007. Dynamic and redundant regulation of LRRK2 and LRRK1 expression. *BMC Neuroscience*, 8, 102.

Bohnen, N.I. et al., 2007. Selective hyposmia and nigrostriatal dopaminergic denervation in Parkinson's disease. *Journal of Neurology*, 254(1), 84-90.

Bonifati, V. et al., 2003a. DJ-1 (PARK7), a novel gene for autosomal recessive, early onset parkinsonism. *Neurological Sciences*, 24(3), 159-160.

Bonifati, V. et al., 2003b. Mutations in the DJ-1 gene associated with autosomal recessive early-onset parkinsonism. *Science*, 299(5604), 256-259.

Bonni, A. et al., 1999. Cell survival promoted by the Ras-MAPK signaling pathway by transcription-dependent and -independent mechanisms. *Science*, 286(5443), 1358-1362.

Bosch, E. et al., 2000. Genetic structure of north-west Africa revealed by STR analysis. *European Journal of Human Genetics*, 8(5), 360-366.

Bosch, E. et al., 2001. High-resolution analysis of human Y-chromosome variation shows a sharp discontinuity and limited gene flow between northwestern Africa and the Iberian Peninsula. *American Journal of Human Genetics*, 68(4), 1019-1029.

Bossers, K. et al., 2009. Analysis of gene expression in Parkinson's disease: possible involvement of neurotrophic support and axon guidance in dopaminergic cell death. *Brain Pathology*, 19(1), 91-107.

Braak, H. & Braak, E., 2000. Pathoanatomy of Parkinson's disease. *Journal of Neurology*, 247 Suppl 2, II3-10.

Braak, H. et al., 2003. Staging of brain pathology related to sporadic Parkinson's disease. *Neurobiology of Aging*, 24(2), 197-211.

Braak, H. et al., 2004. Stages in the development of Parkinson's disease-related pathology. *Cell and Tissue Research*, 318(1), 121-134.

Braak, H. & Del Tredici, K., 2004. Poor and protracted myelination as a contributory factor to neurodegenerative disorders. *Neurobiology of Aging*, 25(1), 19-23.

Braak, H. et al., 2006. Pathology associated with sporadic Parkinson's disease--where does it end? *Journal of Neural Transmission. Supplementum*, (70), 89-97.

Bras, J.M. et al., 2005. G2019S dardarin substitution is a common cause of Parkinson's disease in a Portuguese cohort. *Movement Disorders*, 20(12), 1653-5.

Bras, J. et al., 2009. Complete screening for glucocerebrosidase mutations in Parkinson disease patients from Portugal. *Neurobiology of Aging*, 30(9), 1515-1517.

Bray, N.J. et al., 2003. Cis-acting variation in the expression of a high proportion of genes in human brain. *Human Genetics*, 113(2), 149-153.

Bray, N.J. et al., 2004. Allelic expression of APOE in human brain: effects of epsilon status and promoter haplotypes. *Human Molecular Genetics*, 13(22), 2885-2892.

Brooks, A.I. et al., 1999. Paraquat elicited neurobehavioral syndrome caused by dopaminergic neuron loss. *Brain Research*, 823(1-2), 1-10.

Brooks, D.J., 1991. Detection of preclinical Parkinson's disease with PET. *Neurology*, 41(5 Suppl 2), 24-27.

Buckland, P.R., 2004a. Allele-specific gene expression differences in humans. *Human Molecular Genetics*, 13 (2), R255-260.

Buckland, P.R. et al., 2004b. A high proportion of polymorphisms in the promoters of brain expressed genes influences transcriptional activity. *Biochimica Et Biophysica Acta*, 1690(3), 238-249.

Büeler, H., 2009. Impaired mitochondrial dynamics and function in the pathogenesis of Parkinson's disease. *Experimental Neurology*, 218(2), 235-246.

Bustin, S.A. et al., 2005. Quantitative real-time RT-PCR--a perspective. *Journal of Molecular Endocrinology*, 34(3), 597-601.

Carballo-Carbajal, I. et al., 2010. Leucine-rich repeat kinase 2 induces alpha-synuclein expression via the extracellular signal-regulated kinase pathway. *Cellular Signalling*, 22(5), 821-827.

Cavalli-Sforza, L.L. & Piazza, A., 1993. Human genomic diversity in Europe: a summary of recent research and prospects for the future. *European Journal of Human Genetics*, 1(1), 3-18.

Chaâbani, H. & Cox, D.W., 1988. Genetic characterization and origin of Tunisian Berbers. *Human Heredity*, 38(5), 308-16.

Change, N., Mercier, G. & Lucotte, G., 2008. Genetic screening of the G2019S mutation of the LRRK2 gene in Southwest European, North African, and Sephardic Jewish subjects. *Genetic Testing*, 12(3), 333-9.

Chartier-Harlin, M. et al., 2004. Alpha-synuclein locus duplication as a cause of familial Parkinson's disease. *Lancet*, 364(9440), 1167-1169.

Cheung, V.G. et al., 2005. Mapping determinants of human gene expression by regional and genome-wide association. *Nature*, 437(7063), 1365-1369.

Chiba-Falek, O. & Nussbaum, R.L., 2001. Effect of allelic variation at the NACP-Rep1 repeat upstream of the alpha-synuclein gene (SNCA) on transcription in a cell culture luciferase reporter system. *Human Molecular Genetics*, 10(26), 3101-3109.

Chiba-Falek, O., Lopez, G.J. & Nussbaum, R.L., 2006. Levels of alpha-synuclein mRNA in sporadic Parkinson disease patients. *Movement Disorders*, 21(10), 1703-1708.

Cho, J. et al., 2007. The G2019S LRRK2 mutation is rare in Korean patients with Parkinson's disease. *The Canadian Journal of Neurological Sciences*, 34(1), 53-5.

Clark, I.E. et al., 2006. Drosophila pink1 is required for mitochondrial function and interacts genetically with parkin. *Nature*, 441(7097), 1162-1166.

Clark, L.N. et al., 2006. Frequency of LRRK2 mutations in early- and late-onset Parkinson disease. *Neurology*, 67(10), 1786-91.

Colombo, R., 2000a. Age and Origin of the PRNP E200K Mutation Causing Familial Creutzfeldt-Jacob Disease in Libyan Jews. *American Journal of Human Genetics*, 67(2), 528–531

Colombo, R., 2000b. Age estimate of the N370S mutation causing Gaucher disease in Ashkenazi Jews and European populations: A reappraisal of haplotype data. *American Journal of Human Genetics*, 66(2), 692-7.

Covy, J.P., Van Deerlin V.M. & Giasson, B.I. 2006., Lack of evidence for Lrrk2 in alpha-synuclein pathological inclusions. *Annals of Neurology*, 60(5), 618-619.

Covy, J.P. & Giasson, B.I., 2009. Identification of compounds that inhibit the kinase activity of leucine-rich repeat kinase 2. *Biochemical and Biophysical Research Communications*, 378(3), 473-477.

Cossu, G. et al., 2007. LRRK2 mutations and Parkinson's disease in Sardinia--A Mediterranean genetic isolate. *Parkinsonism & Related Disorders*, 13(1), 17-21.

Criscuolo, C. et al., 2006. PINK1 homozygous W437X mutation in a patient with apparent dominant transmission of parkinsonism. *Movement Disorders*, 21(8), 1265-1267.

Croisier, E. & Graeber, M.B., 2006. Glial degeneration and reactive gliosis in alpha-synucleinopathies: the emerging concept of primary gliodegeneration. *Acta Neuropathologica*, 112(5), 517-530.

Dächsel, J.C. et al., 2007a. Identification of potential protein interactors of Lrrk2. *Parkinsonism & Related Disorders*, 13(7), 382-5.

Dächsel, J.C. et al., 2007b. Lrrk2 G2019S substitution in frontotemporal lobar degeneration with ubiquitin-immunoreactive neuronal inclusions. *Acta Neuropathologica*, 113(5), 601-6.

Dachsel, J.C. et al., 2010. Heterodimerization of Lrrk1-Lrrk2: Implications for LRRK2-associated Parkinson disease. *Mechanisms of Ageing and Development*. Available at: http://www.ncbi.nlm.nih.gov/pubmed/20144646 [Accessed March 16, 2010].

Dagda, R.K., Zhu, J. & Chu, C.T., 2009. Mitochondrial kinases in Parkinson's disease: converging insights from neurotoxin and genetic models. *Mitochondrion*, 9(5), 289-298.

Dekker, M.C.J. et al., 2004. PET neuroimaging and mutations in the DJ-1 gene. *Journal of Neural Transmission*, 111(12), 1575-1581.

Del Tredici, K. et al., 2002. Where does parkinson disease pathology begin in the brain? *Journal of Neuropathology and Experimental Neurology*, 61(5), 413-426.

Deng, H. et al., 2006. Genetic analysis of LRRK2 mutations in patients with Parkinson disease. *Journal of the Neurological Sciences*, 251(1-2), 102-6.

Deng, J. et al., 2008. Structure of the ROC domain from the Parkinson's disease-associated leucine-rich repeat kinase 2 reveals a dimeric GTPase. *Proceedings of the National Academy of Sciences of the United States of America*, 105(5), 1499-504.

De Rosa, A. et al., 2009. Genetic screening for LRRK2 gene G2019S mutation in Parkinson's disease patients from Southern Italy. *Parkinsonism & Related Disorders*, 15(3), 242-4.

Di Fonzo, A. et al., 2005. A frequent LRRK2 gene mutation associated with autosomal dominant Parkinson's disease. *Lancet*, 365(9457), 412-415.

Di Fonzo, A. et al., 2006. Comprehensive analysis of the LRRK2 gene in sixty families with Parkinson's disease. *European Journal of Human Genetics*, 14(3), 322-331.

Di Fonzo, A. et al., 2007. ATP13A2 missense mutations in juvenile parkinsonism and young onset Parkinson disease. *Neurology*, 68(19), 1557-62.

Dixon, A.L. et al., 2007. A genome-wide association study of global gene expression. *Nature Genetics*, 39(10), 1202-1207.

Djaldetti, R. et al., 2008. Clinical characteristics of Parkinson's disease among Jewish Ethnic groups in Israel. *Journal of Neural Transmission*, 115(9), 1279-84.

Djarmati, A. et al., 2004. Detection of Parkin (PARK2) and DJ1 (PARK7) mutations in early-onset Parkinson disease: Parkin mutation frequency depends on ethnic origin of patients. *Human Mutation*, 23(5), 525.

van Duijn, C.M. et al., 2001. Park7, a novel locus for autosomal recessive early-onset parkinsonism, on chromosome 1p36. *American Journal of Human Genetics*, 69(3), 629-634.

Duke, D.C. et al., 2006. Transcriptome analysis reveals link between proteasomal and mitochondrial pathways in Parkinson's disease. *Neurogenetics*, 7(3), 139-48.

Eblan, M.J. et al., 2006. Glucocerebrosidase mutations are not found in association with LRRK2 G2019S in subjects with parkinsonism. *Neuroscience Letters*, 404(1-2), 163-5.

Emre, M., 2003. What causes mental dysfunction in Parkinson's disease? *Movement Disorders*, 18 Suppl 6, S63-71.

Enard, W. et al., 2002. Intra- and interspecific variation in primate gene expression patterns. *Science*, 296(5566), 340-343.

Engelender, S. et al., 1999. Synphilin-1 associates with alpha-synuclein and promotes the formation of cytosolic inclusions. *Nature Genetics*, 22(1), 110-114.

Ervin, J.F. et al., 2007. Postmortem delay has minimal effect on brain RNA integrity. *Journal of Neuropathology and Experimental Neurology*, 66(12), 1093-9.

Esteban, E. et al., 2004. Genetic relationships among Berbers and South Spaniards based on CD4 microsatellite/Alu haplotypes. *Annals of Human Biology*, 31(2), 202-212.

Exner, N. et al., 2007. Loss-of-function of human PINK1 results in mitochondrial pathology and can be rescued by parkin. *The Journal of Neuroscience*, 27(45), 12413-12418.

Faccio, L. et al., 2000. Characterization of a novel human serine protease that has extensive homology to bacterial heat shock endoprotease HtrA and is regulated by kidney ischemia. *The Journal of Biological Chemistry*, 275(4), 2581-2588.

Farrer, M. et al., 2001. Lewy bodies and parkinsonism in families with parkin mutations. *Annals of Neurology*, 50(3), 293-300.

Farrer, M. et al., 2004. Comparison of kindreds with parkinsonism and alpha-synuclein genomic multiplications. *Annals of Neurology*, 55(2), 174-179.

Farrer, Matthew J, Gibson, Rachel & Hentati, Faycal, 2008. The ancestry of LRRK2 Gly2019Ser parkinsonism – Authors' reply. *Lancet Neurology*, 7(9), 770-771.

Feany, M.B. & Bender, W.W., 2000. A Drosophila model of Parkinson's disease. *Nature*, 404(6776), 394-398.

Fearnley, J.M. & Lees, A.J., 1991. Ageing and Parkinson's disease: substantia nigra regional selectivity. *Brain*, 114 (Pt 5), 2283-2301.

Ferrer, I., 2009. Early involvement of the cerebral cortex in Parkinson's disease: convergence of multiple metabolic defects. *Progress in Neurobiology*, 88(2), 89-103.

Ferreira, J.J. et al., 2007. High prevalence of LRRK2 mutations in familial and sporadic Parkinson's disease in Portugal. *Movement Disorders*, 22(8), 1194-201.

Flores, C. et al., 2000. Northwest African distribution of the CD4/Alu microsatellite haplotypes. *Annals of Human Genetics*, 64(Pt 4), 321-7.

Forno, L.S., 1996. Neuropathology of Parkinson's disease. *Journal of Neuropathology and Experimental Neurology*, 55(3), 259-272.

Fuchs, J. et al., 2007. Phenotypic variation in a large Swedish pedigree due to SNCA duplication and triplication. *Neurology*, 68(12), 916-22.

Fuchs, J. et al., 2008. Genetic variability in the SNCA gene influences alpha-synuclein levels in the blood and brain. *The FASEB Journal*, 22(5), 1327-1334.

Fujiwara, H. et al., 2002. alpha-Synuclein is phosphorylated in synucleinopathy lesions. *Nature Cell Biology*, 4(2), 160-4.

Funayama, M. et al., 2002. A new locus for Parkinson's disease (PARK8) maps to chromosome 12p11.2-q13.1. *Annals of Neurology*, 51(3), 296-301.

Funayama, M. et al., 2005. An LRRK2 mutation as a cause for the parkinsonism in the original PARK8 family. *Annals of Neurology*, 57(6), 918-21.

Fung, H. et al., 2006a. Genome-wide genotyping in Parkinson's disease and neurologically normal controls: first stage analysis and public release of data. *Lancet Neurology*, 5(11), 911-916.

Fung, H. et al., 2006b. Lack of G2019S LRRK2 mutation in a cohort of Taiwanese with sporadic Parkinson's disease. *Movement Disorders*, 21(6), 880-1.

Gaig, C. et al., 2006. LRRK2 mutations in Spanish patients with Parkinson disease: frequency, clinical features, and incomplete penetrance. *Archives of Neurology*, 63(3), 377-82.

Gaig, C. et al., 2007. G2019S LRRK2 mutation causing Parkinson's disease without Lewy bodies. *Journal of Neurology, Neurosurgery, and Psychiatry*, 78(6), 626-628.

Galter, D. et al., 2006. LRRK2 expression linked to dopamine-innervated areas. *Annals of Neurology*, 59(4), 714-9.

Gan-Or, Z. et al., 2008. Genotype-phenotype correlations between GBA mutations and Parkinson disease risk and onset. *Neurology*, 70(24), 2277-83.

Gandhi, S. et al., 2006. PINK1 protein in normal human brain and Parkinson's disease. *Brain: A Journal of Neurology*, 129(Pt 7), 1720-1731.

Gasser, T. et al., 1998. A susceptibility locus for Parkinson's disease maps to chromosome 2p13. *Nature Genetics*, 18(3), 262-265.

German, D.C. et al., 1989. Midbrain dopaminergic cell loss in Parkinson's disease: computer visualization. *Annals of Neurology*, 26(4), 507-514.

Gershoni-Baruch, R. et al., 2001. Familial Mediterranean fever: prevalence, penetrance and genetic drift. *European Journal of Human Genetics*, 9(8), 634-7.

Giasson, B.I. et al., 2006. Biochemical and pathological characterization of Lrrk2. *Annals of Neurology*, 59(2), 315-22.

Gibb, W.R. & Lees, A.J., 1991. Anatomy, pigmentation, ventral and dorsal subpopulations of the substantia nigra, and differential cell death in Parkinson's disease. *Journal of Neurology, Neurosurgery, and Psychiatry*, 54(5), 388-396.

Gibb, W.R., 1992. Neuropathology of Parkinson's disease and related syndromes. *Neurologic Clinics*, 10(2), 361-376.

Gilad, Y. et al., 2006. Expression profiling in primates reveals a rapid evolution of human transcription factors. *Nature*, 440(7081), 242-245.

Gilks, W.P. et al., 2005. A common LRRK2 mutation in idiopathic Parkinson's disease. *Lancet*, 365(9457), 415-416.

Gillardon, F., 2009. Interaction of elongation factor 1-alpha with leucine-rich repeat kinase 2 impairs kinase activity and microtubule bundling in vitro. *Neuroscience*, 163(2), 533-539.

Giordana, M.T. et al., 2007. Neuropathology of Parkinson's disease associated with the LRRK2 Ile1371Val mutation. *Movement Disorders*, 22(2), 275-278.

Gitler, A.D. et al., 2009. Alpha-synuclein is part of a diverse and highly conserved interaction network that includes PARK9 and manganese toxicity. *Nature Genetics*, 41(3), 308-315.

Gloeckner, C.J. et al., 2006. The Parkinson disease causing LRRK2 mutation I2020T is associated with increased kinase activity. *Human Molecular Genetics*, 15(2), 223-32.

Gloeckner, C.J. et al., 2009. The Parkinson disease-associated protein kinase LRRK2 exhibits MAPKKK activity and phosphorylates MKK3/6 and MKK4/7, in vitro. *Journal of Neurochemistry*, 109(4), 959-968.

Goetz, C.G., 2002. Jean-Martin Charcot and the aging brain. *Archives of Neurology*, 59(11), 1821-1824.

Goker-Alpan, O. et al., 2004. Parkinsonism among Gaucher disease carriers. *Journal of Medical Genetics*, 41(12), 937-940.

Goldberg, M.S. & Lansbury, P.T., 2000. Is there a cause-and-effect relationship between alpha-synuclein fibrillization and Parkinson's disease? *Nature Cell Biology*, 2(7), E115-9.

Goldwurm, S. et al., 2005. The G6055A (G2019S) mutation in LRRK2 is frequent in both early and late onset Parkinson's disease and originates from a common ancestor. *Journal of Medical Genetics*, 42(11), e65.

Goldwurm, S. et al., 2006. LRRK2 G2019S mutation and Parkinson's disease: a clinical, neuropsychological and neuropsychiatric study in a large Italian sample. *Parkinsonism & Related Disorders*, 12(7), 410-9.

Goldwurm, S. et al., 2007. Evaluation of LRRK2 G2019S penetrance: relevance for genetic counseling in Parkinson disease. *Neurology*, 68(14), 1141-3.

Gómez-Santos, C. et al., 2002. MPP+ increases alpha-synuclein expression and ERK/MAP-kinase phosphorylation in human neuroblastoma SH-SY5Y cells. *Brain Research*, 935(1-2), 32-9.

Göring, H.H.H. et al., 2007. Discovery of expression QTLs using large-scale transcriptional profiling in human lymphocytes. *Nature Genetics*, 39(10), 1208-1216.

Gorostidi, A. et al., 2009. LRRK2 G2019S and R1441G mutations associated with Parkinson's disease are common in the Basque Country, but relative prevalence is determined by ethnicity. *Neurogenetics*, 10(2), 157-159.

Grasbon-Frodl, E.M. et al., 1999. Two novel point mutations of mitochondrial tRNA genes in histologically confirmed Parkinson disease. *Neurogenetics*, 2(2), 121-127.

Gray, C.W. et al., 2000. Characterization of human HtrA2, a novel serine protease involved in the mammalian cellular stress response. *European Journal of Biochemistry / FEBS*, 267(18), 5699-5710.

Greggio, E. et al., 2006. Kinase activity is required for the toxic effects of mutant LRRK2/dardarin. *Neurobiology of Disease*, 23(2), 329-41.

Greggio, E. et al., 2008. The Parkinson disease-associated leucine-rich repeat kinase 2 (LRRK2) is a dimer that undergoes intramolecular autophosphorylation. *The Journal of Biological Chemistry*, 283(24), 16906-14.

Greggio, E. et al., 2009. The Parkinson's disease kinase LRRK2 autophosphorylates its GTPase domain at multiple sites. *Biochemical and Biophysical Research Communications*, 389(3), 449-454.

Greggio, E. & Cookson, M.R., 2009. Leucine-rich repeat kinase 2 mutations and Parkinson's disease: three questions. *ASN Neuro*, 1(1), e00002

Gregory, A. et al., 2008. Neurodegeneration associated with genetic defects in phospholipase A(2). *Neurology*, 71(18), 1402-1409.

Grünblatt, E. et al., 2004. Gene expression profiling of parkinsonian substantia nigra pars compacta; alterations in ubiquitin-proteasome, heat shock protein, iron and oxidative stress regulated proteins, cell adhesion/cellular matrix and vesicle trafficking genes. *Journal of Neural Transmission*, 111(12), 1543-73.

Gründemann, J. et al., 2008. Elevated alpha-synuclein mRNA levels in individual UV-laser-microdissected dopaminergic substantia nigra neurons in idiopathic Parkinson's disease. *Nucleic Acids Research*, 36(7), e38.

Guo, L., Wang, W. & Chen, S.G., 2006. Leucine-rich repeat kinase 2: relevance to Parkinson's disease. *The International Journal of Biochemistry & Cell Biology*, 38(9), 1469-1475.

Gutala, R.V. & Reddy, P.H., 2004. The use of real-time PCR analysis in a gene expression study of Alzheimer's disease post-mortem brains. *Journal of Neuroscience Methods*, 132(1), 101-107.

Häbig, K. et al., 2008. RNA interference of LRRK2-microarray expression analysis of a Parkinson's disease key player. *Neurogenetics*, 9(2), 83-94.

Hampshire, D.J. et al., 2001. Kufor-Rakeb syndrome, pallido-pyramidal degeneration with supranuclear upgaze paresis and dementia, maps to 1p36. *Journal of Medical Genetics*, 38(10), 680-682.

Han, B. et al., 2008. Expression of the LRRK2 gene in the midbrain dopaminergic neurons of the substantia nigra. *Neuroscience Letters*, 442(3), 190-194.

Hardy, J. et al., 2009. The genetics of Parkinson's syndromes: a critical review. *Current Opinion in Genetics & Development*, 19(3), 254-265.

Harrison, P.J. et al., 1991. Terminal coma affects messenger RNA detection in post mortem human temporal cortex. *Brain Research. Molecular Brain Research*, 9(1-2), 161-4.

Hashimoto, M. et al., 1999. Oxidative stress induces amyloid-like aggregate formation of NACP/alpha-synuclein in vitro. *Neuroreport*, 10(4), 717-721.

Hatano, T. et al., 2007. Leucine-rich repeat kinase 2 associates with lipid rafts. *Human Molecular Genetics*, 16(6), 678-690.

Hauser, M.A. et al., 2005. Expression profiling of substantia nigra in Parkinson disease, progressive supranuclear palsy, and frontotemporal dementia with parkinsonism. *Archives of Neurology*, 62(6), 917-21.

Hayashita-Kinoh, H. et al., 2006. Down-regulation of alpha-synuclein expression can rescue dopaminergic cells from cell death in the substantia nigra of Parkinson's disease rat model. *Biochemical and Biophysical Research Communications*, 341(4), 1088-95.

Healy, D.G. et al., 2008. Phenotype, genotype, and worldwide genetic penetrance of LRRK2-associated Parkinson's disease: a case-control study. *Lancet Neurology*, 7(7), 583-90.

Healy, D.G. et al., 2004. Tau gene and Parkinson's disease: a case-control study and meta-analysis. *Journal of Neurology, Neurosurgery, and Psychiatry*, 75(7), 962-965.

Healy, D.G. et al., 2006. NR4A2 genetic variation in sporadic Parkinson's disease: a genewide approach. *Movement Disorders*, 21(11), 1960-1963.

Healy, D.G. et al., 2008. Phenotype, genotype, and worldwide genetic penetrance of LRRK2-associated Parkinson's disease: a case-control study. *Lancet Neurology*, 7(7), 583-90.

Heo, H.Y. et al., 2010. LRRK2 enhances oxidative stress-induced neurotoxicity via its kinase activity. *Experimental Cell Research*, 316(4), 649-656.

Hering, R. et al., 2004. Extended mutation analysis and association studies of Nurr1 (NR4A2) in Parkinson disease. *Neurology*, 62(7), 1231-1232.

Hernandez, D.G. et al., 2005. Clinical and positron emission tomography of Parkinson's disease caused by LRRK2. *Annals of Neurology*, 57(3), 453-6.

Hicks, A.A. et al., 2002. A susceptibility gene for late-onset idiopathic Parkinson's disease. *Annals of Neurology*, 52(5), 549-555.

Higashi, S. et al., 2007a. Expression and localization of Parkinson's disease-associated leucine-rich repeat kinase 2 in the mouse brain. *Journal of Neurochemistry*, 100(2), 368-81.

Higashi, S. et al., 2007b. Localization of Parkinson's disease-associated LRRK2 in normal and pathological human brain. *Brain Research*, 1155, 208-19.

Higashi, S. et al., 2009. Abnormal localization of leucine-rich repeat kinase 2 to the endosomal-lysosomal compartment in lewy body disease. *Journal of Neuropathology and Experimental Neurology*, 68(9), 994-1005.

Hilker, R. et al., 2001. Positron emission tomographic analysis of the nigrostriatal dopaminergic system in familial parkinsonism associated with mutations in the parkin gene. *Annals of Neurology*, 49(3), 367-376.

Hishikawa, N. et al., 2001. Widespread occurrence of argyrophilic glial inclusions in Parkinson's disease. *Neuropathology and Applied Neurobiology*, 27(5), 362-372.

Holdorff, B., 2002. Friedrich Heinrich Lewy (1885-1950) and his work. *Journal of the History of the Neurosciences*, 11(1), 19-28.

Hope, A.D. et al., 2004. Alpha-synuclein missense and multiplication mutations in autosomal dominant Parkinson's disease. *Neuroscience Letters*, 367(1), 97-100.

Hornykiewicz, O., 2008. Basic research on dopamine in Parkinson's disease and the discovery of the nigrostriatal dopamine pathway: the view of an eyewitness. *Neuro-Degenerative Diseases*, 5(3-4), 114-117.

Howells, D.W. et al., 2000. Reduced BDNF mRNA expression in the Parkinson's disease substantia nigra. *Experimental Neurology*, 166(1), 127-135.

Hsu, C.H. et al., 2010. MKK6 binds and regulates expression of Parkinson's disease-related protein LRRK2. *Journal of Neurochemistry*. Available at: http://www.ncbi.nlm.nih.gov/pubmed/20067578 [Accessed March 16, 2010].

Hsu, L.J. et al., 2000. alpha-synuclein promotes mitochondrial deficit and oxidative stress. *The American Journal of Pathology*, 157(2), 401-410.

Hu, Y. & Tong, Y., 2010. A trojan horse for Parkinson's disease. *Science Signaling*, 3(116), pe13.

Huang, Y. et al., 2008. LRRK2 and parkin immunoreactivity in multiple system atrophy inclusions. *Acta Neuropathologica*, 116(6), 639-46.

Hulihan, M.M. et al., 2008. LRRK2 Gly2019Ser penetrance in Arab-Berber patients from Tunisia: a case-control genetic study. *Lancet Neurology*, 7(7), 591-4.

Hurley, M.J. et al., 2007. Striatal leucine-rich repeat kinase 2 mRNA is increased in 1-methyl-4-phenyl-1,2,3,6-tetrahydropyridine-lesioned common marmosets (Callithrix jacchus) with L-3, 4-dihydroxyphenylalanine methyl ester-induced dyskinesia. *The European Journal of Neuroscience*, 26(1), 171-7.

Hutton, M. et al., 1998. Association of missense and 5'-splice-site mutations in tau with the inherited dementia FTDP-17. *Nature*, 393(6686), 702-705.

Iaccarino, C. et al., 2007. Apoptotic mechanisms in mutant LRRK2-mediated cell death. *Human Molecular Genetics*, 16(11), 1319-1326.

Ibáñez, P. et al., 2004a. Causal relation between alpha-synuclein gene duplication and familial Parkinson's disease. *Lancet*, 364(9440), 1169-1171.

Ibáñez, P. et al., 2004b. Absence of NR4A2 exon 1 mutations in 108 families with autosomal dominant Parkinson disease. *Neurology*, 62(11), 2133-4.

Illarioshkin, S.N. et al., 2007. A common leucine-rich repeat kinase 2 gene mutation in familial and sporadic Parkinson's disease in Russia. *European Journal of Neurology*, 14(4), 413-7.

Imai, Y. et al., 2008. Phosphorylation of 4E-BP by LRRK2 affects the maintenance of dopaminergic neurons in Drosophila. *The EMBO Journal*, 27(18), 2432-43.

Inden, M. et al., 2006. PARK7 DJ-1 protects against degeneration of nigral dopaminergic neurons in Parkinson's disease rat model. *Neurobiology of Disease*, 24(1), 144-158.

Ingram, C.J.E. et al., 2007. A novel polymorphism associated with lactose tolerance in Africa: multiple causes for lactase persistence? *Human Genetics*, 120(6), 779-788.

Isaias, I.U. et al., 2006. Striatal dopamine transporter binding in Parkinson's disease associated with the LRRK2 Gly2019Ser mutation. *Movement Disorders*, 21(8), 1144-1147.

Ishihara, L. et al., 2006. Clinical features of Parkinson disease patients with homozygous leucine-rich repeat kinase 2 G2019S mutations. *Archives of Neurology*, 63(9), 1250-4.

Ishihara, L. et al., 2007. Screening for Lrrk2 G2019S and clinical comparison of Tunisian and North American Caucasian Parkinson's disease families. *Movement Disorders*, 22(1), 55-61.

Iwatsubo, T., 2003. Aggregation of alpha-synuclein in the pathogenesis of Parkinson's disease. *Journal of Neurology*, 250 Suppl 3, III11-4.

Jaleel, M. et al., 2007. LRRK2 phosphorylates moesin at threonine-558: characterization of how Parkinson's disease mutants affect kinase activity. *The Biochemical Journal*, 405(2), 307-17.

Jellinger, K.A., 1999. Post mortem studies in Parkinson's disease--is it possible to detect brain areas for specific symptoms? *Journal of Neural Transmission. Supplementum*, 56, 1-29.

Jellinger, K.A., 2004. Lewy body-related alpha-synucleinopathy in the aged human brain. *Journal of Neural Transmission*, 111(10-11), 1219-1235.

Jesnowski, R. et al., 2002. Ribosomal highly basic 23-kDa protein as a reliable standard for gene expression analysis. *Pancreatology*, 2(4), 421-424.

Johnson, J. et al., 2004. SNCA multiplication is not a common cause of Parkinson disease or dementia with Lewy bodies. *Neurology*, 63(3), 554-6.

Jorgensen, N.D. et al., 2009. The WD40 domain is required for LRRK2 neurotoxicity. *PloS One*, 4(12), e8463.

Junqué, C. et al., 2005. Amygdalar and hippocampal MRI volumetric reductions in Parkinson's disease with dementia. *Movement Disorders*, 20(5), 540-544.

Kachergus, J. et al., 2005. Identification of a novel LRRK2 mutation linked to autosomal dominant parkinsonism: evidence of a common founder across European populations. *American Journal of Human Genetics*, 76(4), 672-80.

Kalaitzakis, M.E. et al., 2008. Controversies over the staging of alpha-synuclein pathology in Parkinson's disease. *Acta Neuropathologica*, 116(1), 125-128; author reply 129-131.

Kay, D.M. et al., 2005. Escaping Parkinson's disease: a neurologically healthy octogenarian with the LRRK2 G2019S mutation. *Movement Disorders*, 20(8), 1077-8.

Kay, D.M. et al., 2006. Parkinson's disease and LRRK2: frequency of a common mutation in U.S. movement disorder clinics. *Movement Disorders*, 21(4), 519-23.

Kay, D.M. et al., 2007. Heterozygous parkin point mutations are as common in control subjects as in Parkinson's patients. *Annals of Neurology*, 61(1), 47-54.

Khan, N.L. et al., 2002. Clinical and subclinical dopaminergic dysfunction in PARK6-linked parkinsonism: an 18F-dopa PET study. *Annals of Neurology*, 52(6), 849-853.

Khateeb, S. et al., 2006. PLA2G6 mutation underlies infantile neuroaxonal dystrophy. *American Journal of Human Genetics*, 79(5), 942-948.

Kim, S. & Webster, M.J., 2009. Postmortem Brain Tissue for Drug Discovery in Psychiatric Research. *Schizophr Bull*, 35(6), 1031-1033.

Kingsbury, A.E. et al., 1995. Tissue pH as an indicator of mRNA preservation in human post-mortem brain. *Brain Research. Molecular Brain Research*, 28(2), 311-8.

Kingsbury, A.E. et al., 2001. Metabolic enzyme expression in dopaminergic neurons in Parkinson's disease: an in situ hybridization study. *Annals of Neurology*, 50(2), 142-149.

Kitada, T. et al., 1998. Mutations in the parkin gene cause autosomal recessive juvenile parkinsonism. *Nature*, 392(6676), 605-608.

Knight, J.C., 2003. Functional implications of genetic variation in non-coding DNA for disease susceptibility and gene regulation. *Clinical Science*, 104(5), 493-501.

Knight, J.C. et al., 2003. In vivo characterization of regulatory polymorphisms by allele-specific quantification of RNA polymerase loading. *Nature Genetics*, 33(4), 469-475.

Kösel, S. et al., 1998. Novel mutations of mitochondrial complex I in pathologically proven Parkinson disease. *Neurogenetics*, 1(3), 197-204.

Krüger, R. et al., 1998. Ala30Pro mutation in the gene encoding alpha-synuclein in Parkinson's disease. *Nature Genetics*, 18(2), 106-108.

Kumar, A. et al., 2010. The Parkinson's disease associated LRRK2 exhibits weaker in vitro phosphorylation of 4E-BP compared to autophosphorylation. *PloS One*, 5(1), e8730.

Kwan, T. et al., 2009. Tissue effect on genetic control of transcript isoform variation. *PLoS Genetics*, 5(8), e1000608.

Kushnareva, Y., Murphy, A.N. & Andreyev, A., 2002. Complex I-mediated reactive oxygen species generation: modulation by cytochrome c and NAD(P)+ oxidation-reduction state. *The Biochemical Journal*, 368(Pt 2), 545-553.

Langston, J.W. et al., 1983. Chronic Parkinsonism in humans due to a product of meperidine-analog synthesis. *Science*, 219(4587), 979-980.

Lashley, T. et al., 2008. Expression of BRI2 mRNA and protein in normal human brain and familial British dementia: its relevance to the pathogenesis of disease. *Neuropathology and Applied Neurobiology*, 34(5), 492-505.

Lautier, C. et al., 2008. Mutations in the GIGYF2 (TNRC15) gene at the PARK11 locus in familial Parkinson disease. *American Journal of Human Genetics*, 82(4), 822-33.

Le, W. et al., 2003. Mutations in NR4A2 associated with familial Parkinson disease. *Nature Genetics*, 33(1), 85-89.

Lee, S.B. et al., 2007. Loss of LRRK2/PARK8 induces degeneration of dopaminergic neurons in Drosophila. *Biochemical and Biophysical Research Communications*, 358(2), 534-539.

Lees, A.J., 2007. Unresolved issues relating to the shaking palsy on the celebration of James Parkinson's 250th birthday. *Movement Disorders*, 22 Suppl 17, S327-334.

Lees, A.J., Hardy, J. & Revesz, T., 2009. Parkinson's disease. *Lancet*, 373(9680), 2055-2066.

Leroy, E. et al., 1998a. Deletions in the Parkin gene and genetic heterogeneity in a Greek family with early onset Parkinson's disease. *Human Genetics*, 103(4), 424-427.

Leroy, E. et al., 1998b. The ubiquitin pathway in Parkinson's disease. *Nature*, 395(6701), 451-452.

Lesage, S. et al., 2005a. G2019S LRRK2 mutation in French and North African families with Parkinson's disease. *Annals of Neurology*, 58(5), 784-7.

Lesage, S. et al., 2005b. LRRK2 haplotype analyses in European and North African families with Parkinson disease: a common founder for the G2019S mutation dating from the 13th century. *American Journal of Human Genetics*, 77(2), 330-2.

Lesage, S. et al., 2006. LRRK2 G2019S as a cause of Parkinson's disease in North African Arabs. *The New England Journal of Medicine*, 354(4), 422-3.

Lesage, S. et al., 2007. Frequency of the LRRK2 G2019S mutation in siblings with Parkinson's disease. *Neuro-Degenerative Diseases*, 4(2-3), 195-8

Lesage, S. et al., 2008. Is the common LRRK2 G2019S mutation related to dyskinesias in North African Parkinson disease? *Neurology*, 71(19), 1550-2.

Lesage, S. & Brice, A., 2009. Parkinson's disease: from monogenic forms to genetic susceptibility factors. *Human Molecular Genetics*, 18(R1), R48-59.

Lesage, S. et al., 2010. Parkinson's disease-related LRRK2 G2019S mutation results from independent mutational events in humans. *Human Molecular Genetics*. Available at: http://www.ncbi.nlm.nih.gov/pubmed/20197411 [Accessed March 16, 2010].

Levecque, C. et al., 2004. Association of polymorphisms in the Tau and Saitohin genes with Parkinson's disease. *Journal of Neurology, Neurosurgery, and Psychiatry*, 75(3), 478-80.

Lewis, P.A. et al., 2007. The R1441C mutation of LRRK2 disrupts GTP hydrolysis. *Biochemical and Biophysical Research Communications*, 357(3), 668-71.

Li, X. et al., 2005. Geographic and ethnic differences in frequencies of two polymorphisms (D/N394 and L/I272) of the parkin gene in sporadic Parkinson's disease. *Parkinsonism & Related Disorders*, 11(8), 485-491.

Li, X. et al., 2007. Leucine-rich repeat kinase 2 (LRRK2)/PARK8 possesses GTPase activity that is altered in familial Parkinson's disease R1441C/G mutants. *Journal of Neurochemistry*, 103(1), 238-47.

Li, X. et al., 2010. Enhanced striatal dopamine transmission and motor performance with LRRK2 overexpression in mice is eliminated by familial Parkinson's disease mutation G2019S. *The Journal of Neuroscience*, 30(5), 1788-1797.

Li, Y. et al., 2002. Age at onset in two common neurodegenerative diseases is genetically controlled. *American Journal of Human Genetics*, 70(4), 985-993.

Lim, S., Fox, S.H. & Lang, A.E., 2009. Overview of the extranigral aspects of Parkinson disease. *Archives of Neurology*, 66(2), 167-172.

Lin, X. et al., 2009. Leucine-rich repeat kinase 2 regulates the progression of neuropathology induced by Parkinson's-disease-related mutant alpha-synuclein. *Neuron*, 64(6), 807-827.

Lincoln, S. et al., 1999. Low frequency of pathogenic mutations in the ubiquitin carboxy-terminal hydrolase gene in familial Parkinson's disease. *Neuroreport*, 10(2), 427-429.

Lincoln, S.J. et al., 2003. Parkin variants in North American Parkinson's disease: cases and controls. *Movement Disorders*, 18(11), 1306-1311.

Liou, A.K.F. et al., 2008. Wild-type LRRK2 but not its mutant attenuates stress-induced cell death via ERK pathway. *Neurobiology of Disease*, 32(1), 116-24.

Litvan, I. et al., 2003. Movement Disorders Society Scientific Issues Committee report: SIC Task Force appraisal of clinical diagnostic criteria for Parkinsonian disorders. *Movement Disorders*, 18(5), 467-486.

Liu, Y. et al., 2002. The UCH-L1 gene encodes two opposing enzymatic activities that affect alpha-synuclein degradation and Parkinson's disease susceptibility. *Cell*, 111(2), 209-218.

Liu, Z. et al., 2008. A Drosophila model for LRRK2-linked parkinsonism. *Proceedings of the National Academy of Sciences of the United States of America*, 105(7), 2693-8.

Lo, H.S. et al., 2003. Allelic variation in gene expression is common in the human genome. *Genome Research*, 13(8), 1855-1862.

Lockhart, P.J. et al., 2004. Multiplication of the alpha-synuclein gene is not a common disease mechanism in Lewy body disease. *Journal of Molecular Neuroscience*, 24(3), 337-342.

Lohmann, E. et al., 2003. How much phenotypic variation can be attributed to parkin genotype? *Annals of Neurology*, 54(2), 176-185.

Lowe, J. et al., 1990. Ubiquitin carboxyl-terminal hydrolase (PGP 9.5) is selectively present in ubiquitinated inclusion bodies characteristic of human neurodegenerative diseases. *The Journal of Pathology*, 161(2), 153-160.

Lu, C. et al., 2005. The LRRK2 I2012T, G2019S, and I2020T mutations are rare in Taiwanese patients with sporadic Parkinson's disease. *Parkinsonism & Related Disorders*, 11(8), 521-2.

Lücking, C.B. et al., 2000. Association between early-onset Parkinson's disease and mutations in the parkin gene. *The New England Journal of Medicine*, 342(21), 1560-1567.

MacLeod, D. et al., 2006. The familial Parkinsonism gene LRRK2 regulates neurite process morphology. *Neuron*, 52(4), 587-93.

Mandel, S. et al., 2005. Gene expression profiling of sporadic Parkinson's disease substantia nigra pars compacta reveals impairment of ubiquitin-proteasome subunits, SKP1A, aldehyde dehydrogenase, and chaperone HSC-70. *Annals of the New York Academy of Sciences*, 1053, 356-75.

Maraganore, D.M. et al., 1999. Case-control study of the ubiquitin carboxy-terminal hydrolase L1 gene in Parkinson's disease. *Neurology*, 53(8), 1858-1860.

Maraganore, D.M. et al., 2004. A limited role for DJ1 in Parkinson disease susceptibility. *Neurology*, 63(3), 550-553.

Maraganore, D.M. et al., 2005. High-resolution whole-genome association study of Parkinson disease. *American Journal of Human Genetics*, 77(5), 685-693.

Maraganore, D.M. et al., 2006. Collaborative analysis of alpha-synuclein gene promoter variability and Parkinson disease. *JAMA*, 296(6), 661-70.

Martinat, C. et al., 2006. Cooperative transcription activation by Nurr1 and Pitx3 induces embryonic stem cell maturation to the midbrain dopamine neuron phenotype. *Proceedings of the National Academy of Sciences of the United States of America*, 103(8), 2874-2879.

Martí-Massó, J. et al., 2009. Neuropathology of Parkinson's disease with the R1441G mutation in LRRK2. *Movement Disorders*. Available at: http://www.ncbi.nlm.nih.gov/pubmed/19735093.

Marx, F.P. et al., 2003. Identification and functional characterization of a novel R621C mutation in the synphilin-1 gene in Parkinson's disease. *Human Molecular Genetics*, 12(11), 1223-1231.

Mata, I.F. et al., 2002. Single-nucleotide polymorphisms in the promoter region of the PARKIN gene and Parkinson's disease. *Neuroscience Letters*, 329(2), 149-152.

Mata, I.F. et al., 2005. LRRK2 R1441G in Spanish patients with Parkinson's disease. *Neuroscience Letters*, 382(3), 309-11.

Mata, I.F. et al., 2006a. LRRK2 in Parkinson's disease: protein domains and functional insights. *Trends in Neurosciences*, 29(5), 286-93.

Mata, I.F. et al., 2006b. LRRK2 mutations are a common cause of Parkinson's disease in Spain. *European Journal of Neurology*, 13(4), 391-4.

Mata, I.F. et al., 2008a. Glucocerebrosidase gene mutations: a risk factor for Lewy body disorders. *Archives of Neurology*, 65(3), 379-382.

Mata, I.F. et al., 2009a. Lrrk2 R1441G-related Parkinson's disease: evidence of a common founding event in the seventh century in Northern Spain. *Neurogenetics*. Available at: http://www.ncbi.nlm.nih.gov/pubmed/19308469.

Mata, I.F. et al., 2009b. LRRK2 mutations in patients with Parkinson's disease from Peru and Uruguay. *Parkinsonism & Related Disorders*, 15(5), 370-373.

Matsumine, H. et al., 1997. Localization of a gene for an autosomal recessive form of juvenile Parkinsonism to chromosome 6q25.2-27. *American Journal of Human Genetics*, 60(3), 588-596.

Mattit, H. et al., 2006. Familial Mediterranean fever in the Syrian population: gene mutation frequencies, carrier rates and phenotype-genotype correlation. *European Journal of Medical Genetics*, 49(6), 481-486.

McInerney-Leo, A., Gwinn-Hardy, K. & Nussbaum, R.L., 2004. Prevalence of Parkinson's disease in populations of African ancestry: a review. *Journal of the National Medical Association*, 96(7), 974-9.

McKeith, I.G. et al., 2005. Diagnosis and management of dementia with Lewy bodies: third report of the DLB Consortium. *Neurology*, 65(12), 1863-1872.

Micieli, G. et al., 2003. Autonomic dysfunction in Parkinson's disease. *Neurological Sciences*, 24 Suppl 1, S32-34.

Meldgaard, M. et al., 2006. Validation of two reference genes for mRNA level studies of murine disease models in neurobiology. *Journal of Neuroscience Methods*, 156(1-2), 101-110.

Melrose, H. et al., 2006. Anatomical localization of leucine-rich repeat kinase 2 in mouse brain. *Neuroscience*, 139(3), 791-4.

Melrose, H.L. et al., 2007. A comparative analysis of leucine-rich repeat kinase 2 (Lrrk2) expression in mouse brain and Lewy body disease. *Neuroscience*, 147(4), 1047-58.

Messeguer, X. et al., 2002. PROMO: detection of known transcription regulatory elements using species-tailored searches. *Bioinformatics*, 18(2), 333-334.

Miklossy, J. et al., 2006. LRRK2 expression in normal and pathologic human brain and in human cell lines. *Journal of Neuropathology and Experimental Neurology*, 65(10), 953-63.

Miklossy, J. et al., 2007. Lrrk2 and chronic inflammation are linked to pallido-ponto-nigral degeneration caused by the N279K tau mutation. *Acta Neuropathologica*, 114(3), 243-254.

Miller, G.J. et al., 1996. Increased activation of the haemostatic system in men at high risk of fatal coronary heart disease. *Thrombosis and Haemostasis*, 75(5), 767-771.

Miller, R.M. et al., 2004. Dysregulation of gene expression in the 1-methyl-4-phenyl-1,2,3,6-tetrahydropyridine-lesioned mouse substantia nigra. *The Journal of Neuroscience*, 24(34), 7445-54.

Miller, R.M. et al., 2006. Robust dysregulation of gene expression in substantia nigra and striatum in Parkinson's disease. *Neurobiology of Disease*, 21(2), 305-13.

Milosevic, J. et al., 2009. Emerging role of LRRK2 in human neural progenitor cell cycle progression, survival and differentiation. *Molecular Neurodegeneration*, 4, 25.

Mizuta, I. et al., 2006. Multiple candidate gene analysis identifies alpha-synuclein as a susceptibility gene for sporadic Parkinson's disease. *Human Molecular Genetics*, 15(7), 1151-1158.

Moran, L.B. et al., 2006. Whole genome expression profiling of the medial and lateral substantia nigra in Parkinson's disease. *Neurogenetics*, 7(1), 1-11.

Moran, L.B. et al., 2007. Analysis of alpha-synuclein, dopamine and parkin pathways in neuropathologically confirmed parkinsonian nigra. *Acta Neuropathologica*, 113(3), 253-63.

Morgan, N.V. et al., 2006. PLA2G6, encoding a phospholipase A2, is mutated in neurodegenerative disorders with high brain iron. *Nature Genetics*, 38(7), 752-754.

Morley, M. et al., 2004. Genetic analysis of genome-wide variation in human gene expression. *Nature*, 430(7001), 743-747.

Motulsky, A.G., 1995. Jewish diseases and origins. *Nature Genetics*, 9(2), 99-101.

Mueller, J.C. et al., 2005. Multiple regions of alpha-synuclein are associated with Parkinson's disease. *Annals of Neurology*, 57(4), 535-541.

Munhoz, R.P. et al., 2008. The G2019S LRRK2 mutation in Brazilian patients with Parkinson's disease: phenotype in monozygotic twins. *Movement Disorders*, 23(2), 290-4.

Murakami, T. et al., 2007. PINK1, a gene product of PARK6, accumulates in alpha-synucleinopathy brains. *Journal of Neurology, Neurosurgery, and Psychiatry*, 78(6), 653-654.

Mutez, E. et al., 2010. Transcriptional profile of Parkinson blood mononuclear cells with LRRK2 mutation. *Neurobiology of Aging*.
Available at: http://www.ncbi.nlm.nih.gov/pubmed/20096956..

Myers, A.J. et al., 2007. A survey of genetic human cortical gene expression. *Nature Genetics*, 39(12), 1494-1499.

Myhre, R. et al., 2008. Genetic association study of synphilin-1 in idiopathic Parkinson's disease. *BMC Medical Genetics*, 9, 19.

Najim al-Din, A.S. et al., 1994. Pallido-pyramidal degeneration, supranuclear upgaze paresis and dementia: Kufor-Rakeb syndrome. *Acta Neurologica Scandinavica*, 89(5), 347-352.

Neumann, J. et al., 2009. Glucocerebrosidase mutations in clinical and pathologically proven Parkinson's disease. *Brain*, 132(Pt 7), 1783-1794.

Ng, C. et al., 2009. Parkin protects against LRRK2 G2019S mutant-induced dopaminergic neurodegeneration in Drosophila. *The Journal of Neuroscience*, 29(36), 11257-11262

Niell, B.L. et al., 2003. Genetic anthropology of the colorectal cancer-susceptibility allele APC I1307K: evidence of genetic drift within the Ashkenazim. *American Journal of Human Genetics*, 73(6), 1250-60.

Nichols, W.C. et al., 2005. Genetic screening for a single common LRRK2 mutation in familial Parkinson's disease. *Lancet*, 365(9457), 410-412.

Nichols, W.C. et al., 2009. Mutations in GBA are associated with familial Parkinson disease susceptibility and age at onset. *Neurology*, 72(4), 310-316.

Nishioka, K. et al., 2006. Clinical heterogeneity of alpha-synuclein gene duplication in Parkinson's disease. *Annals of Neurology*, 59(2), 298-309.

Ohl, F. et al., 2005. Gene expression studies in prostate cancer tissue: which reference gene should be selected for normalization? *Journal of Molecular Medicine*, 83(12), 1014-1024.

Ohta, E., Kubo, M. & Obata, F., 2010. Prevention of intracellular degradation of I2020T mutant LRRK2 restores its protectivity against apoptosis. *Biochemical and Biophysical Research Communications*, 391(1), 242-247.

Okubadejo, N.U. et al., 2006. Parkinson's disease in Africa: A systematic review of epidemiologic and genetic studies. *Movement Disorders*, 21(12), 2150-6.

Okubadejo, N. et al., 2008a. Analysis of Nigerians with apparently sporadic Parkinson disease for mutations in LRRK2, PRKN and ATXN3. *PLoS ONE*, 3(10), e3421.

Okubadejo, N.U., 2008b. An analysis of genetic studies of Parkinson's disease in Africa. *Parkinsonism & Related Disorders*, 14(3), 177-82.

Orr-Urtreger, A. et al., 2007. The LRRK2 G2019S mutation in Ashkenazi Jews with Parkinson disease: is there a gender effect? *Neurology*, 69(16), 1595-602.

Osuntokun, B.O. et al., 1987. Neurological disorders in Nigerian Africans: a community-based study. *Acta Neurologica Scandinavica*, 75(1), 13-21.

Ozelius, L.J. et al., 2006. LRRK2 G2019S as a cause of Parkinson's disease in Ashkenazi Jews. *The New England Journal of Medicine*, 354(4), 424-5.

Paisán-Ruíz, C. et al., 2004. Cloning of the gene containing mutations that cause PARK8-linked Parkinson's disease. *Neuron*, 44(4), 595-600.

Paisán-Ruíz, C. et al., 2005. LRRK2 gene in Parkinson disease: mutation analysis and case control association study. *Neurology*, 65(5), 696-700.

Paisán-Ruíz, C. et al., 2006. Testing association between LRRK2 and Parkinson's disease and investigating linkage disequilibrium. *Journal of Medical Genetics*, 43(2), e9.

Paisán-Ruíz, C. et al., 2008. Comprehensive analysis of LRRK2 in publicly available Parkinson's disease cases and neurologically normal controls. *Human Mutation*, 29(4), 485-490.

Paisan-Ruiz, C. et al., 2009. Characterization of PLA2G6 as a locus for dystonia-parkinsonism. *Annals of Neurology*, 65(1), 19-23.

Pankratz, N. et al., 2002. Genome screen to identify susceptibility genes for Parkinson disease in a sample without parkin mutations. *American Journal of Human Genetics*, 71(1), 124-135.

Pankratz, N. et al., 2003. Significant linkage of Parkinson disease to chromosome 2q36-37. *American Journal of Human Genetics*, 72(4), 1053-1057.

Pankratz, N. et al., 2009. Genomewide association study for susceptibility genes contributing to familial Parkinson disease. *Human Genetics*, 124(6), 593-605.

Papadopoulos, V.P. et al., 2008. The population genetics of familial mediterranean fever: a meta-analysis study. *Annals of Human Genetics*, 72(Pt 6), 752-61.

Papapetropoulos, S. et al., 2008. Is the G2019S LRRK2 mutation common in all southern European populations? *Journal of Clinical Neuroscience*, 15(9), 1027-30.

Parisiadou, L. et al., 2009. Phosphorylation of ezrin/radixin/moesin proteins by LRRK2 promotes the rearrangement of actin cytoskeleton in neuronal morphogenesis. *The Journal of Neuroscience*, 29(44), 13971-13980.

Park, J. et al., 2006. Mitochondrial dysfunction in Drosophila PINK1 mutants is complemented by parkin. *Nature*, 441(7097), 1157-1161.

Parkkinen, L., Soininen, H. & Alafuzoff, I., 2003. Regional distribution of alpha-synuclein pathology in unimpaired aging and Alzheimer disease. *Journal of Neuropathology and Experimental Neurology*, 62(4), 363-367.

Pastinen, T. & Hudson, T.J., 2004. Cis-acting regulatory variation in the human genome. *Science*, 306(5696), 647-650.

Pastinen, T. et al., 2004. A survey of genetic and epigenetic variation affecting human gene expression. *Physiological Genomics*, 16(2), 184-193.

Pastinen, T., Ge, B. & Hudson, T.J., 2006. Influence of human genome polymorphism on gene expression. *Human Molecular Genetics*, 15 Spec No 1, R9-16.

Pchelina, S.N. et al., 2008. Screening for LRRK2 mutations in patients with Parkinson's disease in Russia: identification of a novel LRRK2 variant. *European Journal of Neurology*, 15(7), 692-6.

Perez-Pastene, C. et al., 2007. Lrrk2 mutations in South America: A study of Chilean Parkinson's disease. *Neuroscience Letters*, 422(3), 193-7.

Perry, G. et al., 2008. Leucine-rich repeat kinase 2 colocalizes with alpha-synuclein in Parkinson's disease, but not tau-containing deposits in tauopathies. *Neuro-Degenerative Diseases*, 5(3-4), 222-4.

Pimentel, M.M.G. et al., 2008. A study of LRRK2 mutations and Parkinson's disease in Brazil. *Neuroscience Letters*, 433(1), 17-21.

Pirkevi, C. et al., 2009. A LRRK2 G2019S mutation carrier from Turkey shares the Japanese haplotype. *Neurogenetics*, 10(3), 271-273.

Pittman, A.M. et al., 2005. Linkage disequilibrium fine mapping and haplotype association analysis of the tau gene in progressive supranuclear palsy and corticobasal degeneration. *Journal of Medical Genetics*, 42(11), 837-846.

Plowey, E.D. et al., 2008. Role of autophagy in G2019S-LRRK2-associated neurite shortening in differentiated SH-SY5Y cells. *Journal of Neurochemistry*, 105(3), 1048-56.

Plun-Favreau, H. et al., 2007. The mitochondrial protease HtrA2 is regulated by Parkinson's disease-associated kinase PINK1. *Nature Cell Biology*, 9(11), 1243-1252.

Polymeropoulos, M.H. et al., 1996. Mapping of a gene for Parkinson's disease to chromosome 4q21-q23. *Science*, 274(5290), 1197-1199.

Polymeropoulos, M.H. et al., 1997. Mutation in the alpha-synuclein gene identified in families with Parkinson's disease. *Science*, 276(5321), 2045-2047.

Punia, S. et al., 2006. Absence/rarity of commonly reported LRRK2 mutations in Indian Parkinson's disease patients. *Neuroscience Letters*, 409(2), 83-8.

Qing, H. et al., 2009. Lrrk2 phosphorylates alpha synuclein at serine 129: Parkinson disease implications. *Biochemical and Biophysical Research Communications*, 387(1), 149-152.

al Rajeh, S. et al., 1993. A community survey of neurological disorders in Saudi Arabia: the Thugbah study. *Neuroepidemiology*, 12(3), 164-78.

Ramachandiran, S. et al., 2007. Divergent mechanisms of paraquat, MPP+, and rotenone toxicity: oxidation of thioredoxin and caspase-3 activation. *Toxicological Sciences*, 95(1), 163-171.

Ramirez, A. et al., 2006. Hereditary parkinsonism with dementia is caused by mutations in ATP13A2, encoding a lysosomal type 5 P-type ATPase. *Nature Genetics*, 38(10), 1184-1191.

Richardson, J.R. et al., 2005. Paraquat neurotoxicity is distinct from that of MPTP and rotenone. *Toxicological Sciences*, 88(1), 193-201.

Richardson, J.R. et al., 2006. Developmental exposure to the pesticide dieldrin alters the dopamine system and increases neurotoxicity in an animal model of Parkinson's disease. *The FASEB Journal*, 20(10), 1695-1697.

Richardson, J.R. et al., 2007. Obligatory role for complex I inhibition in the dopaminergic neurotoxicity of 1-methyl-4-phenyl-1,2,3,6-tetrahydropyridine (MPTP). *Toxicological Sciences*, 95(1), 196-204.

Risch, N. et al., 1995. Genetic analysis of idiopathic torsion dystonia in Ashkenazi Jews and their recent descent from a small founder population. *Nature Genetics*, 9(2), 152-9.

Risch, N. et al., 2003. Geographic distribution of disease mutations in the Ashkenazi Jewish population supports genetic drift over selection. *American Journal of Human Genetics*, 72(4), 812-22.

Rizzu, P. et al., 2004. DJ-1 colocalizes with tau inclusions: a link between parkinsonism and dementia. *Annals of Neurology*, 55(1), 113-118.

Ross, O.A. et al., 2006. Lrrk2 and Lewy body disease. *Annals of Neurology*, 59(2), 388-93.

Ross, O.A. et al., 2007. Lack of evidence for association of Parkin promoter polymorphism (PRKN-258) with increased risk of Parkinson's disease. *Parkinsonism & Related Disorders*, 13(7), 386-388.

Ross, O.A. et al., 2008. Analysis of Lrrk2 R1628P as a risk factor for Parkinson's disease. *Annals of Neurology*, 64(1), 88-92.

Rothman, K.J., 1990. No adjustments are needed for multiple comparisons. *Epidemiology*, 1(1), 43-46.

Saha, S. et al., 2009. LRRK2 modulates vulnerability to mitochondrial dysfunction in Caenorhabditis elegans. *The Journal of Neuroscience*, 29(29), 9210-9218.

Sakaguchi-Nakashima, A. et al., 2007. LRK-1, a C. elegans PARK8-related kinase, regulates axonal-dendritic polarity of SV proteins. *Current Biology*, 17(7), 592-598.

Santos-Rebouças, C.B. et al., 2008. Co-occurrence of sporadic parkinsonism and late-onset Alzheimer's disease in a Brazilian male with the LRRK2 p.G2019S mutation. *Genetic Testing*, 12(4), 471-3.

Satoh, J. & Kuroda, Y., 2001. A polymorphic variation of serine to tyrosine at codon 18 in the ubiquitin C-terminal hydrolase-L1 gene is associated with a reduced risk of sporadic Parkinson's disease in a Japanese population. *Journal of the Neurological Sciences*, 189(1-2), 113-117.

Santpere, G. & Ferrer, I., 2009. LRRK2 and neurodegeneration. *Acta Neuropathologica*, 117(3), 227-46.

Satake, W. et al., 2009. Genome-wide association study identifies common variants at four loci as genetic risk factors for Parkinson's disease. *Nature Genetics*, 41(12), 1303-1307.

Sasieni, P.D., 1997. From genotypes to genes: doubling the sample size. *Biometrics*, 53(4), 1253-1261.

Saunders-Pullman, R. et al., 2006. Increased frequency of the LRRK2 G2019S mutation in an elderly Ashkenazi Jewish population is not associated with dementia. *Neuroscience Letters*, 402(1-2), 92-6.

Schiesling, C. et al., 2008. Review: Familial Parkinson's disease--genetics, clinical phenotype and neuropathology in relation to the common sporadic form of the disease. *Neuropathology and Applied Neurobiology*, 34(3), 255-271.

Schlossmacher, M.G. et al., 2002. Parkin localizes to the Lewy bodies of Parkinson disease and dementia with Lewy bodies. *The American Journal of Pathology*, 160(5), 1655-67.

Schober, A., 2004. Classic toxin-induced animal models of Parkinson's disease: 6-OHDA and MPTP. *Cell and Tissue Research*, 318(1), 215-224.

Schoenberg, B.S. et al., 1988. Comparison of the prevalence of Parkinson's disease in black populations in the rural United States and in rural Nigeria: door-to-door community studies. *Neurology*, 38(4), 645-6.

Schlossmacher, M.G. et al., 2002. Parkin localizes to the Lewy bodies of Parkinson disease and dementia with Lewy bodies. *The American Journal of Pathology*, 160(5), 1655-67.

Scott, W.K. et al., 2000. Fine mapping of the chromosome 12 late-onset Alzheimer disease locus: potential genetic and phenotypic heterogeneity. *American Journal of Human Genetics*, 66(3), 922-932.

Scott, W.K. et al., 2001. Complete genomic screen in Parkinson disease: evidence for multiple genes. *JAMA: The Journal of the American Medical Association*, 286(18), 2239-2244.

Sharma, M. et al., 2006. The sepiapterin reductase gene region reveals association in the PARK3 locus: analysis of familial and sporadic Parkinson's disease in European populations. *Journal of Medical Genetics*, 43(7), 557-562.

Shimura, H. et al., 2000. Familial Parkinson disease gene product, parkin, is a ubiquitin-protein ligase. *Nature Genetics*, 25(3), 302-305.

Shin, N. et al., 2008. LRRK2 regulates synaptic vesicle endocytosis. *Experimental Cell Research*, 314(10), 2055-65.

Shojaee, S. et al., 2008. Genome-wide linkage analysis of a Parkinsonian-pyramidal syndrome pedigree by 500 K SNP arrays. *American Journal of Human Genetics*, 82(6), 1375-1384.

Shojaee, S. et al., 2009. A clinic-based screening of mutations in exons 31, 34, 35, 41, and 48 of LRRK2 in Iranian Parkinson's disease patients. *Movement Disorders*, 24(7), 1023-1027.

Simes, R.J., 1986. An improved Bonferroni procedure for multiple tests of significance. *Biometrika*, 73(3), 751-754.

Simón-Sánchez, J. et al., 2006. LRRK2 is expressed in areas affected by Parkinson's disease in the adult mouse brain. *The European Journal of Neuroscience*, 23(3), 659-66.

Simón-Sánchez, J. et al., 2009. Genome-wide association study reveals genetic risk underlying Parkinson's disease. *Nature Genetics*, 41(12), 1308-1312.

Simunovic, F. et al., 2009. Gene expression profiling of substantia nigra dopamine neurons: further insights into Parkinson's disease pathology. *Brain*, 132(Pt 7), 1795-1809.

Sina, F. et al., 2009. R632W mutation in PLA2G6 segregates with dystonia-parkinsonism in a consanguineous Iranian family. *European Journal of Neurology*, 16(1), 101-104.

Singleton, A.B. et al., 2003. alpha-Synuclein locus triplication causes Parkinson's disease. *Science*, 302(5646), 841.

Skipper, L. et al., 2004. Linkage disequilibrium and association of MAPT H1 in Parkinson disease. *American Journal of Human Genetics*, 75(4), 669-677.

Skipper, L. et al., 2005. Comprehensive evaluation of common genetic variation within LRRK2 reveals evidence for association with sporadic Parkinson's disease. *Human Molecular Genetics*, 14(23), 3549-3556.

Slatkin, M., 2004. A population-genetic test of founder effects and implications for Ashkenazi Jewish diseases. *American Journal of Human Genetics*, 75(2), 282-93.

Smith, A.J.P. & Humphries, S.E., 2009. Characterization of DNA-binding proteins using multiplexed competitor EMSA. *Journal of Molecular Biology*, 385(3), 714-717.

Smith, W.W. et al., 2005a. Leucine-rich repeat kinase 2 (LRRK2) interacts with parkin, and mutant LRRK2 induces neuronal degeneration. *Proceedings of the National Academy of Sciences of the United States of America*, 102(51), 18676-81.

Smith, W.W. et al. 2005b. Alpha-synuclein phosphorylation enhances eosinophilic cytoplasmic inclusion formation in SH-SY5Y cells. *The Journal of Neuroscience*, 25(23), 5544-52.

Smith, W.W. et al., 2006. Kinase activity of mutant LRRK2 mediates neuronal toxicity. *Nature Neuroscience*, 9(10), 1231-1233.

Spanaki, C., Latsoudis, H. & Plaitakis, A., 2006. LRRK2 mutations on Crete: R1441H associated with PD evolving to PSP. *Neurology*, 67(8), 1518-9.

Spillantini, M.G. et al., 1997. Alpha-synuclein in Lewy bodies. *Nature*, 388(6645), 839-40.

Spillantini, M.G. et al., 1998. alpha-Synuclein in filamentous inclusions of Lewy bodies from Parkinson's disease and dementia with lewy bodies. *Proceedings of the National Academy of Sciences of the United States of America*, 95(11), 6469-73.

Stewart, S. et al., 1999. Kinase suppressor of Ras forms a multiprotein signaling complex and modulates MEK localization. *Molecular and Cellular Biology*, 19(8), 5523-5534.

Stranger, B.E. et al., 2007. Population genomics of human gene expression. *Nature Genetics*, 39(10), 1217-1224.

Strauss, K.M. et al., 2005. Loss of function mutations in the gene encoding Omi/HtrA2 in Parkinson's disease. *Human Molecular Genetics*, 14(15), 2099-2111.

Squillaro, T. et al., 2007. Frequency of the LRRK2 G2019S mutation in Italian patients affected by Parkinson's disease. *Journal of Human Genetics*, 52(3), 201-4.

Sutherland, G. et al., 2007. A functional polymorphism in the parkin gene promoter affects the age of onset of Parkinson's disease. *Neuroscience Letters*, 414(2), 170-173.

Sutherland, G.T. et al., 2009a. Haplotype analysis of the PARK 11 gene, GIGYF2, in sporadic Parkinson's disease. *Movement Disorders*, 24(3), 449-452.

Sutherland, G.T. et al., 2009b. Do polymorphisms in the familial Parkinsonism genes contribute to risk for sporadic Parkinson's disease? *Movement Disorders*, 24(6), 833-838.

Tain, L.S. et al., 2009. Rapamycin activation of 4E-BP prevents parkinsonian dopaminergic neuron loss. *Nature Neuroscience*, 12(9), 1129-1135.

Taira, T. et al., 2004. DJ-1 has a role in antioxidative stress to prevent cell death. *EMBO Reports*, 5(2), 213-218.

Takahashi, H. & Wakabayashi, K., 2001. The cellular pathology of Parkinson's disease. *Neuropathology: Official Journal of the Japanese Society of Neuropathology*, 21(4), 315-322.

Takahashi, M. & Yamada, T., 1999. Viral etiology for Parkinson's disease--a possible role of influenza A virus infection. *Japanese Journal of Infectious Diseases*, 52(3), 89-98.

Tan, E.K. et al., 2004. Genetic analysis of DJ-1 in a cohort Parkinson's disease patients of different ethnicity. *Neuroscience Letters*, 367(1), 109-112.

Tan, E.K. et al., 2005a. The G2019S LRRK2 mutation is uncommon in an Asian cohort of Parkinson's disease patients. *Neuroscience Letters*, 384(3), 327-9.

Tan, E.K. et al., 2005b. Impaired transcriptional upregulation of Parkin promoter variant under oxidative stress and proteasomal inhibition: clinical association. *Human Genetics*, 118(3-4), 484-488.

Tan, E.K. et al., 2006. PINK1 mutations in sporadic early-onset Parkinson's disease. *Movement Disorders*, 21(6), 789-793.

Tan, E.K. et al., 2007a. The LRRK2 Gly2385Arg variant is associated with Parkinson's disease: genetic and functional evidence. *Human Genetics*, 120(6), 857-863.

Tan, E.K. et al., 2007b. Analysis of LRRK2 Gly2385Arg genetic variant in non-Chinese Asians. *Movement Disorders*, 22(12), 1816-1818.

Tan, E.K. et al., 2007c. LRRK2 G2019S founder haplotype in the Chinese population. *Movement Disorders*, 22(1), 105-7.

Tan, E.K. et al., 2008. LRRK2 R1628P increases risk of Parkinson's disease: replication evidence. *Human Genetics*, 124(3), 287-288.

Tanner, C.M. et al., 1999. Parkinson disease in twins: an etiologic study. *JAMA*, 281(4), 341-346.

Taymans, J., Van den Haute, C. & Baekelandt, V., 2006. Distribution of PINK1 and LRRK2 in rat and mouse brain. *Journal of Neurochemistry*, 98(3), 951-61.

Teare, M.D., Heighway, J. & Santibáñez Koref, M.F., 2006. An expectation-maximization algorithm for the analysis of allelic expression imbalance. *American Journal of Human Genetics*, 79(3), 539-543.

Teismann, P. & Schulz, J.B., 2004. Cellular pathology of Parkinson's disease: astrocytes, microglia and inflammation. *Cell and Tissue Research*, 318(1), 149-161.

Thiruchelvam, M. et al., 2000. Potentiated and preferential effects of combined paraquat and maneb on nigrostriatal dopamine systems: environmental risk factors for Parkinson's disease? *Brain Research*, 873(2), 225-234.

Thomas, M.G. et al., 2002. Founding mothers of Jewish communities: geographically separated Jewish groups were independently founded by very few female ancestors. *American Journal of Human Genetics*, 70(6), 1411-1420.

Tobin, J.E. et al., 2008. Haplotypes and gene expression implicate the MAPT region for Parkinson disease: the GenePD Study. *Neurology*, 71(1), 28-34.

Toda, T. et al., 2003. Toward identification of susceptibility genes for sporadic Parkinson's disease. *Journal of Neurology*, 250 Suppl 3, 40-43.

Toft, M. et al., 2006. Glucocerebrosidase gene mutations and Parkinson disease in the Norwegian population. *Neurology*, 66(3), 415-417.

Tomiyama, H. et al., 2006. Clinicogenetic study of mutations in LRRK2 exon 41 in Parkinson's disease patients from 18 countries. *Movement Disorders*, 21(8), 1102-8.

Touitou, I., 2001. The spectrum of Familial Mediterranean Fever (FMF) mutations. *European Journal of Human Genetics*, 9(7), 473-83**.**

Twelves, D., Perkins, K.S.M. & Counsell, C., 2003. Systematic review of incidence studies of Parkinson's disease. *Movement Disorders*, 18(1), 19-31.

Uchikado, H. et al., 2006. Alzheimer disease with amygdala Lewy bodies: a distinct form of alpha-synucleinopathy. *Journal of Neuropathology and Experimental Neurology*, 65(7), 685-697.

Valente, E.M. et al., 2001. Localization of a novel locus for autosomal recessive early-onset parkinsonism, PARK6, on human chromosome 1p35-p36. *American Journal of Human Genetics*, 68(4), 895-900.

Valente, E.M. et al., 2004. Hereditary early-onset Parkinson's disease caused by mutations in PINK1. *Science*, 304(5674), 1158-1160.

Van Den Eeden, S.K. et al., 2003. Incidence of Parkinson's disease: variation by age, gender, and race/ethnicity. *American Journal of Epidemiology*, 157(11), 1015-1022.

Veeramah, K.R. et al., 2008. Sex-Specific Genetic Data Support One of Two Alternative Versions of the Foundation of the Ruling Dynasty of the Nso' in Cameroon. *Current Anthropology*, 49(4), 707-714.

Venderova, K. et al., 2009. Leucine-Rich Repeat Kinase 2 interacts with Parkin, DJ-1 and PINK-1 in a Drosophila melanogaster model of Parkinson's disease. *Human Molecular Genetics*, 18(22), 4390-4404.

Vilariño-Güell, C. et al., 2008. ATP13A2 variability in Parkinson disease. *Human Mutation*, 30(3), 406-410.

Vogt, I.R. et al., 2006. Transcriptional changes in multiple system atrophy and Parkinson's disease putamen. *Experimental Neurology*, 199(2), 465-78.

Wadsworth, J.D.F. et al., 2006. Phenotypic heterogeneity in inherited prion disease (P102L) is associated with differential propagation of protease-resistant wild-type and mutant prion protein. *Brain*, 129(Pt 6), 1557-1569.

Wakabayashi, K. et al., 2000. NACP/alpha-synuclein-positive filamentous inclusions in astrocytes and oligodendrocytes of Parkinson's disease brains. *Acta Neuropathologica*, 99(1), 14-20.

Wang, D. et al., 2008. Dispensable role of Drosophila ortholog of LRRK2 kinase activity in survival of dopaminergic neurons. *Molecular Neurodegeneration*, 3, 3.

Wang, G. et al., 2008. Variation in the miRNA-433 binding site of FGF20 confers risk for Parkinson disease by overexpression of alpha-synuclein. *American Journal of Human Genetics*, 82(2), 283-289.

Wang, L. et al., 2008. The chaperone activity of heat shock protein 90 is critical for maintaining the stability of leucine-rich repeat kinase 2. *The Journal of Neuroscience*, 28(13), 3384-3391.

Warren, L. et al., 2008. A founding LRRK2 haplotype shared by Tunisian, US, European and Middle Eastern families with Parkinson's disease. *Parkinsonism & Related Disorders*, 14(1), 77-80.

Weale, M.E. et al., 2001. Armenian Y chromosome haplotypes reveal strong regional structure within a single ethno-national group. *Human Genetics*, 109(6), 659-674.

West, A.B. et al., 2005. Parkinson's disease-associated mutations in leucine-rich repeat kinase 2 augment kinase activity. *Proceedings of the National Academy of Sciences of the United States of America*, 102(46), 16842-7.

West, A.B. et al., 2002. Functional association of the parkin gene promoter with idiopathic Parkinson's disease. *Human Molecular Genetics*, 11(22), 2787-2792.

West, A.B. et al., 2005. Parkinson's disease-associated mutations in leucine-rich repeat kinase 2 augment kinase activity. *Proceedings of the National Academy of Sciences of the United States of America*, 102(46), 16842-7.

West, A.B. et al., 2007. Parkinson's disease-associated mutations in LRRK2 link enhanced GTP-binding and kinase activities to neuronal toxicity. *Human Molecular Genetics*, 16(2), 223-32.

Westerlund, M. et al., 2008a. Developmental regulation of leucine-rich repeat kinase 1 and 2 expression in the brain and other rodent and human organs: Implications for Parkinson's disease. *Neuroscience*, 152(2), 429-36.

Westerlund, M. et al., 2008b. Lrrk2 and alpha-synuclein are co-regulated in rodent striatum. *Molecular and Cellular Neurosciences*, 39(4), 586-91.

White, L.R. et al., 2007. MAPK-pathway activity, Lrrk2 G2019S, and Parkinson's disease. *Journal of Neuroscience Research*, 85(6), 1288-94.

Wider, C. et al., 2009. Phactr2 and Parkinson's disease. *Neuroscience Letters*, 453(1), 9-11.

Williams, J.H., Mepham, B.L. & Wright, D.H., 1997. Tissue preparation for immunocytochemistry. *Journal of Clinical Pathology*, 50(5), 422-428.

Wolozin, B. et al., 2008. Investigating convergent actions of genes linked to familial Parkinson's disease. *Neuro-Degenerative Diseases*, 5(3-4), 182-185.

Wolters, E.C. & Braak, H., 2006. Parkinson's disease: premotor clinico-pathological correlations. *Journal of Neural Transmission. Supplementum*, (70), 309-319.

Wszolek, Z.K. et al., 2004. Autosomal dominant parkinsonism associated with variable synuclein and tau pathology. *Neurology*, 62(9), 1619-22.

Xiromerisiou, G. et al., 2007. Screening for SNCA and LRRK2 mutations in Greek sporadic and autosomal dominant Parkinson's disease: identification of two novel LRRK2 variants. *European Journal of Neurology*, 14(1), 7-11.

Xu, P. et al., 2002. Association of homozygous 7048G7049 variant in the intron six of Nurr1 gene with Parkinson's disease. *Neurology*, 58(6), 881-884.

Yamada, M. et al., 2004. Overexpression of alpha-synuclein in rat substantia nigra results in loss of dopaminergic neurons, phosphorylation of alpha-synuclein and activation of caspase-9: resemblance to pathogenetic changes in Parkinson's disease. *Journal of Neurochemistry*, 91(2), 451-61.

Yamamoto, A. et al., 2005. Parkin phosphorylation and modulation of its E3 ubiquitin ligase activity. *The Journal of Biological Chemistry*, 280(5), 3390-9.

Yan, H. et al., 2002. Allelic variation in human gene expression. *Science*, 297(5584), 1143.

Yang, Y. et al., 2006. Mitochondrial pathology and muscle and dopaminergic neuron degeneration caused by inactivation of Drosophila Pink1 is rescued by Parkin. *Proceedings of the National Academy of Sciences of the United States of America*, 103(28), 10793-10798.

Yao, C. et al., 2010. LRRK2-mediated neurodegeneration and dysfunction of dopaminergic neurons in a Caenorhabditis elegans model of Parkinson's disease. *Neurobiology of Disease*. Available at: http://www.ncbi.nlm.nih.gov/pubmed/20382224.

Yilmaz, E. et al., 2001. Mutation frequency of Familial Mediterranean Fever and evidence for a high carrier rate in the Turkish population. *European Journal of Human Genetics*, 9(7), 553-5.

Yue, Z., 2009. LRRK2 in Parkinson's disease: in vivo models and approaches for understanding pathogenic roles. *The FEBS Journal*, 276(22), 6445-6454.

Zabetian, C.P. et al., 2006a. LRRK2 G2019S in families with Parkinson disease who originated from Europe and the Middle East: evidence of two distinct founding events beginning two millennia ago. *American Journal of Human Genetics*, 79(4), 752-8.

Zabetian, C.P. et al., 2006b. Identification and haplotype analysis of LRRK2 G2019S in Japanese patients with Parkinson disease. *Neurology*, 67(4), 697-9.

Zabetian, C.P. et al., 2007. Association analysis of MAPT H1 haplotype and subhaplotypes in Parkinson's disease. *Annals of Neurology*, 62(2), 137-144.

Zalloua, P.A. et al., 2008. Identifying genetic traces of historical expansions: Phoenician footprints in the Mediterranean. *American Journal of Human Genetics*, 83(5), 633-642.

Zarranz, J.J. et al., 2004. The new mutation, E46K, of alpha-synuclein causes Parkinson and Lewy body dementia. *Annals of Neurology*, 55(2), 164-173.

Zecca, L. et al., 2003. Neuromelanin of the substantia nigra: a neuronal black hole with protective and toxic characteristics. *Trends in Neurosciences*, 26(11), 578-580.

Zhang, J. et al., 2005. The tau gene haplotype h1 confers a susceptibility to Parkinson's disease. *European Neurology*, 53(1), 15-21.

Zhang, Y. et al., 2005. Transcriptional analysis of multiple brain regions in Parkinson's disease supports the involvement of specific protein processing, energy metabolism, and signaling pathways, and suggests novel disease mechanisms. *American Journal of Medical Genetics (Part B, Neuropsychiatric Genetics)*, 137B(1), 5-16.

Zheng, K., Heydari, B. & Simon, D.K., 2003. A common NURR1 polymorphism associated with Parkinson disease and diffuse Lewy body disease. *Archives of Neurology*, 60(5), 722-725.

Zhu, G. et al., 2004. Differential expression of human COMT alleles in brain and lymphoblasts detected by RT-coupled 5' nuclease assay. *Psychopharmacology*, 177(1-2), 178-184.

Zhu, X. et al., 2006a. LRRK2 in Parkinson's disease and dementia with Lewy bodies. *Molecular Neurodegeneration*, 1, 17.

Zhu, X.. et al., 2006b. LRRK2 protein is a component of Lewy bodies. *Annals of Neurology*, 60(5), 617-8; author reply 618-9.

Zimprich, A. et al., 2003. Point mutations in exon 1 of the NR4A2 gene are not a major cause of familial Parkinson's disease. *Neurogenetics*, 4(4), 219-220.

Zimprich, A. et al., 2004a. The PARK8 locus in autosomal dominant parkinsonism: confirmation of linkage and further delineation of the disease-containing interval. *American Journal of Human Genetics*, 74(1), 11-9.

Zimprich, A. et al., 2004b. Mutations in LRRK2 cause autosomal-dominant parkinsonism with pleomorphic pathology. *Neuron*, 44(4), 601-7.

Zlotogora, J., Zeigler, M. & Bach, G., 1988. Selection in favor of lysosomal storage disorders? *American Journal of Human Genetics*, 42(2), 271-273.